Forest Isoprene Emissions: New Insights from a Novel Field Instrument

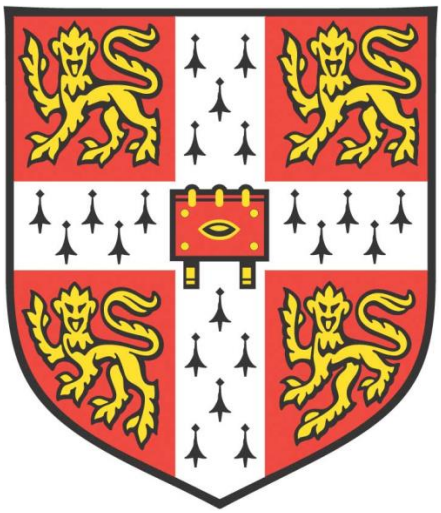

Conor Gordon Bolas

King's College

Centre for Atmospheric Science

Department of Chemistry

University of Cambridge

This dissertation is submitted for the degree of Doctor of Philosophy

April 2019

DECLARATION

This dissertation is the result of my own work and includes nothing, which is the outcome of work done in collaboration except where specifically indicated in the text. It has not been previously submitted, in part or whole, to any university of institution for any degree, diploma, or other qualification.

In accordance with the School of Physics and Chemistry guidelines, this thesis is does not exceed 60,000words, and it contains less than 150 figures.

Signed:_____

Date:_____

Conor Gordon Bolas

August 2019

“If I could have it back

All the time that we wasted

I'd only waste it again

If I could have it back

You know I would love to waste it again”

W. Butler

FOREST ISOPRENE EMISSIONS: NEW INSIGHTS FROM A NOVEL FIELD INSTRUMENT

Conor Gordon Bolas

ABSTRACT

Isoprene is an important biogenic volatile organic compound (VOC) in natural systems. Its emission by certain species of plants depends on solar radiation levels and on temperature, as well as other factors. Once in the atmosphere, it is rapidly transported and oxidised, and the subsequent chemistry of isoprene plays a significant part in determining the oxidising capacity of the troposphere, and therefore atmospheric composition and aerosol formation. The emission of isoprene is also important to the global carbon cycle and the carbon budget of the biosphere. Measurements have highlighted the great spatial and temporal variation of isoprene concentrations within forests and across different forest types, presenting a challenge for understanding overall emissions.

Current understanding of isoprene is limited by the lack of availability of suitable instrumentation for deployment in key field sites. To address this, in this thesis the development of a novel portable gas chromatography instrument suitable for challenging field environments, the iDirac, is described. This instrument has now been deployed in several field campaigns and has demonstrated good stability and a detection limit of ~40 ppt in the field.

Current estimates for global isoprene emission attribute 70% to tropical forests, but these have high levels of uncertainty as a result of under-sampling. This thesis describes a tropical field campaign of both leaf-level and canopy-level measurements of isoprene. Many of the individual tree species had never been measured before.

The distribution of isoprene within a canopy is poorly understood and existing models do not capture effectively the forest vertical isoprene gradient. The factors that drive the vertical concentration gradient are investigated in a novel measurement campaign over summer 2018 in a temperate forest. Measurements at different canopy heights were taken and isoprene was found to follow a strong diurnal profile and reach concentrations of 8ppb. The main driver of the gradient is found to be the insolation at the top of the canopy. The forest experienced stress as a result of higher temperatures and low rainfall in the 2018 heatwave and showed an elevated isoprene emission response that is not well represented in emission models. These measurements constrained a new 1D conceptual model, CamCan, which simulates isoprene concentration at different levels in the forest canopy. An established canopy model is also improved. The model is used to calculate fluxes from the forest and an annual emission of 2.0 Mg is estimated for the 2018 season. This new model is very simple and is capable of representing other forest types.

ACKNOWLEDGEMENTS

Firstly, I would like to acknowledge my supervisors, Prof. Neil Harris and Prof. Rod Jones for their help throughout the course of this PhD and the wealth of invaluable advice and guidance on this project. It has been brilliant!

There are a great many people involved in the many aspects of this thesis, but I would like to thank three in particular – Dr Andrew Robinson, Dr Valerio Ferracci and Zosia Staniaszek. Andrew for unbelievable patience and technical skills as I learned the ropes at the early stages, Valerio for technical help and being good craic out on fieldwork, even when the van gets stuck in the mud and Zosia Staniaszek, who helped develop the CamCan model and put up with me in the final parts of this process.

I am also very grateful to those on the 4th Floor and in wider CAS who have made the whole process really very fun and provided plenty of distraction – that's Anna, Steve, Anika, Andrea, Sarah, Pete, Markus, Battist, Aurelie, Lekan, Lia, Shewei, Bin, Dave, Chiara, Cameron, Arthur, Brendan, Scott, Andrea, Michal and Amy. A special mention to Ray Freshwater down the corridor who helped massively on my endless electronics nightmares. A massive thanks too to Dr Shahrul Nadzir at UKM and Dr Iq Mead at Cranfield University for help and good humour. Dr Alex Archibald, thank you also for the assistance and advice. The Lancaster crew of Dr Kirsti Ashworth, Fred Otu-Larbi, Tom King and Dr Kerneels Jaars need thanking also for all their valuable assistance.

There are those whose work are not mentioned in this thesis, but who have no less been key to my experience. Tabea Koehler who spent six months torturing eucalyptus trees with me, thank you! Also thanks to the Antarctic team at ACE, in particular Julia and Fiona, for helping with that really exciting project.

My trip to Borneo in 2015 was amazing and I am really very grateful to the BALI project team of Dr Sabine Both, Dr Ully Kritzler, Dr Justin Sentian and Unding Jami and all the other RAs that helped us in the jungle! A massive 'shout out' to Dr Matheus Nunes, the arsy fartsy man of the woods, I will never know a richer tapestry than his.

Finally to the others in my life who have been very, very supportive and have helped me get through this PhD. My family and in particular my parents, I guess I should thank them for always letting me do whatever I bloody well wanted. Jerome also, as well as teaching me lots of lessons, you have seen me through this with good humour, patience and cakes, so thank you!

CONTENTS

LIST OF TABLES

LIST OF FIGURES

LIST OF PUBLICATIONS

Schmale, J., Baccarini, A., Thurnherr, I., Henning, S., Efraim, A., Regayre, L., Bolas, C., Hartmann, M., Welti, A., Lehtipalo, K., Aemisegger, F., Tatzelt, C., Landwehr, S., Modini, R., Tummon, F., Johnson, J., Harris, N. R. P., Schnaiter, M., Toffoli, A., Derkani, M., Bukowiecki, N., Stratmann, F., Dommen, J., Baltensperger, U., Wernli, H., Rosenfeld, D., Gysel, M., Carslaw, K., (**2019**). Overview of the Antarctic Circumnavigation Expedition: Study of Preindustrial-like Aerosols and Their Climate Effects (ACE-SPACE). *Bulletin of the American Meteorological Society*. https://doi.org/10.1175/BAMS-D-18-0187.1

Nadzir, M. S. M., Cain, M., Robinson, A. D., Bolas, C., Harris, N. R. P., Parnikoza, I., Salimun, E., Mustafa, E. M., Alhasa, K. M., Zainuddin, M. H. M., Ghee, O. C., Morris, K., Khan, M. F., Latif, M. T., Wallis, B. M., Cheah, W., Zainudin, S. K., Yusop, N., Ahmad, M. R., Hussin, W. M.R.W., Salleh, S. M., Hamid, H. H.A., Lai, G. T., Uning, R., Bakar, M. A.A., Ariff, N. M., Tuah, Z., Wahab, M. I.A., Foong, S. Y., Samah, A. A., Chenoli, S. N., Wan Johari, W. L., Zain, C. R.C.M., Rahman, N. A., Rosenstiel, T. N., Yusoff, A. H., Sabuti, A. A., Alias, S. A., Noor, A. Y. M. (**2019**). Isoprene hotspots at the Western Coast of Antarctic Peninsula during MASEC′16. *Polar Science*. http://doi.org/10.1016/j.polar.2018.12.006

Visakorpi, K., Gripenberg, S., Malhi, Y., Bolas, C., Oliveras, I., Harris, N. R. P., Rifai, S., Riutta, T.Riutta, T. (**2018**). Small-scale indirect plant responses to insect herbivory could have major impacts on canopy photosynthesis and isoprene emission. *New Phytologist*, *220*, 799–810. http://doi.org/10.1111/nph.15338

Nadzir, M. S. M., Ashfold, M. J., Khan, M. F., Robinson, A. D., Bolas, C., Latif, M. T., Wallis, B. M., Mead, M. I., Hamid, H. H. A., Harris, N. R. P. Ramly, Z. T. A., Lai, G. T. Liew, J. N., Ahamad, F., Uning, R., Samah, A. A., Maulud, K. N., Suparta, W., Zainudin, S. K., Wahab, M. I. A., Sahani, M., Müller, M., Yeok, F. S., Rahman, N. A., Mujahid, A., Morris, K. I., Sasso, N. D. (**2018**). Spatial-temporal variations in surface ozone over Ushuaia and the Antarctic region: observations from in situ measurements, satellite data, and global models. *Environmental Science and Pollution Research*, *25*, 2194–2210. http://doi.org/10.1007/s11356-017-0521-1

Unpublished:

Bolas, C., Ferracci, V., Robinson, A. D., Mead, M. I., Nadzir, M. S. M., Pyle J. A., Jones, R. L. and Harris, N. R. P. iDirac: a field-portable instrument for long-term autonomous measurements of isoprene and selected VOCs. *Under Review*.

Nadzir, M. S. M., Harris, N. R., Bolas, C., Bran, S. H., Macatangay, R., Ooi, C. G., Yusup, Y., Latif, M. T., Khan, M. F., Harun, M. H., Cheah, W., Ahamad, F., Kho, L. K., Razak, A. A., Jantan, N. M., Mohammad, M., Sentian, J., Yatim, A. N. M., Mohyeddin, N., Mead, M. I., Samah, A. A., Hamid, H. H A., Maulud, K. N., Wahab, M. I. A., Hazmi, I. R., Yaakob, S., Sahani, M., Salimun, E., Jalil, N. A. A., Jansar, K. M., Zain, C. R. C. M., Awang, N., Sabuti, A. A., Alhasa, K. M., Yusoff, A. H., Ariff, N. M., Bakar, M. A. A. Driving factors for isoprene chemistry over an oil palm plantation in Malaysia. *In Preparation*.

Out-Larbi, F., Bolas, C., Ferracci, V., Jones, R. L., Harris, N. R. P., Ashworth, K. Modelling the effect of the 2018 summer heatwave and drought on isoprene emissions in a UK woodland. *In Preparation*.

LIST OF APPENDICES

1 Isoprene and Forests: An Introduction

1.1 This thesis

This thesis will describe the development and deployment of a new instrument capable of atmospheric measurements of isoprene, which is called the iDirac. The focus of the thesis will be on measurements of isoprene using the iDirac. The three prongs of atmospheric chemistry are touched on: laboratory studies, field experiments and numerical modelling.

The three branches of atmospheric chemistry are equally important in understanding the atmosphere surrounding our planet. Only using laboratory studies can we parameterise the factors used in numerical models to describe atmospheric processes. Only using models can we hope to investigate the endlessly complicated structure and dynamics of our geographically expansive atmosphere. And only with practical field studies can we demonstrate the processes uncovered in lab studies and verify our models. Field studies themselves also unveil questions and further misunderstandings of our atmospheric system.

The development of the iDirac, a novel gas chromatograph has allowed measurements to be taken of isoprene, an important trace gas in the troposphere and take high time resolution measurements with a flexibility that has not been possible before. In the following thesis, the deployment of the iDirac is described in two different forest

environments to measure isoprene and further understand how forests emit this important atmospheric constituent.

The distribution of isoprene in a forest and its distribution is inherently important in understanding how it may affect the local and global chemical balance of the atmosphere. Here, experiments are described that reveal insight into forest isoprene and how it is distributed vertically through a canopy. It is hence possible to model these processes and this provides a tool for asking questions about under-sampled forest environments.

1.2 Aims of this chapter

This chapter aims to provide insight into the background of isoprene research. In such a broad multi-disciplinary area, there is a wealth of information and literature available on previous studies and the current state of understanding. The aims of this chapter are to:

1. Explain what isoprene is and where is comes from.
2. Describe how it reacts in the atmosphere and why this is important.
3. Investigate how the forest is structured and what studies have previously been conducted.
4. Evaluate the current methods for measuring isoprene.
5. Highlight unanswered questions.

1.3 The Earth's atmosphere

1.3.1 Structure

Most of the atmosphere is concentrated in the lower 50 km, and above this, mass gets very scarce. There is an exponential drop of pressure as you rise through the atmosphere, as atmospheric pressure is due to the mass of the air above.

The nature of the atmosphere changes as you go higher, with distinct layers as described in Figure 1. The lowest layer, with which this thesis is concerned is the troposphere, which contains most of the mass of the atmosphere, is where the life on Earth lives and where the vast majority of the emissions occur. Above the troposphere is the stratosphere, which is characterised by its stable structure and a temperature that increases with height. Above the stratosphere, the atmosphere thins further to form the mesosphere and beyond this the thermosphere extends into space. Each transition is characterised by a temperature inversion and the boundaries are called the tropopause, stratopause and mesopause respectively.

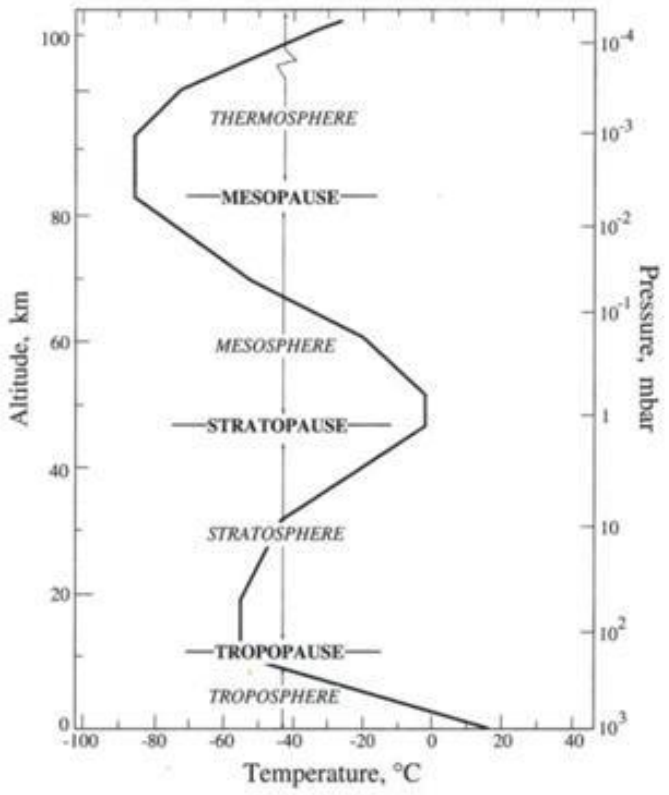

Figure 1 Diagrammatic representation of the atmosphere temperature and pressure profile, showing layers and boundaries (Seinfeld & Pandis, 2006)

1.3.2 Composition

The atmosphere is composed primarily of nitrogen, oxygen and argon, with dry volume fractions of 78.08 %, 20.95 % and 0.95 % respectively. The atmosphere can be considered to extend up to 500 km, a thin envelope around the planet, and is extremely important for life on Earth, despite its size relative to the Earth itself. There are a range of physical and chemical process that govern the composition and dynamics of the atmosphere. In addition to the main constituents of air, the atmosphere contains a rich cocktail of trace gases. These drive a complex sequence of reactions and can affect life on Earth either directly as pollutants, or indirectly by shifting the climate (Seinfeld & Pandis, 2006).

1.3.3 Characteristics of the troposphere

The troposphere is the location of this study and where isoprene is emitted. It extends to the boundary with the stratosphere at the tropopause, which may be located from 9 km at the polar regions to 17 km at equatorial regions, but also varies with time of year (Seinfeld & Pandis, 2006).

The troposphere is characterised by heavy influence from the surface of the Earth, where

there is a rapid exchange of heat and momentum. Heating of the surface and the movement of air parcels drives extensive mixing of the air and emitted gases.

The troposphere can be further divided into two layers, the planetary boundary layer (PBL) and the free troposphere. The free troposphere is defined by having less influence from the turbulence of the surface and being generally more stable. Further structure can be found in the PBL with urban canopy layers or roughness sub layers. However stratification is possible in the PBL and the actual dynamics depend on many factors (Deardorff, 1972).

The PBL changes in form with time of day, following a diurnal pattern of increasing in height during the day and lowering during the night or during cool spells as a result of atmospheric stability from radiative transfer. Over the ocean the marine boundary layer (MBL) is significantly shallower than its counterpart on land during the day, but higher at night. This is due to the rapid radiative loss of heat from the land compared to the ocean. Due to increased surface roughness of urban areas, the PBL over rural areas is typically shallower than that over urban areas. The height of the PBL can affect the concentration of pollutants, acting as a 'lid' of the atmosphere and restricting vertical transport. Figure 2 shows a diagrammatic representation of the PBL over different environments, with different scale processes highlighted (Seinfeld & Pandis, 2006).

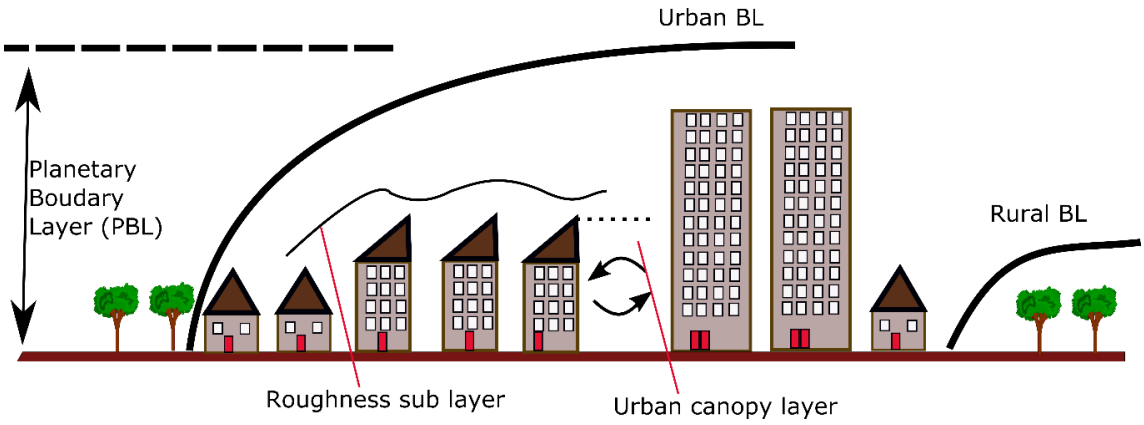

Figure 2 Diagram of the features of the PBL in urban and rural environments (adapted from Oke, 2015) (Not to scale)

As the majority of pollutant and trace gas emissions are at the surface, when considering their dispersion and concentration it is important to think about the structure of the immediate atmosphere.

Much of the activity of the PBL and its nature around the globe is driven by insolation and convection as a result of surface heating. Instability arising from a temperature gradient causes air parcels to rise and disperse. The surface albedo and cloud cover can strongly affect these processes. Other, larger scale processes in the PBL are driven by advection over rough surfaces with physical items causing drag on air movement and hence turbulence or the convergence or divergence of horizontal flows (Seinfeld & Pandis, 2006).

An important concept in the PBL is that of oxidising capacity, that the capability of the atmosphere to remove pollutants by oxidations. The main oxidants in the PBL are the hydroxyl radical (OH, daytime primarily), ozone (O_3) and the nitrate radical (NO_3, night-time primarily). These species react typically with volatile organic compounds (VOC) in the atmosphere and hence reduce the VOC loading of the PBL (Seinfeld & Pandis, 2006). This is a key concept in isoprene chemistry and is discussed further in Section 1.5.

The scope of this thesis examines local emissions of isoprene; hence, global movements of air or synoptic scale movements are not considered in depth here. There are a range of forces that govern movements of air around the Earth, forming circulation cells and surface movement of air masses over vast areas, however due to the localised emissions of isoprene and its short lifetime these forces do not become relevant for this study.

1.4 Isoprene

Emissions of carbon from living plants into the atmosphere can take many forms. Aside from carbon dioxide from respiration, plants emit a wide range of biogenic volatile organic compounds (BVOC) which make up a significant proportion of the total VOC emitted into the atmosphere. Of these emissions, the greatest is that of isoprene (2-methyl-1,3-butadiene, C_5H_8) which is a short chain unsaturated hydrocarbon. Global emissions of isoprene are comparable to that of methane (Sharkey & Yeh, 2001) but as its lifetime is short, atmospheric concentrations fluctuate widly. Anthropogenic sources of VOC come from industry and consist of a wide array of different trace compounds. Other BVOCs include the monoterpenes and sesquiterpenes which are derivatives of isoprenoid compounds and are emitted also from vegetation (Noe, Peñuelas, & Niinemets, 2008). A wide range of VOCs are also produced from decaying matter and microbial activity (Bäck et al., 2010; Kuzma et al., 1995).

1.4.1 How and why is isoprene emitted from plants

Isoprene emission from plants is a widely studied phenomenon and the possible reason for its emission has attracted wide attention. It has been found that only certain species of plants emit isoprene, that some emit none, and that even very similar or closely related species can have completely different emission profiles.

1.4.1.1 Pathway for isoprene production in plant cells

The physiological route for isoprene emission typically follows a complex metabolic pathway, utilising the carbon dioxide (CO_2) absorbed in photosynthesis. Isoprene can take up to 2% of photosynthetically fixed carbon (Sharkey & Loreto, 1993) at 30^{o}C, representing a relatively large proportion of the productivity of photosynthesis for production of a by-product. Typically isoprene is produced in the chloroplasts of cells, as a branch of the methylerythritol 4-phosphate (MEP) pathway which is key in producing isoprenoid compounds for functions such as protein anchoring or protein prenylation among others. At the end stage of the MEP pathway, dimethylallyl pyrophosphate (DMAPP), shown in Figure 3 (RCSB, 2015), is formed. The isomer isopentyl pyrophosphate (IMP) is also formed and can react to form isoprene. Several early schemes were postulated for possible reactions to produce isoprene, including non-enzymatic pathways involving acid catalysis of dimethylallyl diphosphate (DMADP) with proton abstraction (Sanadze, 1990). Recent studies have revealed that the enzyme isoprene synthase is responsible for the enzymatic reaction of DMAPP to form both isoprene and pyrophosphate (Silver & Fall, 1991). Further studies have found the gene responsible for the expression of isoprene synthase (Miller, Oschinski, & Zimmer, 2001). Further investigations have been conducted into isoprene synthase as a route for commercial isoprene production (Chaves et al., 2017) and as an indicator of isoprene emission rate from plants (Josef et al., 2002) for further research in emission potentials.

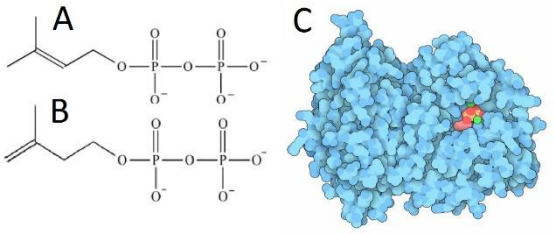

Figure 3 A) DMAPP structure B) IMP structure C) Enzyme image of isoprene synthase

1.4.1.2 Why do plants emit isoprene?

The relatively high energy expenditure in producing isoprene begs the question: why does the plant bother to produce it? Why has it not been eliminated by evolution as an expensive and useless phenomenon? Several reasons have been postulated for its emission, with many studies and discussions centred on this question.

The prevalent theory is that isoprene is emitted as a response to thermal stress (Sharkey, 2013; Sharkey & Singsaas, 1995; Sharkey et al., 2008). Isoprene emisison occurs in plants all round the Earth, but as only one method of relieving thermal stress relative to a plants normal conditions, it is not typically found in any one environment. Many biomolecular studies have been performed that have demonstrated that plants that either don't emit isoprene naturally or that have had that function artificially blocked do not fare well under heat stress. The discovery of the MEP pathway allowed certain steps to be blocked by inhibitor fosmidomycin. Using this inhibitor, studies have been able to show that plants with isoprene production artificially shut-off cannot deal with heat stress as those that still emit isoprene (Velikova & Loreto, 2005). Even when inhibited, it has been shown that the exogenous isoprene can return some degree of thermotolerance (Sharkey, 2001). It has been suggested that isoprene could dissolve in cell membranes, offering a basic thermal protection by stabilising the membrane structure (Siwko et al., 2007; Velikova et al., 2011). These studies have demonstrated that isoprene indeed partitions into the lipid phase and reduces the chance of the membrane undergoing any phase change associated with heat spikes.

Another proposed reason for isoprene production is the protection from damage from O_3 and other reactive oxygen species (ROS). Evidence has shown that isoprene emission can indeed limit visible damage from O_3 exposure (Loreto et al, 2001) and can limit the decrease in photosynthesis activity as a result of oxidative stress (Peñuelas et al, 2005). However, it has also been found that elevated O_3 serves to stifle isoprene synthase production by plants (Fares et al., 2006), thus suggesting that while isoprene does protect a plant from oxidative stress, this is likely a side effect from thermal protection.

Other proposed reasons for isoprene emission include use as a metabolite 'safety valve' or as a signalling factor or insect repellent. Several studies have investigated the idea that isoprene emission is a mechanism to get rid of unwanted or excess metabolites (Rosenstiel et al, 2004). This method however fails to explain either why isoprene emission varies through a forest canopy or why some plants do not possess this ability. Isoprene has been suggested as an insect repellent in a number of cases (Laothawornkitkul et al., 2008;

Laothawornkitku et al., 2008) and also as a signalling compound for the attraction of predatory insects that prevent herbivory (Loivamaki et al, 2008).

1.4.2 Global emission of isoprene

Globally speaking, the emission of isoprene is 500 – 750 Tg annually (Guenther et al., 2006). This equates to around the same quantity of methane emitted globally. Isoprene makes up a third of total emitted VOC, methane makes up a third and the final third is a combination of hundreds of diverse compounds including the monoterpenes, alcohols and alkenes.

As well as being emitted from trees, around the world isoprene is also emitted from phytoplankton in the ocean, which are suggested to do so also as a heat response mechanism, and croplands (Moore, Oram, & Penkett, 1994). Animals even emit small quantities of isoprene (Gelmont, Mead, & Stein, 1981). However the largest emission of isoprene is from the tropics which are suggested to contribute 70% of the total global emission (Michael Keller & Lerdau, 1999). This is due to higher average temperatures and a near-constant growing season combined with higher abundance of forest cover and a higher prevalence of species with isoprene emission potential (Taraborrelli et al., 2012) as well as a general larger coverage around the equator.

Most estimates of global isoprene have come from the Model of Emissions of Gases and Aerosols from Nature (MEGAN) (Guenther et al., 2006). This model provides emission data from emission factor databases and a range of observations from ground measurements and satellites to define variables. Key variables for isoprene are temperature, solar radiation, plant functional type and leaf area index. The model can output both regional and global isoprene emission at a scale of 1 km. An updated version, MEGAN2.1 was put forward in 2012 (Guenther et al., 2012) and includes updated surface land-use models and additional compounds.

1.5 Isoprene chemistry

The chemistry of isoprene in the atmosphere is extremely varied and complex, with a host of compounds produced from a multitude of different reaction pathways. The primary reaction is that with OH during the daytime, the NO_3 radical during the night and to a lesser extent ozonolysis. Oxidation with OH starts a cascade of reactions that can produce many compounds with implications for human health either directly or indirectly and the compounds produced can also have a big effect on the climate and the Earth's radiation balance (Wennberg et al., 2018).

1.5.1 Oxidation of isoprene

The reactions of isoprene with the three main oxidants can have large effects on the chemistry of the troposphere. The three main oxidants are primarily OH in the daytime, O_3 and at night, primarily the NO_3 radical. The oxidising capacity of the atmosphere is strongly affected by the oxidation of isoprene as this alters the concentration of OH. Hence the ability in the troposphere to remove anthropogenic pollutants is reduced as these pollutants are in competition with isoprene for reaction with OH. Where VOC is in high abundance this reacts with OH to form organic peroxy radicals which in turn react with NO to form NO_2, which is a secondary pollutant. This can further photodegrade with sunlight of a specific wavelength that can penetrate to the surface to form an oxygen radical which can react with O_2 rapidly to form O_3 (Kleinman et al., 2003). This is represented below by *Reactions 1, 2* and *3* where the species RH can represent any VOC (Seinfeld & Pandis, 2006). This process is more important in polluted atmospheres where there is an abundance of NO produced from internal combustion engines. In unpolluted primary forests or remote environments, this process is not as relevant, though with extensive land-use change and urbanisation that may change (Latif et al., 2016). In areas with low concentrations of NO_x, reaction with isoprene can actually reduce levels of O_3 in the air by ozonolysis. Reaction with O_3 is a relatively slow process and the lifetime of isoprene with respect to O_3 is 1.3 days (at 30 ppb O_3), compared to reaction with OH which is 1.7 hours (at 0.06 ppt OH) (Seinfeld & Pandis, 2006). However there are emissions of NO_x from bacteria in soils that contribute to this process and may lead to a natural production of O_3 (Hall, Matson, & Roth, 1996). Emissions transported from nearby cities may also contribute to higher levels of NO_x.

$$RH + OH + O_2 \rightarrow RO_2 + H_2O \qquad \textit{Reaction 1}$$

$$RO_2 + NO \rightarrow RO + NO_2 \qquad \textit{Reaction 2}$$

$$NO_2 + O_2 + hv \rightarrow O_3 + NO \qquad \textit{Reaction 3}$$

The presence of O_3 at the surface has negative health implications for humans and the general biosphere, with effects on plant productivity. During Northern Hemisphere summer elevated levels of O_3 have been associated with increased hospitalisations, pulmonary heart disease and assorted respiratory problems among the human population during a study in the US (Knowlton et al., 2004; Koken et al., 2003).

The World Health Organisation (WHO) has determined an O_3 concentration lower threshold of 100 μgm^{-3} (50.9 ppb), above which negative health effects may occur. An upper threshold is set at 240 μgm^{-3} (122.3 ppb), above which acute negative health effects or even death of vulnerable individuals may occur (World Health Organisation, 2005). Damage can also occur to crop species and persistent O_3 levels above 40 ppb have been shown to result in significant damage to various crop species (Mauzerall & Wang, 2001). Future scenarios have been investigated using global models with elevated atmospheric concentrations of NMVOCs and have found increases by 20 – 30 ppb from current day baseline O_3 (~35 ppb) (Sanderson et al., 2003).

1.5.2 Oxidation products of isoprene degradation

Despite high emission, isoprene is only present in the troposphere at a low concentration because the doubly unsaturated molecule is very reactive and reacts rapidly in the air. The main oxidant present in the daytime is OH, which rapidly initiates a sequence of reactions to produce a host of possible products; see Figure 4 (Archibald et al., 2010). It can be seen that the OH radical can attack either of the double bonds, leading to a chain of possible pathways that lead to a host of products. Another important pathway not shown in Figure 4 is the proposed formation of 2-methyltetrols which have been shown to play a key part in the formation of secondary organic aerosols (SOA) (Claeys, 2004). O_3 is an important oxidant in the daytime, also with a plethora of possible oxidation products. In the absence of light, an important oxidant is $NO_3\cdot$ which rapidly oxidises isoprene after the sun has set. (Gebhardt et al., 2008). Of course, the primary products of isoprene oxidation can also react themselves, leading to further complexity.

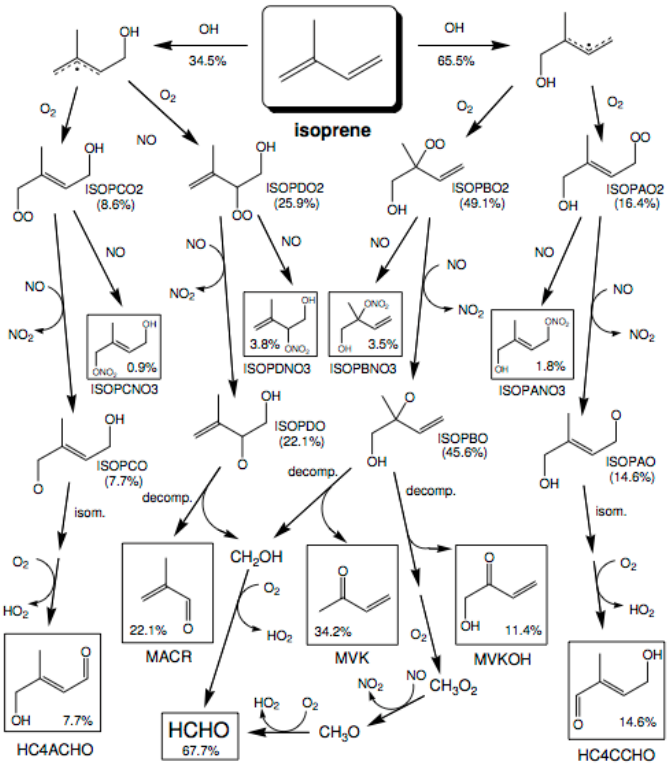

Figure 4 Isoprene oxidation reaction scheme and breakdown products (Archibald et al., 2010)

It is clear that isoprene plays an important part in the composition of the atmosphere, with several of the oxidation products persisting for a longer timeframe than isoprene itself. Hence, to act as an indicator of strong isoprene emission, several oxidation products such as methyl vinyl ketone (MVK), methacrolein (MACR) and formaldehyde (HCHO) can be detected (Jardine et al., 2013).

Some degradation products have other implications for environmental conditions such as the pH of rain water, for example the organic acids formic acid and pyruvic acid found in raindrops over the Amazon Basin (Jacob & Wofsy, 1988). Eventually, the final product of atmospheric oxidation are CO and CO_2 and these have been detected at levels 10-30 ppb higher than the free tropospheric concentrations over areas of high biogenic emission, even without the influence of anthropogenic activities e.g. biomass burning (Jacob & Wofsy, 1988).

1.5.3 Formation of secondary organic aerosol from isoprene

An important component of the atmosphere in heavily forested regions is SOA (Carlton, Wiedinmyer, & Kroll, 2009; Darer et al, 2011) and there is now evidence that isoprene oxidation products can form SOA. In forest environments, SOA has been shown to contain different 2-methyl tetrols as in Figure 5 (Edney et al., 2005). These are produced in various oxidation reactions of isoprene. These tetrol molecules, being highly polar, can condense onto pre-existing particles or accrue with other molecules to create new particles and hence contribute to particulate organic matter. An effect of these SOAs is that they can contribute to radiative forcing (Padhy & Varshney, 2005). SOA has a strong impact on radiation as it interacts with incoming and outgoing solar radiation, either absorbing this energy or scattering it. SOA can also act as cloud condensation nuclei and this can influence the albedo of the atmosphere to a great extent, both by reflecting radiation and by back scattering radiation to Earth. These effects are not fully understood and have been the focus of several studies (Andreae, 1997; Claeys, 2004; Ehn et al., 2014).

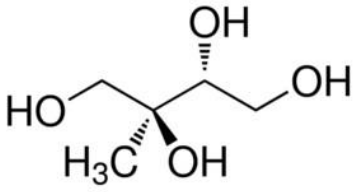

Figure 5 Structure of 2-methyl tetrol

It has recently been suggested that the competition of isoprene with terpenes actually results in an overall decrease in SOA (McFiggans et al., 2019). The suggested mechanism is that isoprene ‘scavenges’ OH and that isoprene peroxy radicals actually scavenge the oxygenated monoterpenes. Currently this is not incorporated in global models, but evidence suggests that this feedback could have a large effect on global SOA concentrations.

1.6 Related compounds: terpenes

In addition to isoprene, there are myriad other VOCs emitted naturally from vegetation. One class of atmospherically relevant compounds are terpenes. Terpenes have many structures but many can be classed as either monoterpenes or sesquiterpenes.

The structure of monoterpenes is closely related to isoprene and generally follow the formula $C_{10}H_{16}$ and can either be cyclic or acyclic. The structure of six common monoterpenes are shown in Figure 6. Monoterpenes have characteristic smells and are used in cosmetics and therapeutics (Breitmaier, 2006). Sesquiterpenes have the general formula $C_{15}H_{24}$ and are less abundant in the atmosphere. Some common sesquiterpenes are shown in Figure 6.

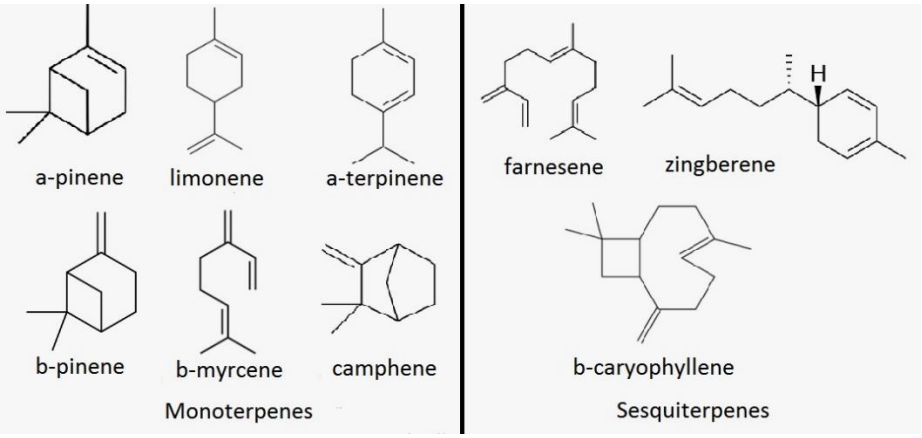

Figure 6 Example structures of monoterpenes and sesquiterpenes

The method of emission of monoterpenes and sesquiterpenes follow similar metabolic pathways as isoprene as described in Section 1.4.1.1 but the terpenes are stored in 'pools' in the plant tissue and emitted gradually, so are more dependent on temperature than light (Kuhn et al., 2007; Staudt et al, 2000). It has been suggested that the primary emission route is due to the volatility of the compounds and is not a direct product of photosynthesis (Seinfeld & Pandis, 2006).

Much of the chemistry of the terpenes is similar to that of isoprene as described in Section 1.5. It has been found in multiple cases that the monoterpenes act as better nuclei for SOA (Lee et al., 2006; Ng et al., 2007).

Different trees have different emission profiles and many trees emit monoterpenes and not isoprene, for example the European Beech (*Fagus sylvatica)* (Moukhtar et al., 2005). Many field campaigns have taken measurements of monoterpenes alongside isoprene (Kuhn et al., 2007; Lamb, Westberg, & Quarles, 1985; Llusia et al, 2014). Atmospheric concentrations are typically found to be lower than isoprene, but they also do not have distinct a diurnal profile as isoprene (Jones, Hopkins, & Lewis, 2011; Langford et al., 2010).

1.7 Forests

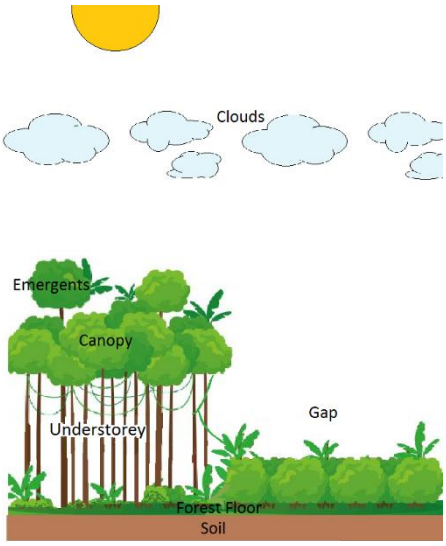

Figure 7 Typical features of a generic forest

Forests are inherently complex environments, and gas emissions in particular have myriad potential sources, sinks and transport processes to be considered (Lowman & Schowalter, 2012). Forest structure can vary widely between different forests and can affect biodiversity greatly (Herbst et al., 2008; Ishii et al., 2004). It is also important in determining the isoprene concentration gradient. The general structure for a forest has various layers (see Figure 7). The forest floor is normally a shaded place with some plant species such as mosses, grasses and ferns in temperate forests and grasses and monocot palms in tropical forests, but has relatively sparse foliage as the upper canopy absorbs most of the light (Herbst et al., 2008; Lieberman et al., 2006). The forest floor atmosphere also feels the greatest effect from the soil, which influences atmospheric chemistry with trace gas emissions (Keller et al., 1983). Temperatures on the forest floor are relatively stable. The understory is the layer between the floor and the canopy, where the biomass is predominantly trunks of larger trees and which is still shaded with a relatively stable temperature (Lowman & Schowalter, 2012). Foliage in the understory is varied, with small trees and shrubs but also mosses and lichens in temperate forests and lianas and creepers in tropical forests (Lieberman et al., 2006). The canopy is the upper area where the majority of the leaves and foliage are, with a temperature that is much more variable and typically with is a lot more exposure to sunlight with shade casting leaves orientated to maximise sun exposure (Givnish, 1988; Lowman & Schowalter, 2012). In a typical forest, isoprene emission would be strongest from the top of the canopy as it has been shown to be dependent on temperature and light. An additional layer is the emergent layer, where particularly large trees have grown higher than the main canopy, where the air is most turbulent and temperature can be highly variable (Lowman & Schowalter, 2012).

In many forests, and particularly in human modified secondary forests, this structure is not as well defined. Where the trees have been felled, there are large areas devoid of larger trees, known as ‘forest gaps’, which have allowed for the rapid colonisation by pioneer species and opportunistic understory species such as grasses, palms, vines or shrubs. In

these gaps there is stronger insolation and so the temperature can get higher but can vary widely as the air is much more turbulent (Lowman & Schowalter, 2012). The foliage can be dense and varied, and hence often isoprene concentration can be higher at ground level, particularly where there are specific strong isoprene emitting species (Fowler et al., 2009).

1.7.1 Isoprene studies in tropical forests

Tropical forests have been the subject of several studies seeking to determine their influence on both local and global atmospheric composition and climate. Alongside grasslands and savannas, they make up a large part of land cover between the tropics of Capricorn and Cancer and have a very large influence on the global carbon cycle and climate. With year-round high temperatures and strong insolation, they are areas of high VOC emission, of which emissions of isoprene make up a large fraction of that (Keller & Lerdau, 1999).

The majority of measurements of tropical forest BVOC have taken place in South America, with several in Africa. A study in Amazonia conducted in 2013 examined the seasonality of isoprene reactivity with OH and found the highest concentration during the wet season, with ~3 times that of the dry season as a result of reduced reactivity with OH. In addition to isoprene a host of other BVOC species were measured and also found to vary similarly to isoprene, with lowest concentrations for all compounds seen at night (Yáñez-Serrano et al., 2015), which is in line with photosynthesis activity. Another large scale experiment that added to understanding of tropical forest atmosphere interactions were the European Studies on Trace Gases and Atmospheric Chemistry as a contribution to the Large-Scale Biosphere-Atmosphere Experiment in Amazonia (LBA-EUSTACH), conducted in 1999. These studies closely examine biogeochemical cycling of carbon, water, energy, trace gases and aerosols in the Amazon and conducted many experiments of fluxes from the forest and made several discoveries on the fate of soil-derived NO_x and the seasonality of aerosols and cloud condensation nuclei (Andreae et al., 2002). The African Monsoon Multidisciplinary Analysis (AMMA) campaign examined the effects of the West African monsoon on VOC emissions and aerosol loading from topical forests in the region. Strong spatial assossiations of isoprene with vegetation were found and there was evidence of deep convection redistributing isoprene from the surface (Ferreira et al., 2010; Marais et al., 2014; Murphy, Oram, & Reeves, 2010).

There have been fewer campaigns in SE Asia to measure forest atmosphere fluxes and ambient concentrations. One crucial difference between SE Asia and those forests in

Amazonia and Africa is the influence of a tropical sea, as well as the differing tree species that form the majority in Borneo. Of these, a recent and extensive campaign was the OP3 campaign in 2008 (Hewitt et al., 2010). Many varied experiments were conducted, including investigations into emissions of primary biological aerosol and BVOC from both primary forests and oil palm plantations. Trace gas concentrations were measured of monoterpenes and other trace gases (Gabey et al., 2010; Jones et al., 2011; Pyle et al., 2011). The BVOC measurements were made with a gas chromatograph with flame ionization detection (GC- FID) and were done at the Bukit Atur Global Atmospheric Watch (GAW) station in the Danum Valley Conservation Area in Sabah, Borneo. As with other isoprene measurements in forests, they were made in a clearing beside a flux tower. Isoprene flux measurements were made in the field during the campaign by virtual disjunct eddy covariance (Fowler et al., 2011; Langford et al., 2010). The isoprene mixing ratios showed a clear diurnal pattern, with a peak as expected at midday when light intensity and temperature are greatest; this pattern was observable for other VOCs measured, though not with the same range as isoprene. Mixing ratios measured were on the order of 1 ppb isoprene, rising to maxima of ~5 ppb and dropping as low as 1 ppt at night time as shown in Figure 8 (Jones et al., 2011). A correlation with temperature and light was observed, but the relationship with temperature was found to be much stronger. A detailed analysis of the difference between monoterpenes and isoprene was completed, finding that a large proportion of the carbon budget to the atmosphere as VOC (~14%) was attributed to the monoterpenes and that the monoterpenes had a large contribution to the destruction of OH (27%) despite a lower concentration (Jones et al., 2011).

A large part of OP3 was dedicated to measuring HO_x radicals to address the discrepancy between measurement and model studies, where the measured level of OH is severely underestimated (Edwards et al., 2013; Hewitt et al., 2009). This discrepancy is thought to be closely linked to the oxidation mechanism of BVOC, particularly isoprene, which exposes a gap in the understanding of the chemistry (Taraborrelli et al., 2012).

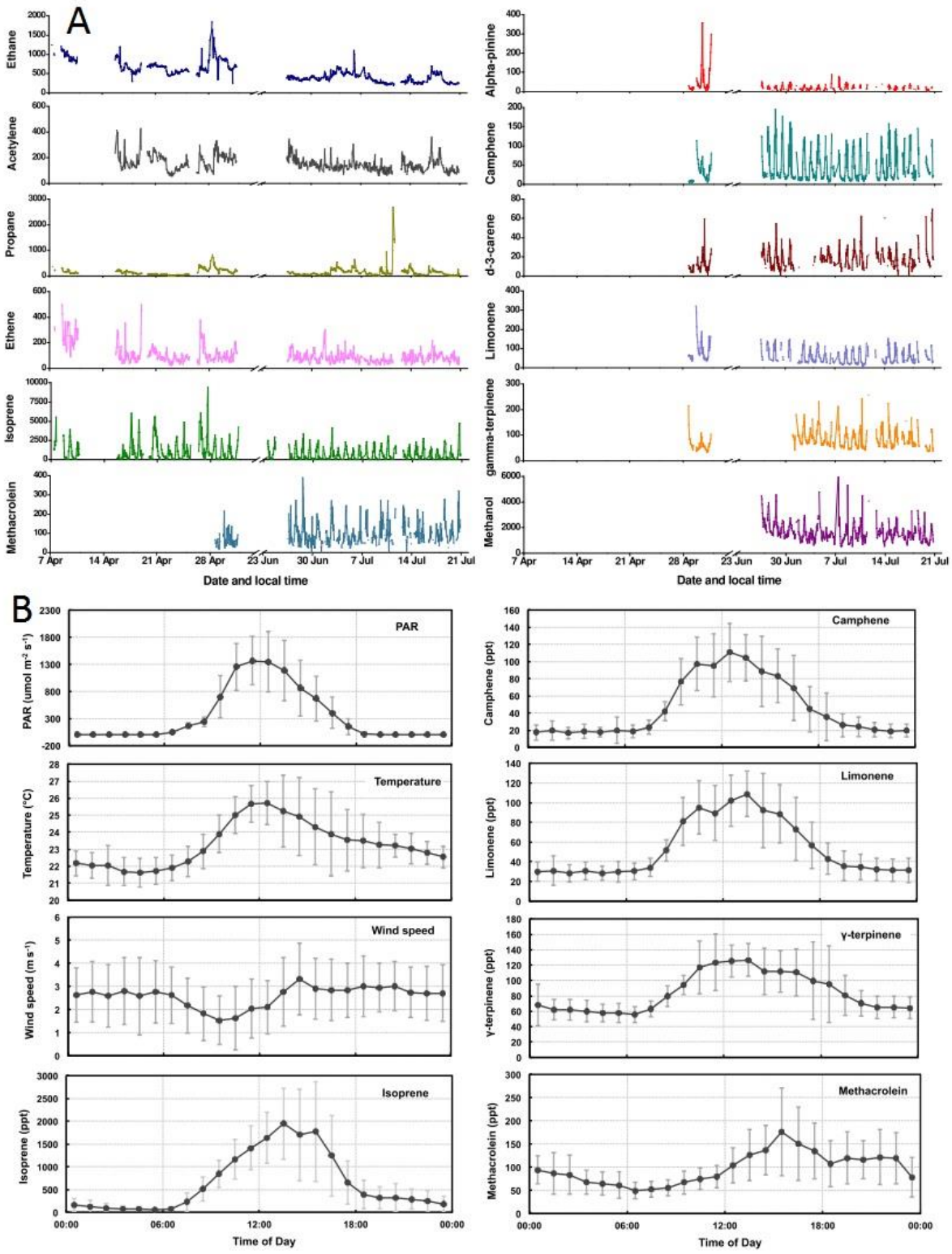

Figure 8 A) VOC measurements taken from OP3, showing time series for each species with mixing ratio of ppt. Isoprene is shown in green B) Daily average plots of several species and meteorological parameters (Jones et al., 2011)

1.7.2 Isoprene studies in temperate forests

Temperate forests can either consist of coniferous or deciduous trees. Of the deciduous trees, several common genera of trees such as *Populus* (aspen) and *Quercus* (oak) contribute huge quantities to global isoprene emission. It should be noted however that not every species of *Populus* or *Quercus* are strong isoprene emitters. Studies have shown that for European isoprene emissions, 70% is due to three oak species (Keenan et al, 2009). Seasonality is a feature that defines temperate forests, with warmer summers and colder winters. This seasonality drives a changing emission profile through the year. There have been many studies examining daily isoprene profiles and tree emission potentials from temperate forests.

To investigate emission potentials, highlighted as a large uncertainty in global isoprene models, several studies have been undertaken around Europe measuring isoprene fluxes from the canopy by eddy covariance (Langford et al., 2017). These studies investigated five study sites across Europe with a diverse array of different species of mixed deciduous trees. The studies derived new emission potentials that have been used to refine the MEGAN model and improve the representation of Europe.

A multitude of field studies in the US have shed light on various aspects of isoprene emission. Studies in Tennessee, US have investigated how isoprene is transported through the canopy and its fate in the atmosphere (Baldocchi et al, 1995). This has shown that isoprene is dependent on leaf age as well as temperature and light and has a significant effect on the local chemistry, affecting to remove both oxidising and acidifying compounds. The Ozarks Isoprene Experiment (OZIE) was a large campaign to investigate the high emission of isoprene from the Ozarks region of Missouri, US (Wiedinmyer et al., 2005). Isoprene and a number of other VOCs were measured and the oak forest area was found to be an extremely strong source of isoprene for the US, earning the nickname the ‘isoprene volcano’. The species in the forest were predominantly *Q. stellata* and *Q. marilandica* which were both measured to be strong emitters. Results from these measurements were used to compare and verify model output from both the MEGAN (Guenther et al., 1993) and the Biogenic Emissions Inventory System (BEIS) (Lamb et al., 1993; Pierce et al., 2004) land-atmosphere emissions models.

It has been found that regional isoprene emission varies widely in temperate forests due to the nature of the tree species distribution and several studies have tried to address this issue with field campaigns calculating regional emission potentials. One study in the south-eastern US postulates that one reason that many models over-represent isoprene is

that some isoprene emitting trees are forming a sub-canopy and are shaded by non-emitting trees, reducing their emission (Yu et al., 2017).

In a northern China temperate mixed forest a study in 2011 also showed typical profiles for isoprene emission and diurnal profiles and showed that isoprene is much more sensitive to temperature and light than monoterpenes (Harley et al., 2011; Li et al., 2006).

A number of canopy models have been proposed to capture the observations from temperate forests. A model used by Lamb et al. (1993) tested new emission inventories for the United States and reported large uncertainties in the model output as a result of limited geographical input and basic assumptions for light and temperature dependence. This model is known as the Biogenic Emissions Inventory System (BEIS) model and became a standard model for estimating land cover BVOC emissions. Another updated model by Lamb et al. (1996) investigated physiological features of the canopy and new ways of representing the light and temperature dependence. This new model demonstrated that incorporating a canopy in land emission models changed the emission by up to a factor of two. This indicates that the canopy structure is important for considering emission into the free atmosphere. Neither of these models calculate the vertical profile, looking instead just at how the canopy affects isoprene emission from the land surface. The vertical profile is calculated in a model by Gao, Wesely, and Doskey, (1993), which incorporates a chemistry scheme that calculates the concentration of isoprene at different heights in the canopy. This study found that the isoprene is strongly dependant on mixing and is actually higher in the lower canopy due to lower chemical reactions and reduced mixing.

The FORCAsT model (Ashworth et al., 2015) provides a comprehensive calculation of different species at different heights. This model incorporates the Guenther (Guenther et al., 2006) emission terms, a complex chemical scheme and terms for turbulent mixing and transport in and above the canopy. The FORCAsT model is discussed in this thesis as a comparison to measurements and a new model.

1.8 Effects of drought on tree isoprene emission

The effect a drought has on a forest can be great, not least because of its effect on physiology and photosynthesis, but also on isoprene emission. Drought can drastically change the emission pattern of the forest and alter the atmospheric processes occurring in that area. Recent research has focussed on the impact that drought may have on isoprene emission.

A laboratory based study in 2004 (Pegoraro et al., 2004) looked at the effect of drought as a drying-rewatering cycle and found isoprene emission to be less sensitive to drought than photosynthesis and stomatal conductance. Only after 12 days of severe drought did the emission rate drop by 64% where photosynthesis and stomatal conductance had both dropped by 92%. Further, isoprene emission recovered faster in the 'recovery' phase. Drought experiments were conducted in 2007 on *Populus alba* saplings (Brilli et al., 2007) which looked closely at isoprene synthase activity and the amount of ^{13}C incorporated into the isoprene, which would indicate how much CO_2 is being used directly from photosynthesis. The study found that under drought ^{13}C incorporation was lower and it found that isoprene production is not supressed until extreme drought conditions were reached. It also found that after the drought passed, isoprene emission was elevated.

In 2015 a study on a real world drought in a forest of the Ozark region of the central US was undertaken (Seco et al., 2015). This dataset confirmed that the isoprene emission is not suppressed to a great extent during a 'natural' drought. It found a decoupling of isoprene and CO_2 fluxes which supports the idea of alternative substrates being used for isoprene synthesis when photosynthesis is drastically reduced (Funk, Mak, & Lerdau, 2004). A study on the same forest from a drought in 2012 highlighted the forest responded to severe drought with a decline in isoprene but that a mild drought in 2011 did not result in the same response (Zheng et al., 2017). This study also assessed the effectiveness of using formaldehyde, a prominent and stable isoprene breakdown product, to detect isoprene emissions via satellite sensing as a proxy for isoprene emission. However, the formaldehyde showed a muted signal and did not accurately predict the isoprene emission rate, possible due to a chemical feedback from atmospheric oxidation.

Another chamber study in 2017 (Bamberger et al., 2017) noted that the combination of heat and drought can bring an eight-fold increase in isoprene emission, representing a carbon loss of 20% of assimilated carbon from photosynthesis. When only heat is applied, without water depletion, these values increase six-fold in isoprene and carbon loss decreases to 12%. This study suggests that this extra drought effect should be factored into existing BVOC models. Model studies in 2018 propose new approaches in how the physiological effects of drought can be incorporated into a new version of MEGAN (Jiang et al., 2018). This study highlights the lack of field campaigns that capture drought behaviour, and that data is taken from the Ozarks drought period of 2011 and 2012.

1.9 Instrumentation to measure isoprene in the field

A wide range of techniques are available for the measurement of VOCs in the atmosphere. The complexity and high number of similarly structured VOCs in the atmosphere requires fine separation of compounds and to determine the concentrations of specific gases, measurements are typically made using gas chromatographs. Both the type of gas chromatograph and the method of sample collection can vary depending on the sample site. Samples may be collected *in-situ* at the field location directly, a grab sample may be taken as air or samples could be collected with the use of an absorbent tube.

Grab samples can either be whole air samples where air samples are collected in an inert vessel or adsorbent tubes, where air samples (or some specific air components) are collected in an inert vessel and analysed at a later date (Heard, 2006). Both methods offer the benefit of simple sampling. While grab samples can be deployed in relatively large numbers, they typically provide low temporal resolution, making this approach unsuitable for capturing the rapidly changing concentrations of isoprene. In addition, reactive compounds can degrade over time before analysis or during desorption (Batterman et al., 2002), so using grab samples for long periods, even with some degree of automation, the sample processing is time- and resource-intensive.

In-situ methods provide a higher confidence measurements and also allow a higher temporal resolution. To date, *in-situ* measurements of isoprene have been carried out using existing commercial bench-top instruments, such as gas chromatographs (Jones et al., 2011) and mass spectrometers (Noelscher et al., 2016; Yáñez-Serrano et al., 2015). These techniques differentiate between VOCs either by fine separation (gas chromatography) or by identification of their molecular ions based on mass-to-charge ratios (mass spectrometry). These instruments, while offering high precision and stability, are not built to withstand field conditions for long periods of time due to their need for power, temperature-controlled environments and specialty carrier gases. This is especially true in under-sampled regions of high isoprene emissions, which are typically in remote or challenging environments (e.g., tropical forests). In these locations instrument size, portability, autonomy, power demand and gas consumption severely limit the length of a deployment. In addition, instrument cost and maintenance limit the number of instruments deployed at any one time, and hence the spatial coverage of a field campaign can be limited.

Novel portable gas chromatography instruments have been developed for uses in

detecting toxic levels of dangerous gases when combined with quadrupole MS (Smith et al., 2004) and have been demonstrated to be operable in harsh conditions. Another system uses a toroidal ion trap analyser with a portable instrument and has also been applied to the detection of chemical warfare agents or other toxic chemicals. A limitation of these portable instruments is the availability of spare parts and the cost of repairs. To develop a home-made instrument would have the benefit of increased tunability, would be cheaper, with more efficient troubleshooting and offer more flexibility in the function of the instrument.

1.10 Open research areas and the aims of this thesis

Isoprene research in forests is a broad field, but many questions remain unanswered and large uncertainties associated with existing research persist. Considering this background to isoprene emission in forests, this thesis aims to address several points.

Research is limited by appropriate instrumentation. A shortcoming of the measurement campaigns described in this chapter is the limitations of available instrumentation. Past field campaigns have used commercial 'bench-top' instruments that are limited by practicality in the field, portability, durability and cost. This identifies a need for a new instrument that is low cost, robust and autonomous and that would allow continuous measurements in challenging or remote conditions. This thesis describes a novel instrument for isoprene concentration measurements that fulfils these criteria. The instrument is a dual column photoionisation detector isothermal gas chromatograph which is called the iDirac. An overview of the iDirac, including its construction, operation and laboratory evaluation will be discussed in Chapter 2.

Tropical forests, despite global importance, are under-sampled. Isoprene emitted from tropical forests has been highlighted as particularly important for global emissions and these areas are also typically under-sampled. Here, a new measurement campaign is described in an attempt to understand the emission of isoprene from tropical forests. This campaign aims to assess the difference between forests of different stages of conversion to oil palm plantation with a series of canopy-level measurements. The emission of isoprene from specific trees is also investigated with a series of leaf-level measurements. The deployment of the iDirac in such an environment and the multiple ways it was used to measure this atmosphere will be described in Chapter 3.

The vertical gradient of isoprene in a forest canopy is poorly understood. It has been established that the distribution of isoprene in a forest canopy is poorly characterised and the tropical measurement campaign has further highlighted shortcomings of this understanding. The main body of work here describes attempts to understand how isoprene is distributed in a temperate forest canopy and what factors affect the vertical mixing. A long-term deployment of the iDirac in a forest in Oxfordshire is described. Using existing infrastructure, vertically distributed measurements investigate the vertical concentration gradient of isoprene in a forest canopy. This campaign, which is described fully over Chapters 4, 5 and 6, aims to lend an insight into what factors affect the isoprene from a temperate forest.

Existing canopy models fail to capture the daily profile or vertical gradient of isoprene. An overarching aim of this study is to be able to gain an understanding of the forest distribution of isoprene and predict what may be seen in certain types of forest. The measurement campaign has been complimented with the construction of a 1D canopy model named CamCan and the improvement of the existing model FORCAsT. Chapter 7 describes how this model is constructed, how it is compared to the existing FORCAsT model and how it compares to our own observations. Using this model, fluxes of isoprene into the free troposphere are estimated for the study site and during a heatwave. Using this model, a greater understanding of the processes at work in a canopy is obtained and potential other scenarios are investigated.

2 iDirac: A Field-portable Instrument for Long-term Autonomous Measurements of Isoprene and Selected VOCs

This chapter is based on a paper currently under review.

Authors: Conor G. Bolas, Valerio Ferracci, Andrew D. Robinson, Mohamed I. Mead, Mohd. Shahrul Mohd. Nadzir, John A. Pyle, Roderic L. Jones and Neil R. P. Harris

Author Contributions:

Conor G. Bolas developed the instrument, designed evaluation experiments, deployed the instrument in the field and wrote the manuscript. Valerio Ferracci assisted in developing and deploying the instrument, performed some evaluation experiments, assisted with data evaluation and reviewed the text. Andrew D. Robinson designed and constructed the original prototype instrument. Mohamed I. Mead and Mohd Shahrul Mohd Nadzir provided technical assistance and advised on data interpretation. John A. Pyle, Roderic L. Jones and Neil R. P. Harris advised on data interpretation and provided guidance on the text.

2.1 Introduction

Due to its high reactivity, isoprene is relatively short-lived, with a typical lifetime of one hour in a temperate forest (Helmig et al., 2002). Local abundances can change rapidly in response to meteorological variations, such as changes in incoming photosynthetically active radiation (PAR), temperature and atmospheric dynamics (Langford et al., 2010). High time resolution data is required to capture changes in isoprene concentrations in real time. Given the importance of isoprene to atmospheric chemistry, it is highly desirable to improve the temporal and spatial coverage of isoprene measurements so that our understanding of its emissions via models can be validated against field data.

Measurements of atmospheric hydrocarbons such as isoprene are challenged by the difficulty in making measurements in remote places. To date, *in-situ* measurements of isoprene have been carried out using existing commercial bench-top instruments, such as gas chromatographs (Jones et al., 2011) and mass spectrometers (Noelscher et al., 2016; Yáñez-Serrano et al., 2015). These techniques differentiate between VOCs either by separation (gas chromatography) or by identification of their molecular ions based on mass-to-charge ratios (mass spectrometry). These instruments, while offering high precision and stability, are not built to withstand field conditions for long periods of time due to their need for power, temperature-controlled environments and specialty carrier gases. This is especially true in under-sampled regions of high isoprene emissions, which are typically remote or challenging environments (e.g., tropical forests). In these locations instrument size, portability, autonomy, power demand and gas consumption significantly limit the length of a deployment. In addition, instrument cost and maintenance limits the number of instruments deployed at any one time, and hence the spatial coverage of a field campaign.

An alternative method to detect environmental VOCs is with grab samples. These can either be whole air samples or adsorbent tubes, where air samples (or some specific air components) are collected in an inert vessel and analysed at a later date. While grab samples can be deployed in relatively large numbers, they typically provide low temporal resolution, making this approach unsuitable to capture the rapidly changing concentrations of isoprene. In addition, reactive compounds can degrade over time before analysis, and using this method for long periods, even with some degree of automation, is time- and resource-intensive.

All the limitations in the instrument currently used for VOC detection drive the need for

a field instrument that is:

- lightweight, so that it is portable and can be installed in environments difficult to access with traditional instrumentation;
- low-power, so that it is capable of running off-grid;
- autonomous, so that it minimises operator involvement and maintenance;
- low gas-use, so that it minimises the cylinder size required and the number of site visits to replace gas cylinders;
- rugged and durable, so that it can withstand challenging environments;
- relatively low-cost, so that multiple instruments can be deployed at one time.

2.2 Aims

Here the development and validation of the iDirac is described, an instrument that fulfils the requirements listed above. It follows on from the philosophy of the μDirac (Gostlow et al., 2010), with portability, modularity, power efficiency and autonomy at the centre of its design. The iDirac also incorporates inexpensive microcontroller board processors for advanced control and remote access to the instrument. The core GC instrument and its operation are described in Section 2.3, while Section 2.5 presents the software used to control the instrument. Instrument performance is discussed in Section 2.6, including calibration, accuracy, precision, sensitivity and separation ability. Results from trial runs in the controlled environment of a laboratory are presented in Section 2.7. Results using this instrument have been published on the impact of herbivory on canopy photosynthesis and isoprene emissions in a UK woodland (Visakorpi et al., 2018) and on isoprene concentrations near the Antarctic peninsula (Nadzir et al., 2019). The aims of this chapter are to:

1. Provide an overview of the iDirac.
2. Describe in detail how the instrument is constructed and operates.
3. Evaluate the instrument performance.

2.3 Practical description of the iDirac

The iDirac is a portable gas chromatograph equipped with a photoionisation detector (GC-PID). The VOCs in an air sample are separated on chromatographic packed columns and then sequentially detected by the PID. The instrument is built in-house and is lightweight, low-power and able to operate for several weeks or months autonomously. Its specifications are shown in Table 1. Section 2.3.1 describes the basic outline of the instrument and Section 2.4 describes the specific configuration of the instrument for isoprene.

Table 1 iDirac specifications

Power	12 W
Weight	10 kg
Voltage Requirements	10–18 V
Dimensions	22 × 61.6 × 49.3 cm
Carrier Gas	High Purity Nitrogen (Grade 5)
Calibration Gas	10 nmol mol^{-1} (or ppb) high-accuracy isoprene in nitrogen
Limit of detection	38 pmol mol^{-1} (or ppt)
Precision	11 %

2.3.1 Core gas chromatograph physical design

The iDirac is built in a modular fashion, so that the various components are housed in six main plastic boxes (Piccolo Polycarbonate Enclosures, IP67) packed in foam inside a protective waterproof case (Peli® 1600), as shown in Figure 9. Details on the boxes and their contents are given below, and shown within the instrument in Figure 9:

- Valve Box, containing eight solenoid valves to control gas flow from the four inlets;
- Control Box, containing microcontroller boards (Arduino and Raspberry Pi), a number of electronic components (e.g.. solid state relays), the flowmeter and SD card for data storage;
- Oven Box, containing the dual-column system, (pre- and main columns), heating

element and Valco valve;

- PID Box, containing the photoionisation detector;
- Pump Box, containing the pump and pressure differential sensor;
- Power Box, containing power regulators and electrical fuses.

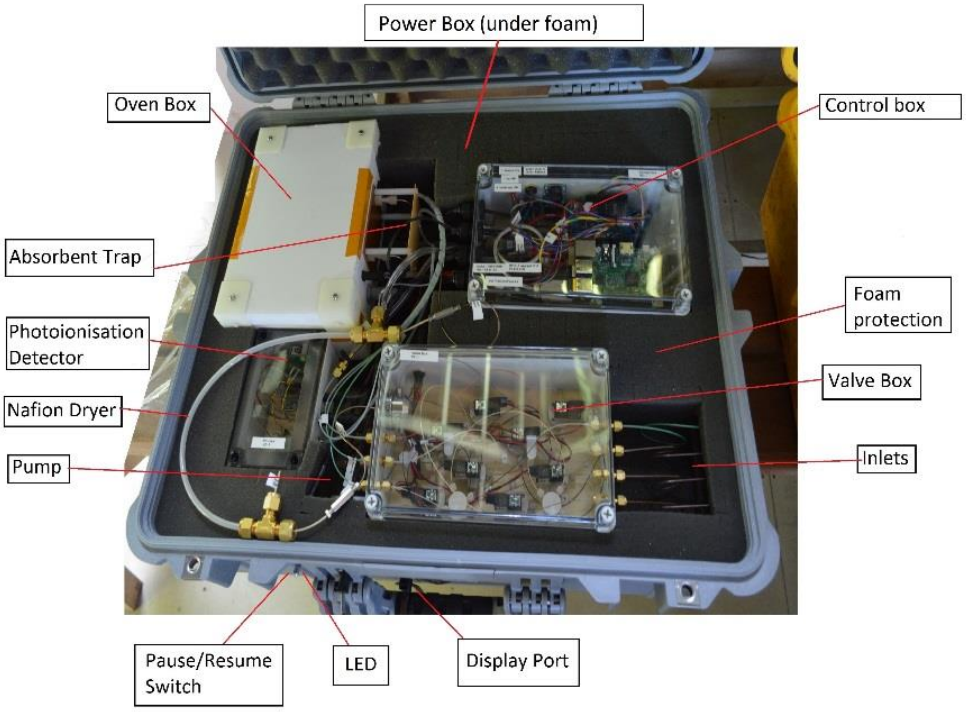

Figure 9 Interior of the iDirac showing the modular design of its component parts inside the Pelicase (22 × 62 × 50 cm)

On the exterior, the iDirac has a power socket, and four inlets for gas input. The inlets are for the nitrogen carrier gas, a calibration gas and two sample lines (sample 1 and sample 2) between which the instrument can alternate.

The general pneumatic design of the instrument is built around two phases in the analysis cycle which are represented schematically in Figure 10: a loading phase (Load Mode – pink), in which the analyte of interest is pre-concentrated on an adsorbent trap, and an injection phase (Inject Mode - purple), in which the analyte is desorbed from the trap and injected onto the columns in the oven for separation and, eventually, detection. These two modes are controlled by a 2-way 10-port Valco valve (VIDV22-3110, mini diaphragm 10 port 2-pos 1/16” 0.75mm, Thames Valco®) in the Oven Box, which is activated by pneumatic actuation, by the set of solenoid valves in the Valve Box and by the pump.

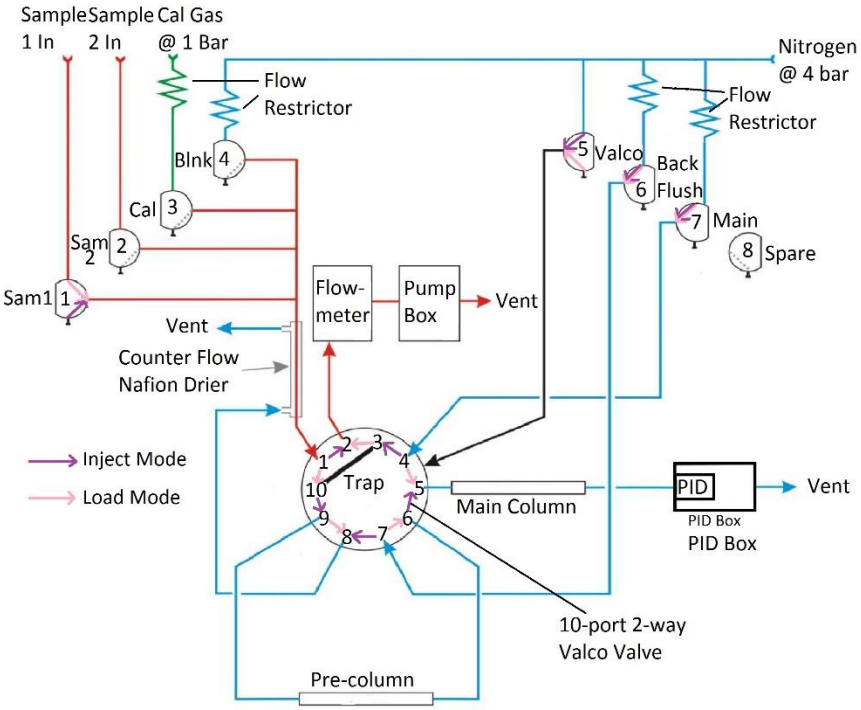

Figure 10 Schematic representation of the iDirac operation. When in Load Mode (valve 5 off - pink), the contents of a gas source chosen between valves 1-4 are pre-concentrated on the adsorbent trap. In Inject Mode (valve 5 on - purple), the VOCs in the trap are injected into the dual-column system for separation and, eventually, detection

In Load Mode (Valco valve not activated, i.e. valve 5 off), one of four inlet gases (either sample 1, sample 2, calibration gas or blank gas) is selected by switching on the appropriate solenoid valve (valves 1, 2, 3, or 4 respectively). By activating the pump, gas is drawn through the selected inlet valve, dried in a Nafion counter-flow system and passed through an adsorbent trap where the analyte is pre-concentrated. The sampled gas is vented into the Pelicase and then to the outside. A flowmeter is placed in series with the sample flow and measures the gas flow through the trap. Once a pre-defined volume of gas has been sampled, the pump stops and the instrument enters Inject Mode.

In Inject Mode, the trap is flash-heated to approximately 300 °C for 9 s to desorb the analyte from the adsorbent material. The Valco valve is then pneumatically activated by switching valve 5 on: the nitrogen carrier flows through the trap in the direction opposite to trap-loading, delivering the desorbed compounds into the dual-column system where they undergo chromatographic separation. The oven consists of a pre-column, which screens for large bulky molecules (e.g., the monoterpenes) whilst allowing smaller molecules through, and a main column, which performs the critical separation of the

relevant analytes. The main column eluent is incident on the PID membrane, where the signal from the changing composition of the gas exiting the main column is detected.

More details on the individual parts of this cycle are given below.

2.3.2 Inlet manifold and sample preparation

The inlet ports protrude from the side of the Pelicase via 1/16” bulkhead unions (Swagelok) and connect directly to the Valve Box, containing eight solenoid valves that act as gas selectors. The sample 1 (via valve 1), sample 2 (via valve 2), calibration gas (via valve 3) and blank nitrogen (via valve 4) lines are all combined in a four-way Silconert-treated stainless steel Valco manifold (Z4M1, 1/16" manifold 4 inlets, Thames Valco). This manifold leads to the adsorbent trap via a Nafion dryer (Nafion gas dryer 12", polypropylene, PermaPure MD-050-12P-2) which drives excess water vapour out of the gas flow by diffusion through a membrane with a counter flow of dry high-purity nitrogen. Valve 5 is a direct line from the nitrogen inlet to the Valco valve for actuation, which requires a higher pressure (typically 4 bar). Valves 6 and 7 control the nitrogen flow through the columns: valve 7 activates the nitrogen flow through both columns in Inject Mode (when valve 5 is on), and through the main column only in Load Mode (when valve 5 is off). Valve 6 activates the nitrogen flow through the pre-column for the backflush in Load Mode. The nitrogen counter-flow needed for the Nafion dryer is provided by valve 6 in Inject Mode and by the pre-column backflush vent in Load Mode. Gas lines downstream from valves 5, 6 and 7 leave the box via manifolds on the side of the box. Valve 8 is a spare valve with no current function.

Flow restrictors upstream from valves 3, 4, 6 and 7 ensure that the flow from the pressurised inlet lines does not exceed the maximum flow through the flowmeter. These restrictors also reduce the gas demand of the instrument. The restrictor tubing used for the calibration line is red PEEK flow restrictor (1/32” OD, 0.005” ID) and the one used for the nitrogen lines is black PEEK (1/32” OD, 0.0035” ID). The rest of the tubing is Silconert-treated stainless steel (Thames Restek, 1/16” OD, 0.04” ID), which does not restrict the gas flow.

2.3.3 Sample adsorption/desorption system

From the Nafion drier, the sample gas passes through ports 1 and 10 of the Valco valve and into the adsorbent trap when the instrument is in Load Mode. The trap consists of wide bore stainless-steel tubing (HI-Chrom, 1/16" OD, 0.046" ID) containing one bed of

adsorbent material between two beds of glass beads, both crimped in place, with a coiled nichrome wire heating element surrounding the section of the tube corresponding to the adsorbent. The adsorption of isoprene and other VOCs takes place on a bed of approximately 10 mg Carboxen 1016 (Supelco, 60/80 mesh, 11021-U); Carboxen 1016 is a carbon molecular sieve that has been selected for its optimised recovery rate of unsaturated short chain hydrocarbons upon thermal desorption. Different sorbent materials can be used for other species. The gas exiting the trap, now scrubbed of VOCs, flows via ports 3 and 2 on the Valco valve into the flowmeter (Sensirion, ASF1430) which monitors the flow rate through the trap. This is then integrated across the duration of sampling to calculate the total volume of gas sampled. When the desired volume is reached, the valves from the sample inlet are closed and the pump is halted to stop the flow of gas through the trap. The heating coil is flash-heated to desorb the analyte from the adsorbent, while the Valco valve is switched to Inject Mode and valve 7 is activated, flushing the desorbed VOCs onto the pre-column in the oven box with the high-purity nitrogen carrier.

2.3.4 Isothermal oven

The flow containing the sample leaves the trap and enters the thermally insulated oven box. This enclosure, housed in insulating material (lightweight display board, Kerbury Group), is heated to 40 ^{o}C using a heating element (PTC element enclosure heater, 15 W 12-24 V 40 C) which is fixed to the base-plate of the oven using conductive paste. A fan mixes the air inside the oven to ensure a uniform temperature throughout.

The sample is injected onto the pre-column (5% RT-1200, 1.75% Bentone-34, SILPT-W, 100/120, 1.0 mm ID, 1/16 "OD SILCO NOC, Custom Packed, Thames Restek, ~70 cm in length) via ports 10 and 9 on the Valco valve. Here, isoprene and other small molecules travel faster through the pre-column than bulky VOCs. After a set time (typically, 30 s), once isoprene has passed through the pre-column, the Valco valve is switched off, with valve 5 closing and valve 6 opening, so that the pre-column is back-flushed. This way lighter species, including isoprene, elute onto the main column while larger molecules that are still in the pre-column when valve 5 is switched off are removed from the column system via the back-flush. This is important to avoid large, less volatile species from entering the main column.

The main chromatographic separation occurs on the main column (OPN-RESL-C,

80/100, 1 mm ID, 1/16"OD, SILCO NOC, Custom Packed, Thames Restek, ~70 cm in length), based on the boiling point and polarity of the VOCs. This way, different species elute onto the detector at different times.

2.3.5 Photoionisation detection system

The sample is directed from the outlet of the main column into a photoionisation detector (PID). The PID (Alphasense Ltd™, PID-AH) operates by ionising any gas diffusing through a membrane covering a krypton lamp. Near-vacuum UV radiation from the lamp ionises any molecule with an ionisation potential of less than or equal to 10.6 eV. Isoprene, with an ionisation potential of 8.85 eV (Bieri et al., 1977), is readily photolysed and hence detected by the PID with a sensitivity of 140% relative to that of isobutylene, which is used by the manufacturer as reference compound in terms of PID response. The ions generated by photoionisation produce a voltage change across an electrode system which is converted to a digital signal by an analogue to digital converter (ADC) (16-Bit ADC 4 Channel, Adafruit). The PID is turned on for the duration of the elution from the dual-column system, and the data is collected at a frequency of 5 Hz. The chromatography run finishes once isoprene has eluted from the main column (typically 60-75 s after starting the back-flush). The data from the PID is then saved to a new file on an SD card by the Arduino Mega. A typical chromatogram showing an isoprene peak is shown in Figure 11.

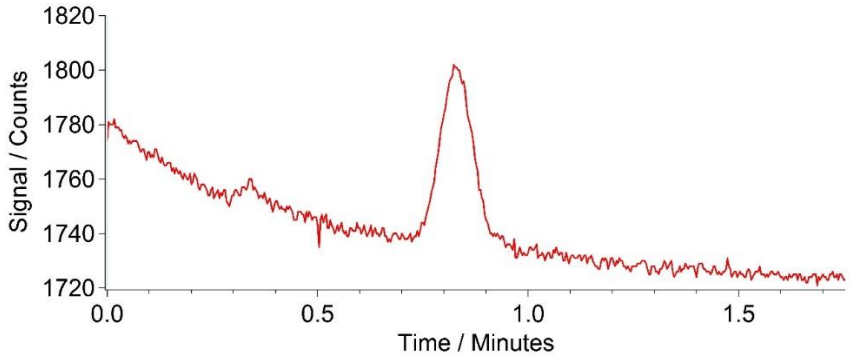

Figure 11 Typical chromatogram from the laboratory showing the isoprene peak detected by the PID at an elution time of approximately 0.8 minutes

2.4 Instrument operation specifications

2.4.1 Carrier gas and calibration gas

Two gas cylinders are required to operate the iDirac: a pure nitrogen supply and a calibration gas. Nitrogen is used as carrier gas through the dual column system, as sample gas for the blank runs and also to actuate the Valco valve. The nitrogen supply is of at least Grade 5 purity (corresponding to $\geq$ 99.999 % nitrogen) to minimise interference from impurities with the detection of isoprene. Typically, high-purity BIP+ Nitrogen (Air Products) is used. The logistics of the measurement dictate the size of the nitrogen cylinder used: for mobile deployments in the field, small portable cylinders (1.2 L) are ideal, whilst larger cylinders (10 L) are more suitable for long-term measurement as they minimise the need for maintenance visits to replace the nitrogen cylinder. Typically, the iDirac can run continuously on a 10 L nitrogen cylinder supplied at 200 bar for approximately two months. The calibration gas consists of a binary gas mixture of approximately 10 nmol mol^{-1} (or ppb) isoprene in nitrogen stored in a Silconert-treated 500 mL stainless steel cylinder (Sample Cylinder Sulfinert, TPED, 1/4", Thames Restek). The use of cylinders with passivated internal walls minimises the adsorption of isoprene on surfaces, which would introduce biases in the measurement. The accurate concentration of the calibration gas is determined by comparison with a primary gas standard. The calibration routine is described in detail in Section 2.6.1.

2.4.2 Power requirements for operation

The instrument requires a power supply between 9 and 18 V. This can either come from mains power or alternatively, a battery. The incoming power is smoothed and regulated with two regulators to stable 5 V and 12 V outlets. The Arduino board monitors the supplied voltage in between runs in the case of the battery losing charge or power cuts. If the voltage drops, the iDirac switches to a power-save mode, where the oven, PID and valves are turned off to conserve power and the instrument waits for 20 minutes before again checking the input voltage. Once it detects a high enough voltage (typically 9 V), it will turn back on the various components.

2.4.3 Flow control through the instrument

The flow through the instrument is driven by either upstream pressure (in the case of the nitrogen and calibration gas flows) or by the pump box (in the case of samples 1 and 2). The pump box is an air-tight container with an inlet line and a vent. A diaphragm pump (DF-18, Boxer) withdraws air from the pump box and vents it outside, reducing the pressure inside the enclosure. The reduced pressure within the pump box causes air (from the sample 1 and 2 inlets) to be drawn through the system, via the trap and the flowmeter. A pressure sensor (differential pressure sensor, Phidgets) monitors the pressure differential between the inside and the outside of the pump box. During a pump cycle, the pump is only activated when the pressure differential falls below a pre-specified value (typically, 20 kPa). This method ensures a uniform flowrate and enables control over low flowrates (~ 20 mL min^{-1}), thus reducing the uncertainty in the volume integration of the air sampled.

2.5 iDirac software and hardware control and data analysis

The iDirac is controlled using a dual Arduino system: an Arduino Micro board controls the gas flow components of the instrument, whilst the main instrument control is achieved with an Arduino Mega board. These two units communicate with all of the sensors inside the instrument and read their outputs. A Raspberry Pi computer acts as the interface between the user and the Arduino boards. A Python script is run on the Raspberry Pi, allowing the user to configure the instrument with the desired parameters and read the sensor output from that of the Arduino. The Raspberry Pi desktop can be accessed remotely via an ad-hoc network, allowing connection with a variety of interfaces. This control system allows many of the parameters described above (e.g., sample volume, time spent in each column) to be changed.

2.5.1 Arduino control of internal electronics

The instrument is controlled primarily using an Arduino Mega 2560 board (Arduino Mega 2560, Arduino). This microcontroller has a number of analogue and digital ports and runs Arduino code (C and C++ commands) to control these ports. An SD breakout board is used (microSD Card Breakout Board, Adafruit) to facilitate the use of an SD card to store data in, while a real time clock (RTC) board is used (Real Time Clock, ChronoDot Ultra-Precise, Adafruit) for time-keeping. Figure 12 illustrates the various connections on the Arduino Mega.

An Arduino Micro board (Arduino Micro, Arduino) controls specifically the altimeter pressure sensor (located in the PID box) and the flowmeter, and sends these readings to the Arduino Mega via a serial port. The use of the Arduino Micro is justified as it simplifies the code on the Arduino Mega, particularly as the flowmeter requires the use of a shifter to convert the RS232 serial signal and several subsequent mathematical manipulations. The Arduino boards do not have a shutdown procedure and can simply be unplugged.

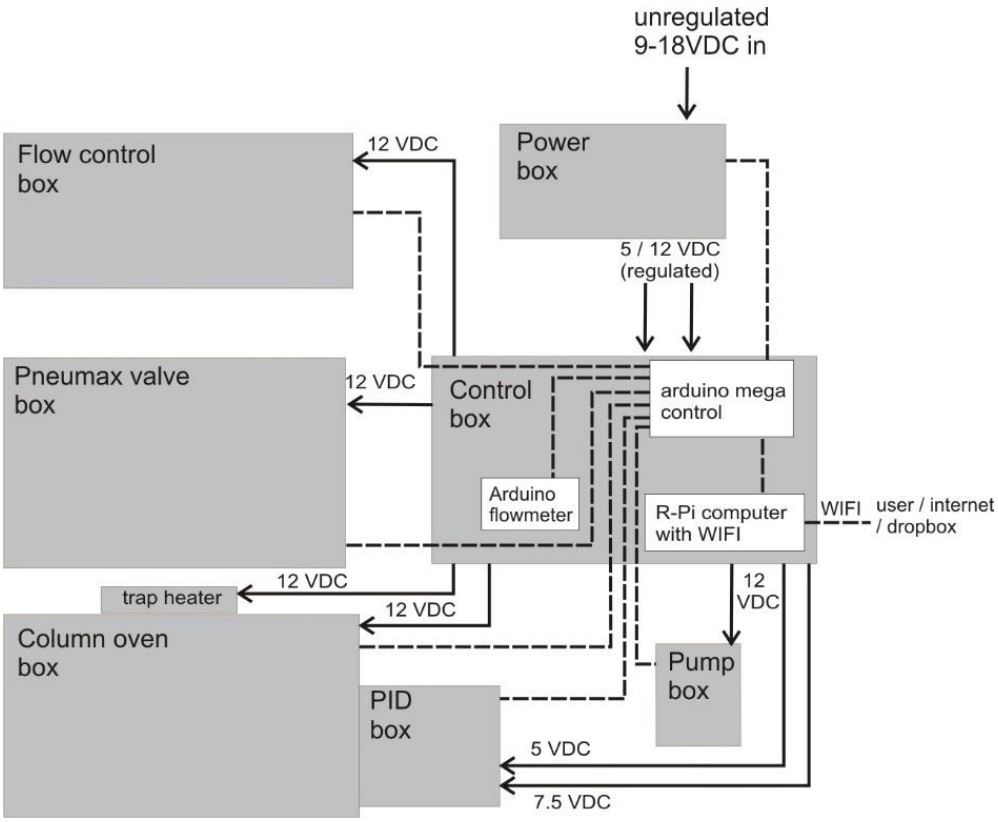

Figure 12 Schematic of Arduino Mega connections to the various components of the iDirac. Black lines indicate power dashed lines indicate a communication line

2.5.2 Description of Raspberry Pi user interface

The iDirac uses a Raspberry Pi (Raspberry Pi Model B V1.1, Raspberry Pi) as a user interface, allowing the instrument to be controlled from a familiar desktop environment. The Raspberry Pi uses a Wi-Fi dongle to set up its own ad-hoc network, which can be connected to laptops and mobile phones in a fashion similar to a standard Wi-Fi network. Once connected to the network, a graphical desktop sharing system such as VNC viewer (VNC Viewer, RealVNC) allows the user to navigate the Raspberry Pi desktop and manipulate the instrument.

Upon opening the Raspberry Pi desktop a purpose-written Python script is launched automatically. A terminal window is opened displaying the serial output from the Arduino Mega and transmitting data to the Arduino Mega via a serial port connection. The latest version of this Python script (Appendix 1) is freely available on GitHub (https://github.com/cgb36/iDirac-scripts). The Python script decodes incoming serial bytes from the Arduino Mega and displays them in a user friendly command line window. It is also possible to restart and shutdown the instrument from the Raspberry Pi desktop. The Raspberry Pi requires a shutdown procedure, which can be done either physically with a switch on the side of the control box, or from the virtual desktop environment.

2.5.3 Processing of chromatograms

To process numerous chromatograms in an automated fashion, a script was created that uses calibration runs to accurately identify isoprene peaks in the sample runs and convert their integrated peak areas into mixing ratios. This script is written in Mathematica (v11.1.1). Figure 13 shows a flow diagram for the main algorithms of the script. Firstly the data is read in, making sure that all the files are the correct size and do not contain any erroneous runs (e.g., corrupted or truncated files) that may jeopardise the running of the script.

The calibration data is processed first. This involves selecting all chromatograms with index ‘C’ and plotting them for visual inspection. The next step is to locate the isoprene peak and to fit a Gaussian curve to it to obtain peak height, width and position (equivalent to elution time), as well as the error in the fit. The elution time of the peak is retained in an interpolated function over time. The blank runs (with index ‘B’) are included in this routine as they effectively represent calibrations with zero isoprene concentration. Subsequently, the peak area is plotted against the calibration volume multiplied by the isoprene concentration in the gas standard to obtain a response curve. A quadratic curve is fit to this data, which captures any slight deviations from linearity. Calibration procedures are described in depth in Section 2.6.1.

The sample chromatograms are then selected as either sample 1 (runs with index ‘S’), or sample 2 (runs with index ‘X’) and, as with the calibration runs, they are plotted to visually inspect the data. Following that, a section of each sample chromatogram is selected as the region where the isoprene peak is likely to reside. This is achieved by interpolating the retention times from adjacent calibration runs to the time of each sample runs, thus ensuring that the isoprene peak is identified correctly. A Gaussian is fitted to

this section of the sample chromatogram, calculate all the peak parameters. The Gaussian function has certain boundaries set, to further ensure that it is fitted to the correct peak. Using the sample peak area, the sample volume and the calibration curve, the isoprene mixing ratio in the sample can be calculated.

When there are insufficient calibration chromatograms to determine the isoprene peak retention time, it can be estimated using the column temperatures from the nearest calibration runs. If the spacing between calibration points is too great or the calibration is done separately to the sampling, the interpolated calibration retention time values may not span the region where the isoprene peak resides. In this case the column temperature and retention time of the most recent calibration chromatograms are used to define a linear relationship. It is then possible to derive the isoprene retention time from the column temperature of the sample chromatogram.

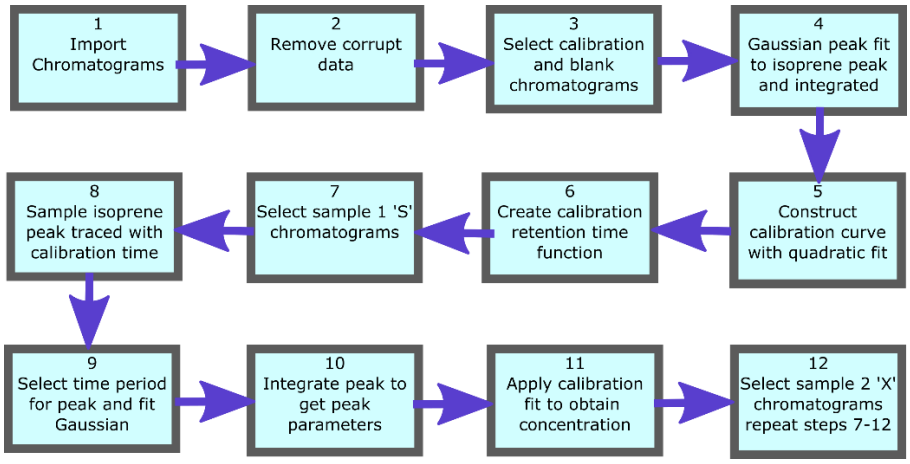

Figure 13 Analysis script flow diagram, describing the key steps to processes large quantities of chromatograms

2.6 Instrument performance

2.6.1 Calibration of output chromatograms

The PID response to isoprene is calibrated using a primary gas standard supplied by the National Physical Laboratory (NPL), certified as containing 5.01 ± 0.25 nmol mol^{-1} (or ppb) isoprene in a nitrogen matrix. The gas mixture is stored in a 10 L Experis cylinder (Air Products); this type of cylinder has been demonstrated to provide maximum stability for VOC mixtures over time (Allen et al., 2018). The primary standard is only used for calibration in the laboratory; for field deployments, a smaller secondary gas standard is used instead. This is prepared manometrically by diluting a higher concentration parent

mixture (100 nmol mol^{-1} isoprene in nitrogen, BOC) to approximately 10 nmol mol^{-1} with high-purity nitrogen (BIP+, Air Products). This secondary gas standard is prepared in a 500 mL Sulfinert-treated stainless steel cylinder (Sample Cylinder Sulfinert, TPED, 1/4", Thames Restek). This type of treated cylinder exhibits very good long-term stability for a number of VOCs (Gary Barone et al. Restek Corporation, 2010). The exact isoprene amount fraction in the secondary standard is determined by validating it against the NPL primary standard. This way the measurements from the iDirac are traceable to accurate primary standards.

Frequent calibration is needed not only to convert chromatography peaks into meaningful atmospheric amount fractions, but also to monitor long-term trends in the detection system, including detector drift and decreasing performance of the adsorbent trap. Any changes in isoprene elution time, which may be caused by changes in oven temperature, can affect the correct peak assignment in chromatograms with multiple peaks. These effects can be easily addressed if frequent calibration chromatograms (which only have, by definition, one peak) are available.

Calibration frequency is specified by the user in the instrument set-up by selecting the number of samples to run between calibrations. For example, a calibration frequency of '4' would correspond to a run of four sample chromatograms, followed by a calibration run. Calibrations can be omitted by inputting '999' (e.g., when there is no access to calibration gas), whilst a calibration-only run can be selected by inputting '0'. It is good practice to perform a calibration run periodically to ensure that the position of the isoprene peak can be traced. The exact number of sample chromatograms that can be run in that time depends on the duration of the chromatographic run (which is designated by the user by specifying an 'inject time' and a 'backflush time') as well as on the volume of air sampled (also specified by the user), which in turn dictates the duration of the step in which the sample is pre-concentrated in the trap.

The calibration cycle is programmed to be preceded and followed by a blank run, in which the system samples from the high-purity nitrogen supply from valve 4. This allows any residual isoprene in the trap to be desorbed before and after calibration, and to monitor the efficiency of desorption over time.

A calibration curve is obtained by varying the volume sampled in each calibration run. When configuring the instrument, the user specifies a calibration volume in mL, which is sampled every other calibration run. For the remaining calibration runs, the instrument is

programmed to sample a volume picked randomly from five possibilities: the user-specified calibration volume, the user-specified calibration volume multiplied by 2 or 4, and the user-specified calibration volume divided by 2 or 4. For instance, for a run configured with a calibration volume of 12 mL, half the calibration runs would be 12 mL samples and half a random mixture of 3, 6, 12, 24 and 48 mL samples. A typical time sequence of isoprene peak areas from different calibration volumes is shown in Figure 14. A calibration curve is then obtained by plotting these peak areas against the effective isoprene concentration (defined as the sample volume multiplied by the isoprene mixing ratio in the calibration cylinder). The zero concentration point is obtained from the blank runs. A quadratic curve is fitted to the calibration data. A typical calibration plot is shown in Figure 15. The equation for the quadratic fit allows the determination of the isoprene amount fraction in the samples by extrapolation or interpolation, provided the sample volume and peak area are known.

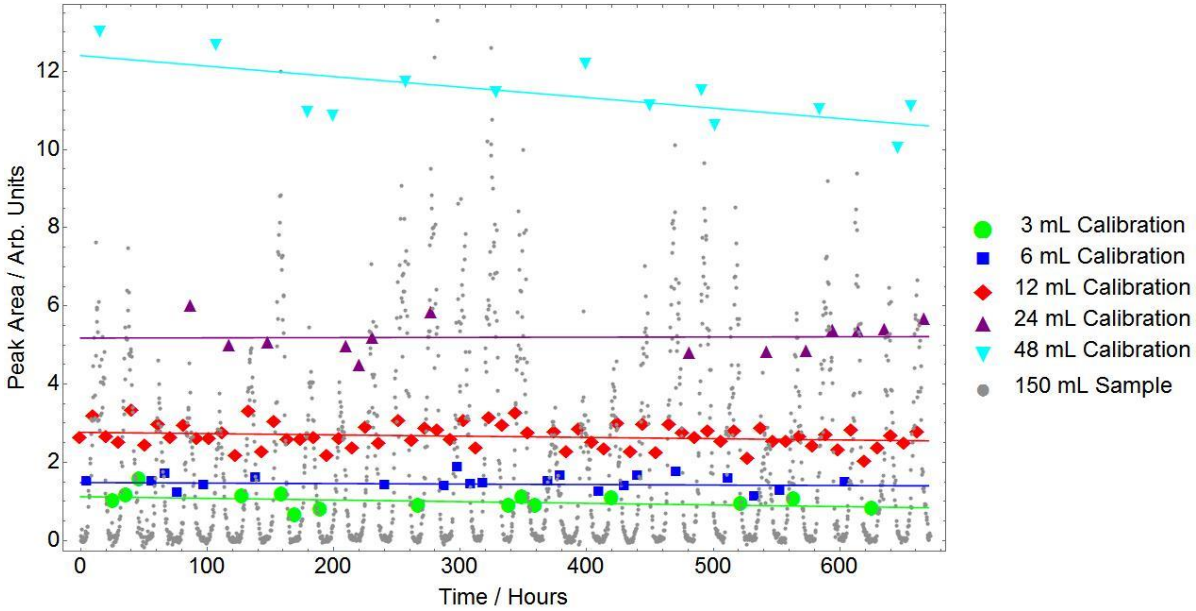

Figure 14 Typical sequence of isoprene peak areas for runs with varying calibration volumes. These are used to produce a calibration curve (see Figure 15). The calibration runs with the standard user-specified sampled volume (red data points) are used to calculate the instrument precision (see Section 2.6.2.1). Peak areas from sample runs (grey data points) are also shown to illustrate how the calibration peak areas span the entire range of sample values, minimising the need for extrapolation. Blank runs are also used and for each calibration point, two zero-value points are produced, these are not shown here to avoid cluttering the plot. This plot is produced using data from 28 days during the Wytham field campaign (see Chapter 5)

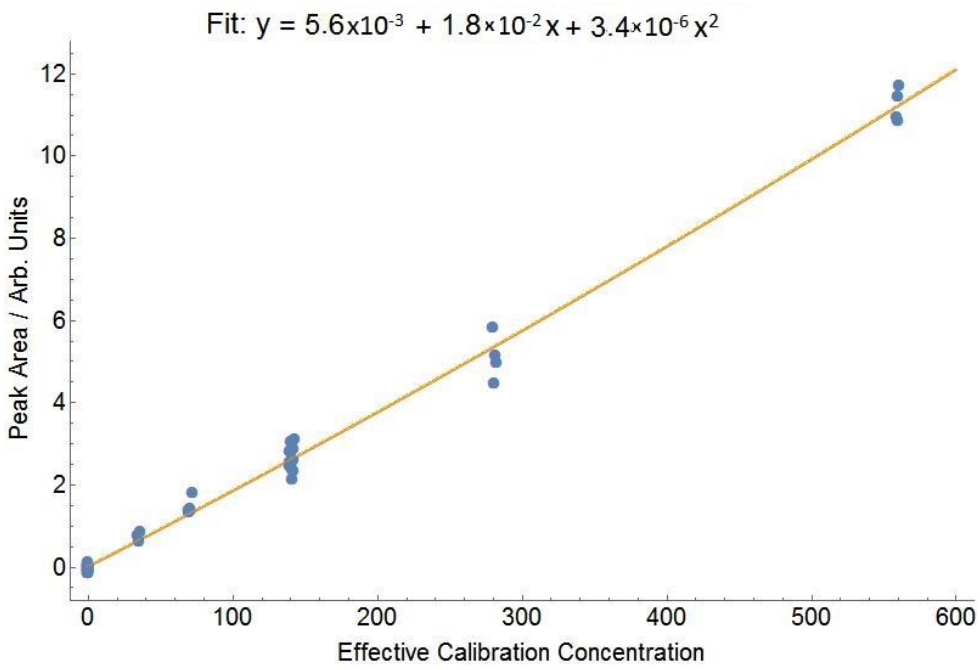

Figure 15 Typical calibration curve for isoprene. The x-axis ('Effective Calibration Concentration') consists in the calibration volume (in mL) multiplied by the isoprene concentration in the gas standard (in ppb)

As interpolation carries lower uncertainty than extrapolation, it is important to choose an appropriate value for the user-specified calibration volume, so that the points in the calibration curve span the entire range of the sample runs (as is the case in Figure 14). Typically, 12 mL is suitable in an environment with relatively low (< 1 ppb) isoprene concentrations (e.g. remote oceans), whilst a higher value (20 mL) is more appropriate when measuring in areas such as tropical forests.

2.6.2 Precision and accuracy of iDirac data

2.6.2.1 Precision

The precision of the instrument is determined as the relative standard deviation in isoprene peak area from calibration chromatograms with the same user-specified volume (typically, more than 50% of the total calibration runs in any given measurement sequence, as detailed in Section 2.6.1) and from the same calibration cylinder. For instance, in the calibration sequence shown in Figure 14 and Figure 15, this corresponds to the runs of 12 mL samples. Upon analysis of the scatter of these data points, the instrument precision is ±11.3% in the field (compared to <5% in the laboratory). This procedure means that the measurement precision can be routinely monitored over time which is especially useful in long deployments.

2.6.2.2 Accuracy

The accuracy of the instrument is dictated primarily by the uncertainty in the isoprene amount fraction in the NPL standard, and how this is propagated to the isoprene amount fraction in the secondary gas standard used in the field. It is therefore essential that the concentration of the secondary calibration cylinder is determined as accurately as possible by comparing it to the NPL primary standard. This is carried out in the laboratory, typically before and after each field deployment.

An example of this concentration determination is shown in Figure 16. XLGENLINE, a generalised least-squares (GLS) software package for low-degree polynomial fitting (Smith, 2010) is used to estimate the final uncertainty in the isoprene amount fraction in the secondary calibration cylinder by inverse regression from the calibration curve. For most secondary calibration cylinders, this is estimated to ~ 7% at the $k = 2$ level (providing a coverage probability of approximately 95%). A similar procedure is applied to calibration and sample data from the field to estimate the uncertainty in the ambient isoprene concentrations. This is estimated to ~20-25 % at the $k = 2$ level.

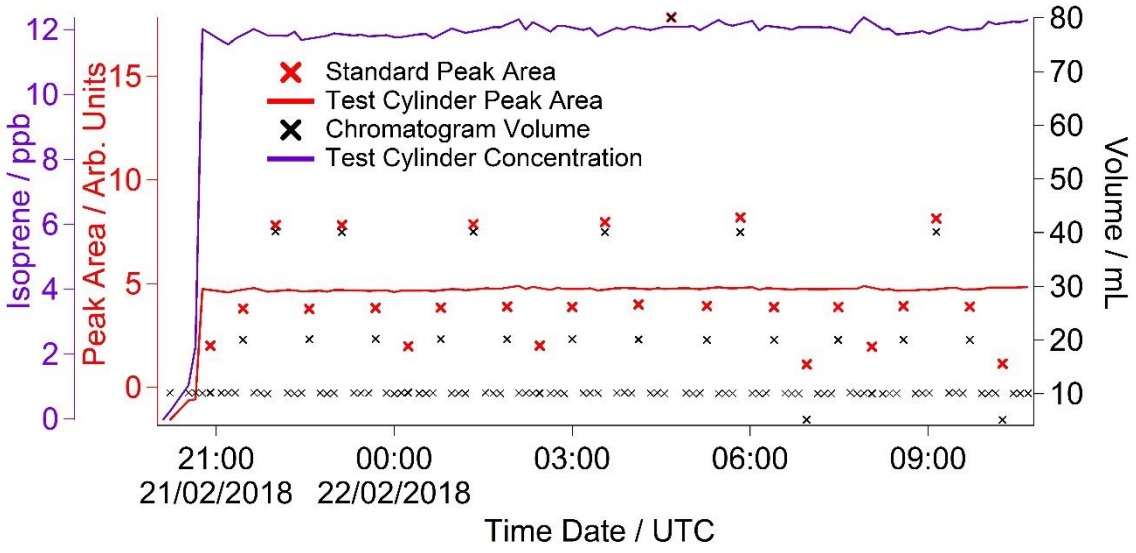

Figure 16 Summary plot of a concentration determination experiment. The primary reference gas mixture is used as the standard in the calibration runs, and the secondary gas mixture under test is used as sample

2.6.3 Sensitivity of the iDirac to isoprene

The instrument's sensitivity can be adjusted by changing the volume of the sample being analysed. For high concentrations (e.g. strong leaf emissions) a smaller volume should be used as the high concentration of isoprene would risk poisoning the adsorption trap. The

instrument has an effective upper volume limit of 250 mL (see Section 2.7.1) and a lower limit of 3 mL. The volume integration becomes unreliable below 3 mL due to the additional uncertainty brought about by the dead volume before the trap (approximately 1.6 mL). On the other hand, when ambient levels of isoprene are low (< 500 ppt), large sample volumes (200 mL) should be used. Sample volumes lower than or equal to 200 mL are used in order not to exceed the trap breakthrough volume (see Section 2.7.1).

The limit of detection is determined for a specific set of runs by allowing a signal-to-noise ratio (S/N) of 3. The blank runs are used to calculate the noise, which is defined as the standard deviation in the PID signal in a section of the blank chromatogram corresponding to the isoprene elution time. The instrument response factor is calculated from the isoprene peak height in the calibration runs and the isoprene amount fraction in the standard. This allows the calculation of the minimum concentration needed to give rise to a signal that would return a S/N of 3. This is identified as the limit of detection and is calculated for two versions of the iDirac, (designated the grey and orange instruments, identical in their design and characterised by the colour of their Pelicase). From the average of 20 calibration chromatograms, limit of detection of the orange iDirac is 108 ppt and that of the grey iDirac is 38.1 ppt. This difference is attributed to the traps used (i.e., a trap with more adsorbent would retain more analyte, resulting in a larger signal), as well as to the performance of the PID detector.

2.7 Tests in the laboratory and field deployments

The iDirac has been tested in a series of laboratory evaluations, at a deployment at a field station in a tropical forest in Sabah, Malaysia and in a research forest in Wytham Woods, UK.

2.7.1 Laboratory tests

2.7.1.1 Intercomparison of two versions of the iDirac

Two iDirac instruments (orange and grey) were compared against one another after the five month deployment in Wytham Woods (Chapter 4-6). The experiment consisted of the two instruments sampling from a chamber containing a controlled isoprene concentration which was varied over time. The orange and grey iDiracs both had inlets inside the chamber with identical filters (polyethersulfone, 0.45µm pore-size) and the same 1.5 m length of PTFE 1/16” tubing, placed as close to one another as possible. The gas within the chamber was well mixed with two large fans. Gas from a 700 ppb isoprene

in nitrogen mixture (BOC) was flow-controlled into the chamber at 80 mL min^{-1} for different time periods to change the concentration. The chamber was not flushed and the only exchange out of the chamber was slight seepage through several small holes around the inlets. The concentration was varied stepwise from 0 to 12 ppb. The instruments were calibrated using the same calibration standard (8.3 ± 0.6 ppb isoprene in nitrogen), which was connected to both instruments via a t-piece.

The results from this experiment are shown in Figure 17. The orange iDirac under-reads by 6.6% relative to the grey iDirac, and this is particularly evident at high concentrations. Figure 18 shows this data as a scatter plot of the 15-minute average values from either instrument, again it can be seen that the orange iDirac under-reads slightly. This discrepancy is accounted for by incorporating a ±6.6 % uncertainty in the measurements. This under-reading is likely due to differences in the absorbent trap, leading to a lower sensitivity for the orange instrument. This is supported by the calibration curve for the orange iDirac, which curves more at high concentrations, resulting in lower peak height than in the grey iDirac for the same concentration. Another artefact of this is that the noise visible on the orange output is greater. Adsorbent traps can be replaced on a regular basis to minimise such artefacts.

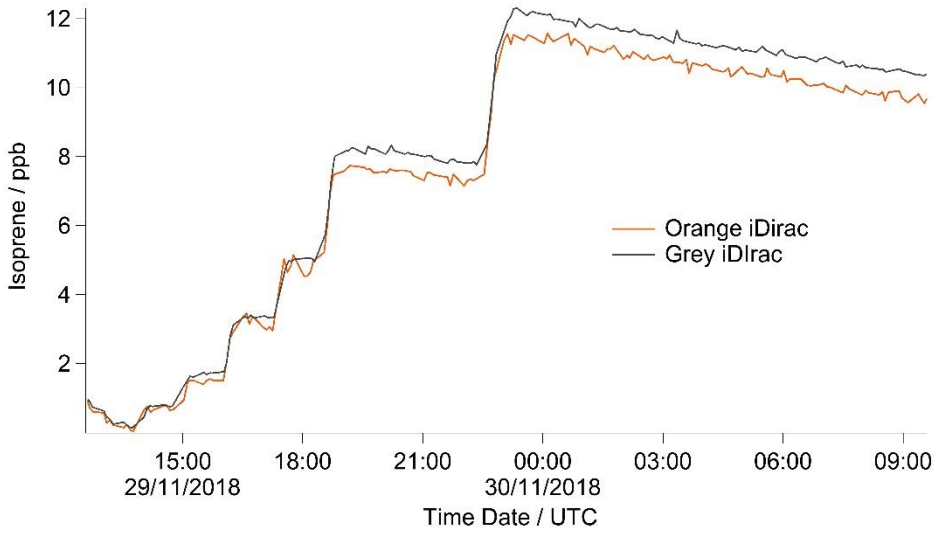

Figure 17 Time series plot showing isoprene mixing ratios from the grey and orange iDiracs

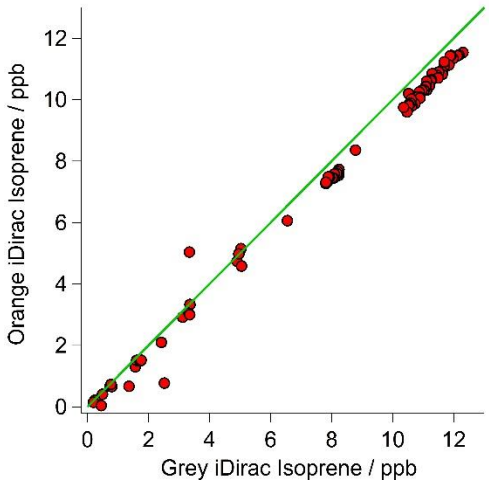

Figure 18 Scatterplot with 1:1 line showing 15 minute average values for the grey and orange iDiracs

2.7.1.2 Breakthrough tests

The breakthrough volume for the adsorbent traps used in the iDirac was determined. This is a test which evaluates what volume of gas is so great as to cause isoprene to pass through the trap in a single sample run. This test is performed by placing an additional adsorbent trap in the instrument upstream of the main trap, at the exit of valves 1-4 from the valve box. Each run sampled 10 mL of an isoprene mixture of known concentration. When the breakthrough volume of the additional trap is exceeded, isoprene effectively 'breaks through' onto the main trap, so that it is injected onto the dual column system and a peak is observed in the chromatograms. The sum of all the volumes of the runs in which isoprene was not observed (i.e., pre-breakthrough) gives the breakthrough volume. This value effectively acts as an upper limit of the volume of gas that the instrument can sample. Figure 19 shows a typical example of such test, in which a breakthrough volume of 250 mL is determined. The instrument is therefore set to sample volumes up to 200 mL, so that the breakthrough volume is never exceeded.

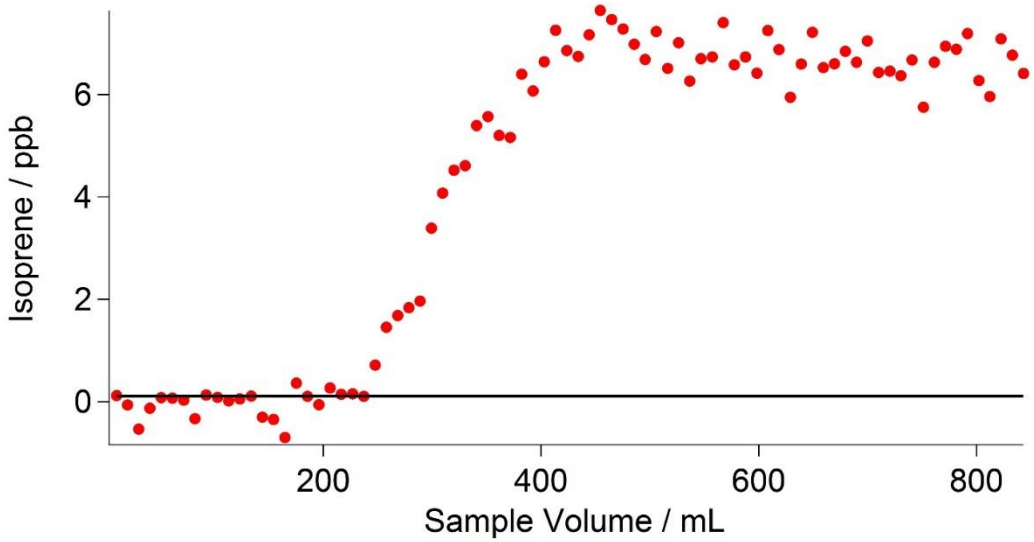

Figure 19 Results of the breakthrough volume tests. Each data point is an individual sample run of 10 mL. A solid black line indicates a threshold (set at LOD of 0.108 ppb), above which the breakthrough volume is exceeded. Negative points are due to a noisy baseline when the instrument does not register a peak

2.7.1.3 Co-elution of interfering species

The PID used in the iDirac is sensitive to all molecules with ionisation energies less than or equal to 10.6 eV, which includes the vast majority of biogenic and anthropogenic VOCs with the exclusion of ethane, acetylene, propane, methanol, formaldehyde and a number of halogenated hydrocarbons. It is therefore possible that species co-eluting at the same time as isoprene might be detected and erroneously identified as isoprene, thus leading to reporting spurious concentrations. The stationary phase in the main column is selected to achieve good separation of isoprene from VOCs of similar polarity and boiling point. This is tested in a series of co-elution experiments, in which the elution time of a number of potentially interfering species was determined and their separation from isoprene assessed. The VOCs under test were chosen based on the column specifications reported by the manufacturer, which identified i- and n-pentane, 1-pentene, trans- and cis-2-butene, 2-methyl-1-butene and 2-methyl-1-pentene as potentially co-eluting with isoprene. Gas samples containing 10-20 ppb of each interfering VOC are prepared in 3 L Tedlar bags by two-step dilutions from the pure substance using high-purity nitrogen. For each interfering species, the iDirac alternated between sampling from one of the Tedlar bags and sampling from a gas cylinder containing only isoprene in nitrogen. The results of these measurements are summarised in Figure 20: Figure 20a illustrates overlaid chromatograms for each species, whilst the individual chromatograms are shown in

Figure 20b-h. Figure 20i summarises the different elution times taking into account the width of each peak (full-width, half maximum) to better assess separation. The isoprene peak is well separated from all interfering VOCs, while poor separation is observed between cis- and trans-2-butene (which are not separated at all and appear as a single peak in Figure 20d) and 2-methyl-1-butene, as well as between i- and n-pentane. These results lend confidence to the unequivocal assignment of the isoprene peak in each chromatogram. Work is ongoing to determine the elution time of a wider range of compounds, including oxygenated products from the oxidation of isoprene.

Co-elution and multiple peaks appearing in a chromatogram are also addressed in the Mathematica script described in Section 2.5.3. To ensure that the isoprene peak is correctly assigned, the script looks for a peak in a relatively narrow region of the chromatogram, which is based on an interpolation of the elution time from the two nearest calibration runs. This algorithm has relatively low tolerance, so that peaks that are more than 4 seconds away from the predicted isoprene elution time are not considered.

A consistent discrepancy is observed in isoprene elution time between the calibration and sample runs. The elution time of isoprene is typically 1.7 s greater in a sample run than in a calibration run. This is an artefact of the trap adsorption process and the resulting tailing of the peak. For large volumes and low concentrations (e.g., a 150 mL field sample at 0.5 ppb), the isoprene band in the adsorbent trap is very broad and resides in the trap for a longer time, so it tails very strongly. For a high-concentration low-volume sample (e.g., a 12 mL calibration run at 10 ppb), the isoprene band in the trap adsorbent is sharp; it desorbs quickly and hence it tails less. This difference in elution times is much smaller than the distance to nearest interfering species (2-methyl-1-pentene, which elutes ~7 s before isoprene).

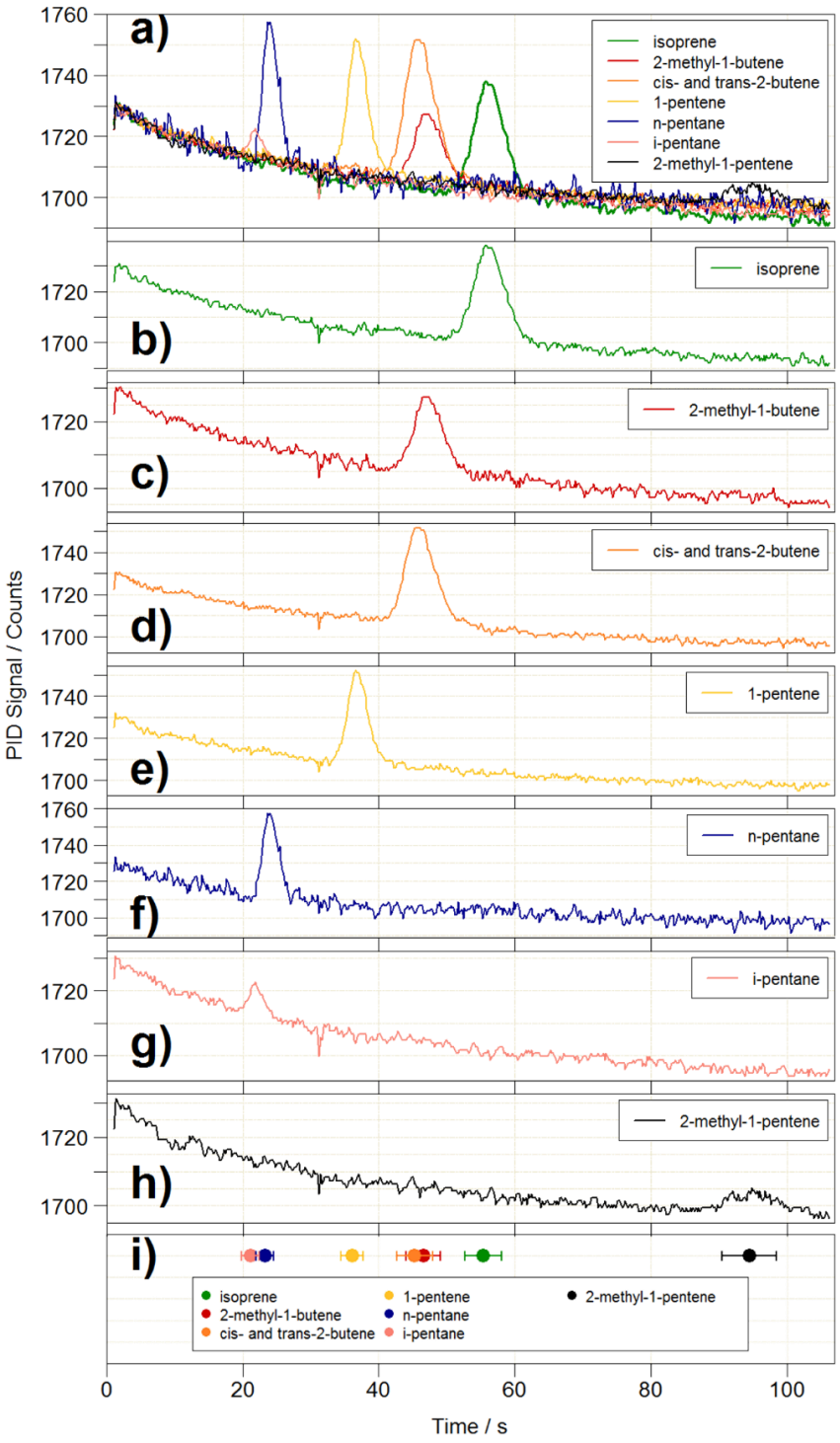

Figure 20 Results of the co-elution tests on the iDirac. a) Overlaid chromatograms of isoprene (green line) and six potential interfering species: 2-methyl-1-butene (red line), cis- and trans-2-butene (orange line), 1-pentene (yellow line), n-pentane (blue line), i-pentane (pink line) and 2-methyl-1-pentene (black line). The chromatograms of each individual species are shown in panels b)-h). The co-elution tests are summarised in h), where the elution time of each species (filled circles) is plotted along with its peak width (FWHM, error bars) to assess peak separation

2.7.2 Deployments of the iDirac in the field

The iDirac has been deployed in several large field campaigns that have provided an opportunity to evaluate the instrument performance. In these field deploymnets it was taken into consideration that the limit of detection for the grey iDirac was 34-40 ppt but the orange iDirac was only 108ppt. Two major field campaigns are described in this thesis.

Following laboratory development and testing, the iDirac had its first field deployment in Sabah (Malaysian Borneo) as part of the Biodiversity and Land-use Impacts on Tropical Ecosystem Function (BALI) Plant Traits campaign. The campaign was successful and demonstrated the capabilities for the iDirac to measure both ambient isoprene and individual leaf chambers. It also highlighted areas for instrument development (e.g., calibration routine) and several issues with instrument function (e.g., warm-up time) that have been addressed in subsequent instrument versions. This campaign ran from May to December 2015 and is described in depth in Chapter 3.

During the field deployments, the iDirac demonstrated its capability in terms of highly time-resolved measurements. For example in a high isoprene environment such as the tropical forest, the time resolution was from 4 - 5 minutes for continuous monitoring of ambient air in the day. This resolution allows the changing atmospheric concentrations of isoprene to be tracked effectively.

An effective evaluation for the performance of the iDirac over a long time period is provided by the WISDOM campaign. This campaign forms the basis for the majority of this thesis and is discussed in detail in Chapters 4–7. The campaign was another successful long term deployment of the iDirac, with successful measurements over six months. In particular the evaluation of the iDirac performance and the drift of the calibration plots are discussed in Section 5.3.1.

2.8 Conclusions and future work

The development and subsequent deployment of the iDirac is described, a novel autonomous GC-PID for isoprene measurements in remote locations. The instrument pre-concentrates ambient VOCs on an adsorbent trap and then separates them in a dual column system kept in an isothermal oven before detection by a photoionisation detector, achieving a limit of detection for isoprene in the field of 35-40 ppt. The rugged design and modular construction make the instrument easily customisable, while the open source

software control results in a straightforward instrument configuration. Designed for field deployments in remote environments with limited power supply, the iDirac weighs 10 kg (excluding gas supply), consumes minimum power and gas, can be run autonomously for months with little maintenance and can be exposed to harsh environmental conditions. The sensitivity and linearity of the instrument response can be tracked effectively with regular calibrations, increasing confidence in the quality of the data. The instrument has been demonstrated to function as desired in a tropical and temperate forest in two lengthy field campaigns, in particular in summer 2018 in an Oxfordshire forest with near continuous operation for almost six months. While this thesis focuses on using the iDirac for isoprene measurements, the instrument configuration can be changed to target different analytes. Future work will focus on monitoring different VOCs (e.g., DMS and ethylene), as well as improving on some of the current limitations of the instrument.

3 DEPLOYMENT OF THE iDIRAC IN TROPICAL FORESTS

3.1 Introduction

Most of the world's isoprene emission comes from tropical areas. Year-round consistency in daylight levels and heat, with the absence of a cold and dark season leads to higher growth rates in plants. As isoprene emission depends strongly on light intensity and temperature, the emission from tropical areas tends to be higher. A combination of a higher density of foliage and these higher emission rates means that the tropics account for 70% of global isoprene emission (Keller & Lerdau, 1999).

Isoprene is a very reactive species and the lifetime is short and at the equator, it is on the timescale of sub-hours (Achakulwisut et al., 2015). The short lifetime means that it is unlikely that it is transported high enough to reach the tropopause. However, isoprene breakdown products and other species have longer lifetimes and hence are more likely to reach higher in the atmosphere (Karl et al., 2007; Kuhn et al., 2007). In addition the photochemical degradation and subsequent reaction cascade of isoprene significantly alters the oxidative capacity of the tropical atmosphere and the concentration of O_3 (Paulot et al., 2012).

Understanding the atmospheric balance of the chemical species around the planet requires a combination of techniques to cover vast geographical areas. These techniques include lab studies, field measurements and modelling. The modelling stage provides the interpolation required to fill in the gaps and field campaigns can then 'ground truth' these models and verify their performance. It is even more key to verify model results in areas of special significance, such as areas of high emission or particular key transport processes such as in the tropics.

In the tropics, due to the often challenging nature of the environment, availability and location of equipment and the inherent challenges in transporting instruments to field sites, field studies are infrequent. As such, these areas are typically under-sampled,

despite their global importance and relevance to atmospheric science. Several large field campaigns have yielded some insight into tropical forest emissions and dynamics but there remains many open questions regarding isoprene emission from these areas. The 2008 intensive field campaign 'oxidant and particle photochemical processes above a South-East Asian rainforest' (OP3) in particular was a substantial field campaign addressing many of the unknowns and issues with the understanding of tropical forest atmospheric chemistry and yielded a great insight into the processes driving the chemistry of the area (Hewitt et al., 2010; Jones et al., 2011; Stone et al., 2011). However, the remaining questions, uncertainties and infrequency of measurements drives a need to undergo field campaigns to try to address this knowledge gap, verify model output and understand emissions in these key areas.

In many tropical areas around the world, large scale land use change is taking place and in Malaysian Borneo this is in the form of forest conversion to palm oil plantation. As a strong isoprene emitter, *Elaeis guineensis* (African oil palm) is likely to change the composition of the air (Hewitt et al., 2009). Also, with much disturbance to the forest, it is likely that the isoprene emission of the different phases of the conversion to oil palm plantation will be different (Stavrakou et al., 2014).

3.2 Aims

In 2015, an opportunity arose to deploy an instrument in a field campaign in an under-sampled region in Malaysian Borneo. In this campaign, there were a number of aims:

1. Deploy and test the iDirac in a first field trial.
2. Develop a method for measuring the emission of an individual leaf using the iDirac.
3. Take targeted measurements of individual leaves to calculate emission factors for tree species, many never sampled before.
4. Measure isoprene concentration at the canopy level in these under-sampled areas to reveal the differences in isoprene profile between different stages of deforestation.

3.3 Experiment description

3.3.1 Overview of the BALI and SAFE projects

The measurements reported in this chapter were made in the secondary and primary forest as part of the Biodiversity And Land-use Impacts (BALI) project. This project examines how the biodiversity, carbon cycle and ecological functioning of a tropical forest ecosystem is influenced by land-use change. The measurements described here were part of a field campaign in BALI called the Plant Traits campaign which examined how the leaf traits of the tallest trees varied across the land disturbance gradient. The BALI project uses the framework of the Stability of Altered Forest Ecosystems (SAFE) project, which is based in an area undergoing huge land-use change on the interface between oil palm plantation and primary forest. The SAFE project is situated across the disturbance gradient from primary forest, through the various stages of development to a mature oil palm plantation. A multitude of sites have been designated as reserved study areas for understanding the land-use change and how the natural ecosystem is affected (Ewers et al., 2011).

3.3.2 Descriptions of the three field sites

Three sites were chosen for isoprene measurements, one in a primary forest, one in a secondary forest and another in an oil palm plantation. A map of the locations of these sites is shown in Figure 21.

Figure 21 Map of Malaysia showing the location of the three study sites

The primary forest location was in the Maliau Basin, a pristine forest that has never been logged. The forest is characterised by high biodiversity, large trees (predominantly *Dipterocarpaceae*) and a typical tropical climate of high humidity, high rainfall and high temperatures. A field research station has been located on the site since 2011 with several study plots, each slightly different in plant composition and aspect. The two sites used for this study were Seraya (4.754° N, 116.950° E) and Belian (4.747° N, 116.970° E). Each plot has large trees, with a canopy height of ~60 m and as a result the shaded understory is generally clear of foliage. The Maliau Basin was measured from July to August 2015.

The secondary forest location was on the interface between the oil palm plantation and the primary forest at the main SAFE study site, which is located near Tawau in Eastern Sabah (Ewers et al., 2011). The forest is characterised by varying levels of disturbance, from 'mature' secondary forest that was selectively logged 30 years prior to cleared land. The understory of the forest generally has dense foliage, with a high concentration of pioneer species; those which grow rapidly on disturbed land. There is an abundance of forest gaps and the trees present are typically much smaller and younger. The broken canopy causes the forest floor to receive more light and heat and there is generally greater air movement. The SAFE project is located at 4.716° N 117.709° E and three study plots were used for ambient measurements; B North, Plot E and the Tower site. B North is a sloping degraded forest with many fallen logs, small saplings, dense undergrowth surrounded in completely logged forest. Plot E is a sloping forest and has more developed trees and is generally less degraded than B North, though with an abundance of undergrowth and pioneer species. The Tower site is the location of the flux tower and is characterised by a large forest clearing that is kept clear of tall vegetation. Measurements from the SAFE site occurred from November to December 2015, which was before a particularly dry period.

The oil palm site was a mature oil palm plantation near Pekan in the state of Pehang on the east coast of the Malaysian Peninsula. The oil palm is typical of a plantation, with a monoculture of *Elaeis guineensis* and very little undergrowth and fewer other species present. A weather station on site provided some meteorological data for the measurements. The instrument inlet was 5 m above the canopy of the oil palm on from the first level of a flux tower situated at 3°26'17.8692" N, 103°23'23.8056" E. A full site description is given in Nadzir et al., (*in prep.*). The oil palm measurements were taken from December 2016 to January 2017.

Table 2 shows an overview of the study sites.

Table 2 Summary of study sites measured

Site	Forest Type	Coordinates	Measurements	Dates Visited
Seraya, Maliau Basin	Primary	4º 44’ N, 116º 58’ E	Leaf traits & ambient levels	Jul-Aug 2015
Belian, Maliau Basin	Primary	4° 44′ N, 116° 58′ E	Leaf traits & ambient levels	Jul-Aug 2015
Plot E, SAFE	Secondary, moderately degraded	4°43'N 117°36'"E	Leaf traits & ambient levels	Nov-Dec 2015
Plot B North, SAFE	Secondary, severely degraded	4°43'N 117°36'"E	Ambient levels	Nov-Dec 2015
Tower Plot, SAFE	Secondary, severely degraded	4°43'N 117°36'"E	Ambient levels	Nov-Dec 2015
Pekan Oil Palm Plantation	Oil palm monoculture	3°26’N, 103°23’E	Ambient levels	Dec 2016 – Jan 2017

3.3.3 Leaf level measurement method

At the primary and secondary forests, there was opportunity to measure isoprene directly from the leaves to obtain a value for the emission factor of that species. The experimental design involved using the iDirac to take samples from cuvettes containing single leaves. The sites sampled are indicated in Table 2.

The measurements focus on leaves taken from the canopy of the tropical trees. The study took leaves from branches cut from the top of the canopy and ran a series of tests on them. The measurements were taken on single leaves and were done for three leaves on a branch. Individual trees typically had one branch sampled, but on occasion two branches were sampled to compare a sun branch to a shade branch. No repeats were done from the same branch, though the same species were sampled repeadly but from different individual trees. Other measurements taken included photosynthesis measurements, leaf reflectance, leaf area and wood density.

The iDirac set-up is shown in Figure 22. The experiment involved taking branches from large trees on the study site, placing this into a bucket of water to minimise stress, and measuring the isoprene concentration from three leaves from that branch. The measurement site was done in the shade of the canopy and out of direct sunlight. The three measurements were preceded with an ambient air measurement of isoprene to get an indication of the background level. The cuvette was a clear plastic Ziploc bag and air from this bag was pumped through an external pump at a rate of 1 $Lmin^{-1}$. Leaves were chosen that represented the entire branch, were of full maturity, of an average size and leaves with herbivory or other physical damage were excluded.

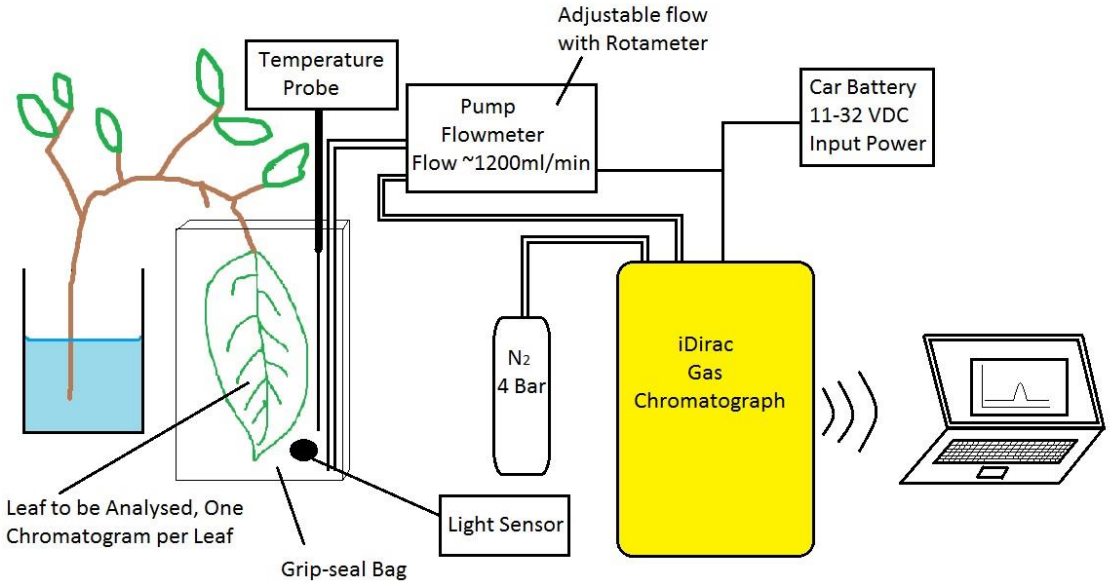

Figure 22 Leaf traits measurement set-up showing how a cuvette was used to sample emission from individual leaves and what other measurements were taken

In addition, a light intensity measurement (photosynthetically active radiation (PAR)) was taken with a Skye Quantum Sensor at the time of the measurement and a temperature probe was placed inside the cuvette.

Before measurements began there was a 30 min warm-up period before the iDirac became operational, where ambient samples were run continuously. If there was a delay in leaf acquisition, the iDirac ran ambient samples so as not to cool down. If the column was allowed to cool, a warm up period was ran again; otherwise the peaks in the chromatogram were shifted and may have become truncated.

To calculate an emission factor for each tree species, the measured background isoprene

mixing ratio is subtracted from the cuvette mixing ratio and is converted to concentration with the ideal gas law and the volume of the sample. From the flow of the pump, it is then possible to calculate the rate of production of isoprene from the leaves in the cuvette. The change of concentration in the cuvette is represented with *Equation 1* (Aneja et al., 2006).

$$\frac{dC}{dt} = \frac{q[C_{air}]}{V} + \frac{IA}{V} - \frac{CLA_w}{V} - \frac{Cq}{V} - R \qquad \textit{Equation 1}$$

Table 3 shows what each term in *Equation 1* represents.

Table 3 Equation terms summary

	Parameter	Unit
C	Chamber concentration	$molm^{-3}$
t	Time	s
q	Flowrate	m^3s^{-1}
C_{air}	Incoming air concentration	$molm^{-3}$
V	Volume	m^3
I	Isoprene emission rate	$molm^{-2}s^{-1}$
A	Area of emitting surface	m^2
L	Wall loss rate	ms^{-1}
A_w	Cuvette inner surface area	m^2
R	Chemical reactions	$molm^{-3}s^{-1}$

Several assumptions allow us to use this equation to calculate I, the isoprene emission of the leaf. Firstly it is assumed that due to the short sampling time of 1-3 minutes and hence short residence time in the cuvette, the wall losses and the chemistry are negligible and they can be set to 0. Secondly, as the volume of the cuvette is small (0.5 L) the system can be assumed to be at steady state so $\frac{dC}{dt} = 0$. The equation can then be rearranged to calculate the emission rate, as shown in *Equation 2.*

$$I = \frac{q(C - C_{air})}{A} \qquad \textit{Equation 2}$$

Once a base rate has been calculated using the concentrations, the flowrate and the area of the leaves in the cuvette, this has to be normalised for light and temperature. To do this the Guenther equations (Guenther et al., 1993) are used to calculate the emission factor at a standard light and temperature, 1000 μmolm^{-2}s^{-1} and 30ºC respectively. These equations are shown in *Equations 3, 4 and 5.*

$$I = I_S C_L C_T \qquad \textit{Equation 3}$$

$$C_L = \frac{\alpha C_{L1} L}{\sqrt{1 + \alpha^2 L^2}} \qquad \textit{Equation 4}$$

$$C_T = \frac{exp\frac{C_{T1}(T - T_S)}{RT_S T}}{1 + exp\frac{C_{T2}(T - T_M)}{RT_S T}} \qquad \textit{Equation 5}$$

In *Equation 3*, I is the emission rate of isoprene, I_s is the emission factor, the emission at a standard temperature and light intensity which is unique to each individual. C_L and C_T are scaling factors for light and temperature respectively. *Equation 4* calculates the normalisation factor for light, C_L, where α and C_{L1} are empirically determined coefficients, 0.0027 and 1.1066 respectively and L is the PAR at the time of measurement. *Equation 5* calculates the normalisation factor for temperature where C_{T1} is empirically determined as 95000 J mol^{-1}, T is the temperature of the measurement, T_s is the standard temperature (303 K), R is the ideal gas constant (8.314 JK^{-1}mol^{-1}), C_{T2} is also empirically determined as 230000 Jmol^{-1} and T_M is the optimum temperature for isoprene production of 314 K (Guenther et al., 1993).

It is these emission factors that are the final values that can be used to compare different trees and species as they have been normalised for light and temperature.

3.3.4 Ambient air isoprene concentration measurement method

While in the tropical forest environment, periods of inactivity where individual trees were not being measured were used to take opportunistic measurements of ambient levels of isoprene and how this varies throughout the day. In many cases, these measurements covered a full 24 hour period, so it was possible to capture the diurnal pattern of isoprene in these locations.

In general, these experiments consisted of the iDirac, securely strapped at a height of 1 m to a tree, with a car battery placed on top and a 1.2 L adjacent nitrogen cylinder also

securely fastened. The tree was chosen in an area that represented each study plot and represented the forest environment. To provide additional waterproofing, a plastic bag was draped over the entire set-up and secured. A typical set-up with and without the waterproof cover is shown in Figure 23. The iDirac was run continuously with a single inlet, without any calibration runs. The PTFE inlet line was 0.05 m long and incorporated a 0.45 µm polyethersulfone filter to avoid particles entering the instrument. To increase the sensitivity of the iDirac the volume of the sample was 100 mL, making it possible to detect the very low concentration of the late evening and early morning. Most of the ambient runs were 24 hours or less, though one run spans 48 hours as the battery was replaced. Calibration of the data was done using the same calibration runs as the leaf traits data and is described in Section 3.3.5. The calibration curve used was chosen as the closest one in time to the ambient run.

Figure 23 iDirac deployed in primary forest to measure ambient isoprene concentration A) With waterproof cover B) Without waterproof cover.

3.3.5 Calibration of the data in the field

Periodic dedicated calibration runs were performed to calibrate the sample data. These calibration runs were completed in the evenings with a field calibration cylinder that had its concentration determined at a later date in the laboratory as discussed in Section 2.6.2.2. No sample runs were done during the calibration period and the runs were ~3 hours long, providing enough chromatograms for a representative calibration curve.

Because of this method of calibration, the sample data isoprene peaks were selected by interpolation of the relationship with retention time and column temperature. The relationship of column temperature and retention time is linear so the isoprene peak can

be accurately selected. This method of calibration was discontinued after this field campaign and periodic calibrations were used instead as described in Section 2.6.1.

To determine which calibration run to use for the data, the nearest calibration run in time for the same instrument was selected so as to give a representative level of sensitivity.

3.3.6 Evaluation of the iDirac performance in the tropical forest

The iDirac performed well in its first field deployment given that it was in the tropical forest environment. Powering an instrument such as this in remote environments is a challenge and hence the measurements were limited to the lifetime of a portable car battery. The environmental conditions did not affect the results, for example there was no evidence that high relative humidity, high temperatures or heavy rain influenced the data quality. Problems that abruptly halted the measurements were technical limitations such as memory allocation or the failure of an internal valve. The occurrence of these problems was useful in the development of protocols for preventing these issues in future deployments. Other issues were human errors such as sucking in bucket-water through the pump or mistakenly using an empty nitrogen cylinder.

One issue that is highlighted in these measurements is the gradual degradation of the absorbent trap. As the instrument absorbs repeat samples with high concentrations of VOCs it seems that there is a gradual poisoning of the trap with non-linear calibration plots indicating poor adsorption and breakthrough of the trap. An extreme example of this issue is when the nitrogen is exhausted, the trap gets heated in the presence of oxygen and causes a dramatic degradation of the trap. This problem has been solved by integrating a fail-safe flowmeter that switches off the trap heater when the nitrogen flow is lowered.

3.4 Results and discussion of leaf level measurements

3.4.1 Results from the leaf level measurements

In total 173 different branches were successfully measured, which corresponded to 162 different trees and 80 species of trees in three locations. The trees sampled represent the tallest trees in the canopy and ranged from primary pristine forest to disturbed secondary forest.

An example of six trees are reported here with the highest isoprene emission factors for the different study plots in Table 4, Table 5 and Table 6. The standard deviation was calculated from the mean of the three measurements that make up each value. For a full

list of all the species measured, see Appendix 2. The thirty highest emitting branches are represented graphically in Figure 24. It is noted that some of the trees on this list have not been identified to date.

Table 4 Isoprene emission data for the highest emitting tree species measured at Plot E at the SAFE site.

Species	Tree Code	Measured emission rate / $nmolm^{-2}s^{-1}$	Measured emission rate standard deviation / $nmolm^{-2}s^{-1}$	Emission factor / $nmolm^{-2}s^{-1}$	Emission factor standard deviation/ $nmolm^{-2}s^{-1}$
Litsea graciae	ESA-T3577-B1S	7.2×10^4	3.7×10^4	3.0×10^6	1.5×10^6
Artocarpus anisophyllus	ESA-T15-B1S	2.4×10^3	2.2×10^3	6.2×10^5	5.7×10^5
Macaranga pearsonii	ESA-T379-B1SH	1.3×10^3	1.3×10^3	1.7×10^5	1.7×10^5
Cleistanthus paxii	ESA-T152-B1SH	3.1×10^3	4.2×10^3	9.4×10^4	1.3×10^5
To be identified	ESA-T377-B1S	7.4×10^2	1.0×10^3	7.4×10^4	1.0×10^5
Macaranga gigantea	ESA-T42-B1S	91	87	7.3×10^4	7.0×10^4

Table 5 Isoprene emission data for the highest emitting tree species measured at Belian at the Maliau Basin.

Species	Tree Code	Measured emission rate / $nmolm^{-2}s^{-1}$	Measured emission rate standard deviation / $nmolm^{-2}s^{-1}$	Emission factor / $nmolm^{-2}s^{-1}$	Emission factor standard deviation/ $nmolm^{-2}s^{-1}$
Dryobalano-ps lanceolata	BEL-T297-B1S	2.1	1.7	2.7×10^4	2.2×10^4
Horsfielda walichii	BEL-T358-B1SH	6.2	2.9	2.0×10^4	9.1×10^3
Lithocarpus gracilis	BEL-T101-B1S	2.2	5.5	1.4×10^4	3.5×10^4
Reinwardtiode -ndron humile	BEL-T285-B1SH	3.2	2.9	9.8×10^3	8.9×10^3
Hydnocarpus woodii	BEL-T337-B1SH	9.2	12	5.1×10^3	6.9×10^3
Shorea parvifolia	BEL-T195-B1S	0.9	0.8	2.8×10^3	2.7×10^3

Table 6 Isoprene emission data for the highest emitting tree species measured at Seraya at the Maliau Basin.

Species	Tree Code	Measured emission rate / $nmolm^{-2}s^{-1}$	Measured emission rate standard deviation / $nmolm^{-2}s^{-1}$	Emission factor / $nmolm^{-2}s^{-1}$	Emission factor standard deviation/ $nmolm^{-2}s^{-1}$
Sindora irpicina	SER-T97-B1S	13	5.5	1.2×10^4	5.3×10^3
Ochanostachys amentacea	SER-T217-B1SH	2.9	5.2	9.1×10^3	1.6×10^4
Parartocarpus bracteatus	SER-T471-B1S	8.3	3.2	6.2×10^3	2.4×10^3
Canarium decumanum	SER-T309-B1S	7.4	6.6	5.5×10^3	5.0×10^3
Dryobalanops lanceolata	SER-T308-B1S	0.7	7.5	3.6×10^3	3.7×10^4
Neonauclea gigantea	SER-T189-B1S	1.0	0.5	3.0×10^3	1.5×10^3

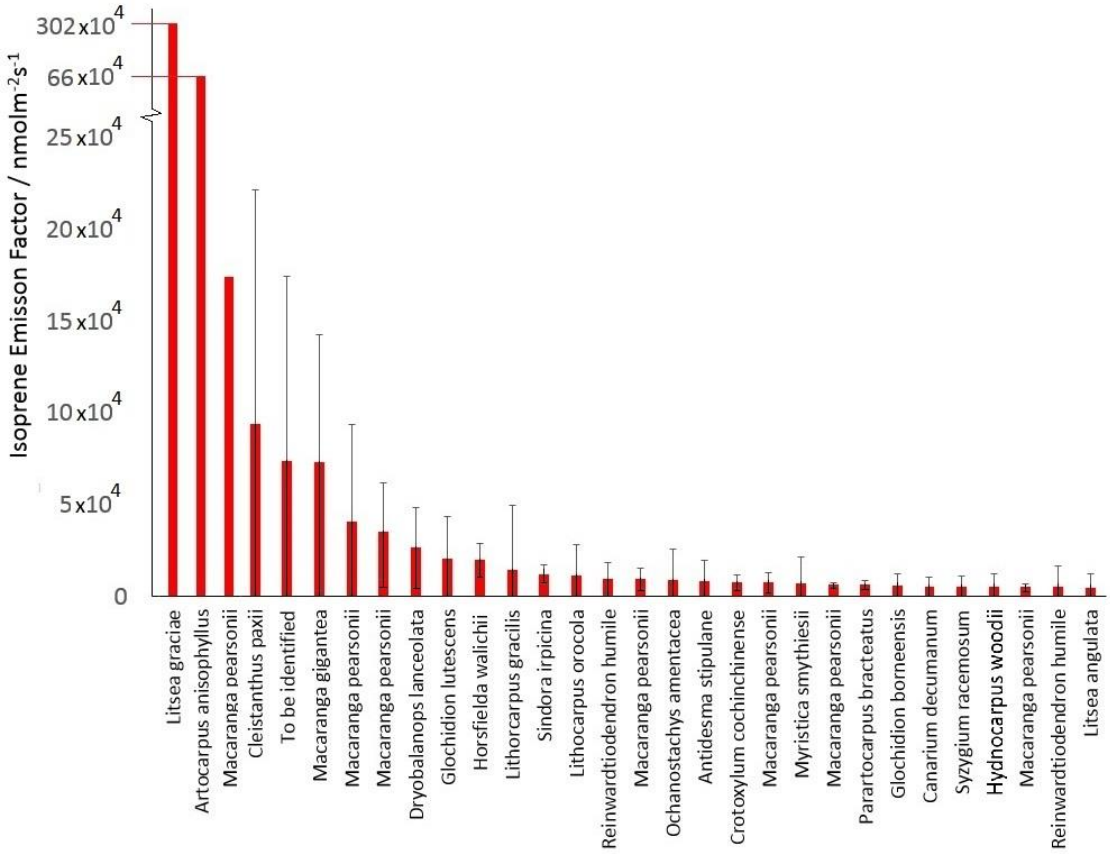

Figure 24 Bar graph showing the 30 highest emitting trees. Individuals with an exceptionally high emission factor have been shown on a cropped portion with error bars omitted to avoid cluttering the plot

3.4.2 Discussion of the leaf level measurements

3.4.2.1 Evaluation of methods to determine emission factor

In the field, and particularly an environment such as that in Malaysian Borneo, there are many challenges to be faced with conducting field experiments. As such, compromises have to be made. The Plant Traits campaign was a campaign that was joined at the last minute, hence the experimental design was constructed at very short notice. The focus was on deploying the iDirac, then a prototype instrument, in the field for the first time. The method used for sampling the emissions from individual leaves had several flaws that could not be remedied in the field without significant delays and rethinking large amounts of the sampling.

Initially the effluent from the LI-COR photosynthesis cuvettes were used for the isoprene measurements, but it was found that the use of the iDirac significantly delayed the measurement schedule and was not practical in field conditions. The benefit of the LI-COR is that the conditions in the cuvette could be controlled and monitored precisely.

The cuvette used for the measurements was a clear Ziploc bag, with limited control of the conditions that the leaf encountered. The material of the bag is not completely inert and could not be kept clean or dry, so wall losses may have been significant or the moisture inside the bag could have affected the stomatal conductance of the leaves. The size of the bag was an issue, as with leaves of vastly differing size different bags had to be used. The flow through the bag was controlled with a pump and maintained at 1 $Lmin^{-1}$, but the air was drawn through holes in the cuvette with differing size and likely varied the residence time in the bag. The bag volume likely changed with each sample as the degree at which the leaf pressed against the walls varied. All these factors likely affected the quality and reliability of the results, despite best efforts to maintain good and repeatable practice.

The site of the measurements likely affected result quality, often measurements were done in shaded conditions under a tarpaulin under the canopy and occasionally it was raining heavily and very cloudy. Such conditions are not ideal for emissions of isoprene from plants, and particularly with higher humidity associated with rain the stomata on the leaves were likely partially shut.

Another aspect that may have affected the result was the shock that could have been experienced by the branch after being cut from the tree. It is generally accepted that a tree branch does not respond immediately to amputation with decreased photosynthesis and that there can be some time before leaves start to decline (Both et al., 2019). This is the technique used globally to measure other plant traits from tree species (Pérez-Harguindeguy et al., 2016). Simple laboratory experiments with a *Eucalyptus globulus* have indicated that isoprene emission continues after amputation and declines very slowly if the branch is placed in water. It is difficult to quantify the effect of this shock on the leaf emission, but this needs to be factored into an uncertainty budget for the measurements.

3.4.2.2 General discussion of the leaf level measurements

From the results of the individual leaf measurements it is clear that there is a lot of variation not only between different tree species, but also between trees of the same species. The values are generally very large, with an extremely large variation across the dataset. From other studies by Langford et al. (2011) values for isoprene emission from the forest are in some cases lower by a factor of 1,000. These differences and large values could be due to experimental difficulties experienced in the field. There is a clear increased signal associated with tree species that have a strong isoprene emission factor.

However there is error associated with each value as a result of the cumulative effect of the iDirac uncertainty, the variation in measurement between adjacent leaves and the environmental conditions at the time of measurement. The largest source of error comes from using the three leaf measurements, which can be orders of magnitude different from each other. In this discussion, the error shown is the standard deviation from the three chromatograms from that branch.

Trees that do not emit isoprene typically result in an apparent negative emission when the ambient sample concentration is greater than that in the cuvette. These values of isoprene emission factors are set to 0 $nmolm^{-2}s^{-1}$ but that within error they may be emitting. It is assumed that if the concentration in the bag is greater than that of the ambient sample then emission has taken place. Variations in the background level have been accounted for by taking the mean of the preceding and proceeding ambient samples. It is often the case that the standard deviation of the mean emission factor is greater than the absolute value, hence within error the species may be a non-emitter.

Many factors affect isoprene emission from a tree, namely the conditions and stresses the tree experience. This means that the habitat and environment of a tree can have a very large effect. Factors such as aspect, soil moisture, CO_2 concentration, age, degree of herbivory and exposure to the tree species of the surrounding forest can all affect the emission of isoprene of an individual tree as discussed in Chapter 1. With these measurements, even after normalising for temperature and light level, the emission factor calculated varies widely even for the same species.

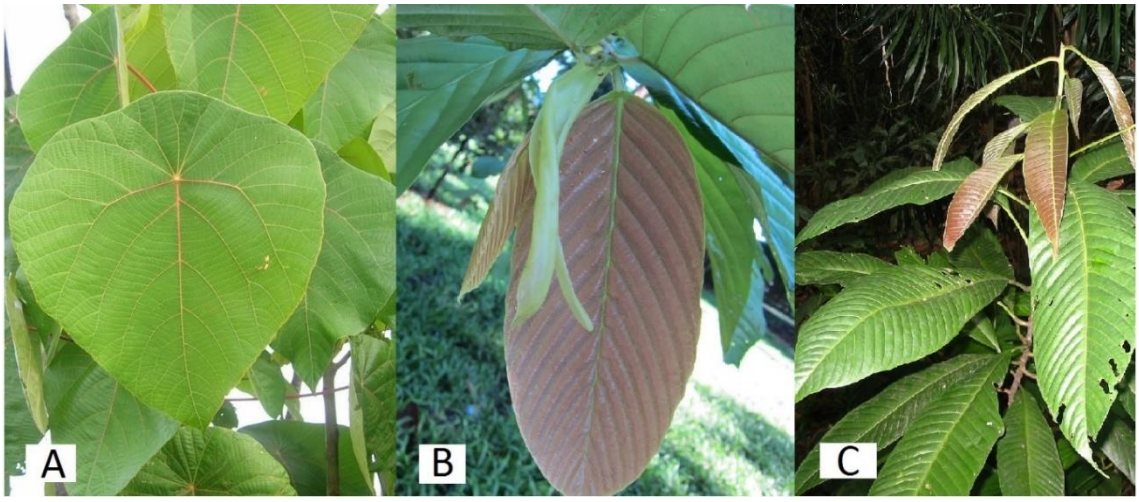

Figure 25 Photographs of A) Macaranga pearsonii B) Parashorea tomentella C) Eusideroxylon zwageri

Three species from the measurements are examined in detail here, the species are selected for the availability of isoprene emission data from multiple individual branches. The trees shown in Figure 25 are *Macaranga pearsonii, Parashorea tomentella and Eusideroxylon zwageri* which represent common trees in the Sabah rainforest and each show different isoprene emission characteristics.

Macaranga pearsonii is a typical pioneer species in the *Euphorbiaceae* family that is commonly found in disturbed forest. The species is fast growing and has large wide leaves. The stems of *M. pearsonii* have a symbiotic relationship with ants and are typically inhabited with an ant colony which can be indicator of forest health (Fiala et al., 1994). Seven different trees were sampled for isoprene emission factor, all from the secondary forest at Plot E and these are shown in Figure 26. Again, high variation is observed between the different trees but every instance of *M. pearsonii* has a high isoprene emission factor.

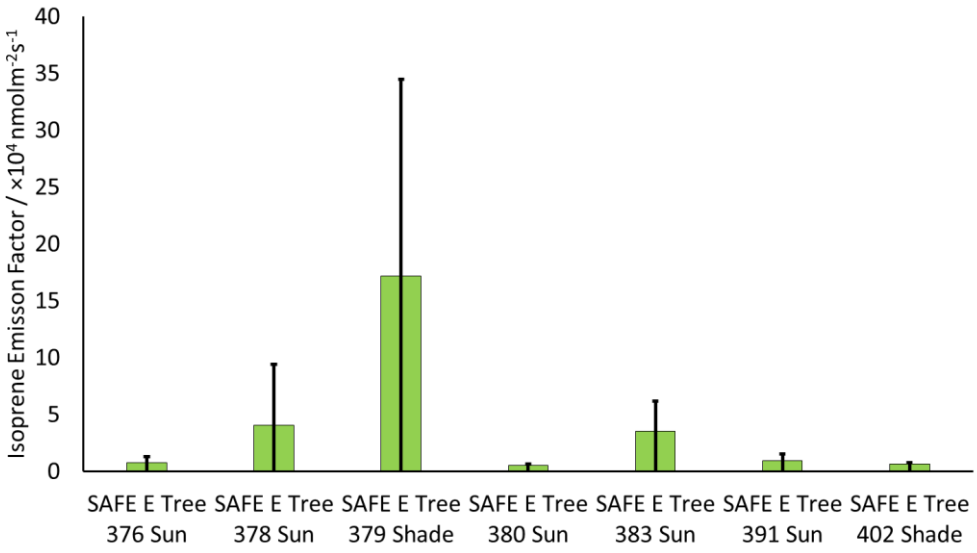

Figure 26 Emission factors for seven Macaranga pearsonii individual trees

In terms of the species distribution, there may be some changes in the isoprene emission structure as the primary forest is sequentially logged. One key pioneer species is *M. pearsonii* and others in the genus *Macaranga* which would likely increase the emission potential of the forest to a great extent. In general it is observed that species sampled from the secondary forest have a higher emission factor. This may be due to the higher temperatures and light intensity in the forest, or it could reflect the changing species distribution in these areas.

Parashorea tomentella is in the *Dipterocarpaceae* family and is a very tall tree native to eastern Borneo. Like many others on the list of species it is threatened by habitat loss. It is a broad leaved evergreen with large leaves. Of the five trees sampled over two field sites at Maliau a positive isoprene emission was not recorded, though the variation in the samples could indicate that it may be a very weak emitter. Figure 27 shows the data for this species and that different trees showed different variations but that each tree indicated no isoprene emission.

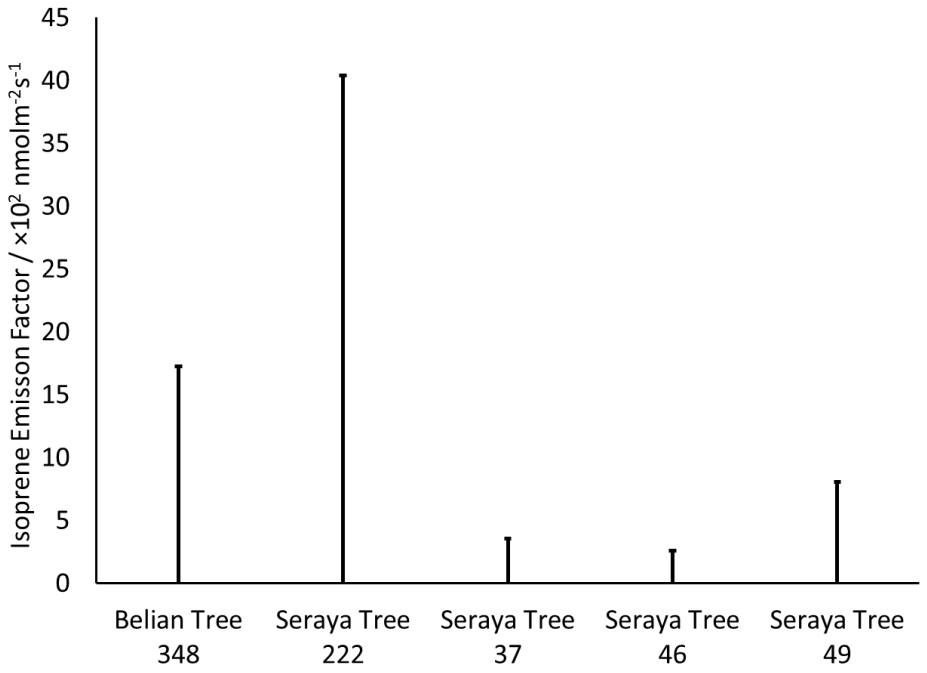

Figure 27 Emission factors for five Parashorea tomentella trees, each value reported is a sun branch and one individual was situated at Belian

Eusideroxylon zwageri is native to the islands of Southeast Asia in the family *Lauraceae* and is a highly prized tree for timber, though is threatened by over exploitation. This very tall tree is slow growing and has large elongated leaves. The isoprene emission factors were measured for 15 individual branches at all three leaf-traits sites and shows highly variable emission data. The emission factors shown in Figure 28 ranged from 2700 to 0 $nmolm^{-2}s^{-1}$ indicating that there is a high degree of variation between trees.

E. zwageri also allowed a comparison between sun and shade branches and between sites as an individual tree from each site was sampled both from a sun branch and a shade branch. Figure 29 shows a summary of this data and reveals that the sun branches appear to show a reduced isoprene emission factor and that at Plot E at the SAFE site *E. zwageri* is not an isoprene emitter, but that the standard deviation indicates that it could emit.

These results do not fit with the hypothesis that the emission factor is increased for sun branches or that the same species have comparable emission factors. This result is limited by the shortcomings of the experimental method and likely demonstrates that there is a high degree of inherent variation between different trees.

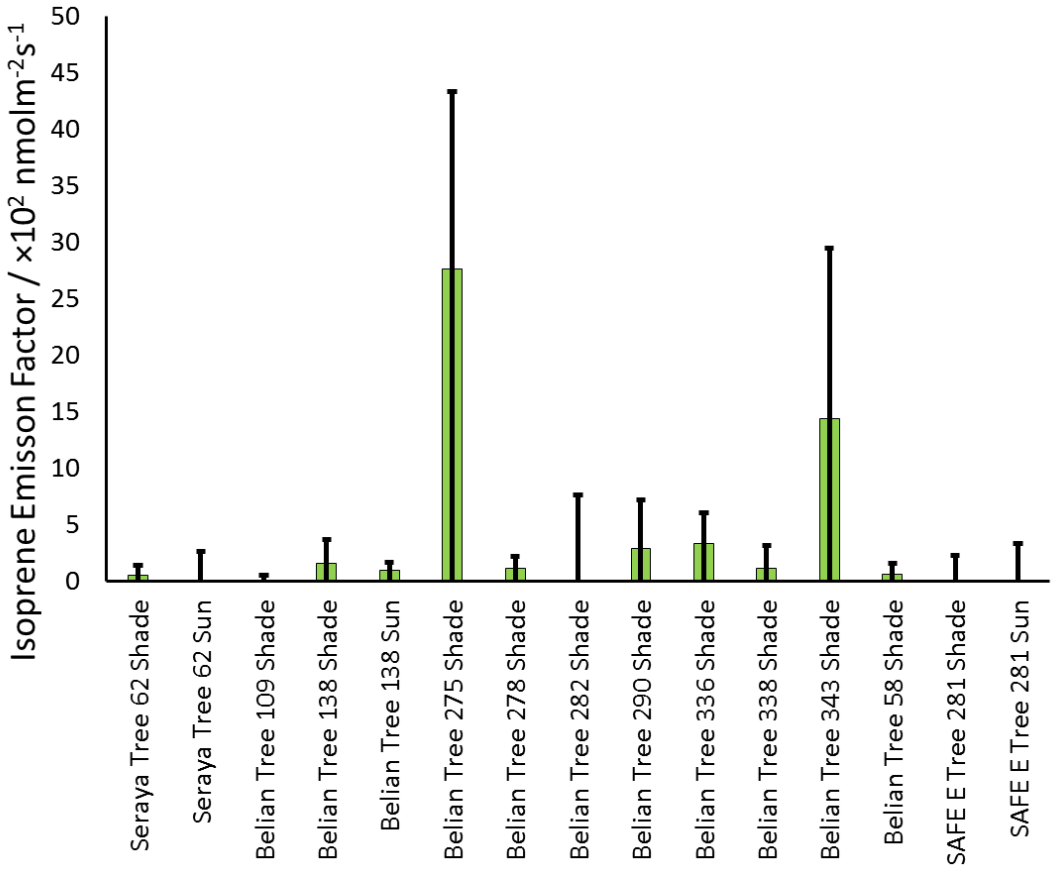

Figure 28 Isoprene emission factors for 15 Eusideroxylon zwageri trees

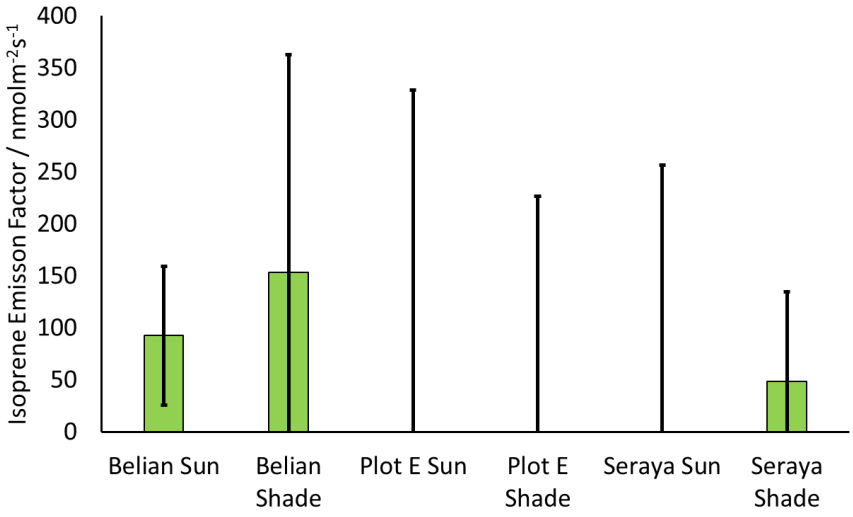

Figure 29 Comparison of sun and shade branches and sites for the isoprene emission factor of Eusideroxylon zwageri

To investigate what conditions have influenced the emission factor of species from the different forest types, further work is required. This study indicates that there are some key differences in emission characteristics between different sites and even between the same species. A future study could focus on determining if the same species are experiencing different conditions between sites and could focus on a couple of key species for study, such as the three described here.

3.5 Ambient isoprene measurements of isoprene concentration

3.5.1 Isoprene concentration profiles from the primary forest

In total four canopy level isoprene concentration profiles were recorded in the primary forest sites. The results of these runs are shown from Figure 30 to Figure 33. The results show a strong diurnal profile of isoprene, with peak isoprene around 14:00 local time but with a high degree of variability. The concentrations typically dropped to 0 ppb at night and the highest concentration reached was ~3 ppb.

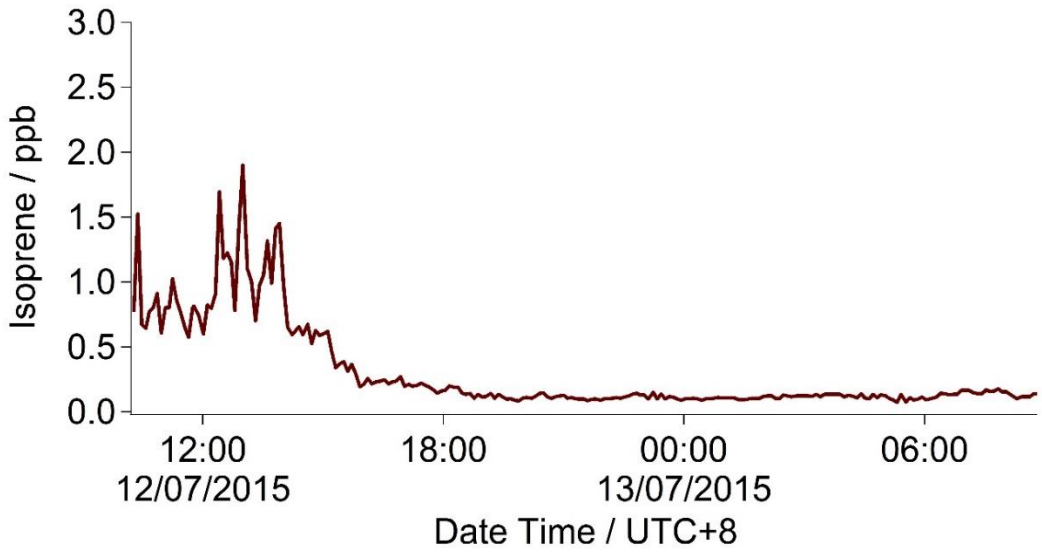

Figure 30 Belian ambient isoprene from 12th-13th July 2015. The inlet was situated at 1 m above the forest floor in a shaded environment with little undergrowth and large tree trunks

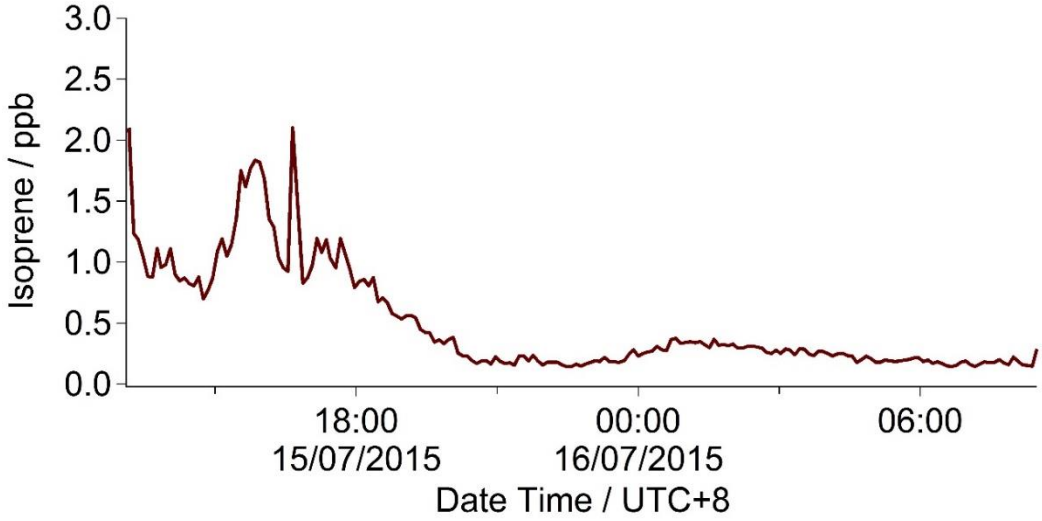

Figure 31 Belian ambient isoprene from 15th-16th July 2015. The inlet was situated at 1m above the forest floor in a shaded environment with minimum undergrowth and large tree trunks

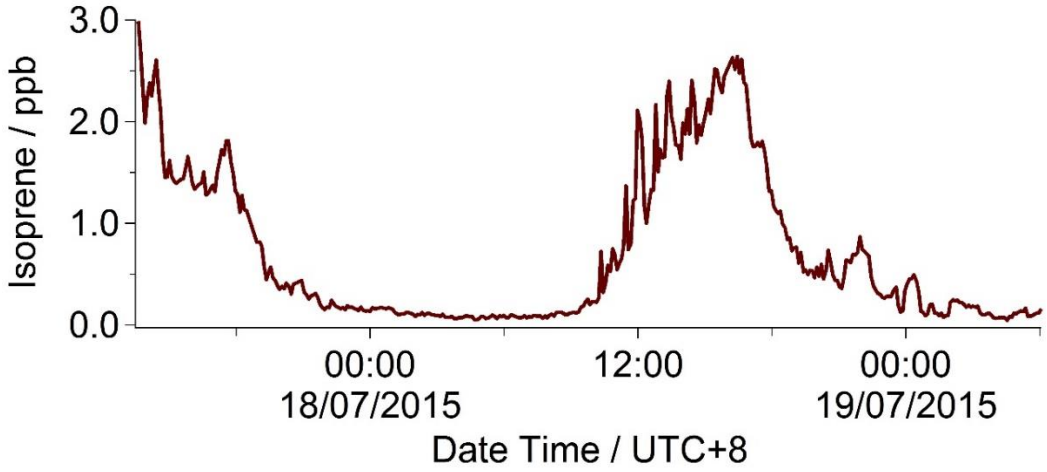

Figure 32 Belian ambient isoprene from 18th-19th July 2015. The inlet was situated at 1m above the forest floor in a shaded environment with minimum undergrowth and large tree trunks

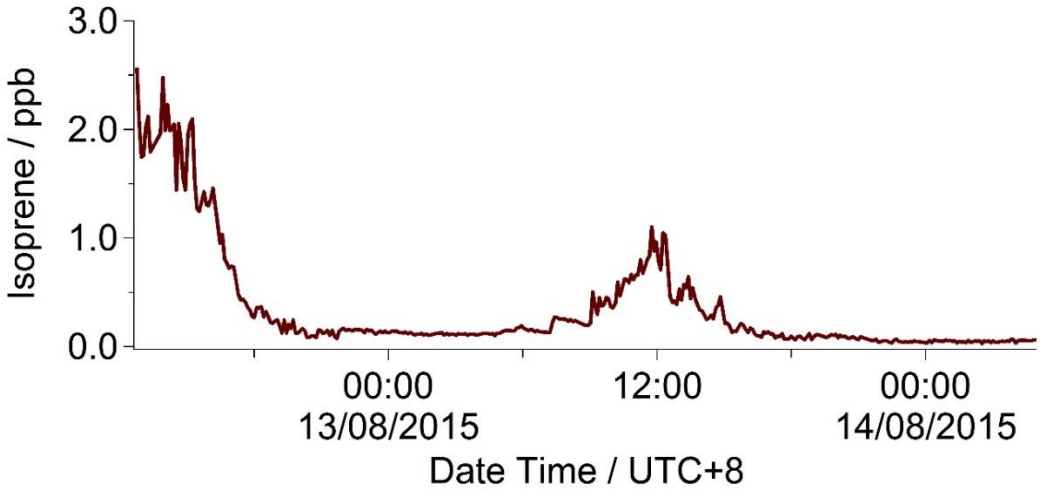

Figure 33 Seraya ambient isoprene from 13th-14th August 2015. The inlet was situated at 1m above the forest floor in a shaded environment with minimum undergrowth and large tree trunks

3.5.2 Isoprene concentration profiles from the secondary forest

In total five canopy level isoprene concentration profiles were recorded for the secondary forest sites. The results of these runs are shown from Figure 34 to Figure 38. The isoprene concentration in the secondary forest showed a diurnal profile with a maximum around 14:00 local time and dropping to 0 ppb at night. The concentrations were much higher, reaching as high as 20 ppb in places. It is also observed that the temporal and spatial variation in the concentration is greater.

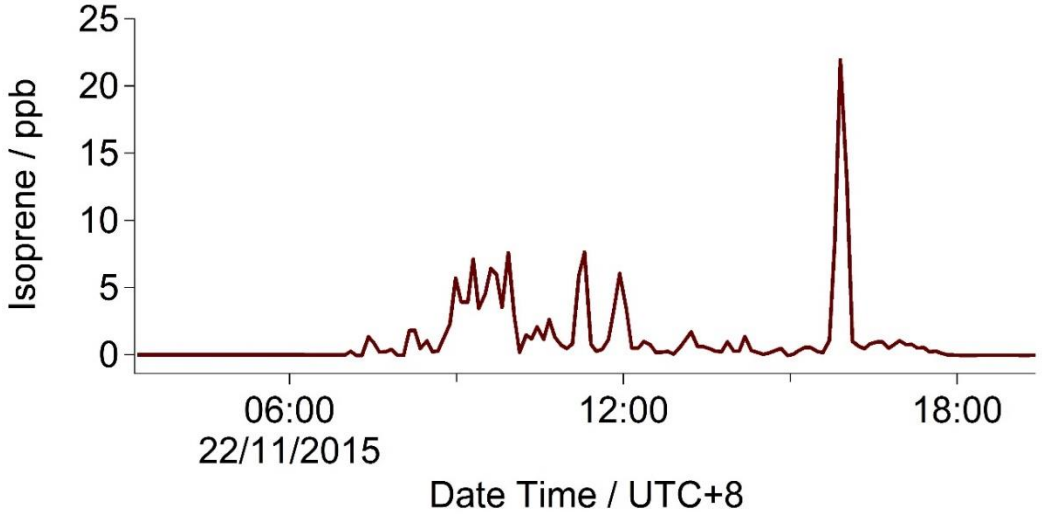

Figure 34 Plot E at the SAFE site ambient isoprene on 22nd November 2015. The inlet is situated at 1 m in a degraded forest, with many small trees and undergrowth and a disturbed canopy

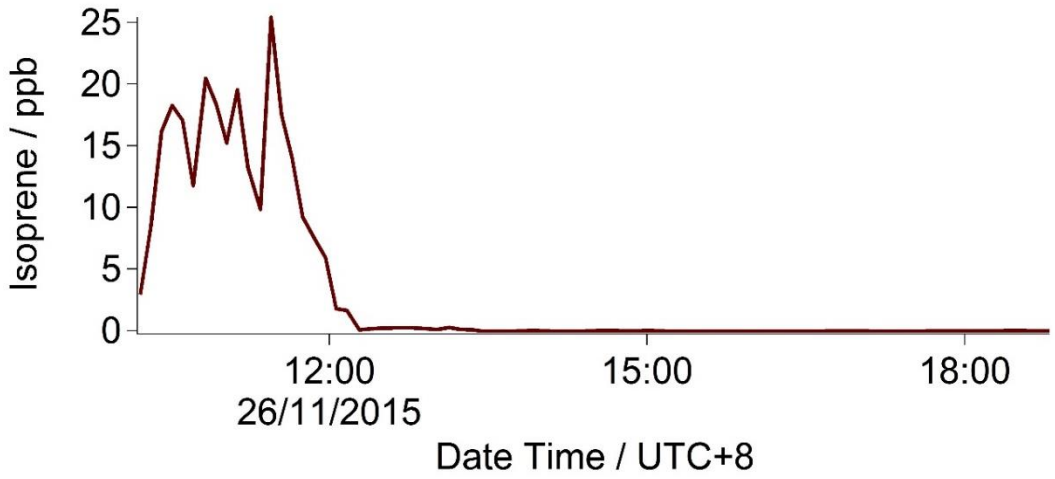

Figure 35 Plot E at the SAFE site ambient isoprene on 26th November 2015. The inlet is situated at 1 m in a degraded forest, with many small trees and undergrowth and a disturbed canopy

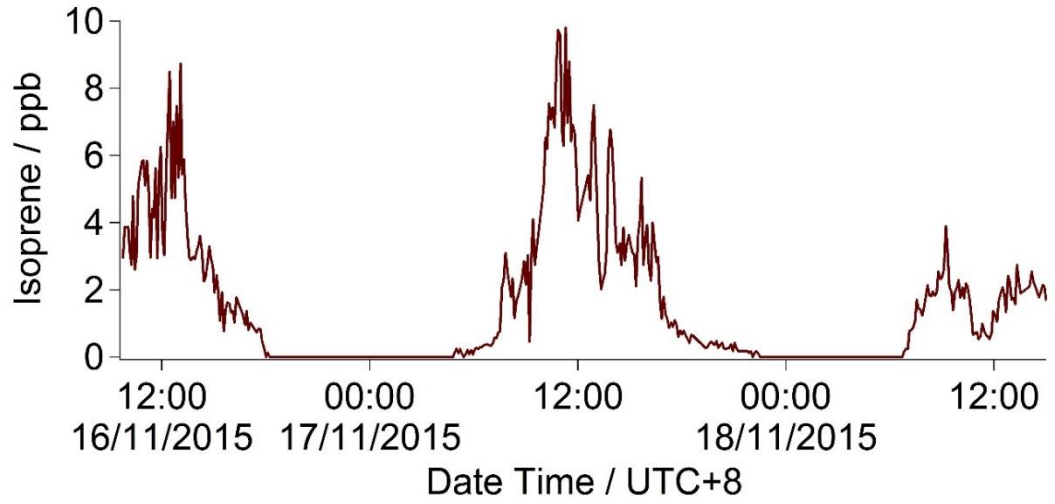

Figure 36 Tower Plot at the SAFE site ambient isoprene from 16th-18th November 2015. The inlet is situated at 1 m in a degraded forest, with many small trees and undergrowth and on the edge of a wide clearing with artificially short grass

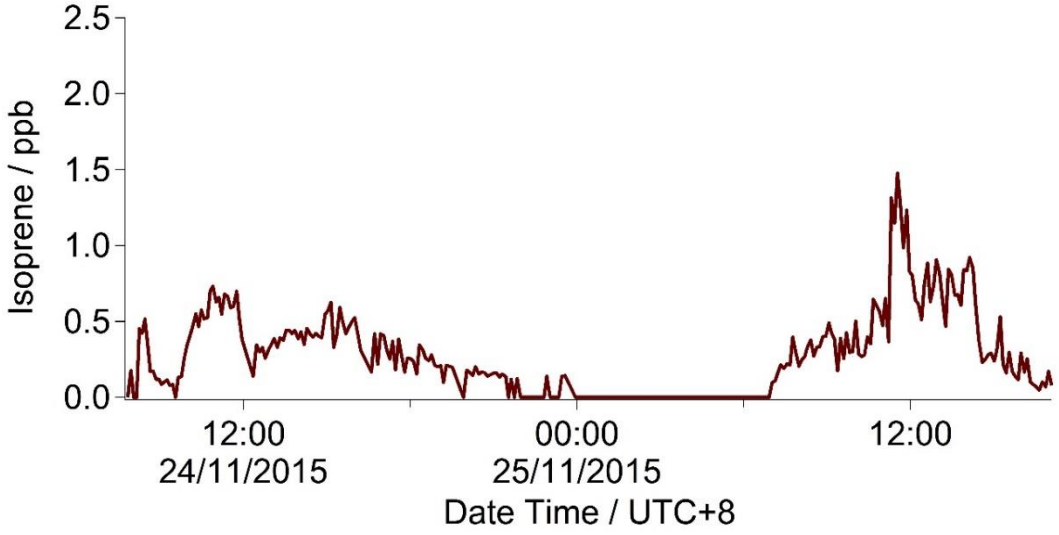

Figure 37 Plot B North at the SAFE site ambient isoprene 24th-25th November 2015. The inlet is situated at 1 m in a severely degraded forest on a steep north-facing slope, with many small trees and undergrowth and a disturbed canopy

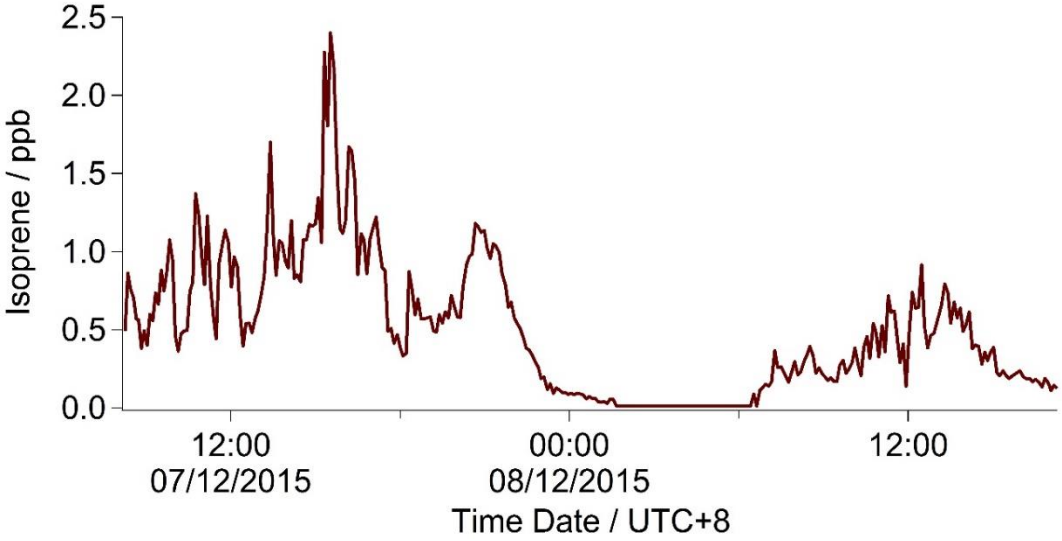

Figure 38 Plot B North at the SAFE site ambient isoprene 7th-8th December 2015. The inlet is situated at 1 m in a severely degraded forest on a steep north-facing slope, with many small trees and undergrowth and a disturbed canopy

3.5.3 Isoprene concentration profiles from the oil palm plantation

In total two canopy level isoprene concentration profiles were recorded for the oil palm site spanning 21 days. Figure 39 and Figure 40 show the results of these runs. Meteorological data was collected for the oil palm site and is shown alongside the isoprene concentration in the below plots. The daily profile of isoprene is strong and shows a maximum around 13:00 local time and dropped to 0 ppb at night. The variation

is not as great as that of the secondary forest and the concentration is consistently higher and reaches levels as high as 35 ppb.

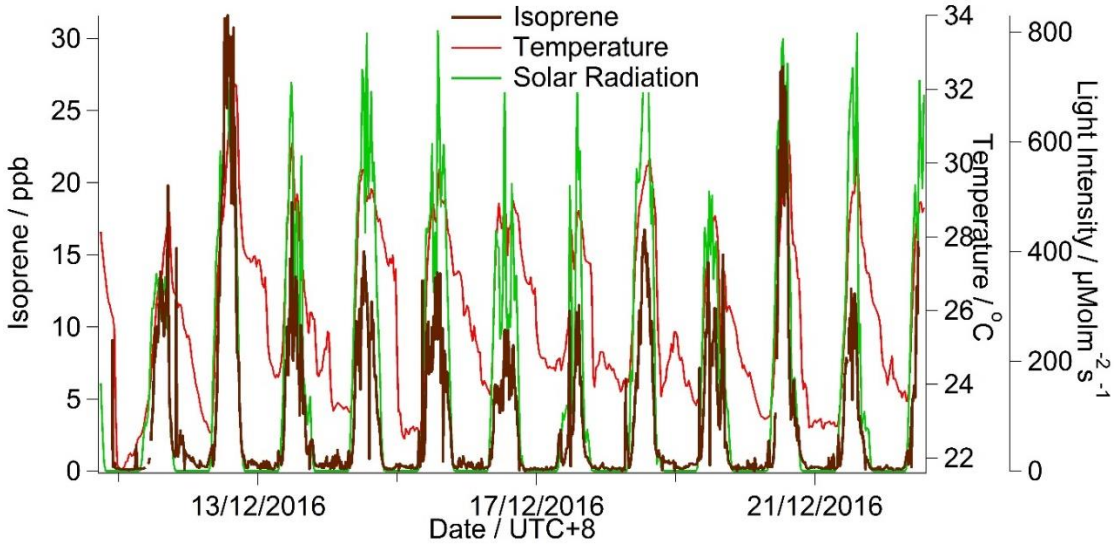

Figure 39 Pekan oil palm plantation ambient isoprene from 10th-22nd December 2016. The inlet is situated at 10 m on a flux tower

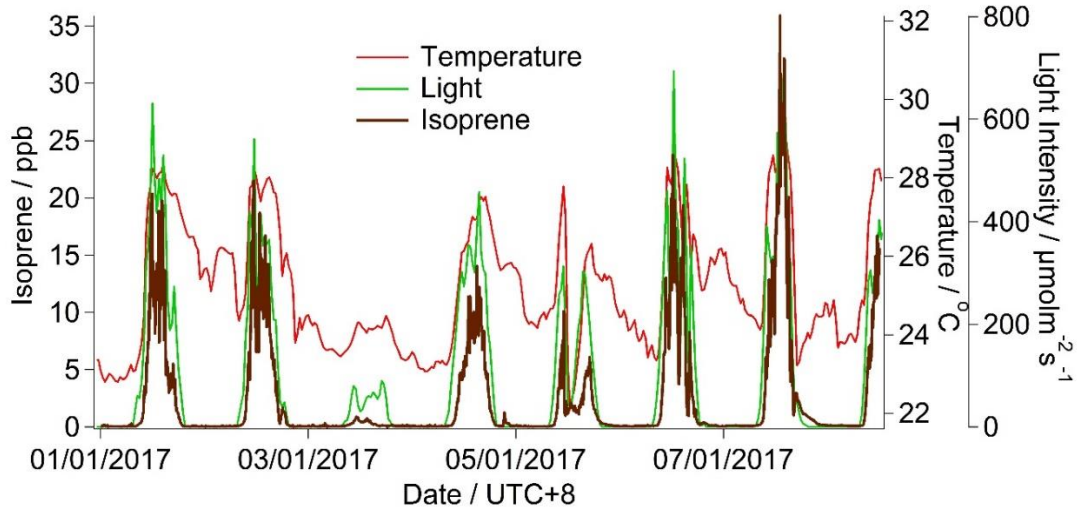

Figure 40 Pekan oil palm plantation ambient isoprene from 1st-8th January 2017. The inlet is situated at 10 m on a flux tower

3.5.4 Discussion of the canopy level measurements

3.5.4.1 Isoprene daily profiles in the primary forest

The low number of ambient runs of over 24 hours in length obtained during this field campaign means that much of the discussion is based on a small sample size. For the primary forest, from the three runs at Belian and one at Seraya in the Maliau Basin Conservation Area, several points can be noted. Due to the forest floor location of the

instrument, the concentration is low despite the high tree density. The isoprene here is likely to be primarily emitted from the top of the tree canopy and transported downwards by diffusion, where contribution from undergrowth is likely minimal as the foliage is sparse and heavily shaded.

The forest canopy of the primary forest is fairly homogenous in structure, with a continuous unbroken, dense and very high canopy with large and straight trunks of large trees forming the understory. This structure likely leads to more stable micrometeorology within the understory, therefore resulting in poor mixing of air from the canopy to the forest floor. This stable atmosphere also results in a typically more uniform isoprene profile through the day, which is less affected by shifts in cloud cover or minor fluctuations in temperature. The stable and shaded canopy may act as a buffer to variations in isoprene concentration due to cloud cover or gusts at the top of the canopy. The factors that affect the mixing in a canopy are investigated in Section 6.4. Further experiments in the tropical forest with investigations into what controls the isoprene transport are required to gain an understanding of the isoprene emission from this forest type.

Isoprene concentration reported during the OP3 campaign in 2008 (Langford et al., 2010) reached peak daily maxima of ~ 1.7 ppb and ~2.3 ppb in the two respective measurements, 20 April – 7 May and 20 June – 20 July respectively. The measurement site for these measurements was the flux tower in the Danum Valley Conservation Area which is situated on top of a hill in a forest clearing. This location is dissimilar to the mesurements in this thesis which likely explains the higher concentrations.

3.5.4.2 Isoprene daily profiles in the secondary forest

In contrast to the primary forest, the secondary forest is characterised by the broken canopy. This includes forest gaps, fallen trees, small shrubs and sparse large trees. This disturbed structure appears to affect the isoprene profile through the day. The diurnal profiles from these forests typically shows a much higher concentration of isoprene and the diurnal profiles have more variation.

The secondary forest contains a higher density of pioneer species and generally is characterised by much more dense undergrowth, which is less shaded as there are reduced numbers of taller trees. Pioneer species, such as the *Macaranga* genera have been found to have a higher emission factor and hence will likely result in higher atmospheric concentrations.

With a more broken canopy, the movement of air would be more turbulent and generally less stable. The result of this is that the isoprene concentration varies much more widely in the secondary forest and spikes in isoprene occur frequently. As a result of the reduced tree cover the entire forest is subject to higher levels of insolation and is susceptible to sudden and randomly varying levels of light as a result of cloud cover that can affect the concentration of isoprene very quickly.

One feature of disturbed forests is the felling of trees and the increased presence of anthropogenic pollutants such as particulate matter, NO_x and ozone. It could be that the trees are emitting isoprene in greater quantities to combat oxidative stress from these increased pollutants. With the increase of NO_x from internal combustion engines or nearby urban areas, increased reactions with isoprene may be producing ozone in higher concentrations, which further accentuates the oxidative stress on the leaves. Mechanical damage in the felling of trees may also increase the isoprene concentration, although this is likely to be a short-lived acute response. Questions surrounding these effects require further study for a full understanding as the factors influencing them are varied and complex.

3.5.4.3 Isoprene daily profiles in the oil palm plantation

The highest concentrations of isoprene are observed in the oil palm plantation. This is likely due to the artificially less-dense canopy structure of the oil palm plantation, where the palm trees are spaced evenly to maximise sun exposure and productivity. The high emission factor for *Elaeis guineensis* is 31.9 $nmolm^{-2}s^{-1}$ (7.8 $mgm^{-2}h^{-1}$) (Misztal et al., 2011). The dominance of the palm trees on the site covering vast swathes of land, the high emission factor, the relatively low (20 m) canopy and the lack of shading for any part of the plant results in high ambient isoprene concentrations. Isoprene concentrations measured by Misztal et al. (2011) as part of the OP3 campaign reached ~25 ppb, which is comparable to the values observed here.

The high isoprene can be expected to have a large impact on the chemistry of the air above the oil palm plantations. In particular the concentration of ozone may increase as described in the cycles in Section 1.5.1.

The meteorological data available at the oil palm site allows an insight into how the atmospheric concentration varies with various factors. It is apparent that the isoprene trend follows the light intensity and temperature extremely closely at the site. With the evenly spaced palm trees it is apparent that the isoprene concentration changes quickly

and this may be due to a well-mixed canopy space, but this requires more study.

A full analysis of the oil palm isoprene concentrations and the chemistry driving atmospheric ozone concentrations is given in Nadzir et al., (*in prep.*).

3.5.4.4 Evaluation of measurement method and general discussion of results

The method for these ambient measurements is simple, and it requires only one inlet at one height. The results show the diurnal profile and the typical values observed for a given location. From the morning increase in isoprene and particularly the evening decline in concentration, an idea can be given about the response of the plants to light and temperature, the mixing of isoprene and also possibly the chemical loss of isoprene. To determine patterns in this data would require long time series and a suite of ancillary measurements which were not present in this dataset.

It is clear from these results that the concentration of isoprene depends strongly on the location of the inlet in the forest. To locate the inlet at the ground in a primary forest when it is shaded results in low concentrations of isoprene. This clearly does not represent the isoprene in that entire forest and does not represent the isoprene that may be emitted to the free troposphere. To measure isoprene at the top of the canopy or above would be required to get an idea of the concentrations from the canopy surfaces. Hence the measurements at the oil palm cannot be directly compared to those in the primary forest as they were recorded above the canopy. The infrastructure required to measure isoprene at the top of the canopy in a primary forest in a remote location would be a practical and expensive challenge as these forest canopies are very dense and can be 90 m high. A flux tower offers a solution but with the drawback that the towers are often located in a clearing which doesn't represent the forest canopy as a whole. These are static and are not able to measure isoprene in different locations.

Even if isoprene is measured from the top of the canopy, no idea is given about the canopy isoprene vertical gradient. What is required is a method to determine the vertical gradient of isoprene, which can then be used to gain an understanding of the isoprene in the forest as a whole. Such an understanding could be determined with multiple inlets at different heights, as described in Chapters 4–7.

3.6 Conclusions on isoprene concentration measurements in a tropical forest

3.6.1 The iDirac proved capable of measurements in a challenging environment

In this field campaign the iDirac was successfully deployed in the tropical rainforest. The deployment demonstrates that the iDirac is capable of two distinct modes of operation and that these can be used to gain an insight on the forest and the atmosphere.

The plant traits campaign was an opportunity to use the iDirac to take discreet samples. The method uses various aspects of the instrument design to good effect and shows that the instrument can be relatively easily transported to challenging environments. Several issues are highlighted in these experiments and certain aspects of the iDirac were not suited to stop-and-start operation.

The ambient measurements tested the long running performance of the instrument. These experiments demonstrate that the iDirac can run for long timeframes unattended in challenging environments. The limiting factor is the availability of power. The iDirac itself is demonstrated to be weather resistant but that the auxiliary power and gas provisions require additional weather proofing.

It is concluded that the iDirac is suitable for fieldwork measurements in remote and challenging locations. It shows good stability for measuring isoprene and the capability of being calibrated at infrequent periods. This field campaign highlights many possible improvements, limitations and issues with the iDirac which are later implemented or resolved for future campaigns.

3.6.2 The isoprene emission factor is recorded for new tropical trees

Measuring the isoprene emission rate with the iDirac and this basic chamber method has been demonstrated to be possible. However there are some flaws and inconsistencies that incur large uncertainties in the data. The data from the iDirac clearly indicates when a tree species results in elevated isoprene levels in the cuvette but for species of lower emission factors, due to ambient variations it is less clear. Calculating emission rates requires assumptions and approximations that also adds to the uncertainty budget.

The data from the Plant Traits measurement campaign highlights some interesting insights into the forest tree species. There is a large variation in isoprene emission factor between trees, between branches and even between leaves. For some leaves measured it

is not clear if the emission is from the leaf itself or a spike in background ambient isoprene. Some of the branches measured register an extremely high isoprene emission factor which has big repercussions for the atmosphere, particularly as most of these species are located in the secondary forest.

3.6.3 There are some key differences in isoprene profile between different forest types

The ambient measurements give insight into the diurnal profile of isoprene for three forest types. The concentrations observed for the sites were indicative both of the species distribution at the site and the meteorological conditions experienced there. It is evident also that the meteorology drives the isoprene concentration very closely.

Each of the forest types displays different isoprene concentration patterns. The primary forest shows lower than expected concentrations and a fairly uniform diurnal profile, this is likely caused by the location of the shady understory under a dense canopy. The secondary forest shows high concentrations and a more sporadic isoprene profile indicative of the altered species distribution in the secondary forest and the disrupted forest canopy. The oil palm plantation shows the highest sustained isoprene concentrations due to the high emission factor of the oil palm with a fairly uniform diurnal profile as a result of the unbroken monoculture of palm trees.

It is highlighted that the location of the instrument inlet does not accurately represent the isoprene distribution in the forest and that only limited information can be obtained from a single time series of isoprene. A different method is proposed that examines the vertical concentration gradient of the forest using multiple inlets which would allow an examination of the vertical forest structure. It is this concept which is the basis for the next four chapters of this thesis.

4 Description and Set-up of an Experiment to Investigate the Vertical Isoprene Gradient in a Temperate Forest

4.1 Introduction

Attempts to study a forest canopy are challenged by their inherent complexity. A dense matrix of different species and types of plants, they vary in composition from the forest floor to the highest branches (Lowman & Schowalter, 2012). The composition of the air throughout a canopy varies as there are a number of sources and sinks for each chemical species within the forest, as well as influences from further afield. The meteorology within the canopy is a strong factor that decides the distribution of these species and understanding this factor is not a trivial task. It is the case that different forest types present many possibilities for different compositions and vertical concentration profiles (Geron et al., 2002).

The isoprene emitted from leaves in a forest can have many different fates. The transport of the isoprene can dictate the concentration of isoprene and this can be important for the possible repercussions for the atmosphere and ecosystem (Sharkey & Monson, 2014). The chemistry of isoprene is extremely important in the destruction of isoprene and this may happen to different extents in different portions of the forest. The highest density of leaves is understood to be where the high degree of isoprene emission occurs from (Sharkey & Singsaas, 1995). The transport from the leaves and the fraction of this emission that reaches the free boundary layer is poorly studied. Equally misunderstood is what fraction of this is transported down through the forest, how this distributes through the different regions of the forest and what fraction is deposited. What happens to the isoprene when it is either in free boundary layer or in the understory of a forest are of

course different, and quantification of this partitioning will lead to a better idea of the final fate of isoprene and the ensuing repercussions.

The Wytham ISoprene iDirac Oak tree Measurements (WISDOM) campaign aimed to address some of these questions and to provide an insight into the forest isoprene concentration patterns. A substantial experiment here is described over three chapters of this thesis that aims to interrogate the forest isoprene and gain a better understanding of the factors controlling the distribution of isoprene in a forest canopy. The design and set-up is discussed in Chapter 4, the results are shown in Chapter 5 and an analysis of these results and subsequent discussion on these are presented in Chapter 6. Subsequently, a modelling study of this forest is presented in Chapter 7.

4.2 Aims

To investigate any chemical species in a forest requires measurements not only in a temporal but in a spatial dimension also. This experiment defines a way to investigate the vertical concentration gradient, and how this changes over the seasons. The aims of this chapter are to:

1. Describe an overview of the rational for the experiment.
2. Give an overview of the experimental set-up.
3. Describe the instruments used for data collection.

4.3 Rationale of WISDOM and the investigation of forest isoprene

4.3.1 Investigations of the vertical isoprene concentration gradient

The vertical concentration gradient in a forest, affects heavily the concentration measured at different levels, as discussed in Chapter 3. The aim of this experiment at Wytham is to better represent the forest isoprene concentration profile to gain a more representative picture for isoprene patterns in a forest. Using this experimental design, the structure and processes in the canopy in terms of isoprene concentration can be studied effectively.

Another aim is to investigate how meteorological conditions affect this vertical gradient and how the meteorology affects the transport of isoprene from the forest into the free troposphere. In the troposphere, isoprene can be important for the global atmospheric chemistry as it is involved in a series of reactions and processes that can repercussions on

human health, biosphere interactions and the radiative transfer of the planet.

4.3.2 The seasonal profile of isoprene concentration

Throughout a growing season, the emission of isoprene is expected to shift, depending not only on sunlight and temperature, but also on the growing stage of the tree. Studies have shown that there is a delay in isoprene emission (Monson et al., 1994) from the onset of bud burst to leaf maturity and that the emission factor is closely related to the age of the leaf. The location of the leaf in the canopy is important for isoprene emission as the degree of shading dictates the rate of emission from that leaf. This experiment aims to demonstrate the seasonal changes observed across the summer and how the forest responds differently to environmental stimuli across this time period.

At the other end of the growing season, the aim is to investigate details of how isoprene production drops off as the leaves become mature and slowly senesce. There is uncertainty about whether the isoprene slowly tails off as a result of shortening days, lower temperatures and less sunshine or if ceases only during leaf senescence. Questions include whether isoprene production ceases before the leaves drop or if the isoprene production ceases only when the leaves have turned brown or fallen off. This change is expected to occur gradually and to have a continuous data series of this time period will allow an assessment of this process.

4.3.3 Long duration evaluation of the iDirac

This experiment will be the longest deployment to date of the iDirac. This provides an opportunity to evaluate the instruments performance and highlight any future improvements.

The forest environment is a challenging one for science equipment. The changing temperature and relative humidity can interfere with the function of an instrument in the field, in particular of the reliability of the sensors that compose the instrument. The forest environment presents a number of challenges to any piece of laboratory equipment, where rainfall, winds, direct insolation, dust, dirt and insects can all interfere with the components of an instrument and cause failure.

The iDirac is designed to be impervious to such threats to its function. Hence, one aim of this study is to evaluate how it performed and how this can be improved for future deployments in other challenging environments.

4.4 Overview of Wytham Woods and the experimental design

4.4.1 Description of Wytham Woods

Wytham woods was chosen for this experiment because of its composition, its location, the existence of a canopy walkway, the availability of auxiliary data and a number of practical considerations. The site has been owned and managed by the University of Oxford since 1942 and has been under constant study. The woodland is 410 hectares in area and contains over 500 plant species and many more animal species (Butt et al., 2009; University of Oxford, 2013). The forest contains a wide array of habitats and different forest environments, with most of the forested area being either ancient semi-natural woodland, secondary woodland or modern plantations. Other non-forest environments at the site include a limestone grassland and some water-logged aquatic environments.

The surrounding landscape contains several features that may influence the bulk air composition of the atmosphere of Wytham. There are several large dual carriageway roads nearby, with the A40 to the north and the A34 to the east. The city of Oxford lies 6 km to the southeast of the experiment site and the Farmoor Reservoir lies 2 km to the southwest. Figure 41 shows the relative location of Oxford and the main roads to Wytham Woods. The climate of Oxfordshire is temperate maritime, with predominant south-westerly winds, typical of much of the United Kingdom (Butt et al., 2009).

Figure 41 Location of Wytham Woods in the United Kingdom

For this experiment, the location chosen was situated in the semi-natural woodland area of the forest. The largest and oldest trees present at the forest are *Quercus robur* (pedunculate oak), with other common species including *Fraxinus excelsior* (ash), *Fagus sylvatica* (beech), *Coryllus avellana* (hazel), *Acer pseudoplatanus* (sycamore) and *Crataegus monogyna* (common hawthorn). The main species and their distribution is shown in Figure 42.

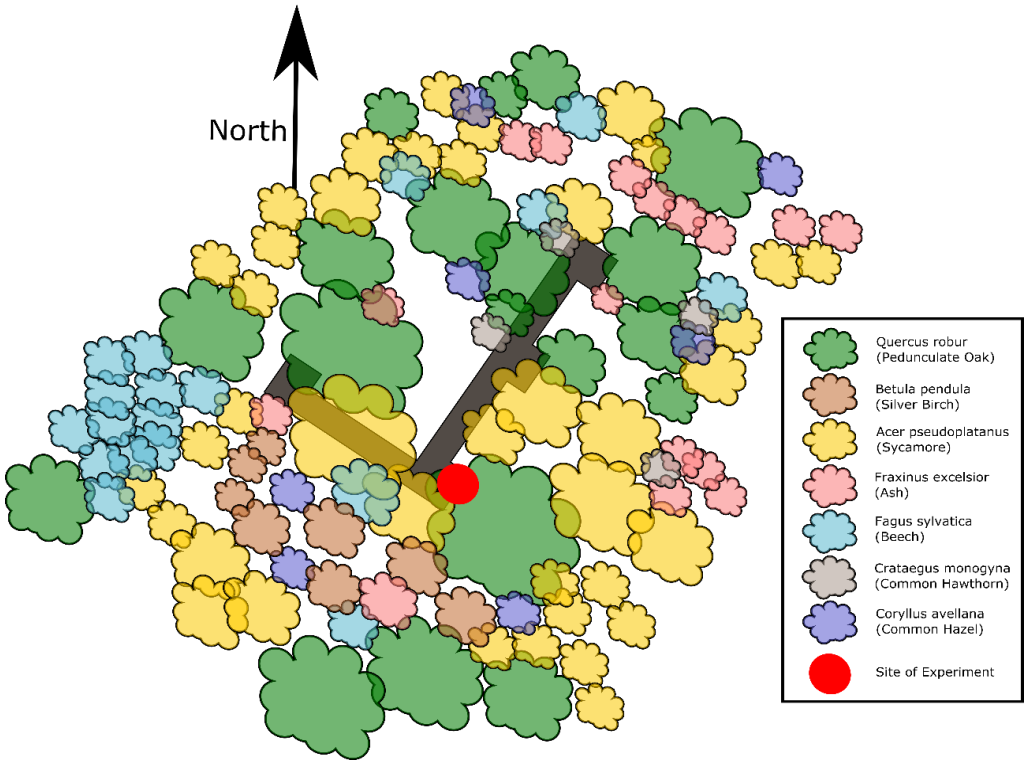

Figure 42 Distribution of nearest tree species surrounding canopy walkway at Wytham Woods. The walkway is represented by the L-shaped feature in the centre of the schematic

To investigate isoprene emissions effectively requires measurements in proximity to emission sources. In temperate woodlands around the world, *Quercus robur* is a known emitter of isoprene. Several studies of isoprene have used oak as the target species, with emission factors varying from 8.03 ± 5.94 $nmolm^{-2}m^{-1}$ (Lehning et al 1999) to 28 $nmolm^{-2}s^{-1}$ (Li et al 2011). Other trees present at the site also have some potential to emit isoprene, with reported emission rates presented in Table 7. It is clear from the reported emission factors that the pedunculate oak is the key isoprene emitting tree in this forest. To maximise the signal from isoprene, it was chosen to set up the experiment as close to an oak individual as possible.

Table 7 Tree species and emission rates

Species	Emission factor
Quercus robur	8.03±5.94 $nmolm^{-2}m^{-1}$ (Lehning et al 1999) 28 $nmolm^{-2}s^{-1}$ (Li et al 2011). 80.0 $\mu gg^{-1}(dw)s^{-1}$ (Possell et al, 2004)
Betula pendula	0.00 $ngg^{-1}(dw)s^{-1}$ (Hakola et al 1998) 0.05 $ngg^{-1}(dw)s^{-1}$ (Hewitt and Street (1992)
Crataegus monogyna	0.03 $ngg^{-1}(dw)s^{-1}$ (Hewitt and Street, 1992)
Acer pseudoplatanus	3.90 $ngg^{-1}(dw)s^{-1}$ (Hewitt and Street, 1992)
Fraxinus excelsior	0.00 $ngg^{-1}(dw)s^{-1}$ (Hewitt and Street, 1992)
Fagus sylvatica	0.00 $ngg^{-1}(dw)s^{-1}$ (Moukhtar et al, 2005)
Coryllus avellana	0.00 $ngg^{-1}(dw)s^{-1}$ (Schurgers et al, 2009)

4.4.2 Physical description of the experimental set-up

To measure the vertical gradient of a species requires several spatially arranged measurements in the vertical dimension. Hence when designing this experiment, the facility to take multiple measurements at the same site but at different heights was required.

Within Wytham Woods there are a number of structures to facilitate forest research. Located in the centre of the semi-natural mature woodland, a canopy walkway facility exists to provide tree-top access to multiple species within the forest canopy. The walkway is located at 51º46'24.2076" N 1º20'18.2076" W, see the map in Figure 41. The University of Oxford allowed use of this facility to enable access to all levels of the forest. A site on the walkway was chosen as close as possible to an oak tree in the southern corner of the 'L'-shaped walkway. For a diagram of the walkway, with surrounding tree species see Figure 42. The location was also chosen due to the accessible height of the canopy.

The experiment was set up with four inlets, each at a different height. Each inlet was

approximately 1.5 m from the trunk of the nearby large oak tree. The inlets were fastened to the canopy walkway at the different heights by different means as described in Section 4.7.1.

4.5 Measurement of parameters in the forest canopy

At each height a range of measurements were taken. Here each measurement technique is described. A diagram of the experimental set-up is shown in Figure 43. The notation of inlets 4 – 1 is used throughout this thesis to represent the heights of the measurements.

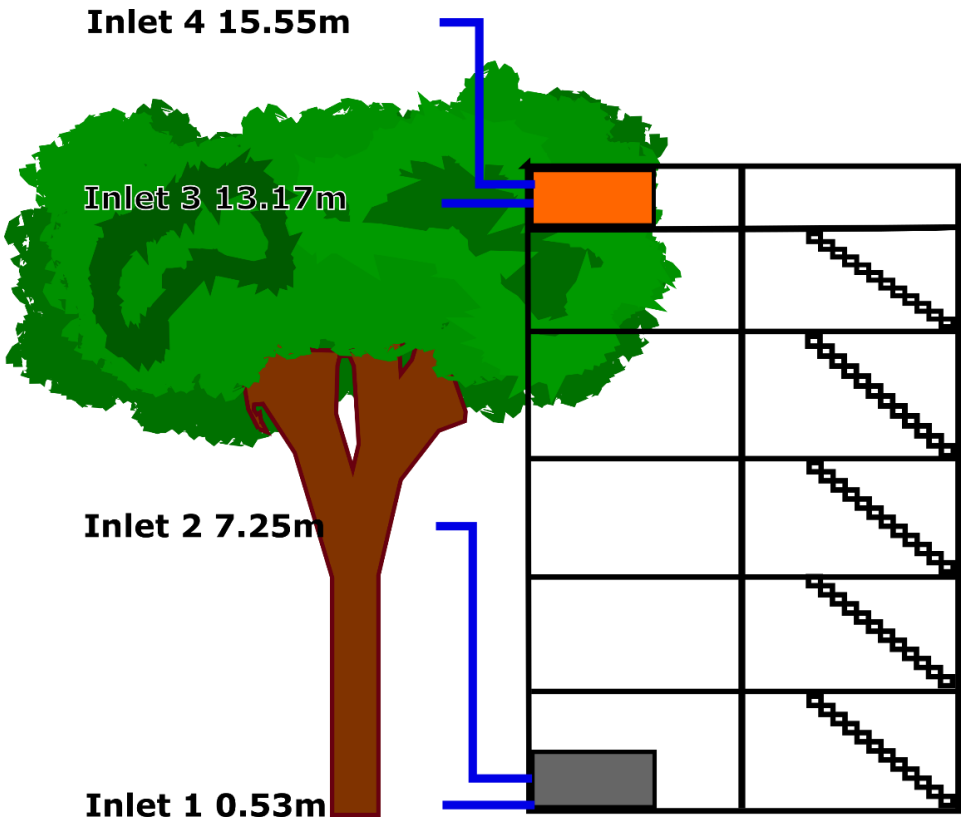

Figure 43 Diagrammatic representation of WISDOM inlet set-up showing four inlets at different heights and two iDiracs on the walkway

4.5.1 Isoprene at four levels in the forest

The iDirac was used for the measurement of isoprene. The iDirac is a dual column isothermal photoionisation detection gas chromatograph, as described in Chapter 2. A picture of the iDirac is shown in Figure 9.

As four inlets were required, two instruments were used, each utilising the functionality of dual sampling. For the majority of the experiment, the grey iDirac was used at the ground for the bottom two inlets (inlet 1 and inlet 2) and the orange iDirac was used on the walkway for the top two inlets (inlet 3 and inlet 4).

The time resolution of the measurements at each inlet was ~20 min which allowed the changes of isoprene concentration on a fine temporal scale to be tracked effectively. The dual inlet functionality was chosen for good spatial resolution. The volume of the sample also dictated the time resolution as the majority of the chromatogram cycle includes a pump cycle which increases in length as the volume of the sample increases. It is not possible to reduce this pumping time in the current configuration as the iDirac sensitivity drops when a lower volume is used, which may affect the measurements in low light or temperatures.

Issues were encountered in the early deployment of the iDirac, particularly with the use of battery power and deployment in low temperatures. Due to the variable resistance of several components in the instrument, dependent on temperature, the measured battery voltage dropped below the instrument set threshold but also below the minimum operating voltage for the Raspberry Pi. Hence, the Raspberry Pi turned off when the high power draw components (oven and trap heater) switched on and the instrument reset itself. This issue was resolved by warming up the instrument with mains power prior to deployment and by disconnecting the Raspberry Pi and using the instrument with Arduino only.

To reduce strain on the internal pump, a pressure differential of 13 kPa was programmed, which increased the lifetime of the pump but resulted in a lower flow. This lower flow meant that the time resolution was further decreased.

Data was collected irregularly at 1-2 week intervals by direct collection from the iDirac micro-SD card. As the Raspberry Pi was not connected, it was not possible to use the ad-hoc network functionality to download data wirelessly. These visits allowed the instrument performance to be assessed and the power supply to be evaluated.

The iDirac was attached to a 10 L high purity nitrogen cylinder at 4 bar and a ~10 ppb isoprene in nitrogen calibration cylinder at 1.5 bar. These were housed in a waterproof Zarges case to protect them from the weather. The power cables and inlet tubes entered the box through a small hole cut in the side of the box. Inside the box, foam padding stopped the cylinders from moving.

4.5.2 Carbon dioxide concentration measurements

A system to log the atmospheric concentration of CO_2 was in place at each inlet height. The CO_2 sensors were developed in-house and consist of a dual channel infrared sensor

with inbuilt logger. The units measured 5.5×12×12 cm and had a small membrane for the diffusion of CO_2. A small temperature sensor was also in place beside the membrane. It was ensured that the membrane surface was always sheltered and facing down to prevent contamination with water. A picture of a CO_2 sensor is shown in Figure 44.

Data collection from these sensors requires a laptop, a serial port connection and the use of Teraterm software to transfer data.

Figure 44 Image of the carbon dioxide in-house sensor showing connection ports and the underside of the sensor with the diffusion membrane and temperature sensor

4.5.3 Measurements of wind with a 3D sonic anemometer

At the top of the canopy was a 3D sonic anemometer (omnidirectional (R3) & asymmetric (R3A) research ultrasonic anemometer, 1590-PK-020, Gill Instruments Ltd) that was able to capture 3D wind data at a time resolution of 1 Hz. The anemometer was deployed fairly late in the season, but is key for modelling and understanding the canopy transport processes. The low-power anemometer was powered with a 110 Ah battery.

The wind data was logged using a home-made Arduino logger, powered with one of the 110 Ah batteries that was used for the iDirac. The logger wrote the serial output from the anemometer to an SD card for further processing.

4.5.4 Temperature and relative humidity sensors

At each inlet height was placed a temperature and relative humidity logger (EL-USB-2-LCD & EL-USB-2, Easylogger Ltd.) which recorded data at a time resolution of 2 minutes. This unit is henceforth referred to as an ‘Easylogger’. These sensors were sheltered from the rain either by placement under the CO_2 logger or under the scaffold structure. They were held in place with either tape or cable ties.

4.5.5 Measurements of photosynthetically active radiation

Light intensity was measured at each height in the canopy with a quantum sensor (Quantum Sensor, Model SQ-100/200/400 Series, Apogee Instruments) and a logging system (Campbell Scientific Ltd.). Light was logged at a time resolution of 2 minutes. Each light sensor was placed on a horizontal platform at each height. At inlet 2 the sensor likely moved very slightly as it was attached to the dangling apparatus and not securely fixed to the scaffolding structure. To ensure it was facing directly up, the rope was pulled tight to reduce dipping of the instruments.

4.6 Other measurements at the site

4.6.1 Photosynthesis and absorbent tube sampling

Photosynthesis measurements were taken of the oak individual's leaves on several occasions during the measurement campaign in collaboration with Lancaster University. The instrument for this was the LI-COR (LI-COR® Potable Photosynthesis System, LI-COR® Biosciences), which was operated from a battery in the field. Two 3-day visits were made with the LI-COR and two different parts of the canopy were sampled – the walkway level and the ground level. Photosynthesis measurements were taken at different temperatures, light intensities and CO_2 concentrations. For an image of the LI-COR in the field see Figure 45.

Figure 45 LI-COR Instrument on the canopy walkway at Wytham Woods

At the same time as the photosynthesis measurements, air was pumped through a Tenax absorbent tube from the effluent from the LI-COR cuvette. On several occasions, vertical profiles of absorbent tubes were taken. The height of the samples was approximately the same height at the iDirac inlets. The volume sampled was 4 L in July and 12 L in August and these were generally sampled at a flowrate of 200 $mLmin^{-1}$. These tubes are analysed using a GC-MS (gas chromatograph-mass spectrometer with quadrapole mass analyser) with a full mass scan range of 50.0-300.0 m/z (Perkin Elmer TurboMass Gold) for a range of volatile organic compounds present in the whole air samples. All of the processing is being done at Lancaster University.

4.6.2 Photographic images of the leaves and canopy cover

With each visit to the site, photos were taken of the forest, the canopy coverage and leaf conditions. Photos were taken with either a Nikon D3200 or a Motorola 4G smartphone. The photos were meant to track the changes in the forest over time. The photo of the canopy was taken at the same location on each occasion. The orientation of the photo was intended to be the same for a fair comparison. The same branchlet was photographed on each visit to track the visual condition of the leaves over time.

4.6.3 Automatic meteorological weather station

The Centre for Ecology and Hydrology (CEH) maintains a comprehensive automatic weather station (AWS) at Wytham Woods as part of their Environmental Change Network (ECN). This weather station collects hourly data which is downloaded periodically. The various factors that are collected are summarized in Table 8. The weather station is situated ~520 m from the measurement location on the canopy walkway and is not situated in a forest. The CEH AWS is located in the Upper Seeds area at Wytham, which is an open limestone grassland area, surrounded by forest.

Table 8 Data collection summary from meteorological station

Measurement	**Unit**	**Note**
Solar radiation	Wm^{-2}	Avg
Net radiation	Wm^{-2}	Avg, range: -100 to 700
Relative humidity	%	Avg
Dry bulb temperature	^oC	Avg, range: -40 to 70
Wind speed	ms^{-1}	Avg, range: 0 to 99
Wind direction	^{o}	Avg, 0^o = magnetic North, range: 0 to 359
Rainfall	mmh^{-1}	Total, range: 0 to 500
Albedo sky	Wm^{-2}	Avg, range: 0 to 1000
Albedo ground	Wm^{-2}	Avg, range: 0 to 1000
Dry bulb air temp. in RH screen	^oC	Avg, range: -40 to 70
Soil temp. at 10cm (bare ground)	^oC	Avg, range: -40 to 70
Soil temp. at 30cm (grass)	^oC	Avg, range: -40 to 70
Surface wetness	Min	Total, total time wetness < 0.8
Soil water content	m^3m^{-3} (%)	Avg volumetric moisture content, range: 0 to 100
Air temp minimum	^oC	Minimum
Air temp max	^oC	Maximum
Maximum wind gust speed	ms^{-1}	Maximum

4.7 Practical description of the inlet set-up

4.7.1 Four inlets at different heights in the canopy

Each inlet had a unique set-up for practical and scientific reasons. For images of each inlet, please see Figure 46. The four inlets were situated at the same location, but vertically distributed at heights; 0.53 m, 7.25 m, 13.17 m and 15.55 m as shown in Figure 43.

The ground inlet (inlet 1) was attached to the scaffolding structure just above the ground and consisted of a 2 m 1/16" PTFE tubing to the iDirac. The inlet was a polypropylene funnel, with a wool plug, fastened with cable ties. The CO_2 sensor was attached 20 cm away and the light sensor was attached to a vertical pole 1 m away, to avoid shading from the inlet or scaffolding tubes. The Easylogger was placed under a scaffolding pole 20cm from the inlet and secured with duct tape. The inlet height was 0.53 m.

The understory inlet (inlet 2) was attached to a T-shaped structure suspended with rope from the top of the canopy. The ¼" tubing was ~13 m long and led to the ground iDirac. Due to the length of the tubing and the volume of flushing required, an external pump was required to supplement the internal pump of the iDirac. This external pump had a flowrate of 1 $Lmin^{-1}$ and had a water absorbent chamber in-line to prevent condensation from building up and damaging the pump. The CO_2 sensor was suspended from a four-way connector so that it hung freely, with the sensor membrane sheltered from rain. The light sensor was connected to the arm of the T-shaped structure, facing upwards. The Easylogger sensor was attached to the T-shaped structure with duct tape. The rope that connected it was pulled tight, so that the T-shaped arm was horizontal. The inlet height was 7.25 m.

The mid-canopy inlet (inlet 3) was fastened to a scaffolding railing 0.5 m from the floor of the canopy walkway. The inlet consisted of a 2 m 1/16" PTFE tube to the walkway iDirac. The inlet was a polypropylene funnel, with a wool plug, fastened with cable ties. The CO_2 sensor was fastened with cable ties and the Easylogger was attached to this with duct tape. The light sensor was 1 m away so as not to be shaded by the railing and dense branches. The inlet height was 13.17 m.

The top-of-canopy inlet (inlet 4) was fastened to a pole which protruded through the top of the oak tree canopy. This pole did not rise higher than the surrounding trees, but was above the highest leaves of the target oak individual. The pole was movable and allowed

access to the loggers. The inlet consisted of a 2 m 1/16" PTFE tubing from the top of the pole to the walkway iDirac. The inlet was a polypropylene funnel, with a wool plug, fastened with cable ties. The CO_2 sensor was fastened with cable ties and the Easylogger was attached to this with duct tape. The light sensor was just above this arrangement. The 3D sonic anemometer was attached to the top of the pole with tight jubilee clips and orientated to face north. The inlet height was 15.55 m.

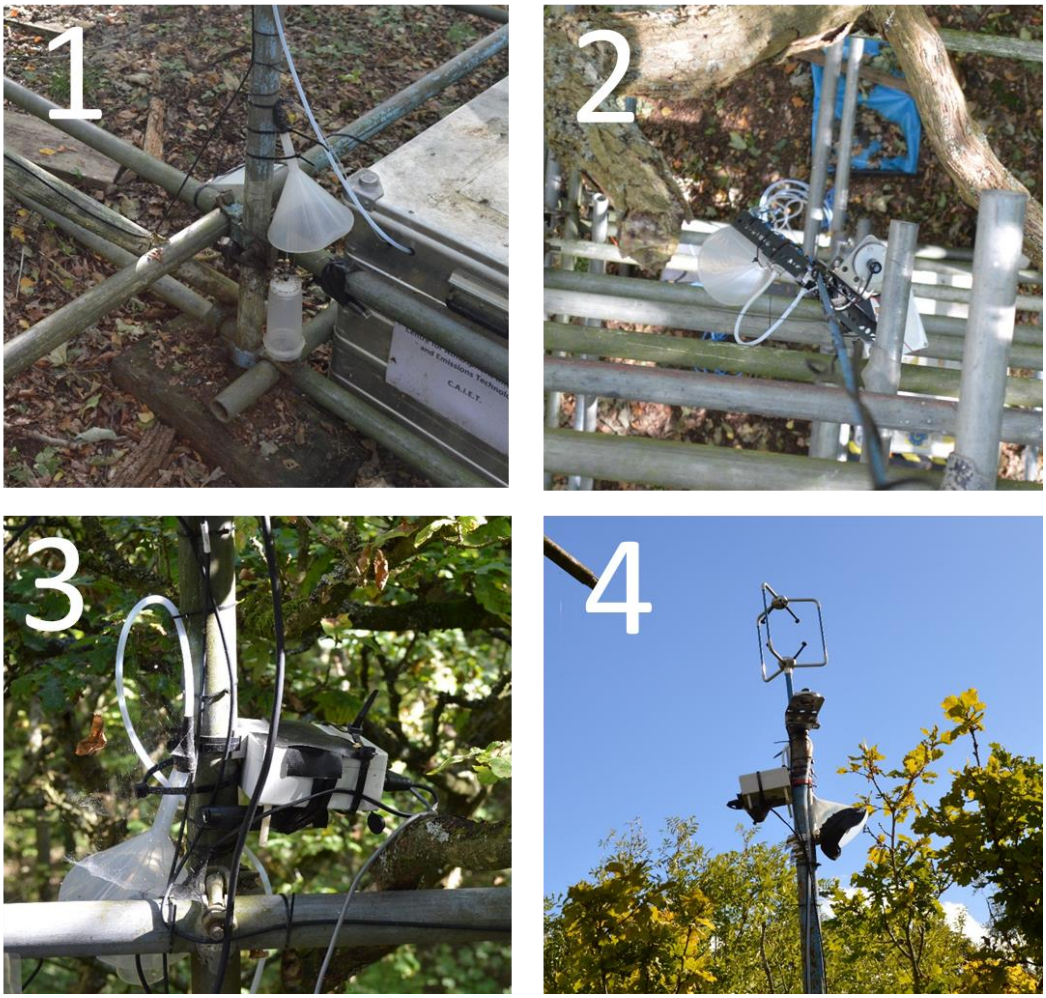

Figure 46 Images of each inlet showing the iDirac inlet, the carbon dioxide sensor and other instruments numbered as for the inlet number

4.7.2 Supplying power to the site

The canopy walkway facility at Wytham Woods does not have a mains power connection. The iDirac GCs, the anemometer and the CO_2 loggers all require a constant 12V supply, which cannot be supplied by batteries alone. The power demands of these instruments are such that a battery would be depleted in several days. A solar powered system was devised

to provide a means for batteries to be trickle charged on site. Two 120 W solar panels (RS Components) were obtained and secured on an elevated pole above the walkway, facing south at a 45^{o} angle to maximise sun exposure.

Two 120 Ah batteries were used to power the iDiracs and CO_2 loggers. To regulate the charging and prevent over-charging, two 10 A charge controllers were put between the solar panels and batteries. A fused junction box was constructed to split the voltage from the battery for the various instruments. For a schematic of the power set-up, please see Figure 47.

With this system, with long days of sunshine, the batteries were charged sufficiently to continue indefinitely. But, despite this complete system, when the days became shorter in the autumn, it was required to replace the batteries occasionally with fully charged ones.

The sonic anemometer required a third battery, but the power demand was low so charging was not necessary for the duration of the field campaign.

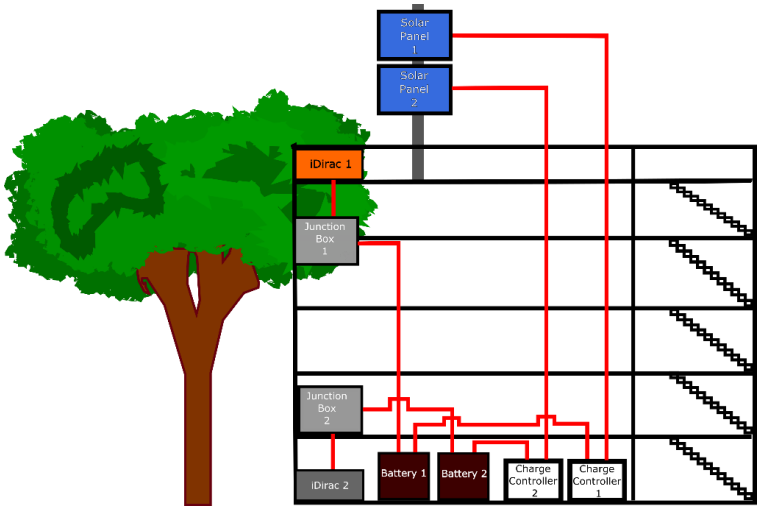

Figure 47 Power supply set-up showing the connections of the solar panels to the batteries and to the iDiracs

4.7.3 Organisation of logistics and data collection

Over the course of summer 2018, 24 fieldtrips were completed using a combination of public transport, rental car and department van. Each trip typically involved downloading all the data from the various loggers, switching batteries for fully charged ones and generally checking the operation of each sensor. On occasion, other tasks and tests were completed. The chalet building at the site provided a storage facility and a dry space to test equipment or troubleshoot.

4.8 Hypotheses on WISDOM and areas of investigation

4.8.1 Meteorology has a large effect on canopy transport

It is hypothesised that the meteorology will have a great effect on the vertical isoprene concentration gradient in the forest. Isoprene emission from vegetation is well known to depend strongly on light and temperature, hence the expectation is that isoprene will be higher on warmer and sunnier days. How rapidly the forest emissions react to fluctuations in PAR and temperature will be investigated as an interesting feature in the data.

It is expected that the wind speed and direction will have a large effect on the isoprene emissions and concentrations and how this is distributed through the forest. The transport of isoprene to the troposphere is likely dependent on the wind speed and it may be that wind directions reveal potential 'hotspots' of isoprene in the forest. It will be possible to examine if during higher wind speeds there is more isoprene transported to the free troposphere or if it is deposited in the forest. With a large town nearby and two busy roads, it may well be the case that air masses from these directions affect the chemistry of isoprene by bringing in NO_x and hence ozone, an isoprene oxidant.

4.8.2 Isoprene concentration has seasonality

With the experiment capturing a great deal of the summer season, it provides a unique opportunity to examine how the forest changes over a longer timescale. By analysing the isoprene concentration over this time period, it will be possible to reveal how the forest is responding to climate stresses and the stage of the development of the forest.

There are several processes in the year of a deciduous tree in a temperate forest that influence the emissions of isoprene. The first process that may yield isoprene is the bud-burst, which occurs as the leaves emerge after winter dormancy. During this campaign, data was collected from late May onwards due to technical limitations. As the leaves reach maturity, their isoprene emission factor likely changes or shifts with meteorological conditions and climactic stresses. It migt be possible to detect this in the data. Toward the end of the growing season, the isoprene is expected to decline as the temperatures become lower and the days shorten, but also as the leaves reach the end of their lifetime.

4.8.3 The heatwave strongly influences isoprene concentration

The climate of 2018 was exceptional, with an extended and colder than average winter and a hotter than average summer period. In particular, in the period from 22nd June to the 8th August the UK faced a heatwave and drought. The UK Met Office declared 2018 the joint hottest summer with 2003, 2006 and 1976 the UK had experienced since 1910 (Met Office, 2018).

It is anticipated that the data collected for the summer at Wytham will provide an insight into a scenario that may become more frequent in the future. Many reports conclude that temperature extremes will become more frequent as a result of anthropogenic emissions affecting climate (IPCC, 2018). With these heightened temperatures, there will be a likely large effect on the biosphere. One major response is likely to be elevated concentrations of biogenic VOCs as isoprene emission has been reported as a response to heat stress.

With heightened isoprene emission of course there would also be a likely knock-on effect on air quality, atmospheric composition and climate. The effects on ozone concentration are unprecedented but may induce a concentration increase, which would incur negative effects on human health. The effects on climate are more indirect, with an increase in aerosol production affecting the radiation balance of the planet.

Hence, this study can shed light on potential future emissions of isoprene from a temperate forest under heightened temperatures. Combined with modelling, it will be possible to examine other scenarios and types of forest to predict potential emissions into the atmosphere.

5 RESULTS FROM THE WISDOM CAMPAIGN

5.1 Aims

The WISDOM campaign, as described in Chapter 4, produced many data sets from the forest, and used auxiliary data provided by the University of Oxford Wytham Woods study site. When raw data is collected during fieldwork, often before this data can be used for analysis, calibration and processing is required. The aims of this chapter are to:

1. Report the raw data series.
2. Summarise calibration and processing procedures.
3. Highlight any limitations of the data or issues.

5.2 Overview of the WISDOM campaign

Overall the WISDOM campaign at Wytham Woods ran from 14th March to 7th November 2018 and data was collected for six months over summer 2018 from 9th May to 6th November. The experiment was initially designed for a short-term deployment in tropical climates, so many aspects were not prepared for a long-term deployment in a temperate environment. As a result, auxiliary measurements were added sequentially over time when sensors became available.

The deployment of two iDiracs allowed us the possibility of evaluating the performance of the instruments over a long timeframe. The timing of WISDOM is the longest continuous deployment the iDirac had undertaken to date.

The site facilities proved to be ideal for an experiment such as this. Access to the various levels of the forest story meant measurements could easily be taken at different locations. Point measurements were taken at the upper canopy level as a result of easy access. The major disadvantage of the canopy walkway for a campaign such as this was the lack of mains power. Power drop-outs were consistently a problem as a result of continuous overcast days failing to charge the batteries.

The experiment was undertaken over the summer with a series of site visits. In total, the

site was visited 24 times. Some key visits are detailed in Table 9.

Table 9 Summary of site visits to Wytham Woods and key activities

Visit #	Date	Activity
1	14th March 2018	Looksee visit.
2	26th–27th April 2018	Set-up installed.
4	9th May 2018	Began CO_2 measurements.
6	25th May 2018	Solar panels in final position. Started walkway isoprene measurements (inlets 3 + 4) successfully.
10	5th July 2018	Started ground isoprene measurements (inlets 1 + 2) successfully.
11	11th–13th July 2018	LI-COR and absorbent tube measurements.
14	10th August 2018	Installed 3D sonic anemometer.
17	29th–31st August 2018	LI-COR and absorbent tube measurements. Installed PAR measurements.
24	6th-7th November 2018	Disassembled experiment.

As the availability of certain sensors affected different measurements, different sensors were added sequentially through the year. A data collection timeline is shown in Figure 48. The gaps shown in Figure 48 are as a result of power drop-outs or instrument failure.

The Upper Seeds meteorological station, as part of the CEH Environmental Change Network provided a wealth of additional general parameters for the whole time period at the site.

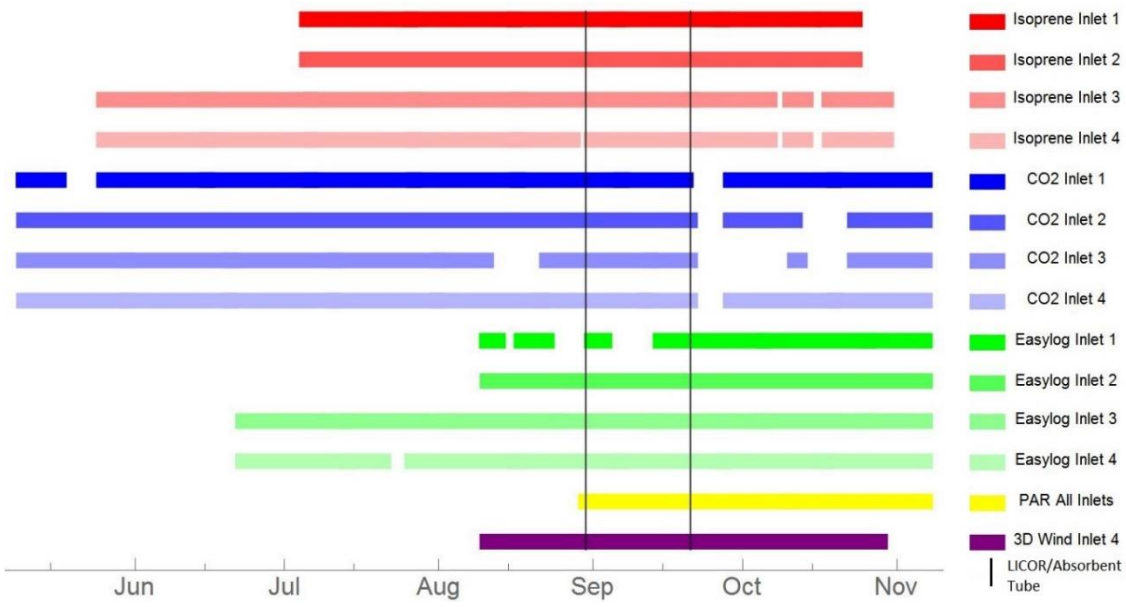

Figure 48 Measurement timeline. Wind data is included here though the sensor was faulty and is not used in the analysis

5.3 Evaluation of the iDirac over long timespans

The iDirac proved capable of measuring isoprene abundances continuously through the day, spanning from concentrations as high as 8 ppb in the height of the summer and to effectively zero at night-time. The long duration of this campaign provides an ideal chance to evaluate how the iDirac performs in a real-world environment over a longer timeframe.

5.3.1 Calibration of the isoprene data and sensitivity drift

The raw chromatograms were processed using the method described in Section 2.5.3 to obtain the peak parameters for the isoprene peak. To account for the effect of drifting sensitivity, the data files were analysed in weekly bins. A calibration curve was constructed for each week, of the type shown in Figure 15. The resulting calibration curves were used to calculate the isoprene concentration in the samples. This allows for the calibrated data to account for any drift in sensitivity as a result of either the degradation of the PID or the gradual poisoning of the absorbent trap. The calibration plots exhibit a clear drift as time progresses, as shown in Figure 49, with calibration chromatograms later in the time series showing lower peak area for the same concentration.

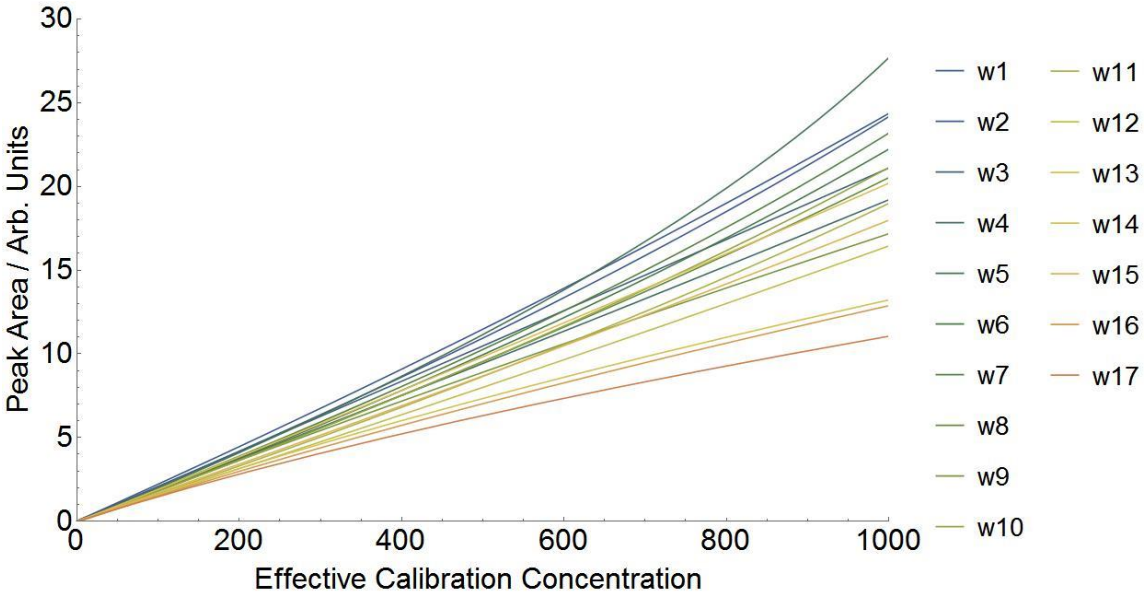

Figure 49 Calibration curves plotted in weekly intervals for the orange iDirac situated on the walkway, showing decreasing sensitivity over time

The lifetime of the absorbent trap can be assessed by examining the calibration curves over time. This drift is attributed to the gradual degradation of the trap as a result of repeated absorption/desorption cycles, with exposure to high concentrations of VOCs and oxygen. It is likely that the absorbent in the trap becomes 'poisoned' over time and eventually needs to be replaced. Ways to mitigate this effect are being contemplated, including using a combination of adsorbent materials within the trap so that large VOCs can be prevented from poisoning the adsorbent bed sensitive to isoprene. Future instrument developments are discussed in Chapter 8.

It may also seem possible that the drop in sensitivity is due to the degradation of the PID. However, this can be ruled out by considering that when the trap is replaced with a new, reconditioned trap then the calibration curve returns to the previous gradient. A possible future development of the iDirac is to implement a direct injection of calibration gas on to the PID that by-passes the absorbent stage. The direct injection could monitor the degradation of the PID without the influence of the absorbent trap and would allow correction of drift as a result of PID sensitivity change.

A slight curvature can be seen in the calibration curves. This behaviour increases over time and is attributed to the occurrence of a slight breakthrough, as at high concentrations and/or high volumes, some isoprene is not absorbed by the trap. This further supports the implementation of more frequent calibration runs in the measurement sequence used.

Decreasing sensitivity would obviously affect the limit of detection of the instrument.

During a particularly long deployment such as that in Wytham Woods, it is important to monitor the sensitivity by means of plots such as that in Figure 49 to better establish a threshold for when the trap needs to be replaced.

5.3.2 Power issues affecting the iDirac

The success of a field campaign depends on a good stable power supply. During this off-grid installation, solar power was used to power the instruments as described in Section 4.7.2. Throughout the WISDOM campaign, the charging of the batteries by the solar panels was variable and often not sufficient to fully recharge the batteries. The set-up relied heavily on fortnightly visits to exchange drained for fully charged batteries.

The iDirac internal voltage divider measures the incoming voltage and so it is possible to trace the output of the battery. It can be seen in Figure 50 that the battery voltage follows a daily cycle, where the battery is charged adequately during the day and then drops slowly during the night. To ensure the battery voltage never drops below the minimum threshold for the instruments, it is essential that the voltage is brought higher at the end of the charging period so that the drop during the night doesn't cause a slow decrease over several days. It can be seen in Figure 50 that on 27th August such an event occurred. This occurrence caused the battery to drop below the threshold value and the iDirac went into 'power-save' mode. This mode, while it saves the battery, has the disadvantage that the column oven heating element switches off. The lowered column oven temperature will adversely affect the retention time of the isoprene peak and hence the results.

A key improvement would be to include a more robust power supply. Where mains power is not available, that could involve improving the charging efficiency of the battery or by using larger solar panels.

Inside the iDirac, an improvement in the design could include a better insulated oven box, which would reduce heat loss and not cool quickly if the heater is switched off. The Arduino script could also be modified so that the 'power-save' mode is not activated for such a long duration. In addition, a different Schottky diode with a smaller voltage drop could be used so as to increase the apparent voltage experienced by the iDirac.

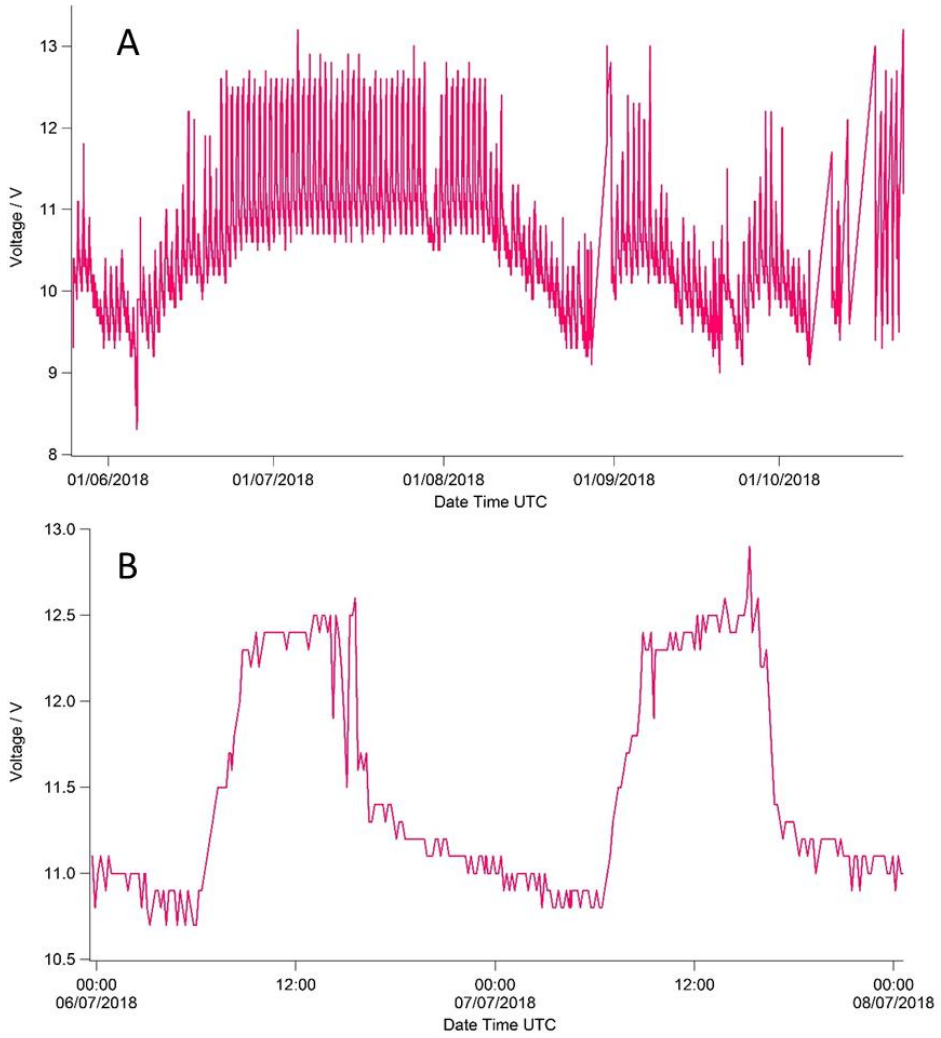

Figure 50 iDirac power supply voltage A) Entire campaign B) Two day example

5.3.3 Stability of the measurements over time

A desired trait of a field instrument is good stability and the iDirac has been developed with this in mind. Over the time period of WISDOM, the stability of the iDirac itself appeared reasonably good. However, two aspects of the instrument appear to jeopardise the ability of the iDirac to run autonomously for such a long time, a pump issue and a software problem.

The internal pump of the iDirac has frequently proven to be a weak point in the current instrument design. The current pumps used (diaphragm pump, model 12KD 1212.106, Boxer Pumps) are small and overheat fairly easily if operated often and under strain. The pressure differential that draws air through the instrument, as described in Section 2.4.3, can be adjusted. If the pump box is not sufficiently air-tight the pressure differential can drop quickly and require the pump to run continuously. The method of drawing air through the pump box involves the pump pulling on a vacuum, which further puts strain

on the performance of the pump. When overheated, the internal coil that drives the pump starts short-circuiting, thus reducing the performance of the pump. Eventually the coil ceases to operate and the entire pump is short-circuited. When this occurs, the power supply to the instrument is interrupted and the iDirac abruptly switches off. At Wytham, the pressure differential was low (13 kPa or 9 kPa) so as to reduce strain on the pump and hence, this effect was observed only ~5 times and did not severely limit the measurements.

The other error that can affect the instrument performance is an occasional software error. This occurs when the data serial buffer from the flowmeter is out of synch with the data received on the Arduino Mega. Despite code improvements, this error does still occur occasionally and causes the flow to be interpreted as 999 $mLmin^{-1}$ and the sample volume to register 0 mL or 999 mL. A likely cause is an interruption of the connection between the Arduino Mega, the Arduino Micro and the flowmeter which can occur when there is a power outage or a power surge. At Wytham this occurred only ~10 times and was not a big problem for the data.

5.4 Overview of each dataset

5.4.1 Isoprene concentration time series

Isoprene data was successfully obtained from the orange iDirac based on the walkway with inlets 3 (13.17 m) and 4 (15.55 m) from 25th May to 29th October 2018. The grey iDirac, based on the ground with inlets 1 (0.53 m) and 2 (7.25 m) collected data from 5th July to 23rd October 2018. This is summarised in Figure 48.

The data collected from the iDirac instruments was in the form of .csv files that required processing with the Mathematica script as described in Section 2.5.3 and shown in Appendix 1. The processing process required the removal of the occasional faulty file. All the data was divided into weekly bins so that the calibration curve used for the data accounted for the gradual sensitivity drop in the instrument as described in Section 5.3.1.

Figure 51 shows the entire time series of isoprene, with all four inlets. The time series has several gaps due to instrument faults. It is important to highlight that the 2018 heatwave from 22nd June to 8th August was captured here, with exceptionally high concentrations of isoprene observed, as high as 8.3 ppb. Concentrations as high as this are exceptional in a temperate forest, and are more commonly associated with tropical forests (Jones et al., 2011).

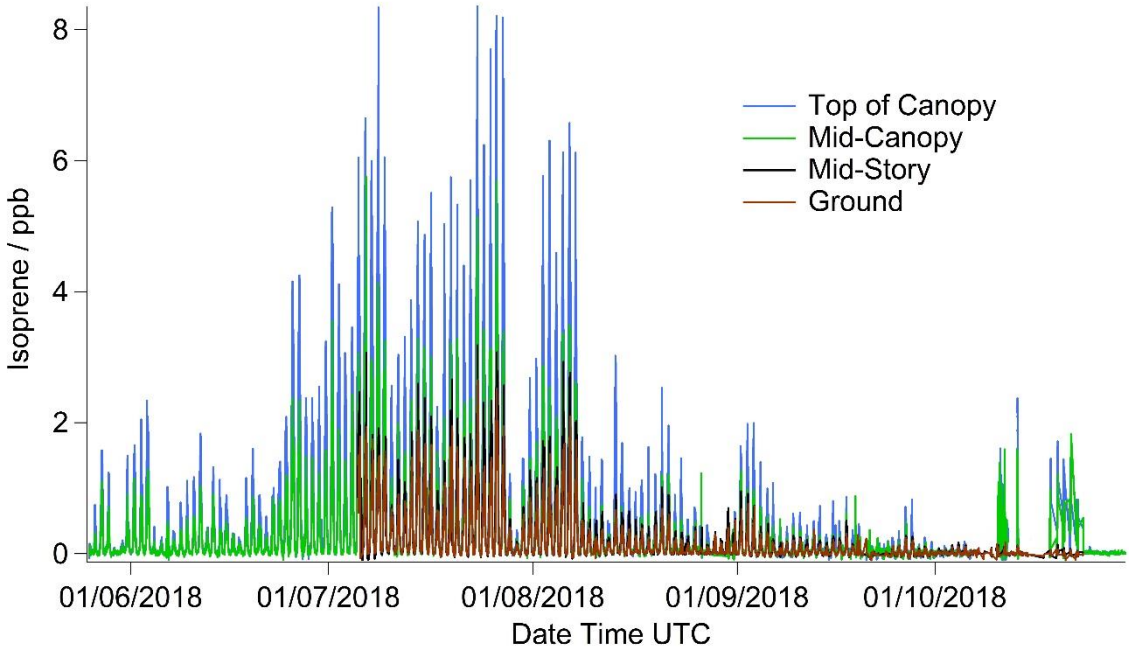

Figure 51 Complete isoprene concentration time series from each inlet

Figure 52 shows typical diurnal cycles with daily isoprene concentration beginning to rise prior to the sunrise, peaking at ~14:00 UTC, and dropping to zero after sunset. During the night, the concentration of isoprene typically dropped below the detection limit of the iDirac. The night-time lower limit was typically reached two hours after the sun had set.

The differences between the four inlet heights is as expected, with highest levels observed at the highest inlet and lowest levels observed at the lowest inlet, which is in agreement with the distribution of leaves in the canopy.

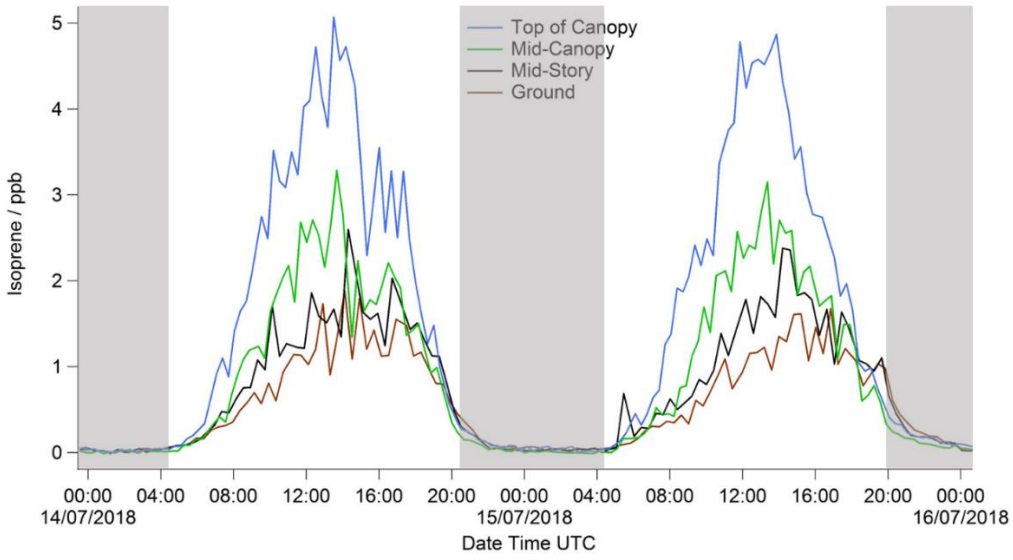

Figure 52 Two day typical isoprene concentration profile, during heatwave showing night as shaded areas

5.4.2 Carbon dioxide concentration time series

5.4.2.1 Carbon dioxide raw data

Carbon dioxide concentrations were logged successfully for all four heights for different time periods (Figure 48). Similar to isoprene, the CO_2 was affected by battery voltage. It also experienced some problems with logging data particular to the sensors that were used. As a result of the power and sensor failures, ~5–10 % of the time series is affected.

The raw data was cleaned and processed before analysis, which involved adding a date stamp to the data. The raw data as calculated internally by the CO_2 logger is reported as a time series in Figure 53. Further correction and calibration of the data is required, as described in Section 5.4.2.2.

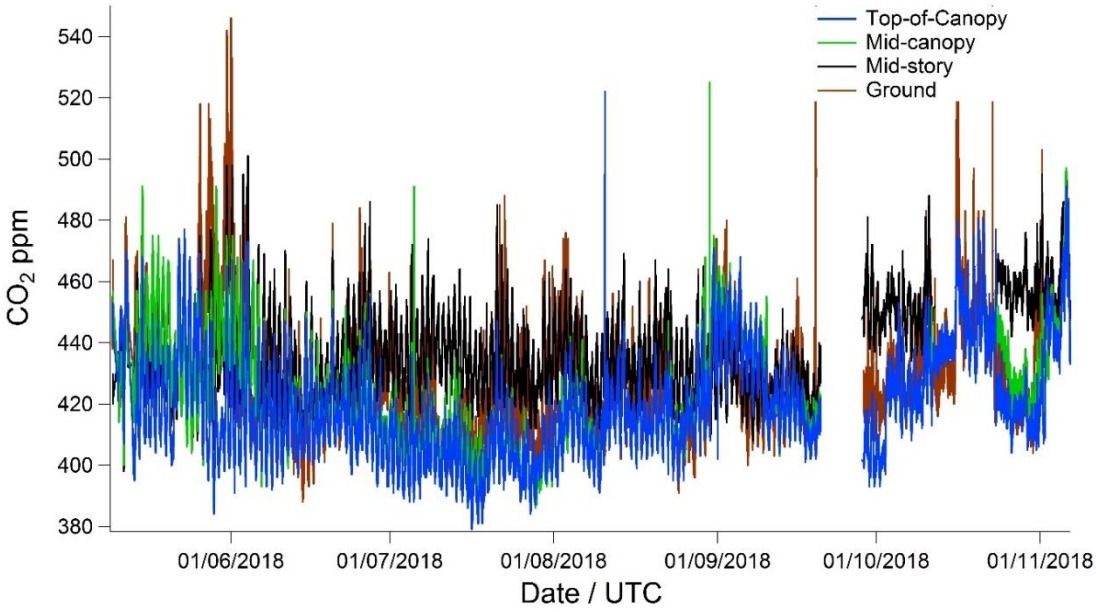

Figure 53 Uncalibrated raw CO_2 concentration time series

5.4.2.2 Calibration of the carbon dioxide concentration data

Before the CO_2 data was used for any analysis, it underwent two post-processing steps to ensure its reliability. One of these steps was to eliminate occasional step shifts in the data series and the other was the absolute calibration, with comparison to known concentrations.

The CO_2 instruments have an internal mechanism for calibration when they are used with calibration standard gases. However, in this case, a calibration gas was not used in the field. This internal calibration manifests as a sudden step shift (either a drop or a jump) in the time series. Using the raw infrared (IR) signal that is also logged from the CO_2 sensor it is possible to calculate CO_2 offline. This utilises the IR-low and IR-high channels logged in the sensor.

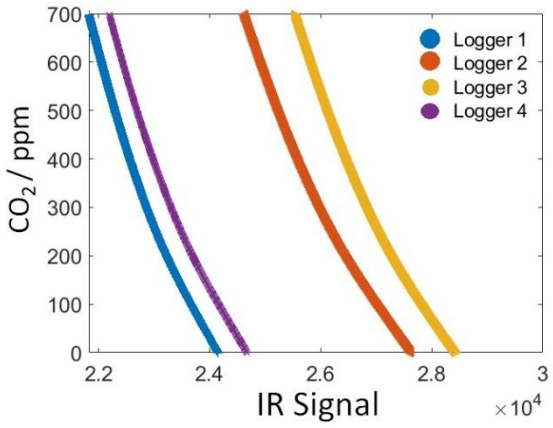

Figure 54 Response curves for each logger showing the IR signal at different CO_2 concentrations

For the absolute calibration, an experiment was constructed where all four sensors were co-located in a small chamber, with an inlet from an accurate CO_2 cylinder to control the concentration of CO_2 inside the chamber. The concentration inside the chamber is measured with the highly precise and accurate Picarro instrument (Picarro G2201-i Isotopic Analyser, Picarro Inc, CA, US). All inlet lines are PTFE inert surface tubing. The flows from the CO_2 cylinder and a nitrogen cylinder are controlled with a flow controller and are changed periodically to alter the concentration inside the chamber. The concentration is allowed to stabilise for ~30 mins before the next adjustment. The concentrations reached were 200, 350, 400, 450, 550 and 700 ppm, as determined by the Picarro. The next step involves measuring the concentration at each level for each sensor, after stabilisation, and constructing a response curve of the IR signals. These response curves are shown in Figure 54.

This response curve is then translated to the raw IR data, so that the CO_2 value for each sensor can be calculated. The result for the chamber tests are shown in Figure 55 and shows a good agreement with the reference Picarro instrument.

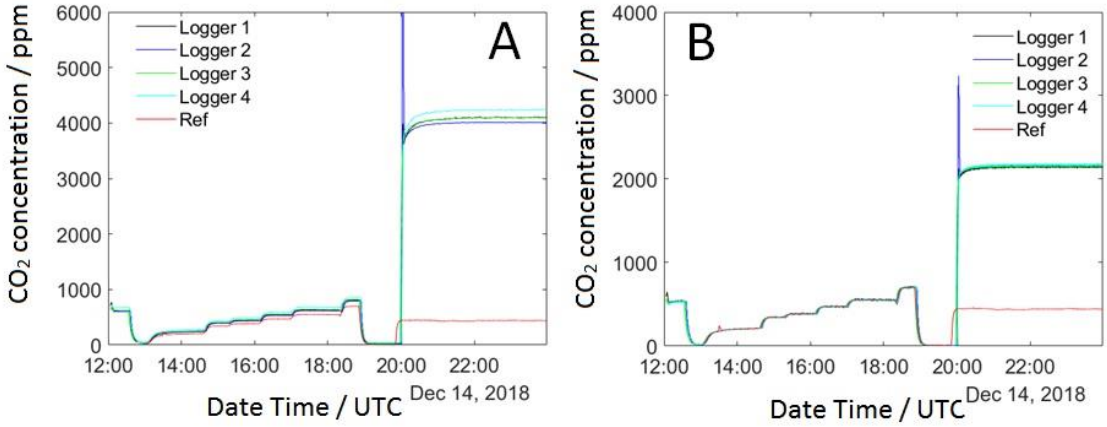

Figure 55 Calibration experiment of CO_2 sensors and Picarro reference using controlled chamber concentrations of CO_2 to construct response curve A) shows data before calibration with on-board CO_2 calculation B) shows data with calculated CO_2 after applying reponse curve

When this response curve is fit to the entire data series however it is clear that there is an issue with the sensor and that the CO_2 values do not match. The sensors have a temperature dependence that is not being accounted for in this absolute calibration and correction. This would require substantial chamber experiments with the sensors to determine a temperature dependence correction factor.

Figure 56 shows the resulting values for the CO_2 sensors. Generally there has been a shift to a lower concentration and in particular the inlet 4 logger has a persistent drift downwards. The values overall seem realistic and the zoomed-in plot shown in Figure 57 does indicate a more sensible scenario of the ground value being higher and gradually getting lower the closer you get to the leaves. It is likely that the absolute values here cannot be used and so comparing the different levels of the canopy is not possible. There is higher confidence that the trend from each logger independently can be used to discern daily trends and daily ranges

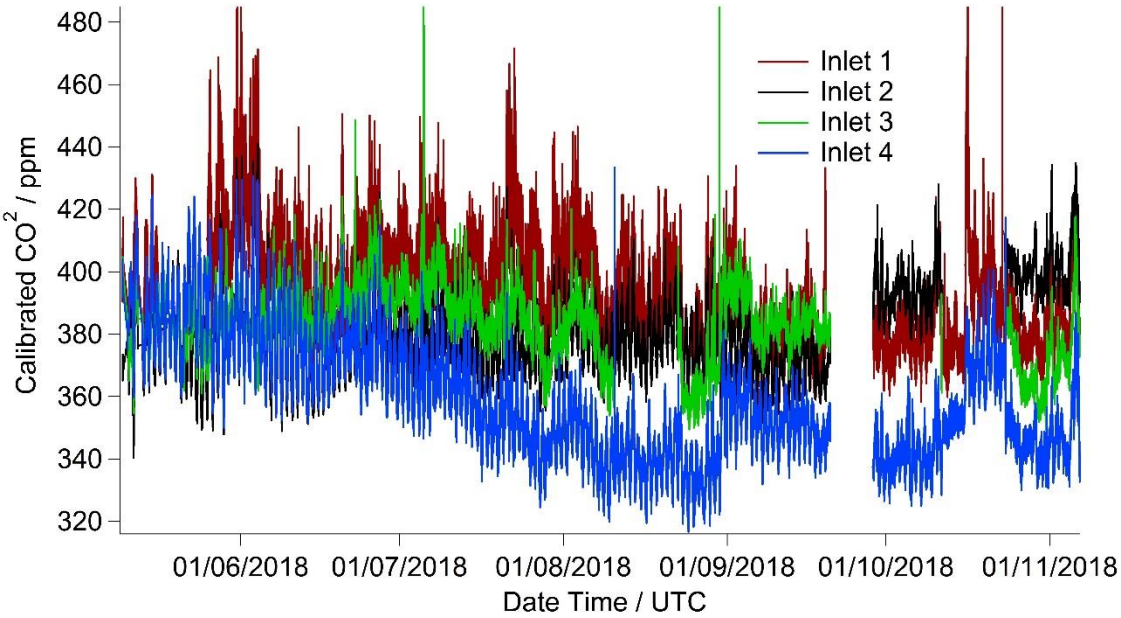

Figure 56 Calibrated and corrected CO_2 concentration data for the entire time series showing the gradual drift of inlet 4

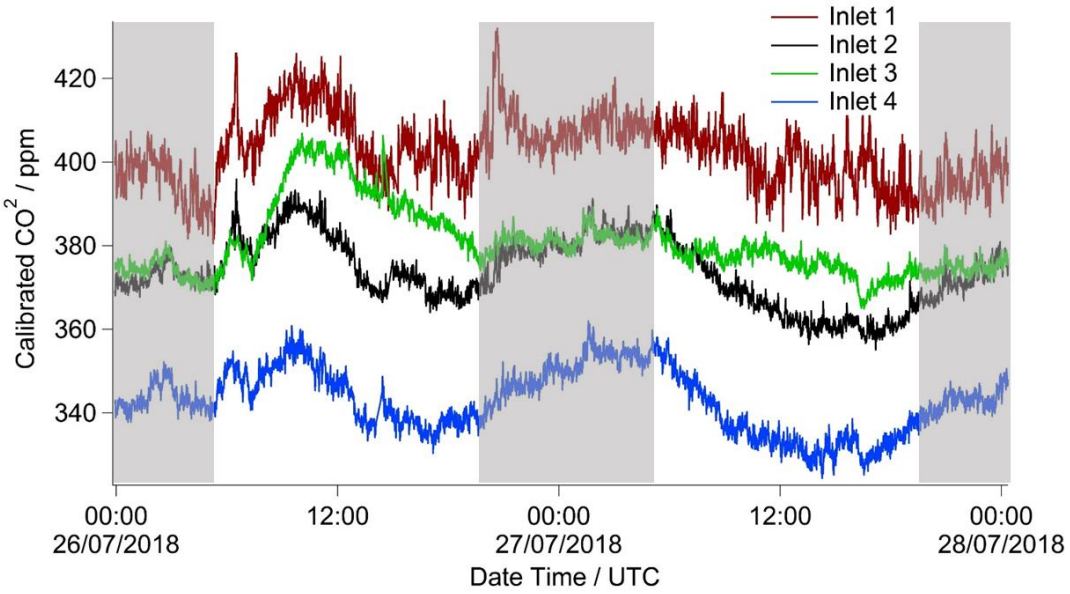

Figure 57 Two-day zoomed period of carbon dioxide concentration showing the daily profile. Night values are represented by shading

5.4.3 Time series of meteorological data

5.4.3.1 Measurements of temperature and relative humidity

Measurements of temperature and relative humidity were taken with the Easylogger mini logger units. These were in place slightly later in the summer than the other sensors due to the availability of the sensors (Figure 48). The temperature time series from these

loggers is shown in Figure 58, with a zoomed period shown in Figure 59.

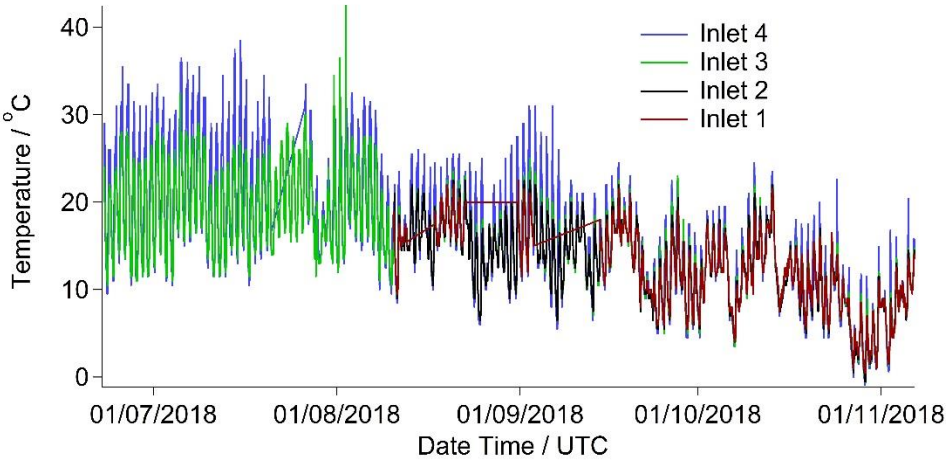

Figure 58 Complete Easylogger temperature measurement data set

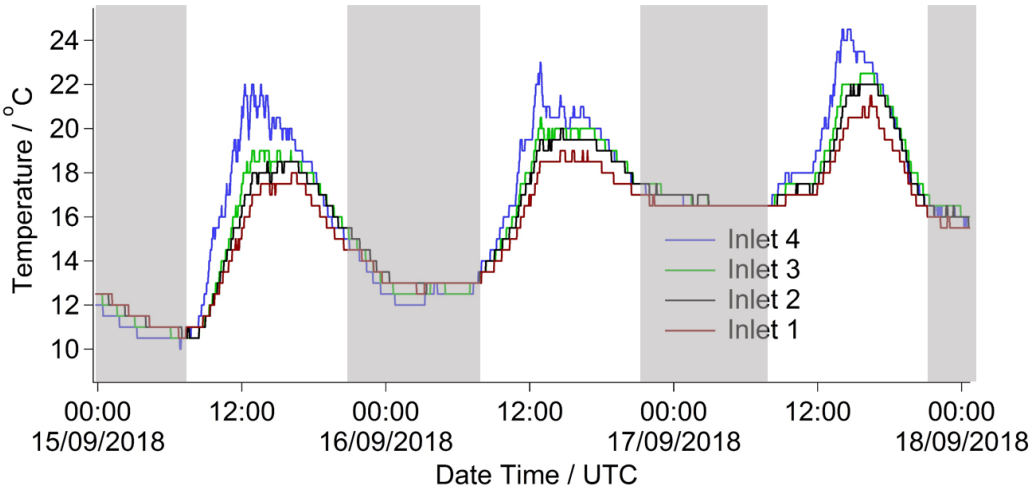

Figure 59 Easylogger Temperature plot, zoomed in to show the diurnal pattern with shaded areas representing night values

The daily pattern of temperature typically consisted of gradually increasing temperatures until two hours after midday, after which the temperature would drop until just before sunrise the next day. The temperature reached a maximum at the height of the summer in July and was disproportionately higher due to the 2018 heatwave from 22nd June to 8th August.

The relative humidity time series from these loggers is shown in Figure 60, with a zoomed period shown in Figure 61. Relative humidity typically reached its maximum just before sunrise and its minimum after midday; in the canopy the lowest relative humidity in the day was at the top of the canopy, and at night the lowest relative humidity was at the ground level. These trends are in line with expectations from transpiration and respiration.

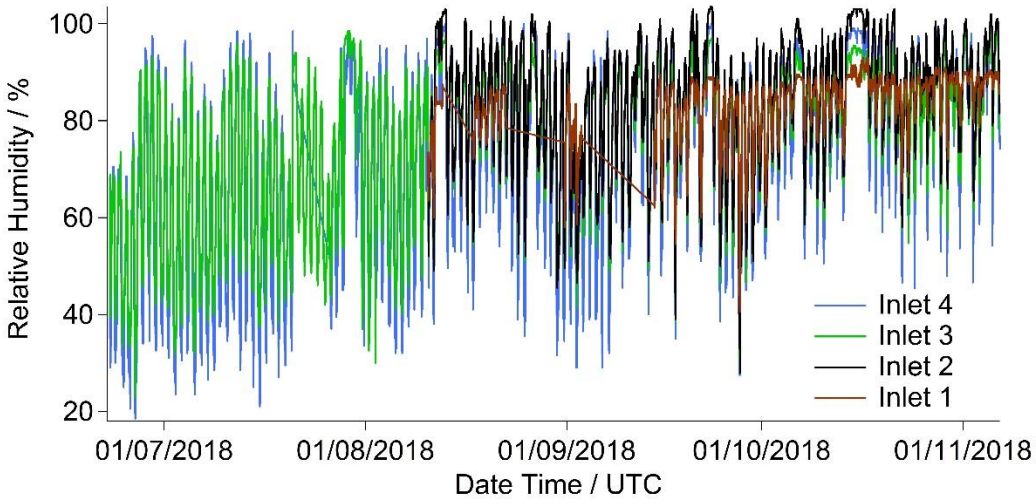

Figure 60 Relative humidity measurements for the entire time period

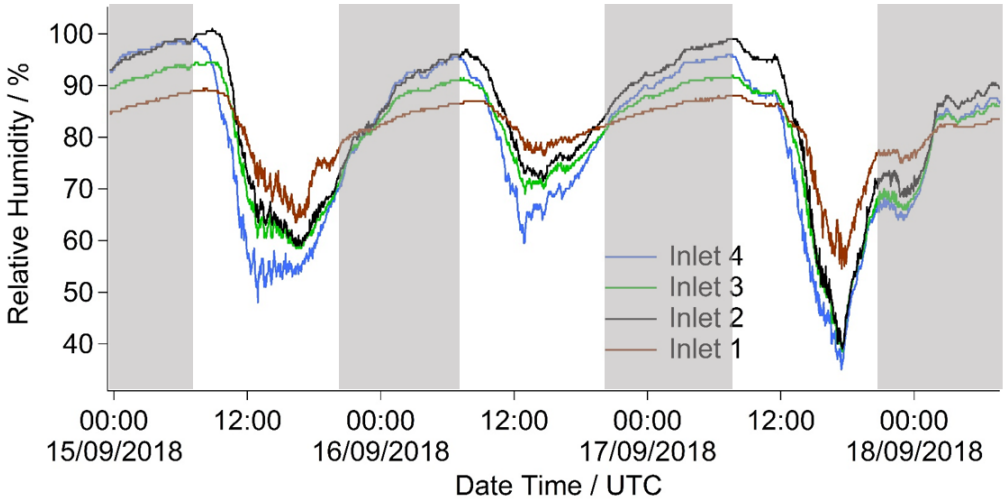

Figure 61 Relative humidity measurements for a select period to demonstrate the diurnal pattern with shaded areas representing the night values

Temperature was also collected with the CO_2 sensors, but the values obtained have an offset that is an artefact of the internal temperature of the logger unit. These temperature values are shown in Figure 62A. The time period covered by the CO_2 sensors exceeds that of the Easyloggers, hence an effort was made to assess the reliability of these temperature measurements. A simple experiment was constructed to compare the CO_2 logger units and the Easylogger units to a standard temperature probe (PT100 fast response air probe, class A, 1m, Pico Technology). It was found that the CO_2 loggers have a mean offset of +1.8^{o}C which is due primarily to heat produced by the logger itself. With this offset applied, the new temperature series is shown in Figure 62B.

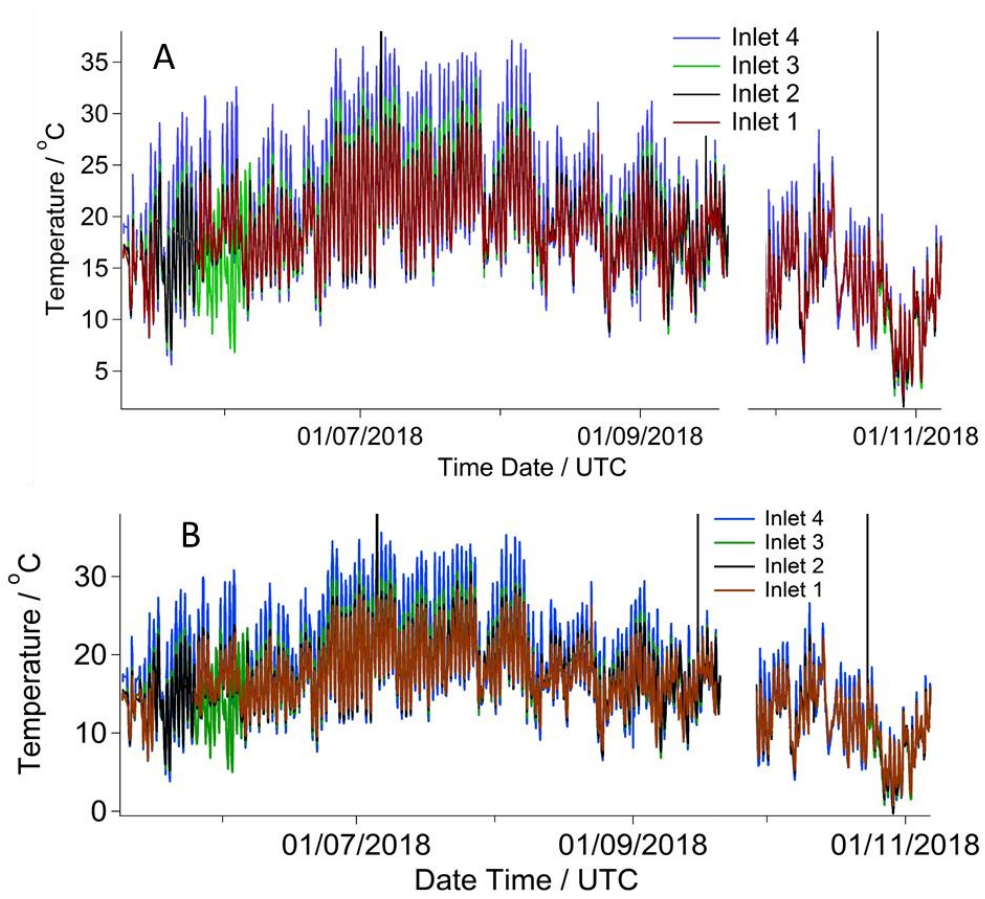

Figure 62 Temperature values from CO_2 sensor temperature probe A) uncorrected data points B) corrected data points

5.4.3.2 Photosynthetically active radiation across the measurement period

Light intensity is an important parameter to record when examining responses from plants. Photosynthetically active radiation (PAR) sensors were deployed to get an idea of the measure of extinction of light through the forest canopy. The sensors were deployed later in the summer because of the availability of the apparatus (Figure 48). The full time series of the PAR measurements is shown in Figure 63, with a zoomed period shown in Figure 64.

Generally the maximum light is just after midday each day and drops to zero at night. As expected, the September data has generally a higher daily maximum.

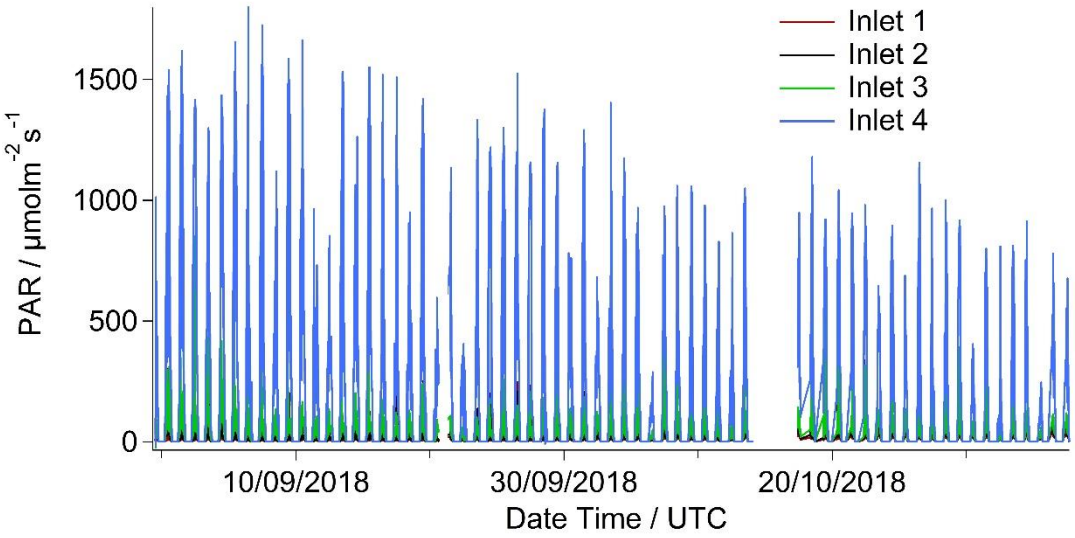

Figure 63 Complete time series of PAR measurements

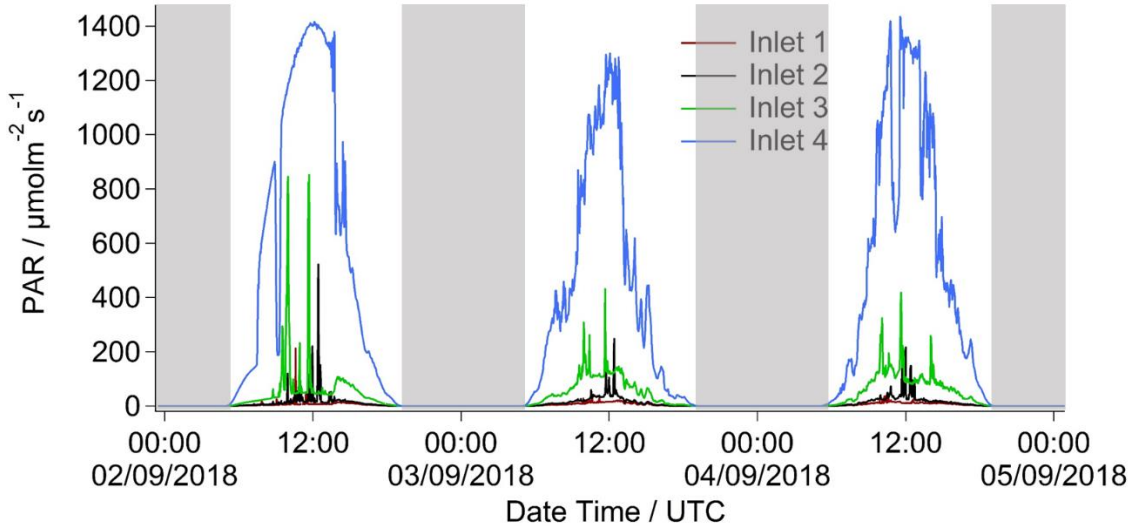

Figure 64 Three-day period to demonstrate diurnal profile of PAR with shaded areas representing night-time

From a brief analysis of the PAR data, it is apparent that the amount of light reaching the forest floor shifts between months. The PAR data was averaged over an hour and the relevant amount of light reaching the forest floor is determined by examining the percentage of each inlet against the inlet above. Table 10 shows the percentages for each inlet. It is observed that later in the season the amount of light penetrating through the canopy increases. This effect can be attributed to the gradual dropping of leaves as the days get colder and shorter, with the reduced leaf cover hence reducing the shade.

Table 10 Percentage of light reaching the forest floor

	September	October	November
% Inlet 1/Inlet 4	1.9	5.1	9.1
% Inlet 2/Inlet 4	3.4	8.1	11.6
% Inlet 3/Inlet 4	11.8	18.4	19.9
% Inlet 1/Inlet 3	16.4	28.1	45.6
% Inlet 2/Inlet 3	30.1	44.4	58.4
% Inlet 1/Inlet 2	55.7	63.4	78.0

This data-set begins at the end of August; hence for much of the analysis the solar radiation from the Upper Seeds AWS is used to infer PAR. To convert the solar radiation data from Upper Seeds to PAR it is first multiplied by 4.6 to convert Wm^{-2} to $\mu molm^{-2}s^{-1}$, followed by conversion to PAR by dividing by 2.4, which represents the proportion of the visible light spectrum that is accounted for with PAR.

To obtain an approximation for inlets 3, 2 and 1 the PAR sensor data is examined to select what percentage of the inlet 4 value is represented by that inlet. For the full dataset, the percentages from September for each inlet relative to inlet 4 are chosen as these most closely represent the summer month leaf coverage. These percentages are 11.81 % for inlet 3, 3.43 % for inlet 2 and 1.92 % for inlet 1. The complete approximated time series for PAR is therefore calculated. A zoomed-in plot of the time series is shown in Figure 65. One disadvantage of this method is that the time resolution is now hourly, however, a visual comparison of derived and measured data as shown in Figure 66, shows for the same day that the approximations used leads to a good representation of the actual data.

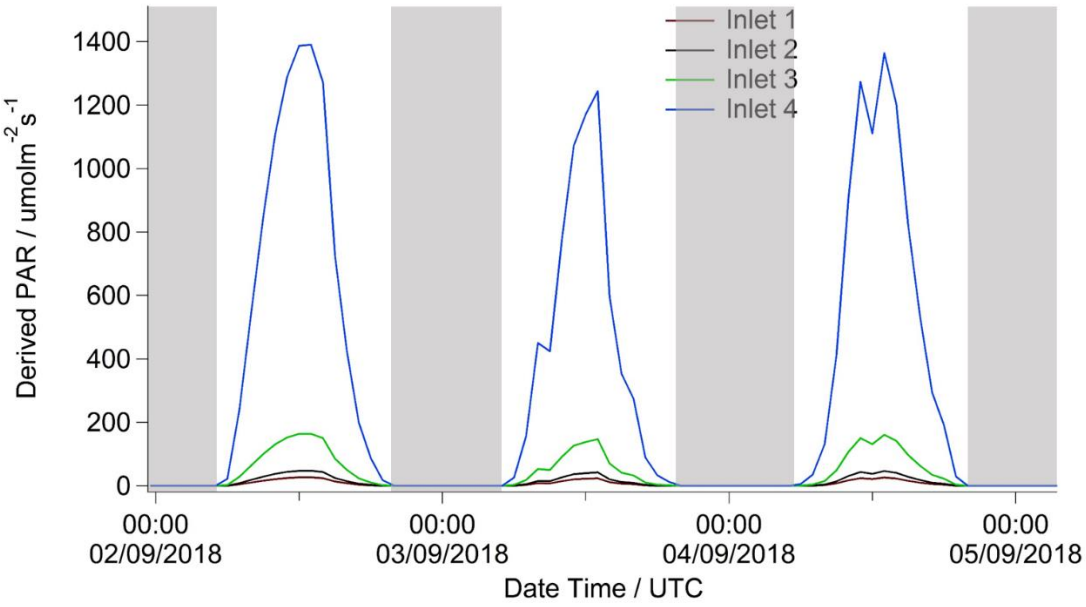

Figure 65 Approximated PAR three-day zoomed period as derived from the Upper Seeds AWS solar radiation and light extinction values with shaded areas representing the night

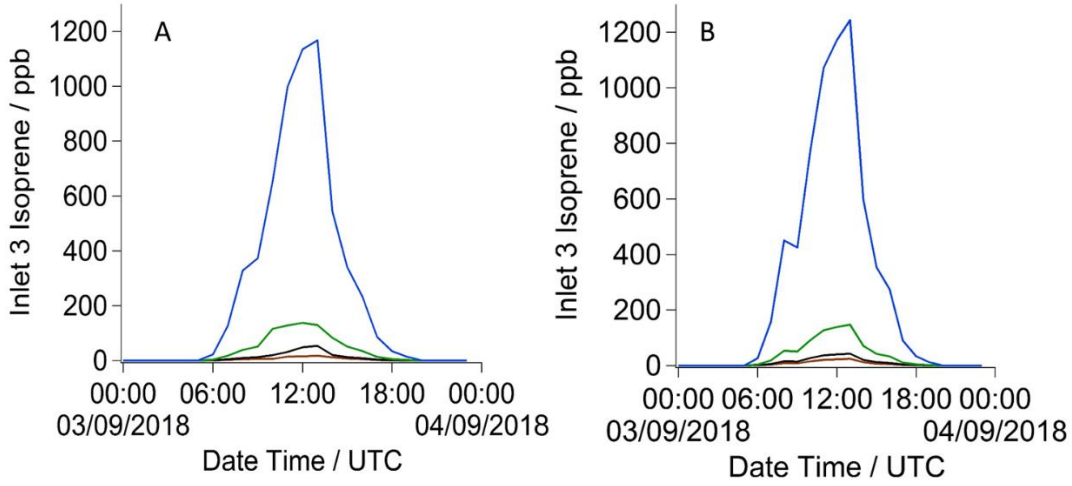

Figure 66 Comparison of derived PAR and measured PAR for all inlets on 3rd September 2018

5.4.3.3 Wind vectors across the measurement time period

The 3D sonic wind anemometer was deployed later in the summer due to the limited availability of the sensor. The anemometer was deployed in the first half of August as shown in Figure 48. For an hourly time series plot of the u, v and w vectors are plotted in Figure 67.

The wind data likely was affected by a faulty sensor. It is clear that the vectors, particularly the w vector do not represent sensible values that are expected for a temperate

forest. These values were not use in the analysis and the wind values were those from the Upper Seeds AWS.

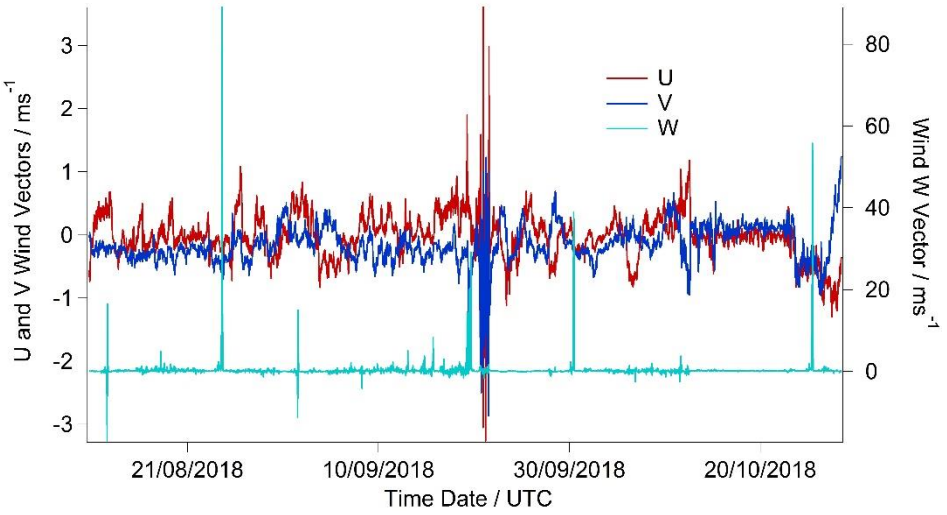

Figure 67 Wind vectors from the 3D sonic anemometer showing suspect values for the w (vertical) vector

5.4.4 Photosynthesis measurements and absorbent tube analysis

Twice during the field campaign, measurements were taken of photosynthesis and whole air composition with Lancaster University. These measurements were taken over three days on two occasions, 11th-13th July and 29th-31st August, and consisted of measurements of photosynthesis from select leaves on the target oak tree, whole air samples at different heights in the canopy and composition analysis of samples taken from the LI-COR leaf cuvette. The results from these measurements are not currently available for analysis and work is under-way to analyse these samples. Analysis of these results is part of future work to understand how the forest changes over time and reacts to a heatwave.

5.5 Photographic time series

Of the two types of routine photos, the canopy photos are shown in Figure 68 and photos of select leaves are shown in Figure 69. The photos are of the same branchlet and the forest canopy from below and show the changes through the season.

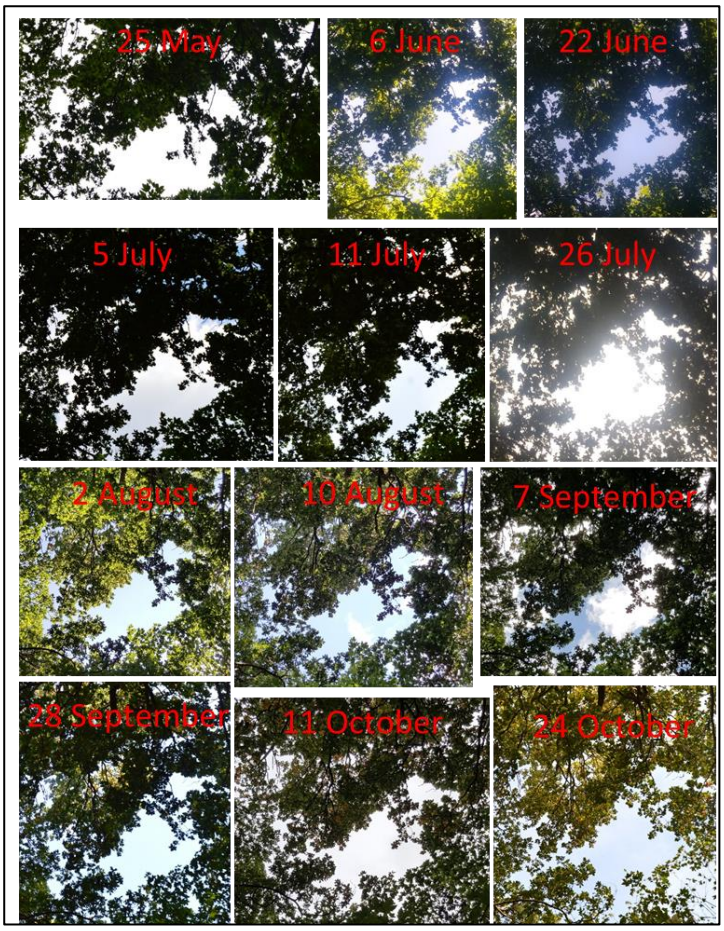

Figure 68 Pictures of a select area of forest canopy through the summer

Figure 69 Picture of select leaves from the walkway through the summer

The photographic results do not appear to display any indication of degradation of tree health. It is apparent from Figure 69 that as the season progresses the leaves darken in

colour which may indicate coming to maturity. The leaf cover as shown in Figure 68 does not seem to visually indicate a shift in cover over the time period indicated. The final image from the 24th October indicates a slightly thinning canopy and paler leaves, though the back lighting of the leaves differs in each photo and it proved difficult to take the same photo on each occasion.

5.6 Summary of results from WISDOM

5.6.1 Performance of instruments

The deployment of as many sensors and instruments in a forest provides an opportunity to evaluate their performance under challenging field conditions.

Collection of meteorological data was achieved with the use of Easylogger USB loggers and proved to be a simple and convenient way of collecting temperature and relative humidity data. The sensors were in general reliable and stable, though evidence suggests that they require shelter as water ingress caused failure on one occasion.

The iDirac isoprene GCs proved themselves to be capable of collecting reliable high resolution isoprene data. When adequately powered, the instruments were only limited by the volume of calibration or carrier gas and did not show a severe sensitivity drop across the field campaign.

The carbon dioxide sensors proved to be suitable for the campaign, but had some operational issues. The data from them after calibration proved to be strongly affected by the temperature in the field and that a complex relationship with temperature and the internal parameters of the sensor meant that the data could not be used for an in-depth analysis. In terms of practicality the instruments were a suitable size for the field but the data transfer proved to be unreliable and the sensor was sensitive to water exposure.

The PAR data was very reliable and highly suitable for such a campaign but the wind anemometer was not correctly configured to collect data. The sonic anemometer was not suitable and requires both mains power supply and a more suitable logging system.

5.6.2 Seasonal variation of each data time series

One aspect of this research that is of interest is the length of the experiment, which encompassed a growing season in a northern hemisphere temperate summer. The data collected will be used to look for patterns in the emission from the trees as the season progresses, capturing the emission from leaves in late spring, through to their senescence

of the leaves with the onset of winter. The data set can be processed and interrogated a number of ways to investigate these factors.

One aspect likely to affect the emission of the forest canopy is the meteorology and the general climactic conditions. In subsequent sections, the data will be compared to meteorological factors to uncover any underlying patterns or indicators of forest stress.

5.6.3 Vertical canopy gradient of each data time series

The position of four inlets at four different heights in the canopy means that the factors can be investigated that determine how isoprene distributes through the canopy. Potential sources and sinks will be investigated, as will the transport of air within the canopy. This information will be used to inform a modelling study that is discussed in Chapter 7.

5.6.4 Effects of the 2018 UK heatwave

The summer of 2018 was exceptional when typical climactic conditions of the British Isles are considered. The month of July saw sustained high temperatures and very low precipitation, leading to heatwave and drought conditions. This meteorology is one that will likely affect the forest in many ways, and this data set gives us a unique opportunity to ask how these extreme conditions affected the forest. With this data set, how the forest has responded to heat stress can be examined and how the forest did or did not recover.

5.7 Conclusion and future work

To conclude, a long-term series of the concentration of isoprene and CO_2 was collected at four heights in the canopy. Isoprene concentrations showed a strong diurnal profile and reached concentrations as high as 8 ppb at the height of the heatwave. Night-time values of isoprene concentration consistently dropped below detection limit. At concurrent heights to these are measurements of temperature, relative humidity and PAR. PAR values have been calculated for the entire time series using the solar radiation data from the AWS. A suite of hourly meteorological data will provide an insight into the factors affecting the Wytham forest site and the conditions at the top of the canopy or site-wide factors such as rainfall or soil moisture. The data collected here will provide valuable insight into the forest canopy and the dynamics of isoprene concentrations in a forest. The data collected has been rigorously validated and calibrated to give high confidence in the values so that robust conclusions may be drawn. This vast dataset will be analysed to realise the relationships between the factors that control the isoprene in the forest.

The WISDOM campaign was the first experiment of its kind using the iDirac to measure isoprene. There were a number of developments in term of the instrumental set-up and practicalities that should be highlighted for future campaigns. Four developments are highlighted here:

- Power was an issue in 2018 and demonstrated that a reliable power supply is key to the success of this experiment. If mains power is not possible, it may be necessary to increase the number or size of the solar panels used to allow for more efficient charging.
- The iDirac inlets should be alternated to increase confidence in inter-instrument variability. Hence the iDirac based on the ground would measure inlets 1 and 3 and the iDirac based on the walkway would measure inlets 2 and 4.
- Reliable 3D sonic anemometers should be installed at each height to allow an in-depth understanding of how the air is moving and in what direction transport is occurring.
- A higher inlet 4 would increase confidence in the above-canopy concentrations. In the future, an improved understanding of the above canopy region could be garnered if the inlet is situated ~2 m higher so as to avoid much of the surface roughness and heterogeneity of the canopy.

6 Discussions on Isoprene in a Temperate Forest

6.1 Introduction

The dataset from WISDOM, described in Chapter 5, provides a unique opportunity to ask lots of questions of the forest. The behaviour of trees in a forest can be altered by a great many factors, including biotic and abiotic stresses. The challenge is to pick which factors directly result in stress response mechanisms such as isoprene emission.

The WISDOM dataset is described in Chapter 5 and extends from late spring to late autumn 2018. 2018 was marked with exceptional weather and this likely had a large effect on the biosphere. The measurements of isoprene appear to indicate that the trees responded very strongly to the higher temperatures and the severely reduced rainfall. By digging further into this time series and looking at average trends and correlations, understanding of how the forest responded and what other factors were involved can be obtained.

Three prongs of analysis are used to interrogate the forest at Wytham. The forest can be assessed as a whole, with an overview of the isoprene and other factors that were measured. This can pull out some seasonal patterns that begin to allow some understanding of the fundamental relationships between the data. The vertically-spaced series of data allows us to ask questions about the mixing within the canopy including what factors affect this and what are the implications of this on the biosphere and climate. Thirdly, the heatwave provides an opportunity to examine how a forest is responding to stress and if it can recover quickly. Several key points will be brought from the data that interrogate this period further.

6.2 Aims

The aims of this chapter are to investigate:

1. How isoprene concentration relates to different meteorological factors.
2. How the vertical mixing varies through a season.

3. What factors are affecting the vertical canopy gradient.
4. The 2018 heatwave and how the forest responded to this abiotic stress.

6.3 Isoprene concentration profiles during WISDOM

6.3.1 Isoprene diurnal cycles

The time series of isoprene shown in Figure 51 shows some features to be investigated further. For the top two inlets, the data series captures the profile in isoprene before, during and after the heatwave. The time series also shows the clear decline of isoprene as the season progresses.

The overall relationship and diurnal cycle of the four inlets is shown in Figure 70. On average, isoprene production is seen to begin at around 06:00 UTC and to decline back to low levels at 22:00 UTC, but this of course changes through the year as the day length changes. Inlet 4 is always significantly higher than inlet 3 when isoprene is present, which is attributed to the proximity to the most irradiated leaves. This plot also shows the time shift of the inlet 1 isoprene concentration maximum daily peak compared to inlet 4. With a time lag of nearly 2 hours, this shift demonstrates that the majority of the isoprene observed at the forest floor is transported from the canopy. The time it takes to transport downwards will cause a delay in the peak, so this can be indicative of the mixing rate of the forest canopy.

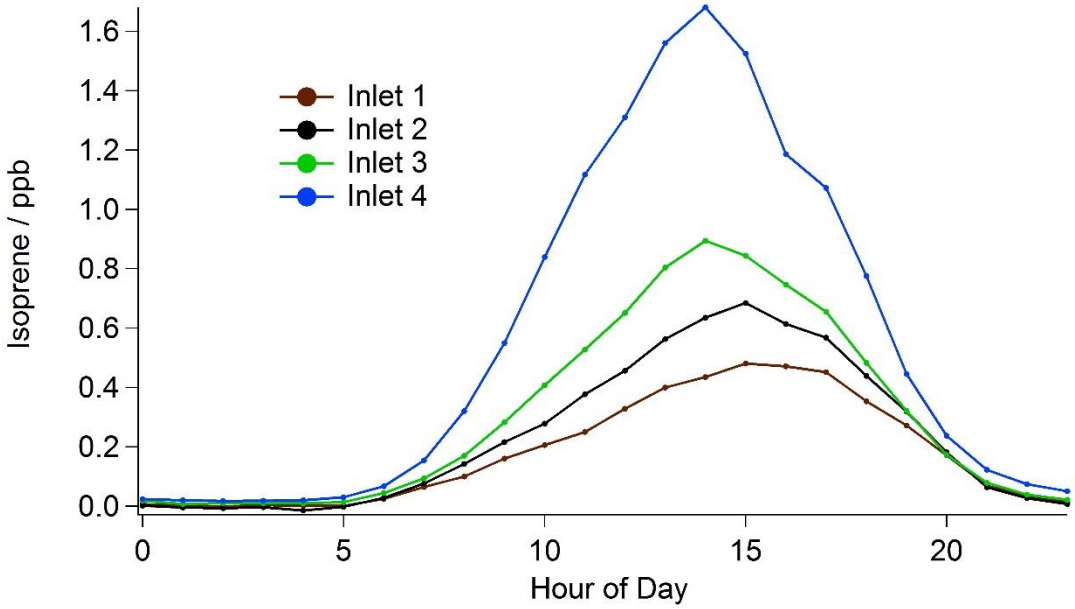

Figure 70 Average diurnal isoprene profile over entire time series. Inlet 1 & 2 5th July to 30th September 2018. Inlet 4 & 3 from 25th May to 30th September 2018

When broken down into smaller time periods, further details become apparent.

Figure 71 shows the isoprene concentration daily profile, averaged over each month. At each inlet it is apparent that the daily maximum is getting earlier later in the season. This may be due to the phenology of the forest changing, or it could be due to the meteorological factors affecting the forest such as the soil temperature causing the tree to heat up faster.

To show an even finer scale, the weekly averages are plotted in Figure 72. In particular here it is clear that there is a six week period of elevated isoprene which is attributed to the heatwave. Again, the daily isoprene peak shifts to earlier in the day later in the year and this is observed for each inlet. The later peak of the lower two inlets can also be observed clearly.

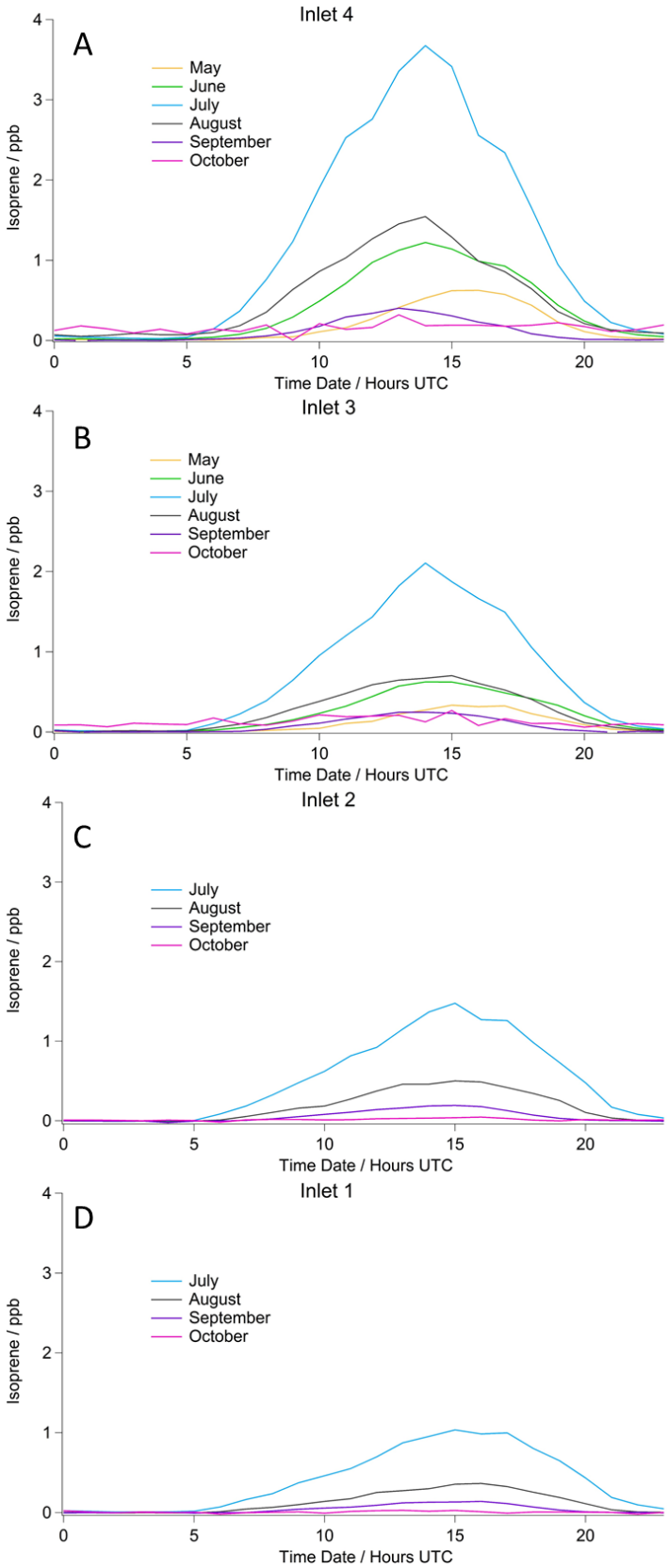

Figure 71 Monthly mean hourly average isoprene diurnal profile A) Inlet 4 B) Inlet 3 C) Inlet 2 D) Inlet 1

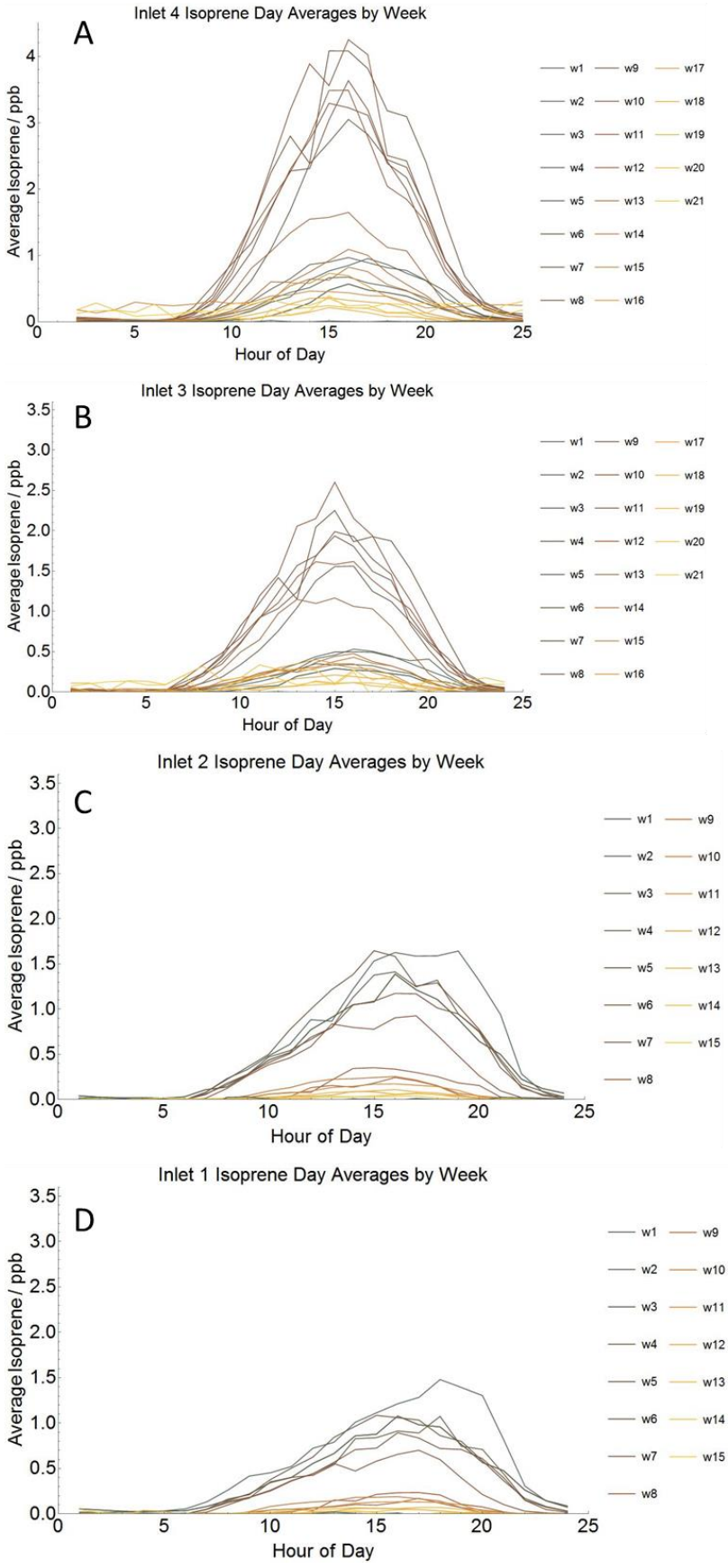

Figure 72 Weekly mean hourly average isoprene diurnal profiles A) Inlet 4 B) Inlet 3 C) Inlet 2 D) Inlet 1

6.3.2 Response of isoprene concentration with temperature

To analyse the changes of isoprene at each of the levels, an hourly average is obtained so that equivalent time periods may be plotted in a scatterplot.

Figure 73 shows the isoprene concentration plotted against temperature, with each inlet indicated. The plot shows that the isoprene concentration increases as temperature increases, as the leaves respond to the heat with increased emission as has been reported widely in the literature. It is understood that the isoprene emission declines above a temperature as low as 32 ^{o}C and that above this temperature, the plant may suffer heat damage but this threshold varies for different regions and species (Singsaas & Sharkey, 2000). This emission profile with respect to temperature varies for different individuals, species and latitude. It can be seen that in the correlation plot shown in Figure 73 that values above 32 ^{o}C show a decline in isoprene concentration, though this may be due to low PAR values. Indeed, in the time series of isoprene concentrations, on three days where temperatures exceed 32 ^{o}C there is a drop in isoprene concentration.

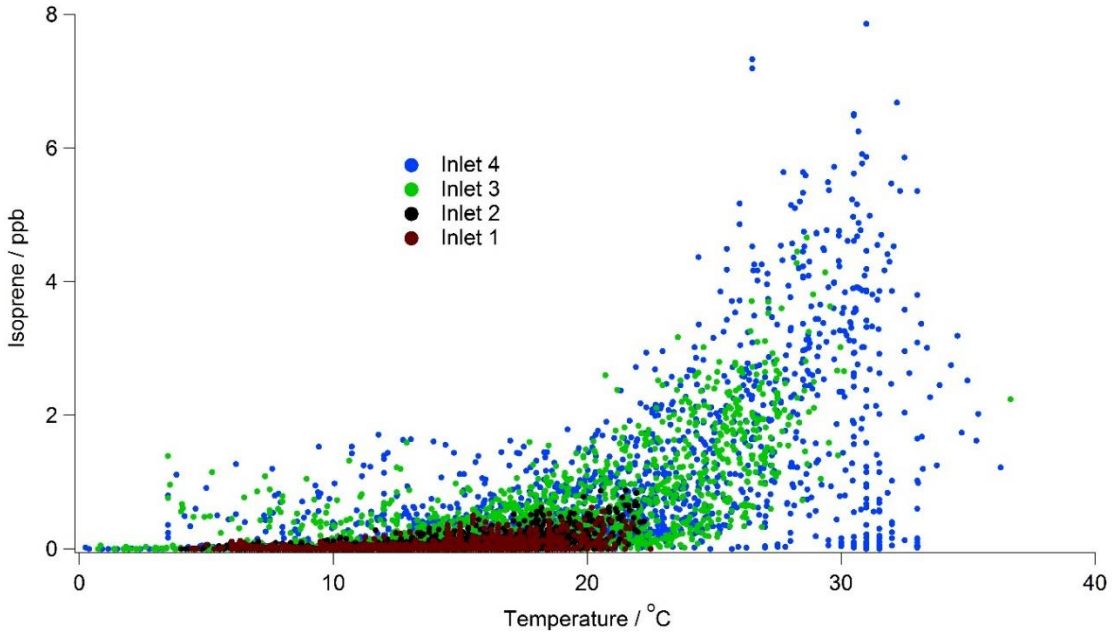

Figure 73 Hourly mean isoprene concentration plotted against hourly mean temperature for each inlet. Inlet 1 & 2 5th July to 19th October 2018. Inlet 4 & 3 from 25th May to 27th October 2018

To examine the relationship of isoprene with temperature in a temporal sense, the average peak isoprene, from 1-5 pm was plotted against the same time period for temperature. It is observed in Figure 74 that at the start of the summer, the isoprene concentration roughly follows the temperatures and the relative size of the temperature differences match those

of the isoprene. It is observed that nearing the end of the season where temperature levels are similar, there is less isoprene observed. This could indicate that isoprene emission has slowed down and may be a demonstration of the aging of the leaves, though the length of the day and decreased soil temperatures likely also affect the emission. The heatwave is clearly visible from 22nd June to 8th August.

The reason for the decoupling of the isoprene concentration from temperature is poorly understood. Several sources suggest when a plant is under stress from heat or drought with reduced photosynthesis, carbon loss as isoprene can up to 50% of total carbon uptake (Brilli et al., 2007; Lerdau & Keller, 1997). This effect can be from the use of alternative substrates to form isoprene from different metabolic pathways (Bamberger et al., 2017; Pegoraro et al., 2004). When under stress, it has been observed that although photosynthesis reduces and stomatal conductance decreases, isoprene production continues and typically even increases. When under stress and photosynthesis is reduced, there is evidence that isoprene is produced from a range of different substrates in the cell chloroplasts (Funk et al., 2004). These substrates however have a finite concentration, or their production may depend on stress related factors, hence when used in fairly high amounts to produce isoprene, their concentration may be lowered. If a drought persists for long enough, the isoprene production can slow down as these substrates are used up, but this does not appear to be observed here.

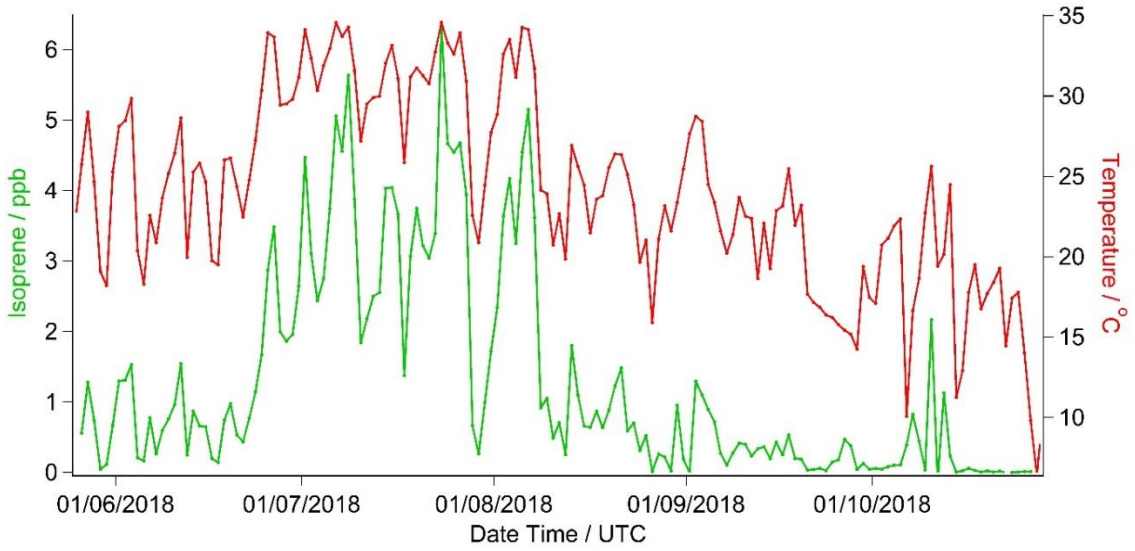

Figure 74 Mean isoprene and temperature from 1- 5pm across the experimental time period at inlet 4

To investigate why the daily isoprene peak gets earlier later in the season as shown in Figure 71 and Figure 72, the average diurnal pattern of temperature for each month at

inlet 4 is shown in Figure 75. The plot shows that in fact the peak temperature in the spring is in fact later than in the autumn. For example, the peak temperature value is at 15:00 UTC for May but for October the peak temperature is at 13:00 UTC. This difference explains why the isoprene peak is earlier because the isoprene concentration has been shown to correlate strongly with temperature.

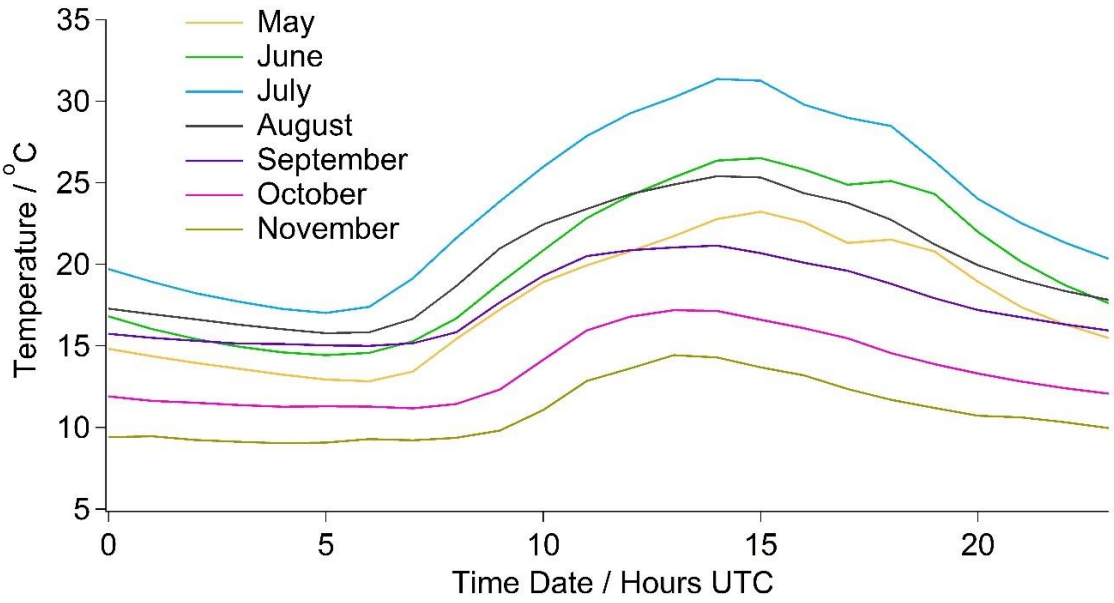

Figure 75 Month average diurnal profiles for temperature as mean hourly values for inlet 4

6.3.3 Isoprene concentration response to PAR

From the scatterplot of mean hourly isoprene concentration with mean hourly PAR, shown in Figure 76, it is shown that isoprene concentration correlates with PAR, but not to the same extent as temperature (Figure 73). The plot shows that the scatter of the isoprene concentration at each value of PAR depends on temperature, so that on sunny but cold days the isoprene concentration is reduced. This supports the idea that isoprene emission is dependent on photosynthesis, which requires light, but that the isoprene emission dependence on temperature is more closely linked, as has been concluded in the literature. This suggests that the isoprene emission is a response to heat stress, which has been investigated in the literature as discussed in Section 1.4.1.2.

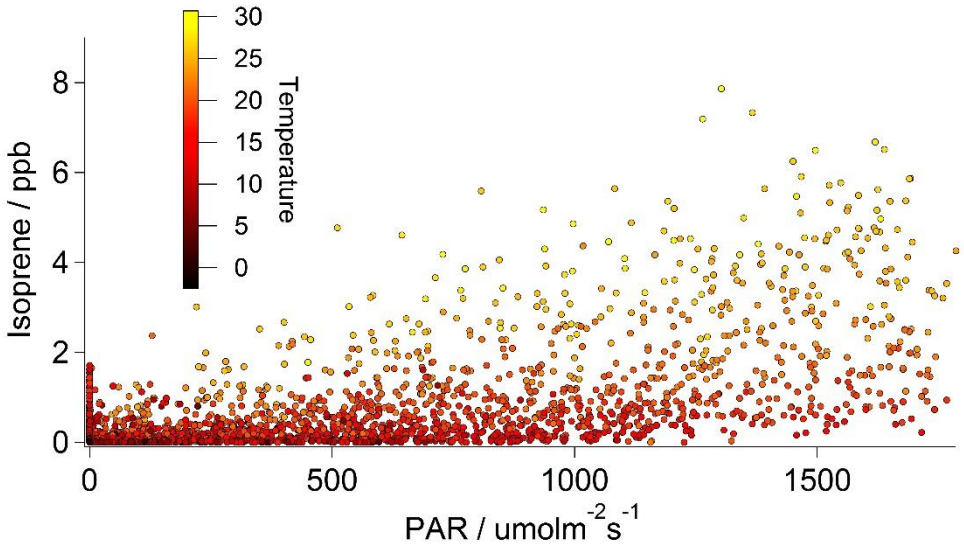

Figure 76 Inlet 4 isoprene against PAR with colour as a function of temperature

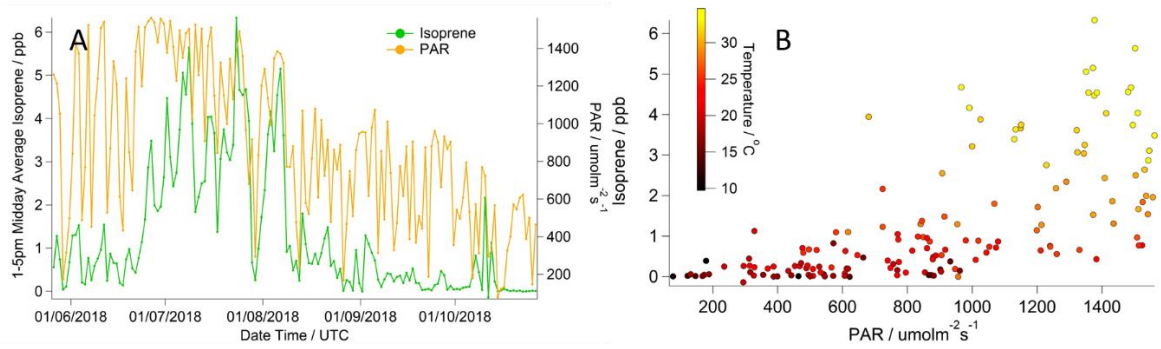

Figure 77 Mean isoprene and PAR from 1-5pm across the experimental time period at inlet 4 as A) time series B) correlation scatter plot with 1 – 5pm mean temperature colour scale

When PAR is plotted against isoprene for the 1-5pm average as shown in Figure 77B, as expected the isoprene concentration follows the PAR values but not as closely as temperature as in Figure 74. The correlation plot shows the same profile as for the entire dataset. The time series in Figure 77A also shows that the profile for PAR is not elevated during the period 22nd June to 8th August but that there are an increased frequency of clear-sky values.

From Figure 78 it is seen that the peak PAR is at the same time each day and that the daily isoprene concentration peak is later and appears to shift over time, as described in Section 6.3.1. As expected, at the forest floor the peak isoprene is four hours later than the peak PAR for that level, whereas the peak isoprene at inlet 4 is 2 hours afterwards. This is likely due to the mixing of isoprene in the forest canopy, soil deposition processes

and the proximity to the leaves, these factors are investigated in a modelling study in Chapter 7. At the forest floor (inlet 1) the distance for the diffusion of isoprene is greater resulting in a later peak.

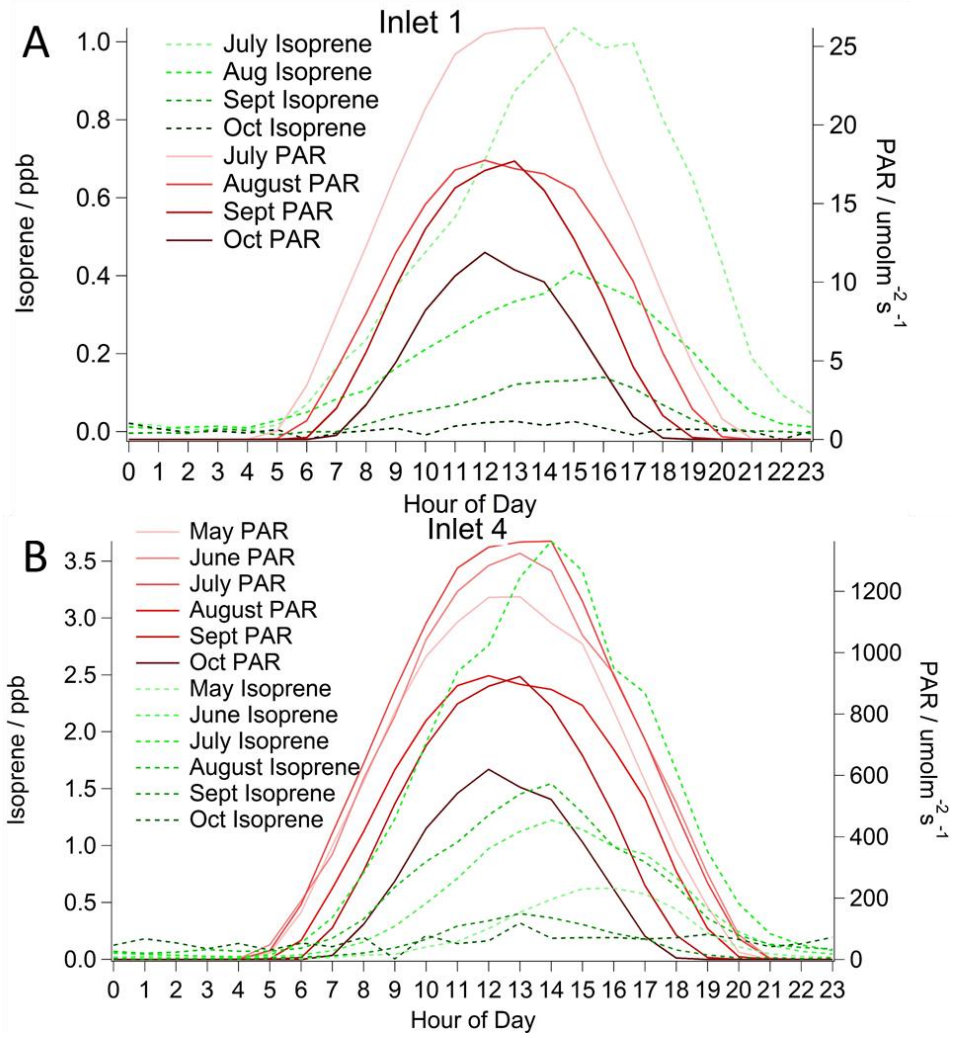

Figure 78 Average monthly diurnal profiles of mean hourly PAR and isoprene concentrations at A) inlet 1 and B) inlet 4

6.3.4 Carbon dioxide diurnal profile

Carbon dioxide is produced and taken in by plants, with predominant respiration during the night and photosynthesis dominating during the day. The function that determines CO_2 uptake follows a similar profile as isoprene, with gross primary productivity giving a good representation of CO_2 uptake (Beer et al., 2010).

It is understood that isoprene is produced in leaves using CO_2 absorbed in photosynthesis (Sharkey et al., 2008). Studies have shown that the carbon atoms in isoprene are directly obtained from absorbed CO_2 (Sharkey & Yeh, 2001). The average daily profile of both isoprene and CO_2 for inlet 4 at the top of the canopy is shown in Figure 79 for the month

of July at the top of canopy and shows an anti-correlation of CO_2 and isoprene. The maximum isoprene occurs just before the CO_2 reaches its daily minimum, likely as a delayed response to photosynthesis.

As with isoprene, a shut-down of photosynthesis and stomatal conductance can occur during heatwaves (Jiang et al., 2018) which effectively changes the emission or absorption of CO_2. Isoprene emissions continue even after photosynthesis has shut down (Bamberger et al., 2017).

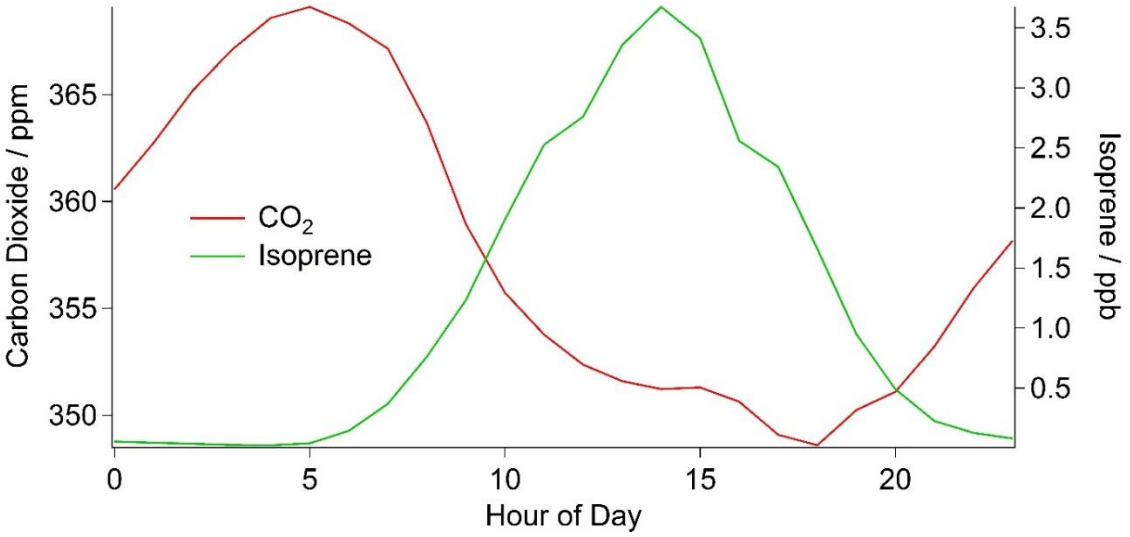

Figure 79 Average daily profiles of mean hourly isoprene concentration and CO_2 concentration at inlet 4 for July 2018

6.3.5 Isoprene and relative humidity

Relative humidity is suggested to influence the emission of isoprene by controlling stomatal conductance (Fall & Monson, 1992). It is important for the consideration of isoprene in the atmosphere as it has been suggested that it enhances secondary organic aerosol formation (Song et al., 2015). Figure 60 shows the diurnal profile of relative humidity and Figure 80 shows an apparent correlation. Relative humidity is closely related to photosynthesis and respiration of the trees, therefore without further study and new measurements of photosynthesis it is not possible to conclude if relative humidity directly influences isoprene concentration. It may also be possible that the temperature relationship with relative humidity is driving this apparent correlation as the temperature of the air strongly affects the relative humidity. Further experiments are required to investigate the effect of relative humidity on stomatal conductance.

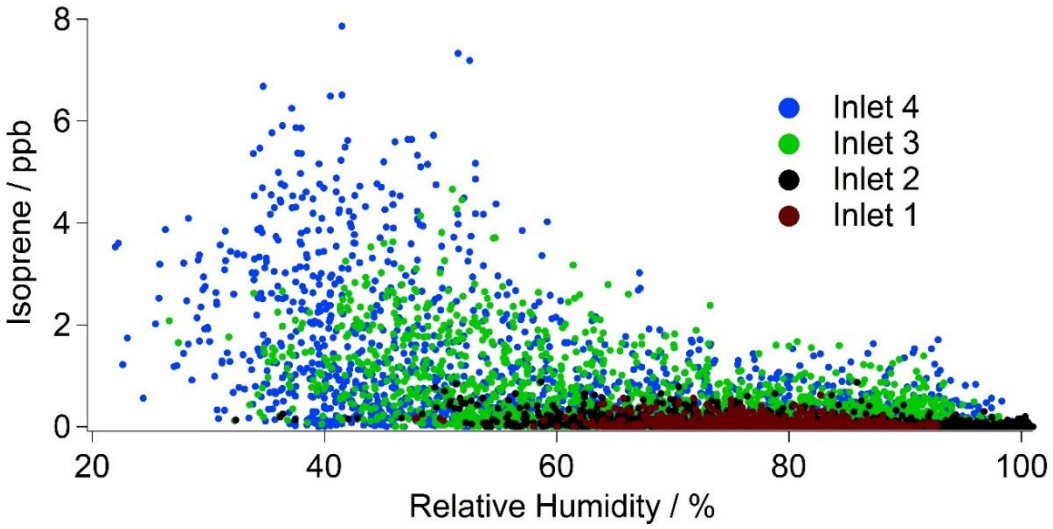

Figure 80 Correlation of mean hourly isoprene with mean hourly relative humidity

6.4 Relationships of meteorology with isoprene

6.4.1 Relationship of isoprene with wind direction and speed

The strength and direction of the wind can affect many aspects of the atmospheric composition at Wytham. For example by increasing the rate of mixing, a higher wind speed would result in lower concentrations. The direction of the wind may affect the concentration by passing over isoprene sources such as a large *Q. robur* individual.

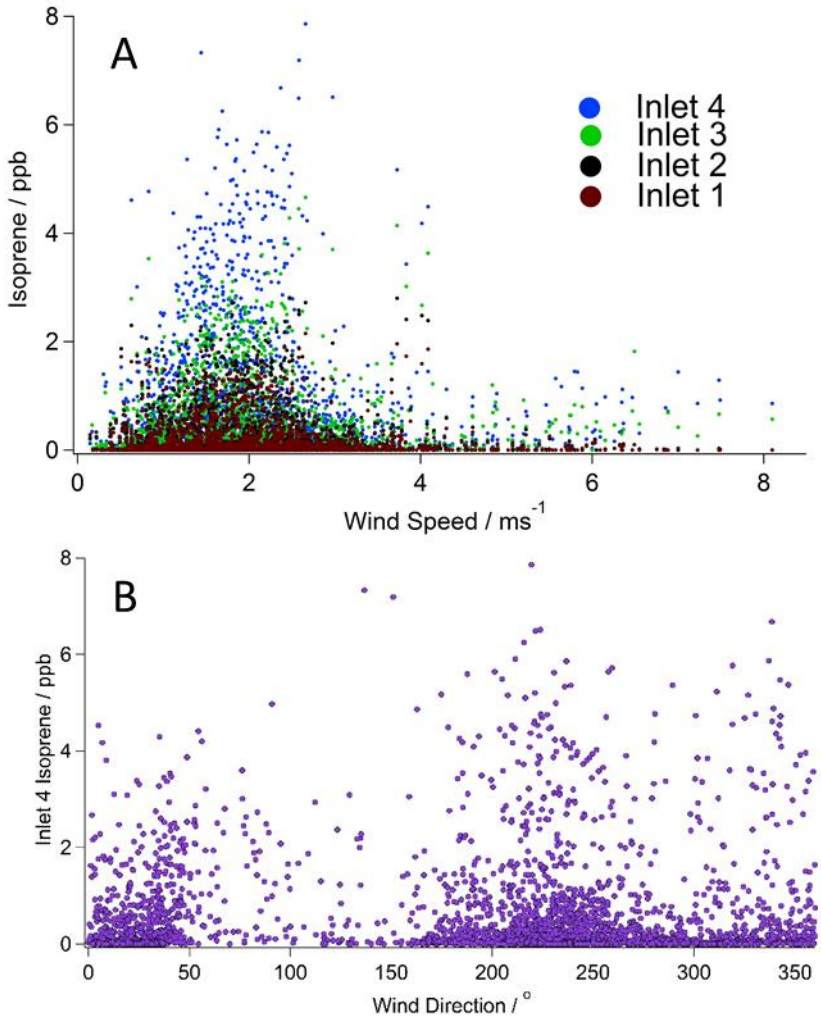

Figure 81 A) Correlation of mean hourly isoprene concentration at each inlet with mean hourly wind speed at inlet 4 B) Correlation of mean hourly isoprene concentration at inlet 4 with mean hourly wind direction at inlet 4

Due to the lifetime of isoprene (1–2 hours in a temperate forest (Pacifico et al., 2009)), it is possible that the effect of local sources such as dense areas of *Q. robur* trees is masked by the meteorological factors. Figure 81A shows the isoprene at each level against the wind speed. It is seen that the wind speed does not affect the isoprene concentration. Odd events such as those at ~4 ms^{-1} are in fact caused by a windy period that was also very warm which would result in a higher isoprene emission from the leaves. Figure 81B shows the wind direction and isoprene correlation and demonstrates which directions typically correlate with higher isoprene. It shows that wind directions from the southwest typically correlate with the highest isoprene, with a mean daytime value of 0.9 ± 1.3 ppb at inlet 4 between 200º and 250º. Some higher concentrations are also correlated with the north-eastern direction with a mean daytime value of 0.6 ± 0.8 ppb at inlet 4 between 0º and 50º. This observation may be due to the distribution of tree species in the forest and

upstream isoprene sources or it could be due to temperature and cloud cover when the wind arrived from these directions.

To assess whether a particularly strong signal is seen from any particular direction that indicates upstream sources, the open source software package Openair for R is employed. This is a tool for analysing air pollution data that was developed as part of a NERC funded knowledge exchange program, led by the Environmental Research Group at King's College London. Openair uses the wind speed and direction values and constructs a convenient graphic to help analyse potential sources of any pollutant. Isoprene measured at inlets 3 and 4 were analysed with Openair using the wind data from the Upper Seeds AWS to investigate if a signal could be observed from any particular direction. As Openair is meant for measurements in the PBL, only inlet 3 and 4 are used here as these inlets are likely influenced more strongly by air movements above the canopy. To avoid skewing the data, all the isoprene values from the night were omitted in this analysis. The output from Openair is shown in Figure 82.

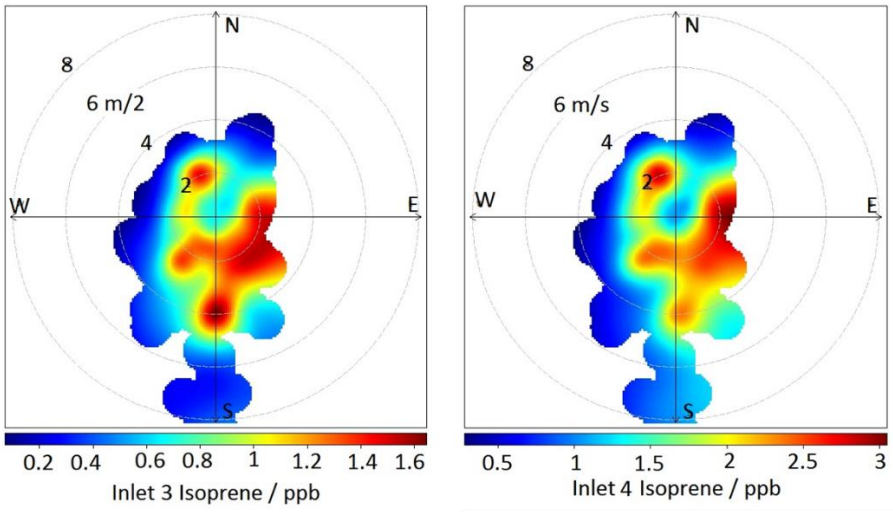

Figure 82 Polar bivariate plots (Openair) from isoprene concentrations at two inlets using the Upper Seeds AWS wind speed and direction data

These bivariate polar plots from Openair show the concentration of isoprene coming from a certain wind direction when the wind is of a certain speed, giving some indication of the proximity to the source. It is tempting to attribute these point sources to individual trees, particularly as the apparent sources of isoprene match approximately the oak trees mapped in Figure 42. This is a useful tool and does seem to shed light on some predominant directions that show higher isoprene concentrations. However, the forest at Wytham is somewhat heterogeneous and the oak distribution is fairly even through this

region of the forest (Lee et al., 2016) so a broader signal is expected. With the turbulence of the forest canopy, it would be highly unlikely that the signal from a multitude of trees were not extremely well mixed when it reached the inlets. Further study is required to investigate advection over the forest and the transport of isoprene from the wider forest.

6.4.2 Can anthropogenic carbon dioxide emission be detected?

Wytham woods is a substantial carbon dioxide sink (Thomas et al., 2011) and in this section, it is investigated whether anthropogenic sources of CO_2 can be detected. Wytham is situated near two large dual carriageway roads with frequent heavy traffic. An increase in CO_2 from certain wind directions may indicate that NO_x and CO from car exhausts have also increased. CO_2 concentration at inlets 3 and 4 were analysed with Openair using the wind data from the Upper Seeds AWS to investigate if a signal can be observed from either the near-by roads to the north and east or the town of Oxford to the southeast. The wind speed measured at the Upper Seeds AWS is taken as an approximation for the top of the canopy wind speed. In Figure 83 the output of Openair is shown.

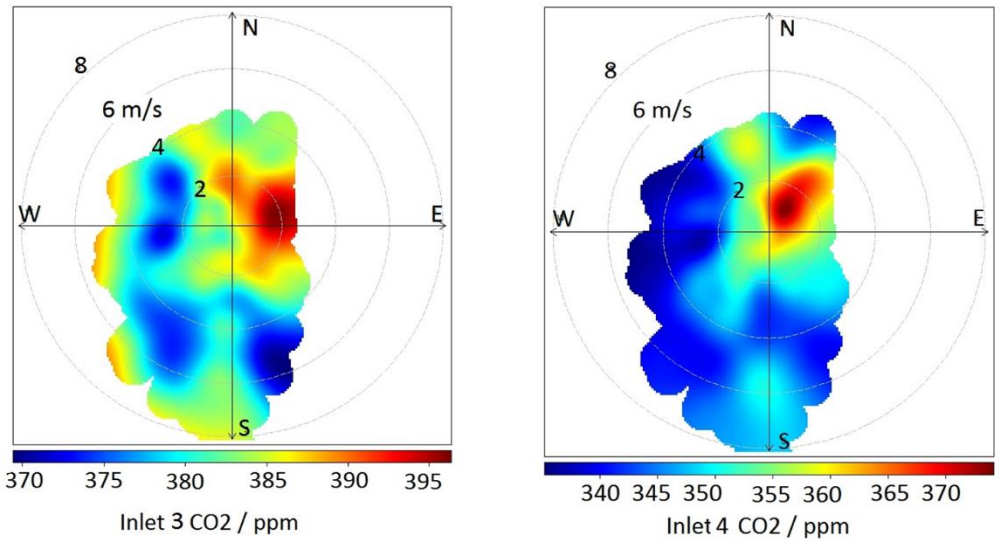

Figure 83 CO_2 polar bivariate plots (Openair) showing the direction of potential CO_2 sources

It can be seen that a similar signal is observed for both inlets. Inlets 3 and 4 get affected by the top of the canopy top wind speed and direction and Figure 83 indicates that these inlets are influenced by a strong CO_2 source to the east northeast of the sensor location. This signal corresponds to a wind speed of just 2 ms^{-1} and the nearest large road is 2 km away to the north with a transport time of 16 min assuming constant wind speed and direction. The road junction to the north northeast is 3.8 km away with a transport time

of 31 min, hence this signal may it is unlikely that this is a signal from either Oxford or the large roads. Possible near-by sources in this direction are the river Thames, a farm or a wetland area. Without further information or measurements it is difficult to conclude anything further.

6.4.3 A metric for vertical mixing

Having inlets at four heights allows questions to be asked of how the isoprene is distributed vertically through the canopy. To represent the gradient, the percentage of each inlet relative to inlet 4 is calculated using the hourly isoprene values. All of the data points when PAR is less than 10 $\mu molm^{-2}s^{-1}$ are removed to exclude instances when the concentration at inlet 4 is ~0 ppb. This percentage value gives a representation for how well the isoprene is mixed to the lower levels. A low percentage indicates weak mixing or slow vertical transport while a high percentage indicates the air in the canopy is better mixed.

6.4.4 Seasonal changes in vertical distribution

When examining the PAR extinction through the canopy for the purposes of deriving PAR values at each inlet height (Figure 63), it is noted that the extinction has a less steep gradient from September to November. This is shown in Table 10. This change can be attributed to the dropping of the leaves at the end of the season causing more light to penetrate the canopy. With respect to isoprene, it may be the case that increased light to the lower levels caused stronger emission there, but the reduced leaf area would increase mixing as leaves would have impeded air movement. It may also be possible that there are other seasonal factors affecting the vertical mixing.

The average peak isoprene concentration from 1-5pm is calculated for each day at each inlet and the percentage of each inlet compared to inlet 4 is calculated. The average percentage for inlet 1 is 34.6 ± 12.0 %, inlet 2 is 45.7 ± 14.1 % and inlet 3 is 56.3 ± 11.2 %. To examine if these values exhibit any seasonality, they are plotted as a time series in Figure 84. This plot shows that across the season there is a high degree of variability and that there is no clear profile across the time series. However it is noted that the values tend to increase at the end of the season, which suggests that there is a seasonal dependence of canopy mixing with the date.

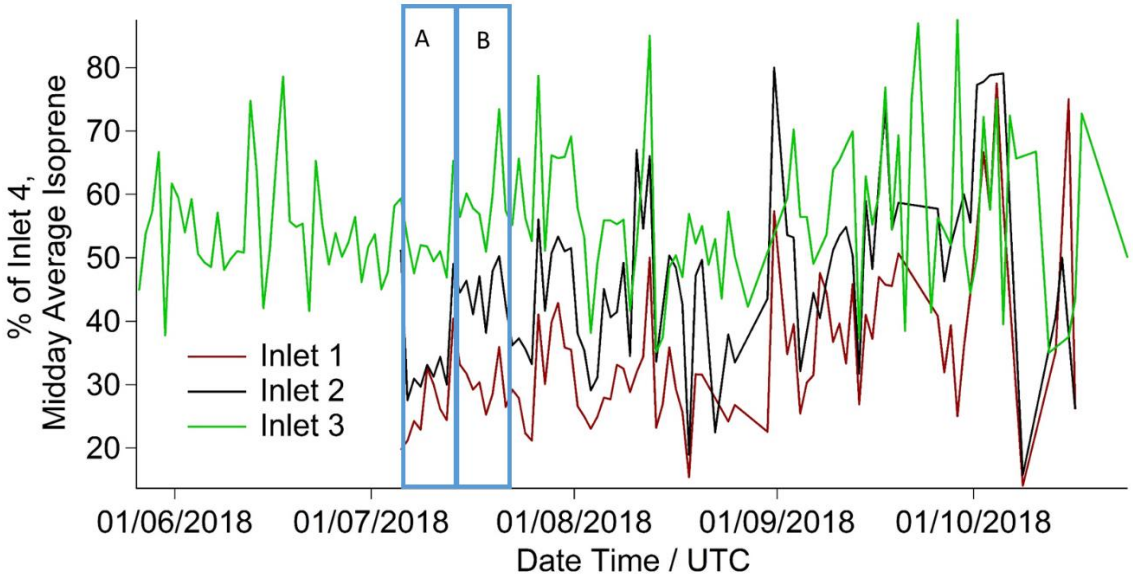

Figure 84 Percentage of isoprene concentration of each inlet over isoprene concentration at inlet 4 plotted for 1 – 5pm daily averages across the experimental period with periods A representing a less well mixed period and B representing a well mixed period

Figure 84 also shows that there are certain periods where the vertical profile of isoprene is different. The period from 6th July to 12th July (A) for example shows a less well mixed canopy, with each inlet displaying lower values. In particular inlet 2 is significantly lower. This suggests that the canopy is more stratified and that the turbulent mixing experienced above the canopy is stifled by the canopy leaf layer and is experienced less the further you go into the understory. The period from 13th – 25th July (B) however is showing a well distributed isoprene profile, indicating that the canopy is better mixed on those days. The following two sections describe efforts to answer the question of what affects the canopy mixing and what factors differ between A and B in Figure 84.

6.4.5 Does top-of-canopy wind speed change the vertical distribution?

A factor that might be expected to have a large impact on mixing in the canopy is wind speed. As the wind speed increases, it is hypothesized that turbulence at the canopy is enhanced as the boundary layer air mass encounters a rough surface. With the turbulence this brings parcels of air from the canopy down into the understory to be diffused to the forest floor. Wind speed at the Upper Seeds AWS is plotted against these fractional values for each inlet to test this hypothesis. These plots are shown in Figure 85.

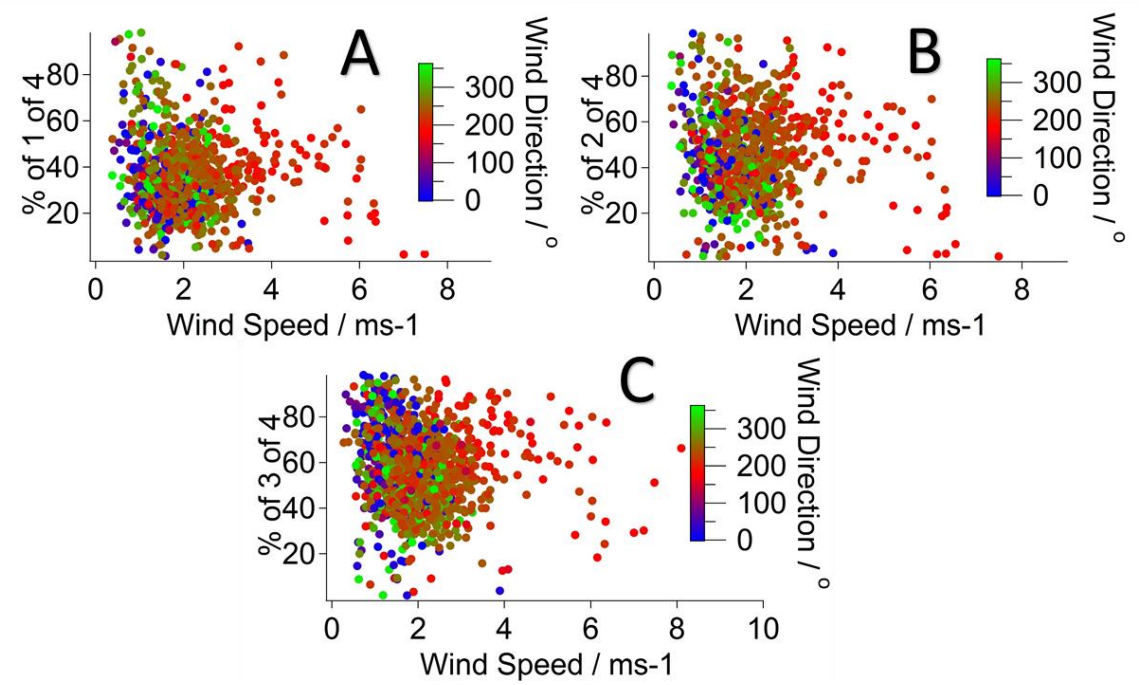

Figure 85 Hourly average wind speed plotted against relative percentage of the isoprene concentration at each inlet to inlet 4 with colour as a function of wind direction A) Inlet 1 relative percentage to inlet 4 B) Inlet 2 relative percentage to inlet 4 C) Inlet 3 relative percentage to inlet 4. Values used when PAR >0 µmolm^{-2}s^{-1}

It can be seen that there is no obvious relationship of the relative percentage of the concentration to wind speed. This result indicates that the canopy gradient is not affected by the wind speed and neither is the mixing. The Upper Seeds data are used, which are measured 500 m away in a field and might not represent the conditions at the top of the canopy. However, as the wind speed is an hourly average it is expected to represent the broad conditions experienced by the Wytham site.

When comparing two regions of contrasting mixing such as regions A and B in Figure 84, the average wind speed for these regions can be considered. For region A the average wind speed is 1.7 ± 0.5 ms^{-1} whereas for region B it is 1.6 ± 0.5 ms^{-1}. This is not statistically significant and any difference is likely due to natural variability and coincidence.

6.4.6 Effect of PAR and temperature on vertical canopy mixing

The fractional abundances for the three lower inlets against the top of the canopy PAR are shown in Figure 86 with the date added with colour coding. There is an observed correlation of PAR with the fractional abundance of isoprene at each inlet.

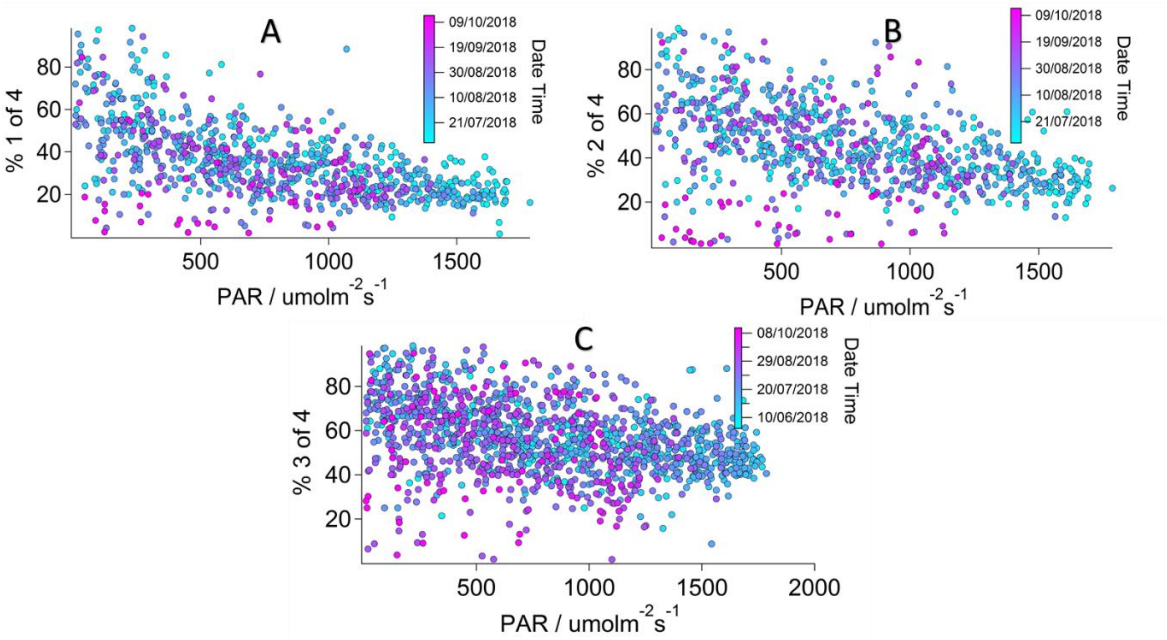

Figure 86 PAR plotted against relative percentage of the isoprene concentration at each inlet to inlet 4 with date colour scale A) Inlet 1 relative percentage to inlet 4 B) Inlet 2 relative percentage to inlet 4 C) Inlet 3 relative percentage to inlet 4. Values used when PAR >0 µmolm^{-2}s^{-1}

It is indicated that as PAR is increased, so the mixing decreases and conversely, at low values of PAR, the canopy is better mixed. A sun-lit canopy would experience a local temperature increase that can explain this observation. To determine if there is a dependence on the temperature, the difference between the inlet temperature is plotted against the fractional inlet concentration in Figure 87.

The hypothesis that the date correlates with the mixing as a seasonal response is discussed in Section 6.4.4. In the plots of fractional isoprene in Figure 86 with date colour coding it is observed that there is a weak correlation.

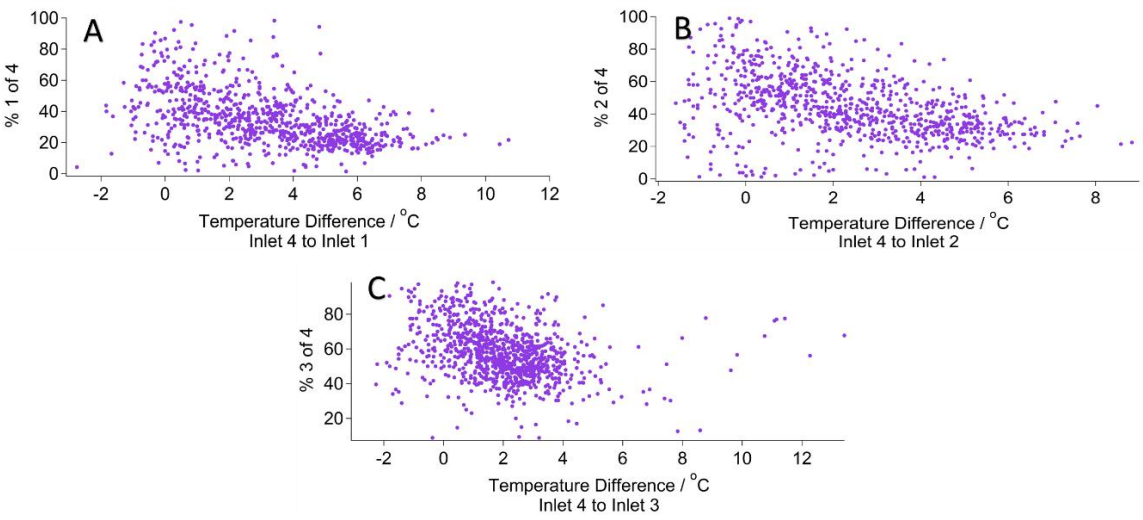

Figure 87 Difference in temperature between inlets plotted against relative percentage of the isoprene concentration at each inlet to inlet 4 A) Inlet 1 relative percentage to inlet 4 B) Inlet 2 relative percentage to inlet 4 C) Inlet 3 relative percentage to inlet 4. Values used when PAR >0 µmolm^{-2}s^{-1}

The heating of the upper canopy drives a stable atmosphere in the understory because the temperatures at the ground are lower than that at the top of the canopy during the day. When this difference is greatest, the least degree of mixing is observed and this is due to suppressed internal convection. For inlet 3 the relationship is not as well defined and this it likely because the inlet is situated in the canopy and is measuring the heated air so the temperature difference between inlet 3 and inlet 4 is typically less. Often in the morning or late evening (when isoprene is present) the upper canopy is cooler than the forest floor, so this inverted temperature profile leads to increased mixing.

The higher temperatures just above the top of the canopy may also explain why higher isoprene is observed there. With increased heating at the bottom of the free PBL enhanced above canopy convection would drive air upwards. Inlet 3, in the mid-canopy would also be affected which is why the observed correlation in Figure 87C is not as strong.

When comparing two regions of contrasting mixing such as regions A and B in Figure 84, the average PAR at the top of the canopy for these regions can be considered. For region A the average PAR is 983 ± 509 µmolm^{-2}s^{-1} whereas for region B it is 840 ± 492 µmolm^{-2}s^{-1}. The high variability is due to the diurnal pattern of PAR. These values indicates that for the stronger vertical gradient (i.e. less mixing) there is higher mean daily PAR which further agrees with the findings above that the insolation at the top of the canopy is a key factor that drives the vertical gradient.

6.5 Impact of 2018 heatwave on isoprene concentration

The 2018 heatwave provides a unique opportunity to investigate how the trees responded to both the temperature and the drought and how they recovered afterwards. Globally there have been few field studies on actual forests during a drought (Jiang et al., 2018), and here the data is interrogated to reveal insights on the forest during this heatwave and drought. It is hypothesized that the drought could lead to increased isoprene emissions but that afterwards the emission is reduced as the metabolites are used up in the cell pathway for the production of isoprene. How the trees respond to different factors after the drought may also have changed.

6.5.1 How is isoprene concentration affected before, during and after?

To analyse the effect the heatwave had on the isoprene levels, the average daily profile was created using time periods shown in Table 11 and Figure 88. The time periods were arbitrarily chosen based on sustained midday high temperatures, with the boundary defined as when the maximum temperature for two adjacent days differed by 4.5 ^{o}C or more. The hourly values were used in each period to get a statistical representation of each time period.

Table 11 Regions selected to represent the different stages of the heatwave

Region	Label	Dates
Before	A	26th May – 23rd June
Heatwave Phase 1	B	24th June – 9th July
Heatwave Phase 1	C	10th July – 27th July
Heatwave Phase 1	D	28th July – 7th Aug
After	E	8th Aug – 5th Oct

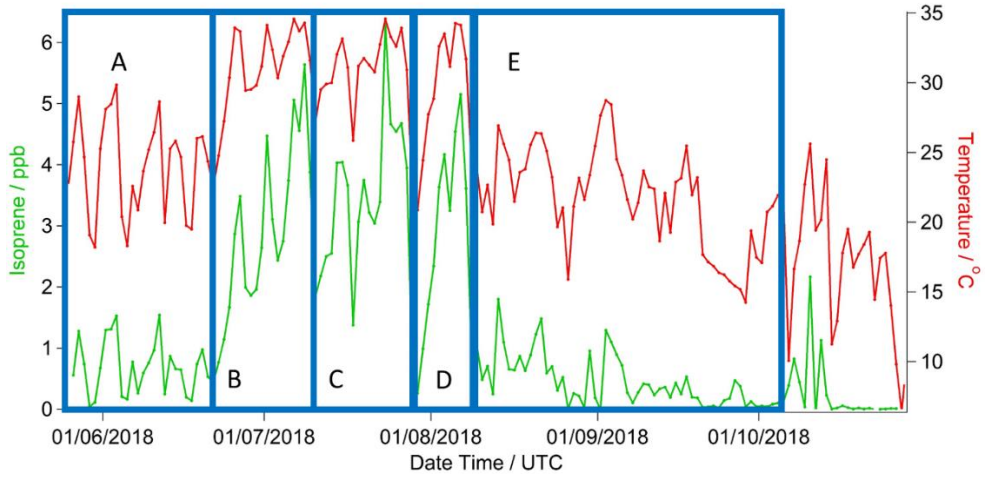

Figure 88 Selected periods to represent 2018 heatwave showing the 1–5pm mean values for both isoprene concentration and temperature and the periods designated A-E as described in Table 11

For inlet 4, the isoprene concentration is plotted in Figure 89. The heatwave period was covered by the measurements in a period of good stability for the iDirac as the long sunny days allowed for adequate charging of the batteries and reliable measurements. It is clear that there is a strong effect as a result of the heatwave, as expected from the elevated temperatures observed and the high PAR. The heatwave produced isoprene concentrations up to eight times higher than the non-heatwave conditions. There is evidence (Bamberger et al., 2017) that suggests that the trees have an additional and alternative heat stress response that may result in elevated isoprene emission. The temperature relationship before, during and after the heatwave is analysed.

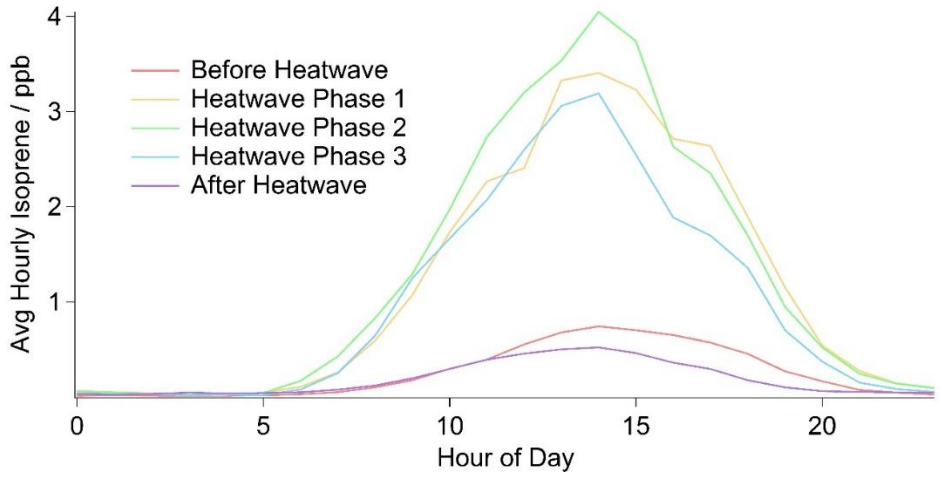

Figure 89 Heatwave mean hourly isoprene concentration average daily profiles shown for the different phases of the heatwave

Figure 89 also shows that the isoprene concentrations after the heatwave are comparable to the period before the heatwave. This could either be an indication that the forest was relatively unaffected afterwards, or it could be a coincidental effect.

6.5.2 Does the relationship with temperature or light change?

To investigate how the temperature or light response of the forest changes over time, the hourly average isoprene concentration is plotted against the hourly average temperature. To this scatterplot a quadratic curve is fit to assess the temperature response at each stage. The time period selected for this analysis are A, B, C, D and E as shown in Figure 88.

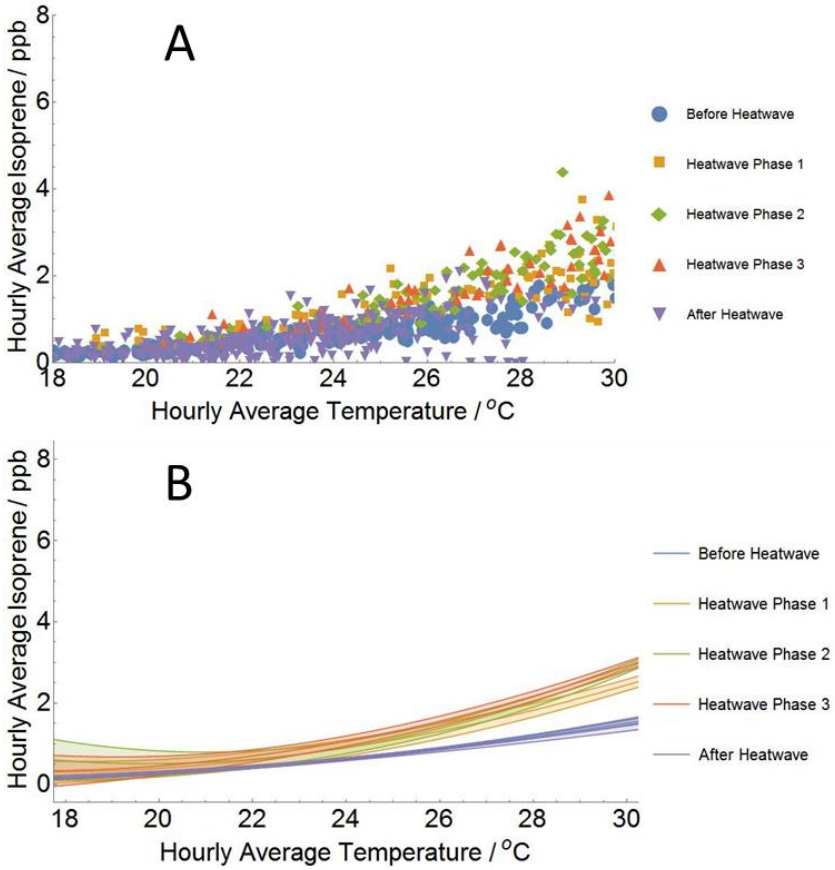

Figure 90 A) Scatterplot of mean hourly isoprene concentration against mean hourly temperature B) Fitted quadratic curves for each period of the heatwave showing the 95% confidence interval in the fitted line for the temperature range observed before and after the heatwave to avoid extrapolation. Isoprene concentration during daylight hours used

Figure 90 shows the scatter plot and the fits of the isoprene concentration against temperature. As expected, the isoprene concentration overall is a lot higher for the three phases of the heatwave. However the degree of the curvature of the temperature response curve is changing. When quadratic fits are applied to the data, the response curve for the

periods before and after the heatwave are not seen to be statistically different. Slight differences were observed for the three phases of the heatwave, with the first phase of the heatwave statistically differing with a shallower curvature. This indicates that it takes some time for the heatwave to fully affect the trees and the initial stress response of isoprene emission is less than that of a persistent heatwave. It has been suggested that there is a memory effect of 10 days where isoprene emission is heightened during drought conditions before being shut-off (Guenther et al., 2006). In this data there is no example of this and the only instances of decreased isoprene were on the 9th and 28th July which were marked with reduced sunlight and temperature and a rain event on the 28th July. Interestingly, the response before and after the heatwave is the same, indicating that the tree has returned to normal and that isoprene repose is not muted after the heatwave.

To investigate if there were more immediate responses to temperature, the before and after period are split into further divisions and are defined as 26th May – 11th June (before 1), 12th June – 23rd June (before 2), 8th Aug – 24th Aug (after 1), 25th Aug – 14th Sept (after 2), 15th Sept – 5th Oct (after 3). In Figure 91 the fitted curves of these finer temporally resolved periods are plotted. It appears that even before the heatwave, there are differences in the temperature response of isoprene that may be natural variability. After the heatwave the trees initially retained a strong temperature response and that this drops to the levels before the heatwave after a couple of weeks. The latest period in the season also shows the lowest temperature response which likely indicate the effect of shortening days, lower temperatures and the dropping of leaves.

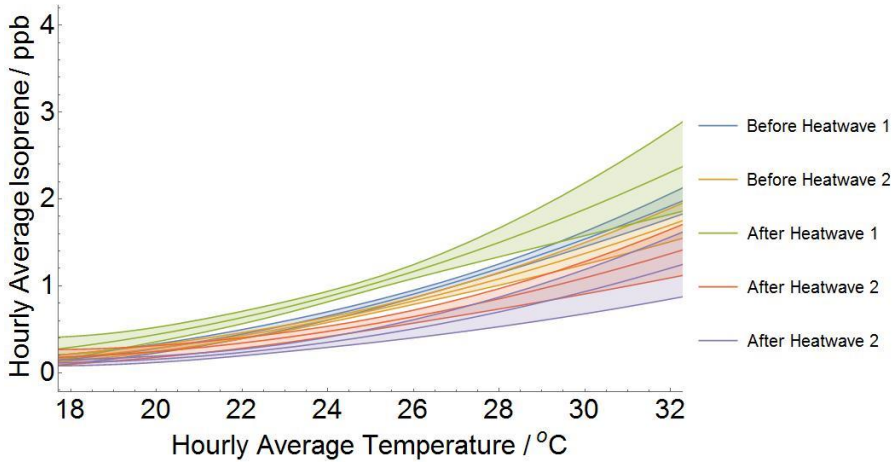

Figure 91 Finer temporal resolution of periods before and after the heatwave showing the 95% confidence interval in the fitted line. Isoprene concentration during daylight hours used

The same approach is used for the light response in the periods A, B, C, D and E. The results are shown in Figure 92 and show that the response for light is essentially unchanged for the five different periods. This is the expectation as the light level for this period was not particularly unusual for a given year and the heatwave is characterised by higher than average temperatures and a lack of rainfall, not the intensity of the sunlight. These plots do show us however that a higher PAR intensity leads to higher isoprene concentration, but that the response is roughly linear and that the response doesn't change in profile for the different periods of the heatwave.

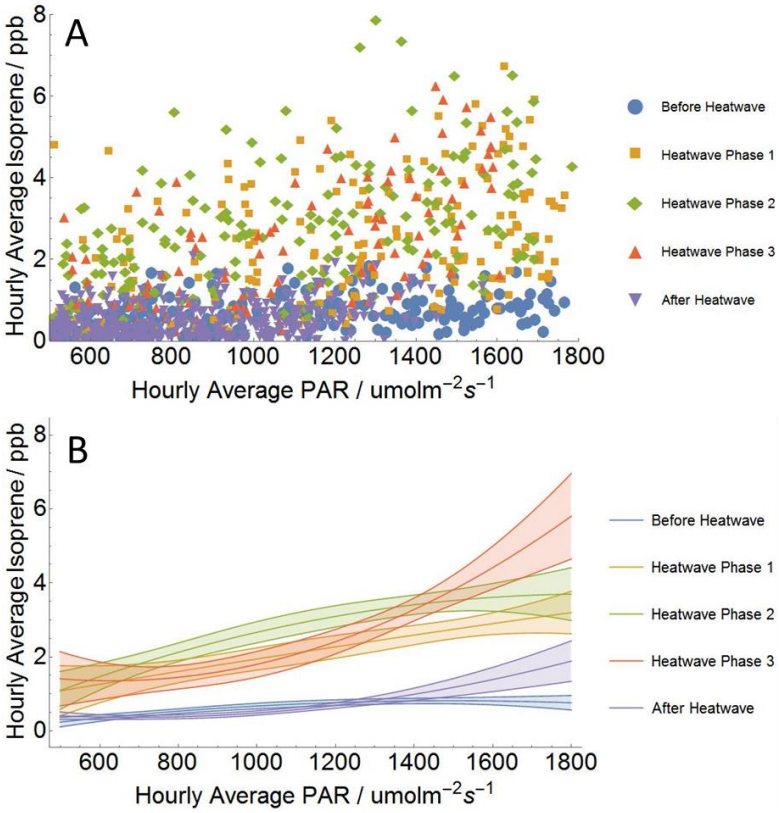

Figure 92 A) Scatterplot of mean hourly isoprene concentration against mean hourly PAR B) Fitted quadratic curves for each period of the heatwave showing the 95% confidence interval in the fitted line for the PAR range observed before and after the heatwave to avoid extrapolation

6.5.3 Isoprene emission as calculated by the Guenther functions

In isoprene studies the standard method for calculating the emission rate of isoprene is to use the equations defined in Guenther et al., (1993) these are *Equations 3*, *4* and *5* and are shown and discussed in Section 3.3.3.

At Wytham the only tree that emits significant levels of isoprene is *Quercus robur* as shown in Table 7 and it has an emission factor, I_s, of 28 nmolm^{-2}s^{-1} (Li et al, 2011). Hence it is possible to calculate an emission rate of *Q. robur* for the time period of the WISDOM experiment using the temperature and PAR values for the canopy. The resulting values are reported in Figure 93.

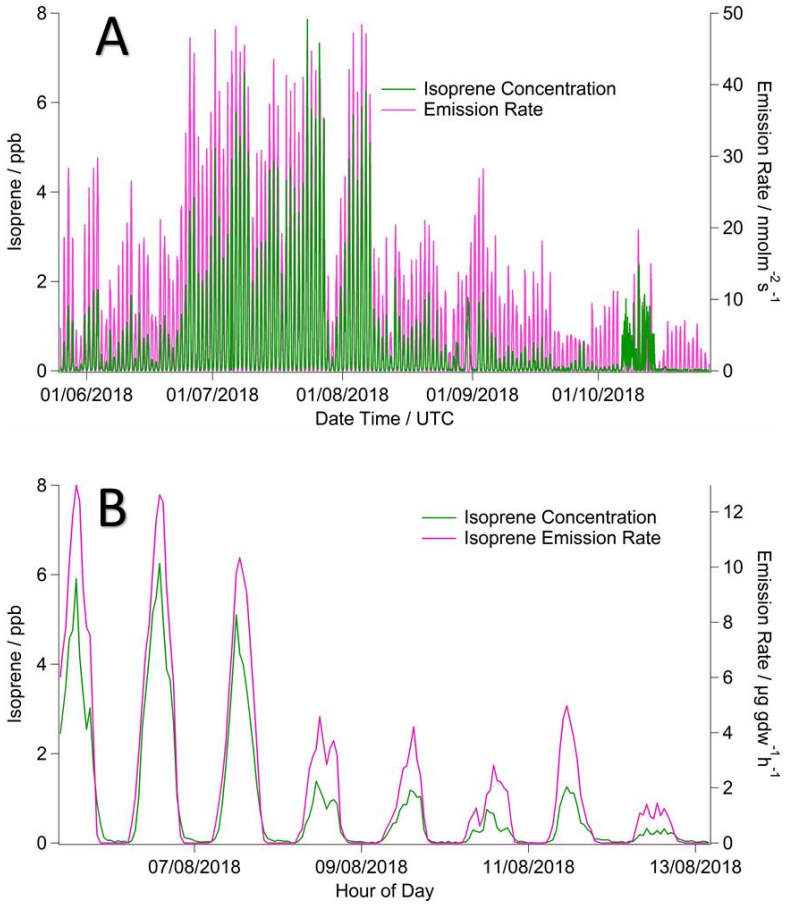

Figure 93 Isoprene emission rate and concentration A) across WISDOM time period B) in a zoomed in portion which shows the diurnal profile in more detail

The isoprene concentration and the estimated emission rate are plotted together in Figure 94. The relationship does not follow a linear dependence because the processes determining the concentration of isoprene such as mixing, chemistry and deposition are not linear. It is noted that the non-zero values of isoprene that occur when the emission rate is 0 nmol m^{-2} s^{-1} are due to the isoprene that lingers after the sun has set. The isoprene concentration decays to zero at night as a result of mixing, deposition and chemical reactions. Although hard to observe, there is also a period when the isoprene concentration is 0 ppb or very low despite a high emission rate and this is because of the

time it takes for the isoprene emission rate to increase to such that can mix through the atmosphere.

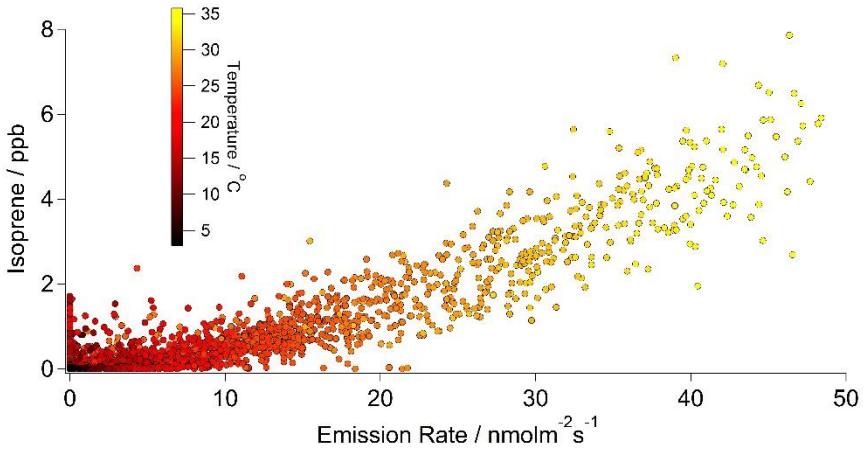

Figure 94 Isoprene emission rate qualitative correlation with mean hourly isoprene concentration at inlet 4

It has been suggested that the Guenther function does not capture periods of drought well (Bamberger et al., 2017) so it may be that a different relationship is observed when split into different periods before, during and after the heatwave. In Figure 95 the concentration and emission are plotted for each time period before, during and after the heatwave. It shows that the relationship before and after the heatwave is more linear and during the heatwave the response is steeper. During the heatwave a much less linear relationship is seen, with a steep gradient. This indicates that the non-linearity of the Guenther equations for isoprene emission, which accounts a plants response to light and temperature, is enhanced. It may be that the heatwave accentuates the shortcomings of the Guenther equation. This implies that the emission equations are not well reflected in the isoprene concentration and that there are some factors not represented with the emission equations, such as mixing and deposition. This increased non-linearity may be why drought events are poorly represented in MEGAN.

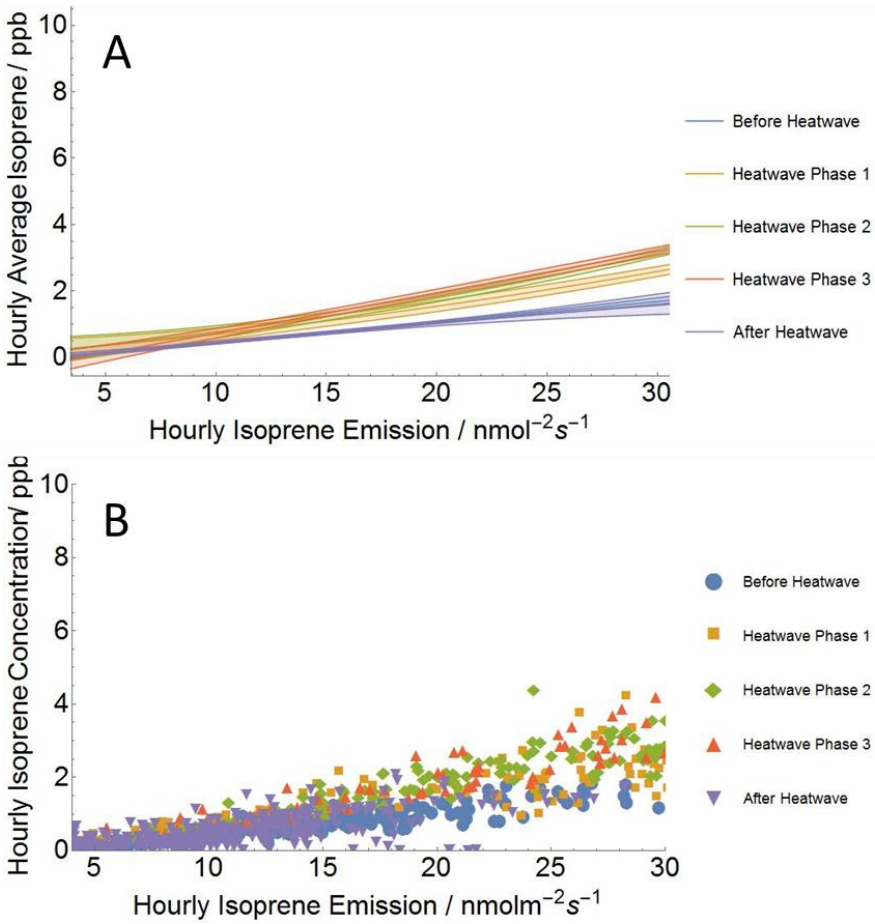

Figure 95 Guenther emission qualitative correlation with measured inlet 4 mean hourly isoprene concentration for periods before, during and after the heatwave as A) scatterplot and B) quadratic fits and 95% confidence interval

6.5.4 Soil water effects on isoprene concentration

One key defining parameter of a drought is the soil water content. This metric was provided by the Upper Seeds AWS as an hourly average. Over the course of the 2018 heatwave the soil water content dropped significantly and was a defining feature of the summer period. Figure 96 shows how the soil water content dropped after every rainfall event and reached low levels and even struggled to recover after the heatwave had passed. It is difficult to analyse the isoprene response to soil water because isoprene concentration is also closely linked to temperature and light.

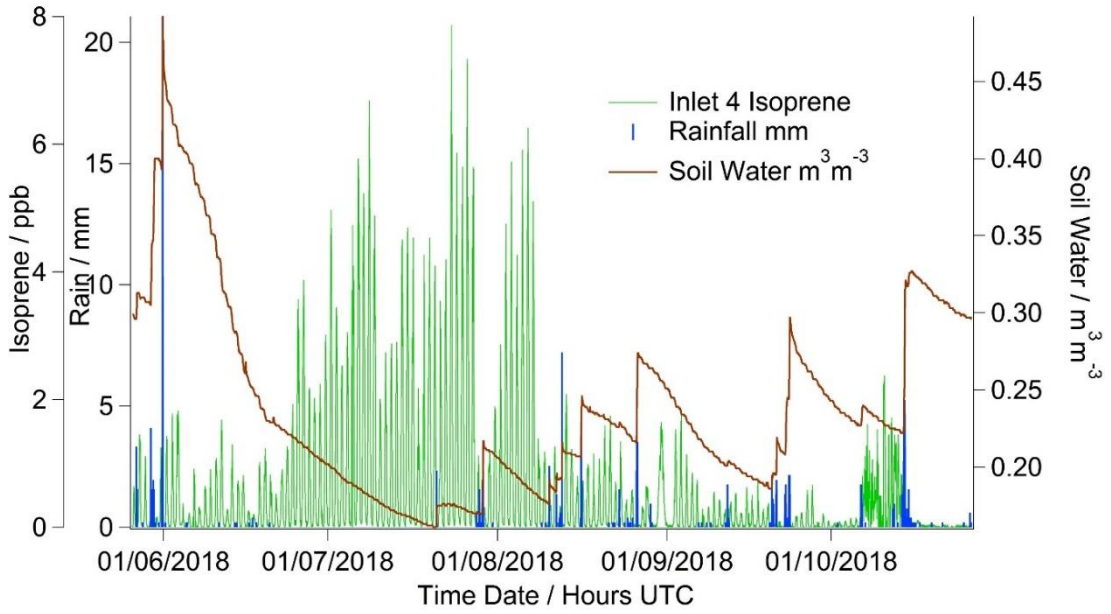

Figure 96 Time series of the soil water content over time and response to rainfall, with hourly average isoprene time series

Figure 96 shows the time series of soil water, isoprene concentration and rainfall. Visually, it appears that there is a negative correlation and as the soil water content decreases, the isoprene concentration decreases. However, this plot does not take into account light and temperature and how they influence the isoprene concentration. Without normalising for these two important variables, it is hard to conclude much from this plot.

To normalise the isoprene concentration, the same equations were used as for calculating the emission factors in Section 6.5.3. Using the isoprene concentration, *Equation 6* shows how the normalised concentration is calculated. For this, the derived PAR at inlet 4 is used, and the dry bulb temperature from the Upper Seeds AWS is used as the temperature.

$$[Iso]_{norm} = \frac{[Iso]}{C_T C_L} \qquad \textit{Equation 6}$$

For this normalisation, an average concentration value is calculated from 1-5pm so that the value represents the peak isoprene concentration. The resulting values from this calculation are almost double the original isoprene concentration.

The correlation plot is shown in Figure 97B and demonstrates that the normalised isoprene follows a similar relationship as the original isoprene. It can be seen that at a lower water content, the isoprene increases.

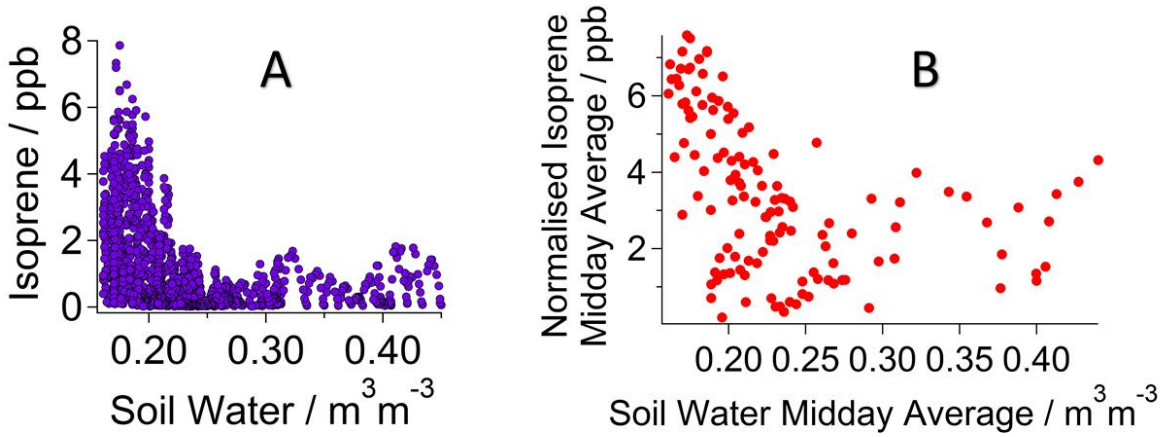

Figure 97 How isoprene concentration at inlet 4 correlates to soil water content A) Hourly mean isoprene concentration against hourly mean soil water B) Normalised isoprene concentration against soil water midday (1-5pm) averages

From this investigation of soil water, it is found that the isoprene emission has two distinct regimes. Above 0.2 m^3m^{-3} it appears that the isoprene concentration does not depend on soil water. Below 0.2 m^3m^{-3} there does seem to be a strong relationship of isoprene with soil water, with a rapid increase of isoprene as the soil water drops. The point at which the trees respond more strongly may correspond to the point where the stomatal conductance decreases as a water conservation measure in times of scarce water. The minimum soil moisture recorded in the summer was 0.161 m^3m^{-3} on the 20th July and the wilting point used in MEGAN is 0.171 m^3m^{-3}. This indicates that that threshold was crossed. However there was no visible 'wilting' as shown in the photographs of leaves in Figure 69. This may be due to the deep and broad rooting system of the trees. The threshold for isoprene shut-off and wilting is likely dependant on the soil type and specific conditions at Wytham. It may also be possible that the soil moisture at the canopy walkway, under the canopy, has higher soil moisture than the open meadow site at Upper Seeds. A more rigorous analysis of the low soil moisture is required to further investigate the relationship to isoprene emission. It is concluded that the tree was highly stressed but a significant 'drop' of isoprene was not observed and the trees did not sustain serious damage. Further study is required to investigate the wilting point of Wytham woods and *Q. robur* in different soil types.

6.6 Conclusions

A number of conclusions are drawn from this study regarding the behaviour of trees in a forest canopy and under drought stress. From this study insights are obtained on the behaviour of the trees in terms of isoprene emission, the vertical canopy mixing of isoprene and response to a heatwave and drought.

6.6.1 Isoprene at Wytham in summer 2018

Over the course of summer 2018 isoprene concentrations at four heights were successfully measured for four months, with five months at the top of the canopy. A summary of the peak isoprene values is presented in Table 12. The maximum isoprene measured was at 14:20 UTC on 23rd July and reached 8.4 ppb, an extremely high concentration for a temperate forest. It is observed that there is a 2 hour lag between the top of canopy peak isoprene concentration and the forest floor peak isoprene concentration, which is attributed to the mixing time of isoprene in the canopy. At each inlet, July showed the highest concentration followed by August, June, May, September and finally October showed the lowest concentrations. At the top of the canopy (15.6m) the average values for peak isoprene in July, August, June, May, September and October were 3.7 ± 1.7 ppb, 1.5 ± 1.7 ppb, 1.2 ± 0.9 ppb, 0.6 ± 0.6 ppb, 0.4 ± 0.4 ppb and 0.3 ± 0.5 ppb respectively.

Table 12 Summary of peak isoprene values across the time series

Height in Canopy / m	Mean Peak Isoprene / ppb	Standard Deviation / ppb
0.5	0.48	0.53
7.3	0.68	0.76
13.2	0.89	0.91
15.6	1.68	1.78

A strong correlation of isoprene concentration is visually observed with temperature at each level in the forest, with some decline in isoprene concentration at high temperatures. This indicates that isoprene is being produced in response to heat stress and that temperatures were reached that severely stressed the tree. The response of isoprene

concentration to light is less strong. In general very little isoprene is observed in the dark. This suggests that isoprene is indeed produced using the products of photosynthesis. These results have been demonstrated previously in the literature and show that the isoprene emission behaviour of the trees at Wytham did not differ from other forest types.

A visual anti-correlation is observed with CO_2 but further analysis is not possible due to the confidence in the CO_2 data. This observation agrees with the expected decrease in CO_2 as a result of photosynthesis, but a lag is observed that may indicate a delay between absorption of CO_2 and production of isoprene.

6.6.2 Factors that drive the vertical canopy isoprene gradient

This study investigates which factors affecting the vertical mixing in the forest canopy. The way in which air and all the various emissions are distributed in the canopy has several implications for the forest. In terms of the proposed function of isoprene as a signalling compound in the case of herbivory, the repercussions of the canopy transport are very important. If the plants, mosses or lichens in the forest detect the isoprene and use this to alter their behaviour then a important metric is how long the isoprene takes to reach them. The structure and type of forest will affect the air movement and mixing and the species distribution will affect strongly the relative abundance of different chemical species. Several studies have investigated the presence of microbial communities that utilise isoprene as a feedstock (Mcgenity et al., 2018). There is evidence that there are bacteria and fungi in the soil (Cleveland et al., 1997) and on leaves (Johan et al., 2000) that use isoprene as a primary source of energy and for carbon assimilation. Where the concentration of isoprene is distributed in the canopy likely affects the habitat and distribution of such microbial communities. This is of course important for the studies of such aspects of the biosphere and has repercussions on the understanding of natural systems.

There is no strong observed seasonal change of the vertical canopy mixing across the summer season. It was hypothesised that the changes in LAI as a result of the aging of the leaves may change the movement of air in the canopy and hence increase the isoprene mixing. The end of season values suggest an increase as the leaves started to drop, but more study is required to firmly conclude this. For the forest floor at 0.5 m, the average percentage relative to the top of the canopy was 34.6 ± 12.0 %, the same value for the understory (7.3 m) was 45.7 ± 14.1 % and for the mid-canopy height (13.2 m) this percentage was 56.3 ± 11.2 %. This method of calculating the percentage of each inlet

relative to the top of canopy inlet is deemed suitable for determining the degree of mixing through the canopy.

The wind speed is investigated as a possible driver of vertical isoprene mixing in the canopy. It is found that the vertical distribution of isoprene at the measurement site does not depend on the top of canopy wind speed or direction. No visual correlation is observed between isoprene percentage fractions of each inlet and the wind speed. The dense canopy of leaves at the measurement site may act as a barrier to air movement and so that the top of canopy wind does not strongly affect the movement of air in the understory.

Another factor investigated as a potential driver of the vertical mixing is the light intensity at the top of the canopy. Here PAR is used to indicate the degree of light intensity at the top of the canopy. The measurements of PAR at the top of the canopy correlate with the isoprene percentage fractions of each inlet, as the higher PAR values resulted in a less well mixed canopy. It is found the difference in temperature between the inlets correlates with the isoprene percentage fractions of each inlet. It is concluded that the vertical mixing is dictated by the light intensity at the top of the canopy which causes a stable atmosphere as the result of a positive temperature gradient. The role of horizontal advection could play a large role in determining the concentration of isoprene at the top of the canopy and this is discussed further in Section 7.3.3.

6.6.3 The effect of a heatwave on isoprene concentrations

This study shows that the effect of higher temperatures and drier conditions can increase the concentration of isoprene in the atmosphere. More isoprene has important consequences for atmospheric chemistry and for the health of the trees, and so could be significant under a warmer and drier climate. This study shows that the isoprene concentration was sustained at ~5.5 times the concentration out with the heatwave, with maximum daily average concentrations for the three phases of the heatwave of 3.4 ± 1.4 ppb, 4.0 ± 1.5 ppb and 3.2 ± 2.1 ppb.

The relationship of isoprene with temperature is investigated across the heatwave periods. As well as a higher isoprene concentration, the heatwave caused an elevated response of the trees to temperature. It was observed that the relationship of isoprene concentration with temperature was different for time periods before and after the heatwave compared with the temperature response during the heatwave. The period after the heatwave shows some heightened temperature response, but not as high as during the heatwave, suggesting that the forest took around one week to recover from the sustained high temperatures.

After the heatwave the tree isoprene response to temperature returned to a similar level as before the heatwave, suggesting that the heatwave had not had a lasting effect on the tree isoprene emission. As discussed in Section 1.8, under heat stress many trees use alternative substrates to source the carbon for the production of isoprene. Eventually these substrates may become exhausted and the tree would struggle to produce isoprene and the tree would become susceptible to damage by heat stress. Also, the tree expends large amounts of energy to produce isoprene and would need time to recover valuable stocks for further metabolic functions. This could weaken the tree and leaving it open to pathological attack, herbivory or other biotic stress factor. In this study it is found that the forest was able to recover from sustained temperatures and there were no lasting effects in terms of isoprene emission.

The soil moisture is investigated as a possible influencing factor on the isoprene emission from trees under drought stress. Using a PAR and temperature normalised hourly value for isoprene concentration, qualitative correlation with soil moisture is investigated. The result suggests that at a soil water content of less that ~0.2 m^3m^{-3} the trees have a heighted isoprene emission. When the soil water decreases below this value there is a sharp increase in isoprene concentration. The minimum soil moisture recorded in the summer was 0.161 m^3m^{-3} on the 20th July and the wilting point used in MEGAN is 0.171 m^3m^{-3}. However a shut-off of isoprene or significant leaf damage due to wilting was not observed. This could be due to the soil type at Wytham and the characteristics of the specific trees at the site but further research is required to investigate this.

This analysis of the measurements taken during WISDOM are investigated further in Chapter 7, where a model is constructed to recreate the measurements, simulate fluxes of isoprene from the forest and investigate other types of forest.

7 MODELLING ISOPRENE IN A FOREST CANOPY

7.1 Introduction

Modelling a forest canopy is inherently difficult because of the complex nature of the forest, with a multitude of species, intricate structure, multiple sources and sinks, varying levels of light and complex micrometeorology. It is possible however to simplify natural systems with assumptions and approximations, which can vastly reduce the complexity of any model. With some simplifications, it may be possible to use a model of a forest canopy to garner insights into the processes affecting the forest emissions and to probe how the situation might change under different conditions.

Existing models have some shortcomings when predicting the concentration of isoprene in a forest canopy. There have been many model studies to represent the transport of emitted species from forests and a recent example is the Chemistry of Atmosphere-Forest Exchange (CAFE) model developed by Wolfe & Thornton, (2011). The CAFE model uses an 800 m high model domain and implicitly assumes that the isoprene is transported to the top of the boundary layer and that the forest is infinite in the horizontal dimension. There is also no deposition to the forest floor in that model. The assumption that the isoprene is transported high into the boundary layer results in the boundary layer effectively acting as a reservoir for isoprene, leading to elevated night-time isoprene values compared to observations (Section 7.3.3.1). The absence of surface deposition also does not capture the vertical isoprene gradient (Section 7.3.3.1). A plot showing model and measurement comparison is shown in Figure 98A (Wolfe et al., 2011). The FORCAsT model (Ashworth et al., 2015) uses the methods from Gao et al., (1993) to represent mixing of species both within and above the canopy. Additionally, the deposition of isoprene to the forest floor was initially absent from FORCAsT. The vertical gradient of isoprene concentration, the night-time value and the absolute values are therefore not well simulated in that model, as shown for a model simulation in Figure 98B.

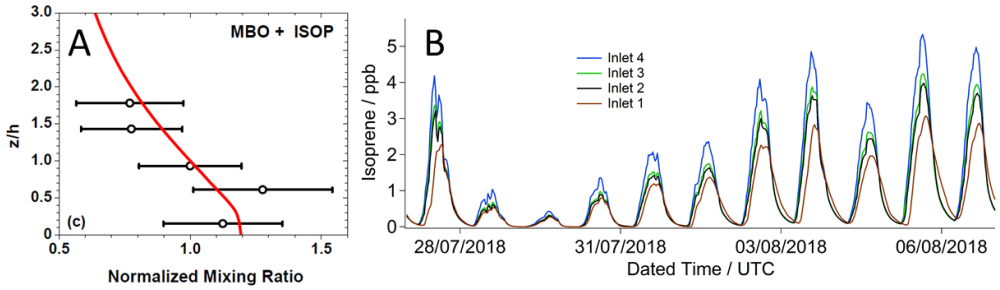

Figure 98 A) Model output for methyl-butanol and isoprene the CAFE model compared to measurements with a PTR-MS with red line showing the model simulation normalised for the canopy height of a coniferous forest (9.3 m) (Wolfe et al., 2011) B) Model output from FORCAsT with parameters set-up for Wytham Woods with output from four levels representing the measurement heights of WISDOM

In this chapter, the new Cambridge canopy 'CamCan' conceptual model is described and evaluated. The CamCan model uses the transport scheme as defined in the CAFE model, but with the model domain capped at 30 m (Section 7.3.1). This approach is justified by investigating a 2D version of the model (Section 7.3.3) which explores horizontal and vertical advection of isoprene over a finite forest. Using the CamCan model with the modified transport scheme, the FORCAsT model was modified to provide an improved representation of isoprene concentrations as described in Section 7.4. The outcome from the simple conceptual model was essential for informing modifications to the complex model used previously, and gave insights into the processes in the complex model and which ones may require modification for better isoprene simulation.

The WISDOM campaign created a unique dataset for constraining canopy models effectively. By having a time series of measurements at four levels in the canopy, it is possible to examine the vertical gradients and use this to verify model output.

The temperate broadleaved forest is only one type of forest and has many differences from other forest types. Using the CamCan model it is possible to investigate other scenarios and what the outcomes may be of different sets of input data. It may be possible to predict the isoprene from different forest types, or even predict the isoprene concentrations for different climate scenarios in the future. Very simple assumptions can hence lead to outcomes which could have potentially large impact on both the forest and the atmosphere. For example, the tropical rainforest is different from the temperate forest, with higher temperature, most intense light, a more diverse distribution of species (Both et al., 2019) and a different forest structure.

7.2 Aims

This chapter describes the construction of a simple canopy model and how this and another more complex model, FORCAsT, can be used to gain an insight into canopy transport processes. The chapters starts by describing the model, its assumptions and inputs in Section 7.3.1 it then describes the output in Section 7.3.4 and evaluates this against the measurements in Section 7.3.5. The FORCAsT model is focussed on in Section 7.4, with a comparison to both CamCan and measurement data. Finally the tropical forest and the oil palm plantations are considered and an attempt to model these forests that were sampled in Chapter 3 is described and evaluated in Section 7.7. The overall aims of this chapter are to:

1. Define and optimise a new simple canopy model (CamCan) that can describe what is observed in the isoprene profile of the Wytham forest canopy.
2. Describe the development of an existing canopy model (FORCAsT), modified and optimised for the Wytham site.
3. Compare and evaluate the performance of the two models.
4. Calculate the flux from the forest using CamCan.
5. Use the new model to try to characterise other forest types.

7.3 A new forest isoprene conceptual model: CamCan

When vastly simplified, it is possible to model the forest system as a conceptual model. Using simple equations to describe the processes in each level, a model was written using the functions in the Mathematica coding language, which is called the 'CamCan' model. This section describes the model's conception, development and how it has been optimised. The model includes representations for isoprene emissions (Section 7.3.1.3), isoprene reaction with OH (Section 7.3.1.4), vertical transport (Section 7.3.1.5) and the structure of the trees (Section 7.3.1.1). The time period reported here is a test set of data from 27th July to 6th August which encompasses a large range of temperatures, isoprene concentrations and wind speeds and so provides an ideal set of conditions to test the model.

7.3.1 Description of the CamCan isoprene model

7.3.1.1 Canopy structure and leaf area distribution

The model starts with a definition of the levels used, for a standard run this would typically be 50 levels each spaced at 0.6 m each with the upper model boundary at 30 m.

The height of the canopy is 16.2 m. A pictorial representation of the model levels, is given in Figure 99, which shows the distribution of the tree and the level spacing. The model represents a continuous forest and for the sake of simplicity in these simulations a vertical column with base area of 1 m^2 is used. Using this definition levels 27, 22, 9 and 1 represent inlets 4, 3, 2, and 1 respectively in the WISDOM campaign.

In CamCan, the forest that is modelled is assumed to be infinite and there is no horizontal advection influencing the conditions in the model column. Hence the fetch of the air masses and potential surrounding sources of isoprene are not considered.

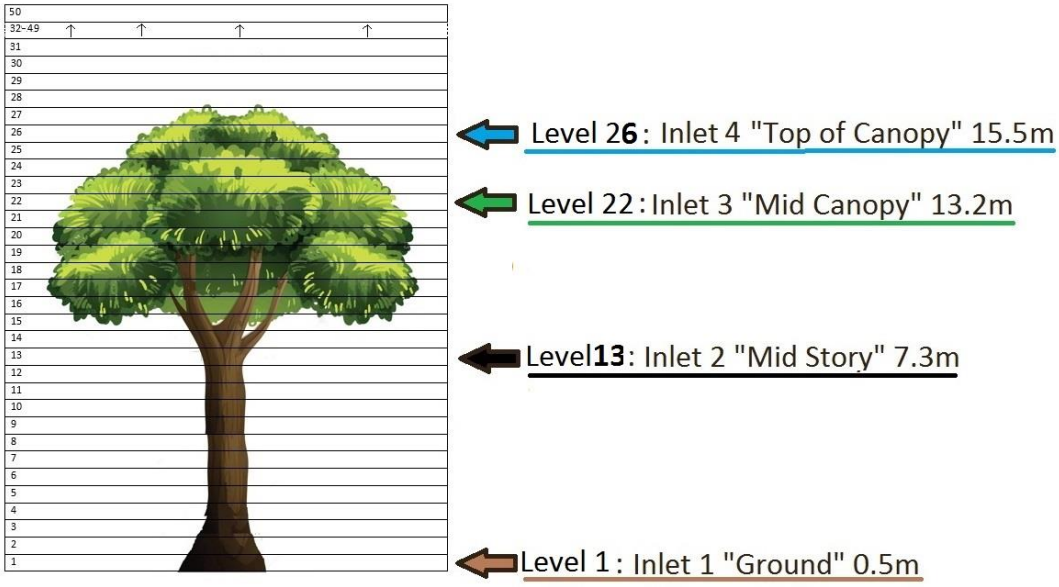

Figure 99 Level spacing, distribution of tree and location of inlets and equivalent levels in the model

The structure of the canopy is next defined by the leaf area index (LAI) of 3.6 m^2m^{-2} for Wytham (Herbst et al., 2008) and the leaf area distribution, which is arbitrarily defined. Figure 99 and Figure 100 show how the forest canopy, the levels and the leaf distribution are represented in the model. This model assumes that the leaf area is evenly distributed within each level and that there is no understory or ground foliage that could emit isoprene. There is also no parameter for the leaf angle, which would determine the efficiency of light absorption. The canopy structure also includes a light extinction factor that decreases at lower levels. This is essentially a scaling factor and is shown in Figure 101 and applied to the isoprene production term to account for the shading of lower leaves by those higher in the canopy.

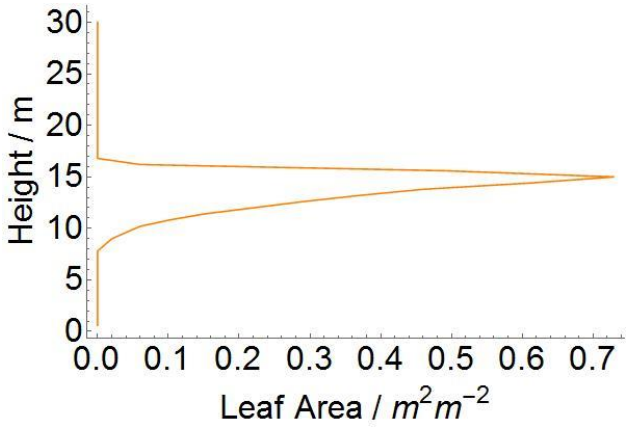

Figure 100 Leaf area distribution as a function of model height

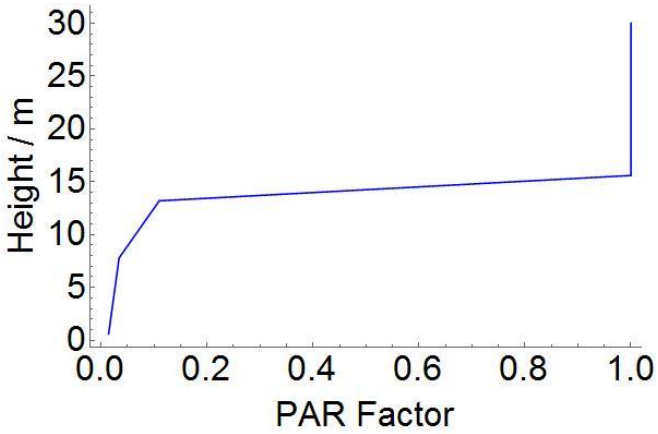

Figure 101 PAR extinction through the canopy as a function of model height

7.3.1.2 Equations describing the processes in each level

Within each level, a number of processes determine the concentration of isoprene. An overview of the level processes is shown in Figure 102. There are unique equations for the top and bottom levels, but each level has an equation to describe the change in isoprene concentration over time. These equations are derived from the equations to control concentration inside a chamber from those by Aneja et al., (2006), which is also used to calculate emission factors in Chapter 3. The equations treat each level as a 'chamber', with a number of factors affecting the concentration within. It is assumed that the levels are instantaneously and perfectly mixed. For each level there is an isoprene production term, a loss term from the chemical reactions and transfer to and from the levels above and below. In the bottom level there is also a ground deposition term. For the top level, it is assumed that isoprene is lost to the free atmosphere and that the air above the top level has an isoprene concentration of 0 ppb. The equations are shown below in *Equations 7, 8* and *9* and the terms in the equations are described in Table 13.

$$\frac{dC_{(t,1)}}{dt} = A_1 I_{(t,1)} - k_{Isop}[OH]_t C_{(t,1)} - \frac{k_{Diff}\left(C_{(t,1)} - C_{(t,2)}\right)}{\Delta z^2} - k_{Dep} C_{(t,1)}$$

Equation 7

$$\frac{dC_{(t,b)}}{dt} = A_b I_{(t,b)} - k_{Isop}[OH]_t C_{(t,b)} - \frac{k_{Diff_{(t,b)}}\left(C_{(t,b-1)} + C_{(t,b+1)} - 2C_{(t,b)}\right)}{\Delta z^2}$$

Equation 8

$$\frac{dC_{(t,bmax)}}{dt} = A_{bmax} I_{(t,bmax)} - k_{Isop}[OH]_t C_{(t,bmax)} - \frac{k_{Diff_{(t,bmax)}}\left(C_{(t,bmax-1)} - 2C_{(t,bmax)}\right)}{\Delta z^2}$$

Equation 9

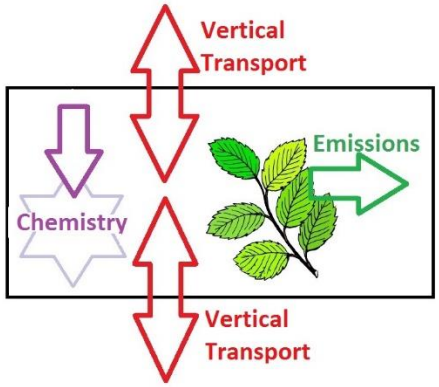

Figure 102 One CamCan level showing processes affecting isoprene concentration

Table 13 Summary of terms used in equations

	Parameter	**Unit**
$C_{(t,b)}$	Chamber concentration	ppb
t	Time	s
b	Level number	NA
[OH]	Concentration of OH	molecules cm^{-3}
I	Isoprene emission rate	$ppbm^{-2}s^{-1}$
A	Area of emitting surface	m^2
k_{isop}	Reaction rate of Isoprene with OH	$molecule^{-1}cm^3s^{-1}$
k_{Diff}	Diffusion coefficient	m^2s^{-1}
k_{Dep}	Deposition velocity	ms^{-1}
z	Height	m
Δz	Level height	m

7.3.1.3 Representing isoprene emissions in CamCan

The isoprene emission from *Quercus robur* is represented with an isoprene production term. This term shown in *Equations 7* to *9*, is taken from Guenther et al., (1993) and these functions are shown in *Equations 1*, *2* and *3* in Section 3.3.3 which take into account a normalisation factor for temperature and light. The emission factor of *Quercus robur* is taken as 10 $nmolm^{-2}s^{-1}$ (Lehning et al., 1999). It is assumed that the only source of isoprene in the forest are the oak trees and that the PAR varied between levels as a result of shading but it is also assumed that the temperature is constant throughout the canopy. Another assumption in the model is that the isoprene emission factor is constant across the season and the value chosen is representative of July emissions as determined by Lehning et al., 1999.

7.3.1.4 Description of model chemical scheme

The chemistry of the CamCan model is represented by the reaction of isoprene with OH. This is a simplification, but it allows other processes in the forest to be calculated effectively and tested for their effect on isoprene concentration. The model calculates OH

concentration using the solar zenith angle and the concentration of background ozone. The photolysis rate of ozone is calculated from an approximation of the solar zenith angle, as shown in *Equation 10* (Hough, 1988).

$$J = 8x10^{-5} * {SZ_{(t)}}^{1.6} * Exp\left(\frac{-0.56}{SZ_{(t)}}\right) \qquad \textit{Equation 10}$$

The reactions used in the calculation of OH are:

$$O_3 + h\nu \xrightarrow{J} O^1D + O_2 \qquad \textit{Reaction 4}$$

$$O^1D + H_2O \xrightarrow{k1} 2OH \qquad \textit{Reaction 5}$$

$$O^1D + M \xrightarrow{k2} O^3P + M^* \qquad \textit{Reaction 6}$$

$$\frac{d[OH]}{dt} = 2k_1[O^1D][H_2O] \qquad \textit{Equation 11}$$

To get an equation for $\frac{d[OH]}{dt}$ with just measurable species and constants, it can be approximated that since *Reaction 5* is very fast the rate of production of OH depends on *Reaction 4.* Since *Reaction 6* is more favourable, the reaction shown in *Reaction 5* occurs only 5% of the time so a factor of 0.05 can be applied to the equation. Hence:

$$\frac{d[OH]}{dt} = 2 * 0.05 * J[O_3] \qquad \textit{Equation 12}$$

Another source of OH is the reaction of O_3 with HO_2. Shown in *Reaction 7.*

$$O_3 + HO_2 \xrightarrow{k3} OH + 2O_2 \qquad \textit{Reaction 7}$$

The rate of this reaction is given by *Equation 13* which contains $[HO_2]$ which can be substituted for different terms for easier calculation.

$$\frac{d[OH]}{dt} = k_3[HO_2][O_3] \qquad \textit{Equation 13}$$

To determine a term for $[HO_2]$, the HO_x cycling reactions have to be considered, these are shown here. *Reaction 7* is an interconversion of HO_x so doesn't affect the concentration, whereas *Reaction 5* is production and *Reaction 8* is destruction.

$$HO_2 + HO_2 \xrightarrow{k4} H_2O_2 + O_2 \qquad \textit{Reaction 8}$$

$$-\frac{d[HO_x]}{dt} = 2k_4[HO_2]^2 + 2k_1[O^1D][H_2O] \quad \textit{Equation 14}$$

$$\therefore -\frac{d[HO_x]}{dt} = 2k_4[HO_2]^2 + 2 * 0.05 * J[O_3] \quad \textit{Equation 15}$$

It is then assumed that HO_x is in steady state so that $\frac{d[HO_x]}{dt} = 0$ then the equation can be rearranged for OH_2:

$$[HO_2] = \sqrt{\frac{0.05 * J[O_3]}{k_4}} \quad \textit{Equation 16}$$

Reaction with CO is also an important sink of OH as shown in *Reaction 9* and *Equation 17*.

$$OH + CO \xrightarrow{k5} +CO_2 + H \quad \textit{Reaction 9}$$

$$\frac{d[OH]}{dt} = -k_5[CO][OH] \quad \textit{Equation 17}$$

Hence all these sources and sinks can be grouped to represent the changes in the total OH.

$$\frac{d[OH]}{dt} = 2 * 0.05 * J[O_3] + k_3[O_3]\sqrt{\frac{0.05 * J[O_3]}{k_4}} - k_5[CO][OH] \quad \textit{Equation 18}$$

Then if, for a given solar zenith angle, it is assumed that the OH is in steady state, then $\frac{d[OH]}{dt} = 0$ and the equation can be rearranged as shown in *Equation 19*.

$$[OH] = \frac{2 * 0.05 * J[O_3] + k_3[O_3]\sqrt{\frac{0.05 * J[O_3]}{k_4}}}{k_5[CO]} \quad \textit{Equation 19}$$

A time series of the OH concentration for the test period as calculated in this method is shown in Figure 103.

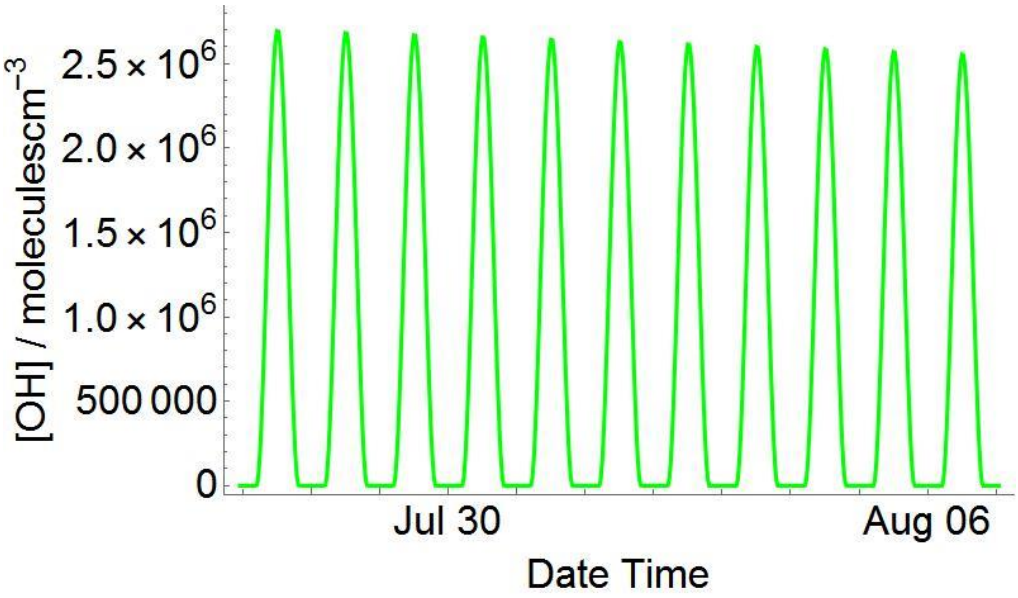

Figure 103 Concentration profile of OH shown for the test period as described in Section 7.3

The rate constants and concentrations of key species used in these calculations are shown in Table 14.

Table 14 Rate constants and species concentrations used to determine concentration of OH

Term	Value	Unit	Reference
k_3	2.32×10^{-15}	molecule^{-1}cm^{3}s^{-1}	Sinha et al., 1998
k_4	1.80×10^{-12}	molecule^{-1}cm^{3}s^{-1}	Christensen et al., 2002
k_5	1.47×10^{-13}	molecule^{-1}cm^{3}s^{-1}	Liu & Sander, 2015
k_{Isop}	1.00×10^{-10}	molecule^{-1}cm^{3}s^{-1}	Karl et al., 2004
$[O_3]$	30	ppb	Lee and Lewis et al., 2006
[CO]	200	ppb	Lee and Lewis et al., 2006

This chemical scheme makes many assumptions to simplify the loss of isoprene as a result of the chemistry. In reality, although the dominant reaction pathway of isoprene oxidation is by OH in the daytime, there are some other processes at work, which are omitted here such as ozonolysis or the night-time reaction with NO_3. The profile of OH also assumes that there are no feedbacks as a result of reaction with isoprene.

7.3.1.5 Representing diffusion between model levels

The diffusion coefficient represents the transport term between the levels. This term changes with the time of day and the level number and accounts for wind speed and the leaf density through the canopy. CamCan incorporates definitions from the CAFE Model (Wolfe & Thornton, 2011) of diffusion coefficient which accounts for the leaves of the canopy acting as an impediment for wind movement. Some functions for the friction velocity are also taken from Yi, (2007). The equations used for the term are shown in Equations 20, 21 and 22 and the parameters used are shown in Table 15. With the influence of the leaf density utilised, the diffusion coefficient function increases as you reach the top of the canopy. Above the model canopy it is assumed constant. The diffusion coefficient profile with model height is shown in Figure 104 and displays how this changes for two examples of wind speed.

$$k_{Diff} = r * 0.3 * 1.25^2 * h * U^{*LEAF} \qquad \textit{Equation 20}$$

$$U^{*LEAF} = U^* * Exp(-\frac{LAI_{cum(b)}}{2}) \qquad \textit{Equation 21}$$

$$U^* = v_{kc} * \frac{u}{Log(\frac{x-d}{z_0})} \qquad \textit{Equation 22}$$

Table 15 Parameters used in calculation of the diffusion coefficient

	Parameter	**Unit**
k_{Diff}	Diffusion coefficient	m^2s^{-1}
r	Near field correction	NA
h	Canopy height	m
U^{*LEAF}	Friction velocity corrected for leaf-density	ms^{-1}
U*	Friction velocity	ms^{-1}
LAI_{cum}	Cumulative leaf area index	m^2m^{-2}
v_{kc}	Von Karman constant	NA
u	Wind speed	ms^{-1}
x	Wind speed reference height	m
d	Zero plane displacement	m
z_0	Roughness length	m

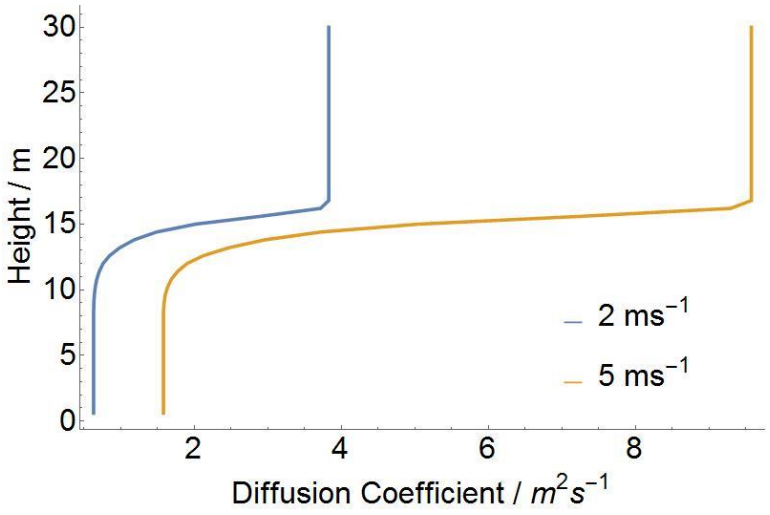

Figure 104 Diffusion coefficient variation with model height showing two examples of different wind speeds

The diffusion coefficient is directly proportional to the wind speed and is shown for level 25 in Figure 105. It can be seen that for the test period there is a period of higher and lower wind speeds, allowing us to assess how effective this approach is at calculating the mixing.

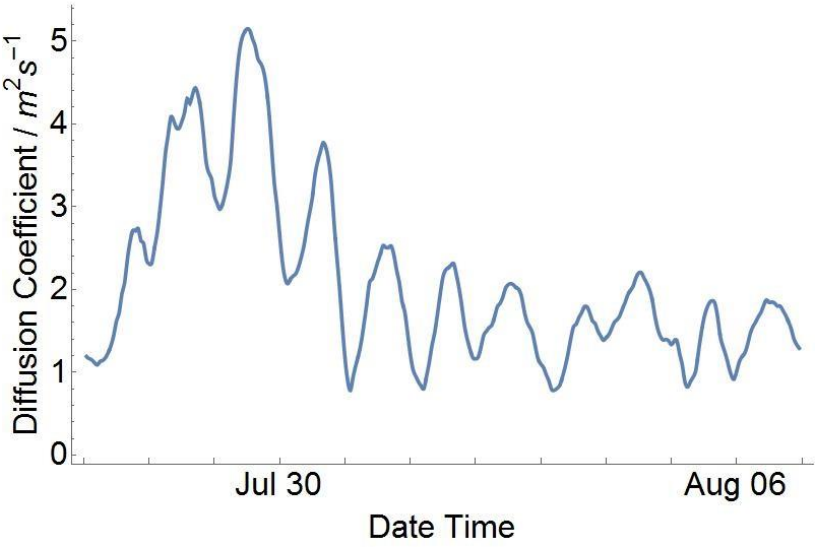

Figure 105 Time series of plot of the calculated diffusion coefficient for level 25 as an example of the differing profile for the test period

7.3.1.6 Representing deposition to the forest floor

In addition to each model process, in level 1 there is a deposition term that represents the uptake of isoprene to the forest floor and heightens the vertical gradient in the forest. In CamCan this is given a value of 0.1 ms^{-1}, chosen based a sensitivity study of possible values. This sensitivity study to investigate the use of other values is discussed in Section 7.3.2.

An assumption in CamCan is that the only surface deposition that is observed is the deposition to the ground. There are no terms for the deposition to other surfaces such as leaves, bryophytes, stems or other surfaces. The term used is also assumed to represent dry deposition velocity, wet deposition and active uptake of isoprene into the soil by bacteria. Use of other surface deposition terms requires future study.

7.3.2 CamCan sensitivity study to surface deposition

The value used for surface deposition rate (k_{dep}) in level 1 of the standard model run is 0.1 ms^{-1}, this value is chosen to best represent the measurements, as shown in Figure 112. This value is key to maintaining a strong vertical gradient in the canopy. To demonstrate how sensitive the model is to other values for surface deposition, two alternative values are run as comparison. The values chosen are 0.01 ms^{-1} and 1 ms^{-1}.

The results are evaluated in the same way as for the standard run for CamCan and are plotted as scatter plots, as shown in Figure 106. It is observed that the deposition rate strongly affects the concentrations calculated in the model. At the lower deposition rate of 0.01 ms^{-1}, the model overestimates the concentration of isoprene significantly for each inlet (Figure 106A) apart from the top of canopy inlet which appears to be well represented. This may be due to the isoprene reaching a higher overall concentration as the rate of loss due to deposition decreases. This improves estimations for the top of the canopy, but it is detrimental to the other inlets. At the higher deposition rate of 1 ms^{-1}, the model appears to predict (Figure 106A) the isoprene concentration at inlets 2, 3 and 4 with a slight underestimation but the concentration at inlet 1 at the forest floor is heavily underestimated.

Hence using the intermediate value of 0.1 ms^{-1} provides a compromise between over and under estimation. It may be possible to use a varying deposition velocity to reflect other processes occurring in the forest other deposition rates if a different vertical profile for transport (the diffusion coefficient, k_{diff}) is used. Further study and trials are required before modifying the model in this way.

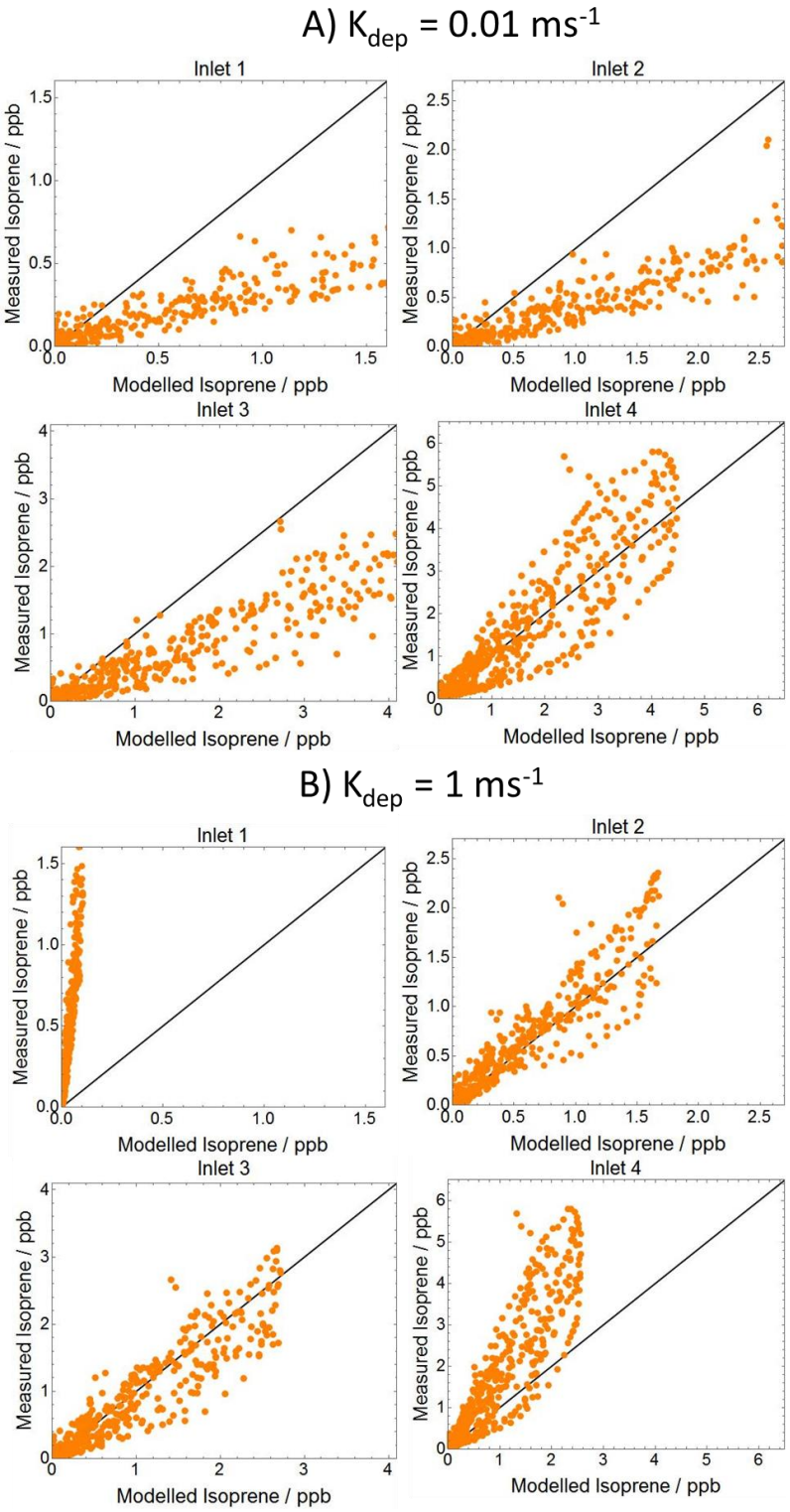

Figure 106 Two examples of model run evaluation scatterplots for two different deposition rates on the test data A) CamCan run with k_{dep} = 0.01 ms^{-1} showing model overestimation B) CamCan run with k_{dep} = 1 ms^{-1} showing model underestimation

7.3.3 A 2D model version to investigate advection

7.3.3.1 1D model with impermeable upper boundary

As described in Section 7.1, many models such as CAFE and FORCAsT use a vertical mixing profile that extends to the boundary layer. Isoprene is hence mixed to this region, and it may account for the decline of isoprene at night. In CamCan it is assumed that transport above 30 m with an exchange of air of 0 ppb isoprene produces a feasible night profile for isoprene. It may be that this is not realistic. It was attempted to use a more 'realistic' variable boundary layer without any transport above into the 1D model to try to represent a more physically realistic model. The vertical profile of the diffusion coefficient, above the current model version of just 30 levels, is shown in Figure 107 and is based on Gao et al., 1993. This model run results in non-zero night-time values as shown in Figure 108. This demonstrates that when this transport 'sink' of isoprene is removed, that the mixing, deposition and chemistry alone are not enough to drop the night values to zero, hence it is concluded that transport from a region with zero isoprene is required. The horizontal transport is investigated below in Section 7.3.3 and demonstrates that this is necessary. The vertical loss to the free troposphere can be thought of as an approximation of such an effect.

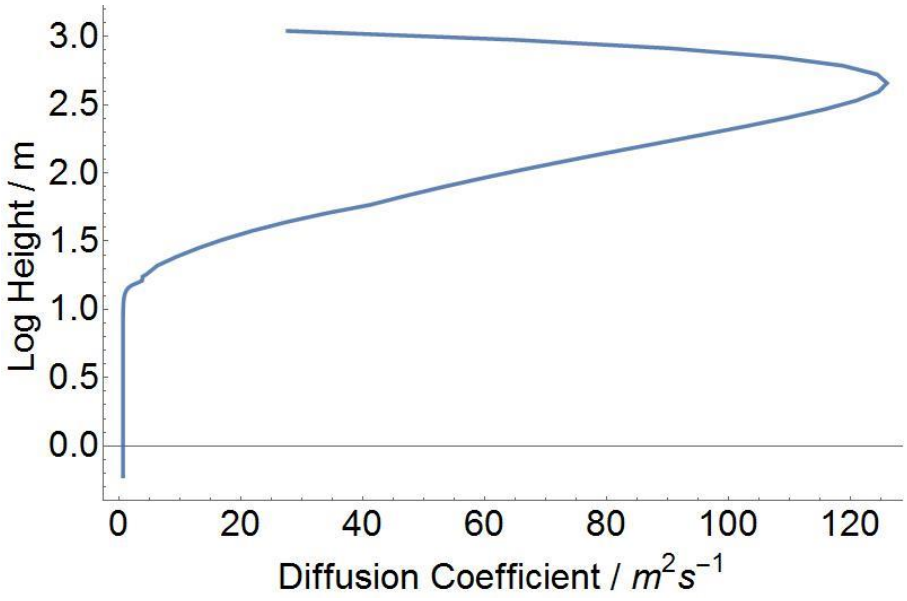

Figure 107 Diffusion coefficient values for model height (logarithmic scale) that accounts for boundary layer in the existing 1D model

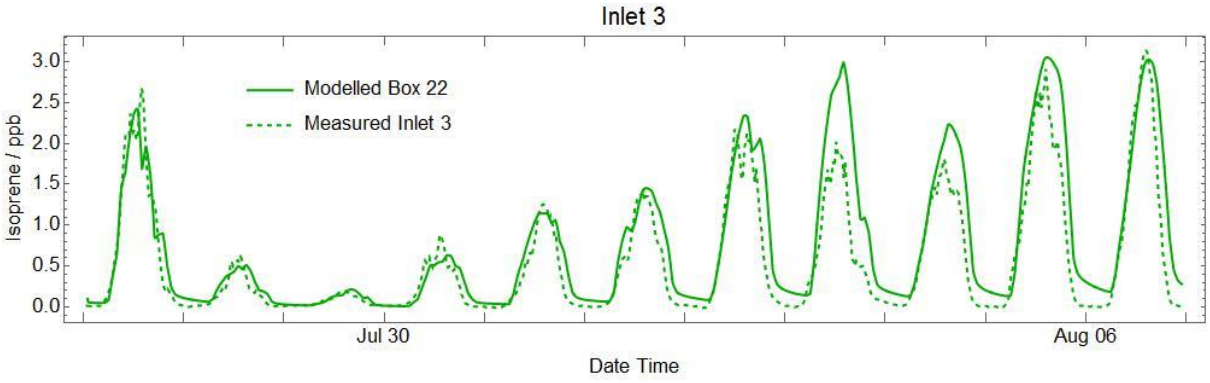

Figure 108 Model output and observations for inlet 3 showing the failure of the model to reach the low values observed in the measurements at night

7.3.3.2 A description of 2D model

In many 1D canopy transport models, the night concentration drop of isoprene is facilitated by inclusion of a loss of isoprene from the top of the model or into a 'reservoir' in the upper model domains. In CamCan the upper limit of the model is 30 m, which is below the boundary layer height. The forest in CamCan is assumed to be infinite in area and there is no consideration of horizontal advection influencing the concentrations. Isoprene can be transported above the model height and the assumed concentration entering the model is 0 ppb. Treating the model like this facilitates a drop off of isoprene when the emission is halted because isoprene is lost and there is no isoprene source.

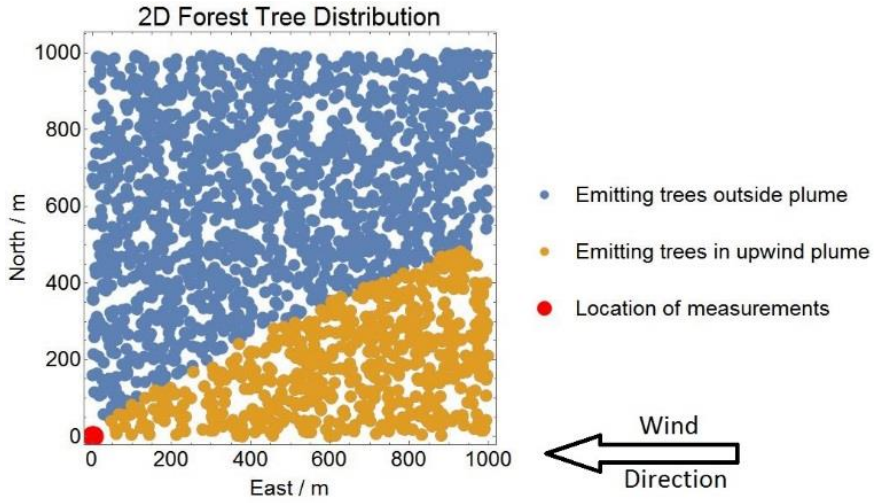

Figure 109 Representation of 2D model forest as a plan view showing an upwind plume for an easterly wind direction and the emitting trees in that plume

To determine if this method and model height realistically represents the modelled system, a 2D model (CamCan2D) was created that uses horizontal advection and the fetch of the forest to obtain appropriate isoprene concentration levels. It is hypothesised that

the true cause of the fast night-time drop-off of isoprene is due to horizontal advection bringing air from beyond the edge of the forest. As the forest is the primary source of isoprene, any air that arrives from beyond this boundary is assumed to have an isoprene concentration of 0 ppb.

This 2D model creates a map of the trees and models the horizontal plume of air from each one using the Pasquill-Gifford dispersion model approach (e.g. Seinfeld & Pandis, 2006). A representation of the 2D surface of the plume with individual trees is shown in Figure 109, which represents one quarter of a square 2 km × 2 km forest with an easterly wind direction. It can be seen that in this model, the isoprene concentration is determined by the influence of the trees upwind of the measurement site. The trees which may influence the measurement are seen in a plume as determined by the Pasquill-Gifford method.

This new model uses the same vertical diffusion scheme in CamCan as described in Section 7.3.1.5. The top level, which extenmds to 800 m, in the 2D model has a minor transport term upwards beyond the model domain.

The 2D model also validates the chosen model height on CamCan. Figure 110 shows how the plume distributes in the vertical plane across the forest, in this case for a representative wind speed of 3 ms^{-1}, with intense spots of tracer concentration indicating proximity to a source (trees). The plot shows that when the wind blows uniformly across a forest of 1 km, the maximum height reached by the plume is ~45 m and that at 30 m the concentration of the tracer species is extremely low. This shows that consideration of the isoprene concentrations above the 1D model domain of 30 m may not be necessary, particularly at Wytham Woods where the largest fetch across a stretch of forest is 1.4 km.

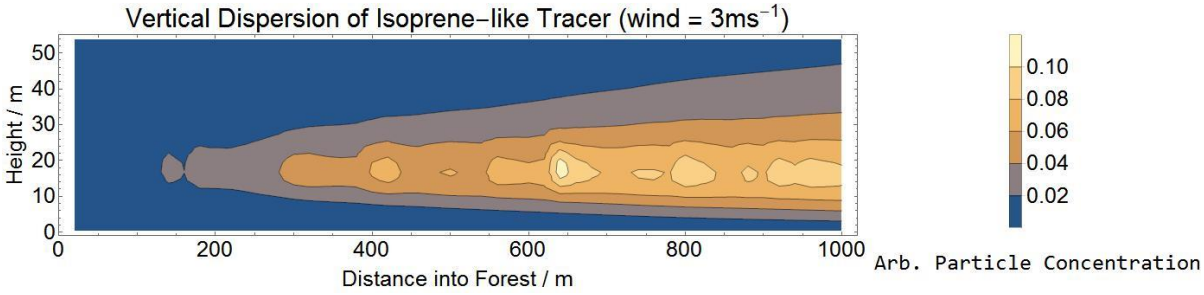

Figure 110 Vertical distribution of the dispersion plume across the forest as calculated by the Pasquill-Gifford method for an isoprene-like tracer

7.3.3.3 Simulation results from CamCan2D

The results of this model for the inlet heights are shown in Figure 111 and shows very similar values as those for CamCan shown in Figure 112. These results prove that when you take the upper level diffusion away and include the horizontal influence of the other tress and advection, the values obtained are similar or the same. This model is a rough representation, so the vertical distribution and the fine concentration profile is not captured as for the 1D CamCan, but the absolute values are comparable. This result is interesting as it demonstrates that the isoprene measured at the measurement site can just as likely be attributed to the isoprene advected across the forest as to the emission from the leaves at the measurement site. Hence, when considering a forest this is strong evidence that horizontal advection is important and that the assumption of isoprene residing higher in the boundary layer may not be accurate.

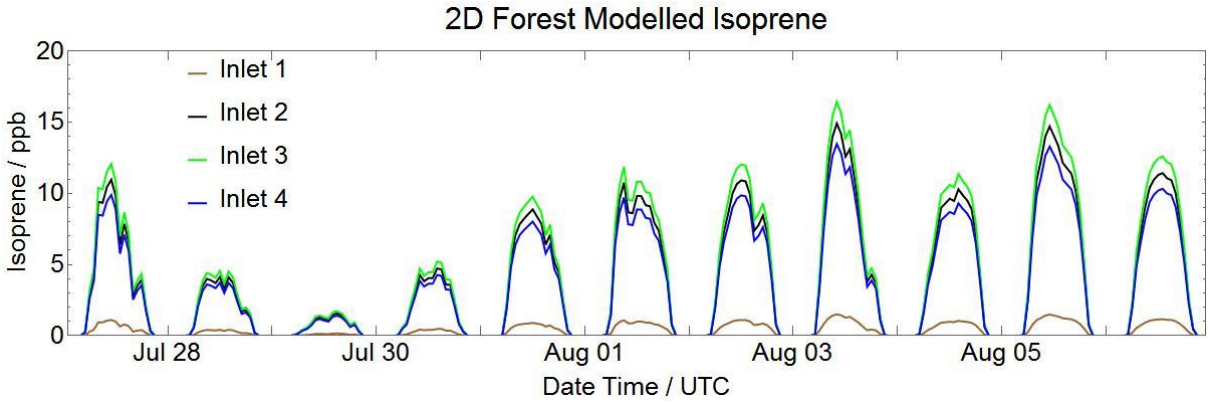

Figure 111 Model output from 2D model showing isoprene concentrations and the vertical gradient for the test period at the same order of magnitude despite the model's simplicity

7.3.4 Canopy isoprene output from the CamCan model

7.3.4.1 Output during the test period

For the period selected, the output is shown in Figure 112. The model consisted of 30 levels, but for clarity only 4 levels that represent the canopy height of the inlets in WISDOM are shown. At first glance the output reveals that inlets 2 and 3 are best represented and that inlets 1 and 4 have limited success. Particularly apparent is that CamCan is underestimating the higher values at inlet 4.

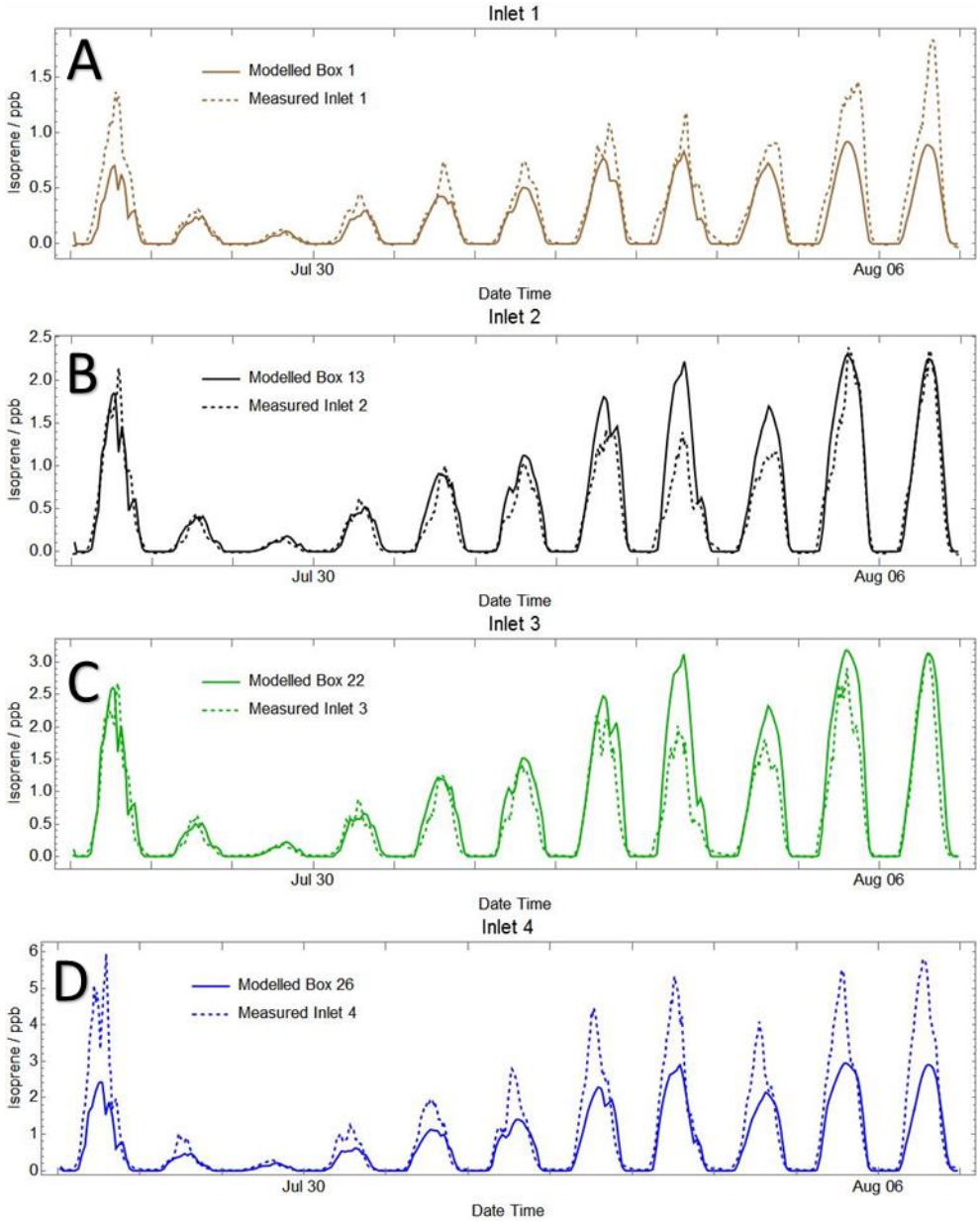

Figure 112 Model output for levels equivalent in height to the measurement inlets A) Inlet 1 and level 1 at the ground B) Inlet 2 and level 13 in the understory C) Inlet 3 and level 22 in the canopy D) Inlet 4 and level 26 above the top of the canopy

7.3.4.2 Output of CamCan for entire measurement time period

CamCan is run for the entire time period and the model output is shown in Figure 113. The model output looks similar to the measurement profile that is shown in Figure 51. From this plot it is apparent that CamCan is not representing the true vertical gradient of the forest isoprene concentration and that level 26 is consistently lower in concentration that level 22. It is also apparent that CamCan appears to capture the heatwave period. Further evaluation and analysis of this is discussed in Section 7.3.5 and Section 7.5.

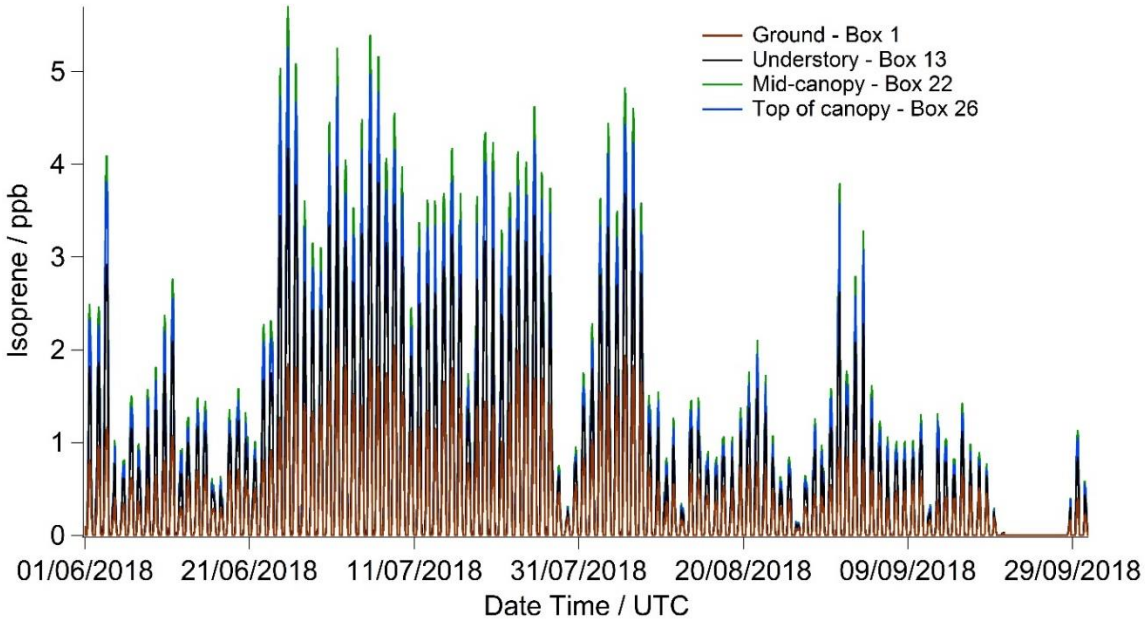

Figure 113 Full output of CamCan showing isoprene concentrations from four levels representing the inlets that were measured from 1st June to 30th September. The 19th – 20th September shows a period where no temperature data was recorded, hence predicted isoprene is 0 ppb

7.3.5 Evaluation of CamCan output

7.3.5.1 General evaluation of CamCan output

To evaluate the output of CamCan, the observations were plotted against the modelled output for each inlet, as shown in Figure 114. It can be seen that the model recreates different inlets differently. Inlets 1 and 4 are underestimated by the model. The reason for the underestimation for inlet 4 is discussed in Section 7.3.5.2. Inlet 1 in the model is level 1, which includes a simplified surface deposition term to represent the uptake of isoprene to the soil. It is likely that the influence of this factor and that of the diffusion term into this level is causing the underestimation. To amend this, a possible solution would be to slow the ground deposition but increase the diffusion to create a 'bottleneck' in the model and observe higher concentrations in this level. It may be possible to vary the deposition rate with time of day, which has been suggested is behaviour of this parameter (Muller, 1992) in line with microbial activity and decreasing temperature gradients. Inlets 2 and 3 are better represented in the model, though it can be seen that there is a slight underestimation. This could be due to the approximation of a smooth transition of diffusion factor from the canopy to the ground and the lack of representation of eddies and turbulence at each level due to the forest matrix.

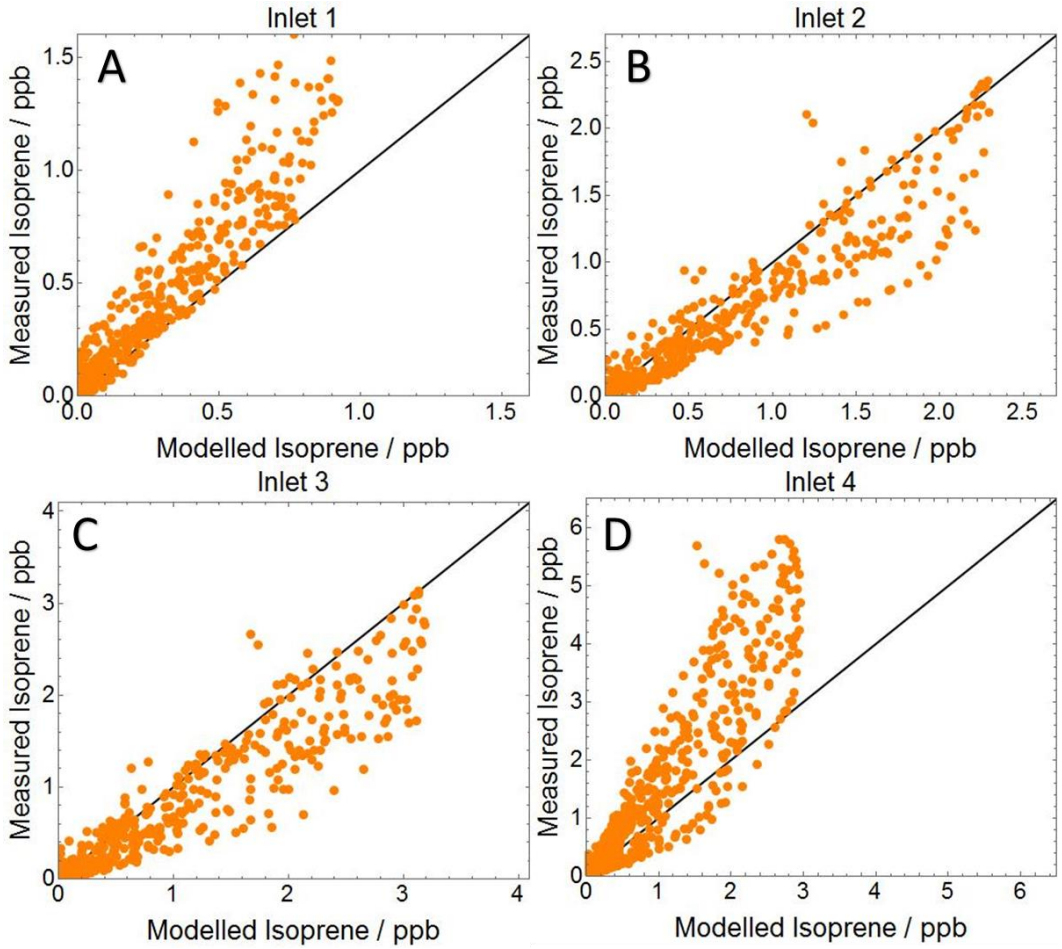

Figure 114 Scatter plots of CamCan against hourly averaged measurements for the test period A) Inlet 1 at the ground B) Inlet 2 in the mid-story C) Inlet 3 mid-canopy D) Inlet 4 above the canopy

7.3.5.2 Concentration inversion at the top of the canopy

The performance of the model with respect to inlet 4 underestimates the concentration of isoprene. Repeat attempts to represent the diffusion differently all result in inlet 4 (level 26) with a lower concentration of isoprene. The reason for this is likely the way the model treats the emission as a function of leaf area, Figure 100 shows that the maximum leaf area is 0.73 m^2m^{-2} in level 25. Hence the highest isoprene is always from this level and the diffusion causes the levels away from this to have a lower concentration. Although inlet 4 is not the highest point of the whole forest it is the highest point of this specific tree. It is hypothesised that the insolation of the leaf surfaces may cause a convective upwelling arising from an increased local temperature gradient from the top of the canopy that is not captured in this model.

7.3.5.3 The timescale of the chemistry scheme

A simple calculation shows that the timescale of the chemistry is not comparable to that of transport.

Equation 23 represents the reaction with OH which is the only chemical reaction in the model. *Equation 24* represents the transport term of isoprene out of the level. Using these equations for level 25 (inlet 3, mid-canopy) and the values shown in Table 16, an estimate for the timescale involved can be obtained.

$$\frac{dC}{dt}(chem.) = -k_{Isop}[OH]C_{Isop} \qquad \textit{Equation 23}$$

$$\frac{dC}{dt}(tran.) = -\frac{k_{Diff}C_{Isop}}{\Delta z^2} \qquad \textit{Equation 24}$$

Table 16 Test values for investigating the timescale of multiple processes in CamCan

	Parameter	**Unit**	**Value**
k_{Isop}	Reaction rate with OH	$molecule^{-1}cm^3s^{-1}$	1×10^{-10}
[OH]	Concentration of OH	$moleculescm^{-3}$	2.5×10^6
C_{Isop}	Concentration of isoprene	ppb	5
k_{Diff}	Diffusion coefficient	m^2s^{-1}	4
Δz^2	Scaling parameter for level height	m^2	0.36

With these values the rate of loss of isoprene with respect to chemistry is 1.25×10^{-3} $ppbs^{-1}$ and the rate of loss due to transport is 55.55 $ppbs^{-1}$. These values indicate that the chemistry is occurring on a very slow timescale and is not primarily responsible for the observed vertical gradient. To further investigate this, CamCan was run with the terms for chemistry removed. The results are shown in Figure 115. This plot shows how the chemistry plays only a minor part in the observed time-series.

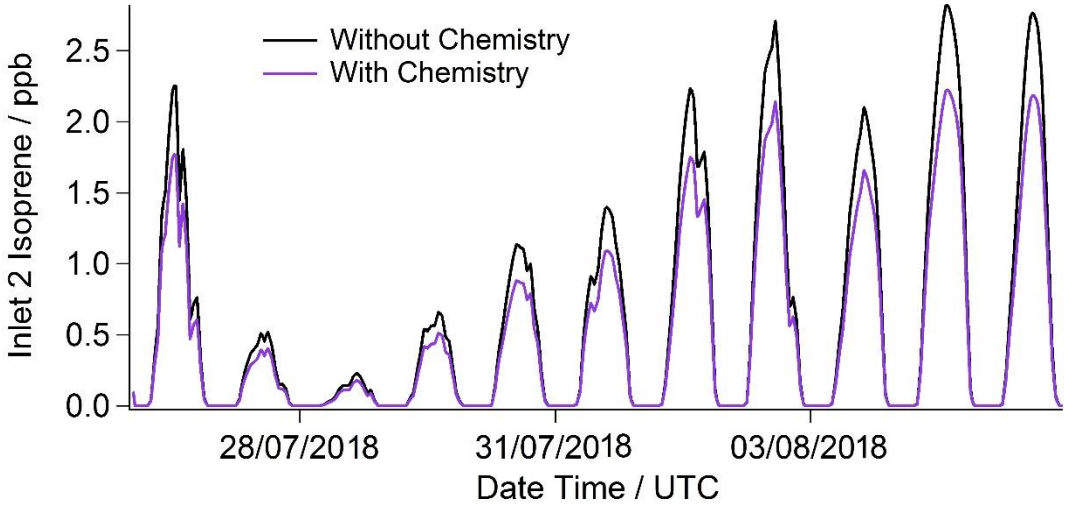

Figure 115 Comparison of modelled output isoprene concentration at inlet 2 (level 13) with and without the chemistry term included for the experimental test period

7.4 The FORCAsT model: an established model

As a way to compare results with a developed and significantly more complex model, the forest at Wytham was modelled with the FORest Canopy Atmosphere Transfer (FORCAsT) model (Ashworth et al., 2015). FORCAsT is a 1D canopy transport model that can simulate the concentrations and fluxes of different VOCs in a canopy and above. The model includes complex chemical reaction schemes that exceed the level of those in the CamCan model and can lend us some understanding of the mass and energy balance of the canopy system. FORCAsT was developed at the University of Michigan, US by Ashworth et al. (2015) and development is now continued at the University of Lancaster, UK. The results shown here were calculated by Fred Otu-Larbi and Kirsti Ashworth at Lancaster as part of the WISDOM campaign.

7.4.1 Description of the FORCAsT model

The simplified structure of FORCAsT is shown in Figure 116. The model is broken down into a single column of multiple levels, which increase in level height as model height increases, with the model reaching a height of 3 to 5 km. The model also includes several layers into the soil.

Each layer of the model has similar processes described as the CamCan model, with vertical transport out of and into each level, but also in a horizontal direction as advection. The loss processes in each level are the chemical reactions and surface deposition. Emission of many more species are included and additionally, turbulence within a level

is characterised. The chemistry, dynamics and land surface treatment in this model is a development of the CACHE model (Forkel et al., 2006). The energy and radiation balance of the model are derived from that of the CUPID soil-plant-atmosphere model (Norman, 1979; Norman & Campbell, 1983). One novelty of the FORCAsT model is that it models the partitioning of the gas phase to the condensable phase for aerosol concentrations.

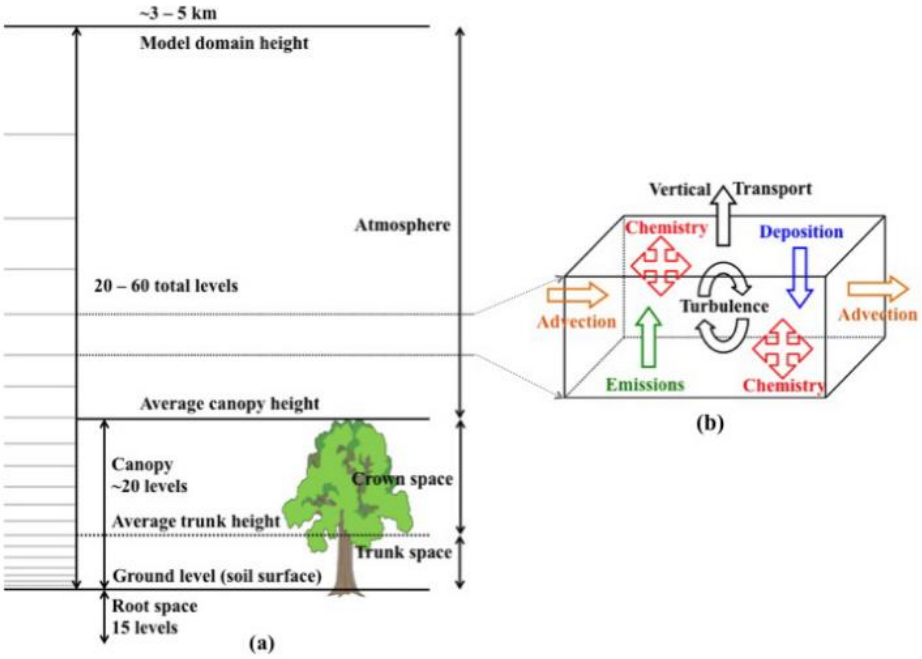

Figure 116 Schematic of FORCAsT model showing the level distribution and the processes affecting each level

The canopy in FORCAsT uses a leaf angle distribution from the leaf area index (LAI) to construct a structure that represents the leaf density and their orientation to incoming radiation. The interception of the sunlight by leaves determines how the sensible and latent heat fluxes are determined for the canopy. The model assumes for the radiation balance that the canopy is spherical. The incoming solar radiation can either be provided by observations or by a default scheme.

The emissions in FORCAsT of BVOCs are derived from parameterisations from Guenther et al., (1995) and monoterpene emissions have a temperature dependent term that is derived from storage pools in the plant tissue (Steinbrecher et al., 1999). For isoprene the scaling factors for light and temperature are those shown in *Equations 1, 2* and *3* in Section 3.3.3. A different emission is calculated for each leaf, depending on what angle class they are and the degree of shading.

The advection terms are included so as to account for the incoming oxidant species that

strongly affect the concentration of many VOCs or the influence of anthropogenic sources away from the forest. The parameterisation of advection is derived from wind speed and the input values are obtained from nearby satellite or observational values.

The deposition in the model of gases is treated as dry deposition using a range of resistances of various parts of the forest surfaces and species specific Henry's law coefficients. The processes governing deposition rate are all explicit and also account for processes like stomatal conductance which varies with light levels, temperature and vapour pressure deficit. These processes are calculated before being passed to the chemistry schemes in FORCAsT. From observations of the performance of CamCan with a ground deposition velocity of 0.1 ms^{-1} the deposition velocity for FORCAsT is increased to improve model output, specifically the evening decrease of isoprene concentration. The FORCAsT deposition velocity has a diurnal profile, with a mean value at the ground for the time series of 0.13 ± 0.51 ms^{-1}.

The turbulence in the model follows K-theory (Blackadar, 1962) and originally used mixing parameters from within the canopy and above by Baldocchi, (1988) and Gao et al., (1993). The model is typically constrained by 3D wind observations at multiple heights. Using the positive results from CamCan, the vertical mixing parameters in the canopy are now defined by those from Wolfe & Thornton, (2011). The diffusion coefficient for FORCAsT above the canopy uses the profile defined by Gao et al., (1993) and hence assumes that the space above the canopy can act as a 'reservoir' for emitted species.

The FORCAsT chemistry schemes involve many species and reactions. It is possible to run the model using either the regional atmospheric chemistry mechanism (RACM) (Geiger et al., 2003; Stockwell et al., 1997) or the Caltech atmospheric chemistry mechanism (CACM) (Chen & Griffin, 2005; Griffin et al., 2002; Griffin et al., 2005). The RACM scheme includes 84 gas phase compounds and 249 reactions concerning these. The isoprene reactions include those from the Mainz Isoprene Mechanism (Pöschl et al., 2000). One of the main developments with FORCAsT was the ability to represent SOA formation and this was done with the CACM chemical mechanism (Griffin et al., 2002, 2005). CACM contains 300 chemical species and 620 reactions, but also added to FORCAsT is new treatment of some monoterpenes to form aerosol and also an update to the peroxy radical reactions which are more aligned with that of RACM.

7.4.2 Output from the FORCAsT model

Prior to optimisation, FORCAsT did not accurately the isoprene observed. In particular the night values were non-zero, the vertical isoprene concentration gradient was not well represented and the absolute values were too low. The output for the model at Wytham, before these parameters were improved is shown in Figure 98B.

The model was first run for the test period as selected for CamCan. This period ran from the 27th July to 6th August 2018 and included sunny periods, cloudy periods and varying wind speeds. The output is compared to the observations in Figure 117. It can be observed that generally there is an over-estimation of isoprene at each level. The model fails to calculate isoprene correctly in particular on day three of the test period.

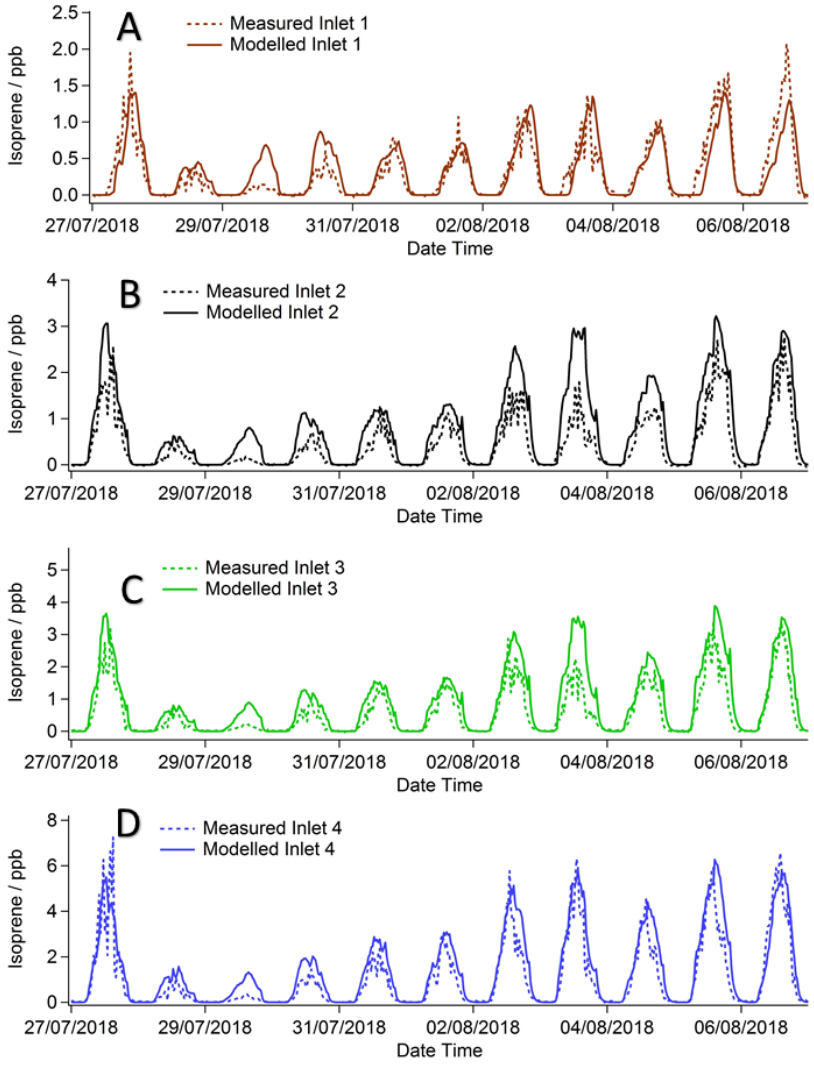

Figure 117 FORCAsT model output for levels equivalent in height to the measurement inlets A) Inlet 1 at the ground B) Inlet 2 dangling mid-story C) Inlet 3 in the canopy D) Inlet 4 above the top of the canopy

7.4.3 Evaluation of the FORCAsT model

In general FORCAsT recreates the measurements in the forest well. It can be seen for Figure 118 that each inlet shows reasonably good agreement. Inlet 1 in particular shows good agreement, with little bias in any direction, but with a high degree of spread, similar to the other inlets. The scatter plots for inlets 2, 3 and 4 show that the FORCAsT model consistently over-predicts isoprene. In terms of the test period time series shown in Figure 117 there are several days where FORCAsT fails to recreate the isoprene concentration. In Section 7.5 several factors are investigated as possible causes for this and other reasons are discussed.

FORCAsT results in a better scaling of the vertical gradient than CamCan. This is achieved by incorporating a steeper light extinction coefficient at the top of the canopy. This means that the few leaves at the very top receive the most light and since this is in the upper level, it experiences the highest isoprene concentration.

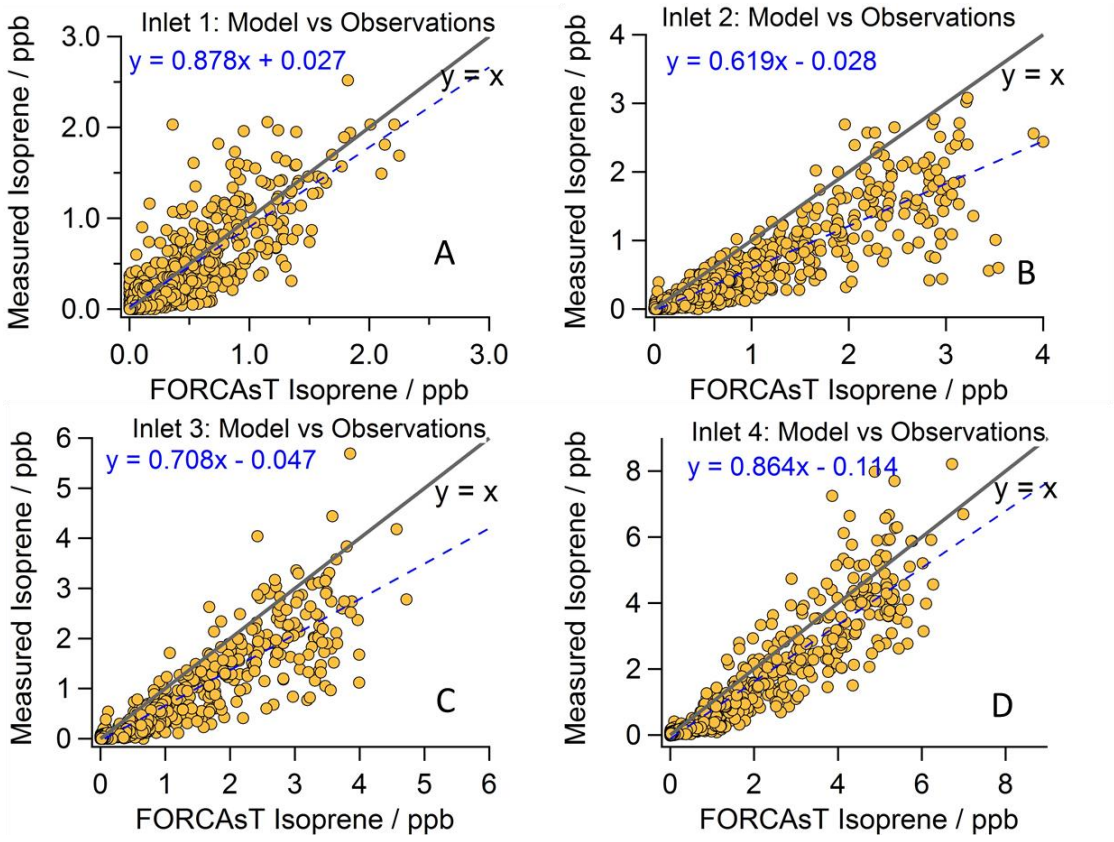

Figure 118 Scatterplot analysis of model vs observations. The black line is the 1:1 line A) Inlet 1 comparison B) Inlet 2 comparison C) inlet 3 comparison D) Inlet 4 comparison

7.5 Comparison and evaluation of CamCan and FORCAsT

7.5.1 General comparison of CamCan and FORCAsT

With different processes represented differently in both CamCan and FORCAsT, it is expected that the model output of isoprene concentration is different. As shown in Figure 112 and Figure 117, both models appear to capture the observations on some occasions, but fail on others. This section aims to investigate how each model may fail to capture the isoprene profiles and what factors might cause this discrepancy.

The entire season was ran for both CamCan and FORCAsT using the optimised parameters as discussed in Section 7.3 and Section 7.4. The dates the model ran were from 1st June 2018 to 30th September 2018. The model output followed the measurements and this time series can be seen in Figure 120B. In this plot it is observed that both models consistently over-predict isoprene across the entire time period. This is further demonstrated as a scatterplot for inlet 3 in Figure 119. This plot also shows that FORCAsT is more successful at predicting isoprene over the entire time period. This result may indicate that some of the simplifications and assumptions used in constructing CamCan need refinement. The inclusion in FORCAsT of reactions of isoprene with O_3 and NO_3 may also explain the lower values outputted and the better agreement.

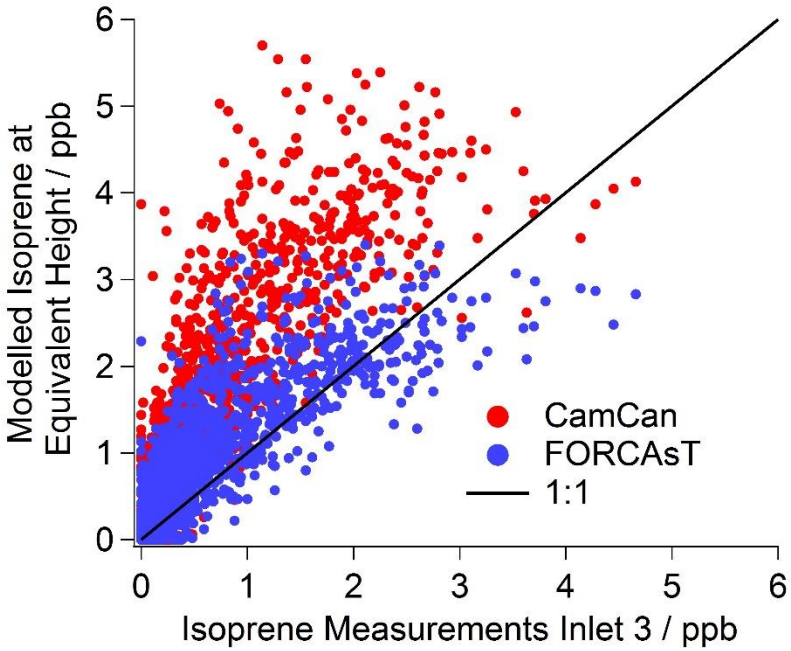

Figure 119 Side-by-side comparison of isoprene concentrations from CamCan and FORCAsT against the observations for the height of inlet 3, showing over-prediction from both models

To investigate where model-measurement disagreements arise, the meteorological data is examined. For this analysis the inlet 3 measurement is used as this is the inlet with best agreement to the measurements using either FORCAsT or CamCan. A number of factors could have contributed to a discrepancy such as soil moisture, wind direction or the changing emission factor resulting from the age of the leaves.

A metric for the model-measurement discrepancy is the model efficiency factor, which is defined and discussed in Section 7.5.2. This value gives an idea of the magnitude of over or under prediction.

During the heatwave, it is seen that the models both over-predict isoprene significantly. As discussed in Section 6.5 it may be that during the heatwave, as a result of lowered soil moisture, the trees emission behaviour changes significantly. In the models this change in behaviour is not captured and hence the models fail to recreate this phenomenon. There is be a degree of seasonality to the isoprene emissions which is not captured by the models, which input just temperature, PAR and plant emission factor to calculate emission. It appears that the models fail to capture the seasonality and the heatwave stress period and hence are not able to capture the trend in isoprene concentration at the height of the summer.

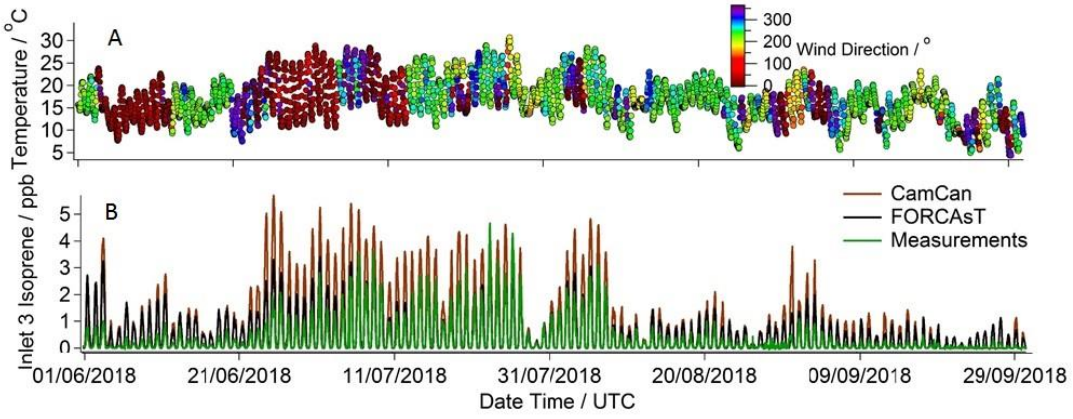

Figure 120 A) Time series of mean temperature and wind direction B) Model outputs from CamCan and FORCAsT with the measurement data

7.5.2 Calculation of a model efficiency factor

To examine how the measurements represent the seasonality of the measurements, a comparison is made of the CamCan and FORCAsT simulated concentrations to the measurements. By assessing the ratio of the measurements to the modelled output a

function can be calculated that can be described as a model efficiency term. This term would represent the value that would need to be multiplied to the model output to reach the correct value for the equivalent measurement. To eliminate the diurnal pattern in the data, the gradient is taken from the scatterplot of the modelled data to the measured isoprene for the equivalent height for each day.

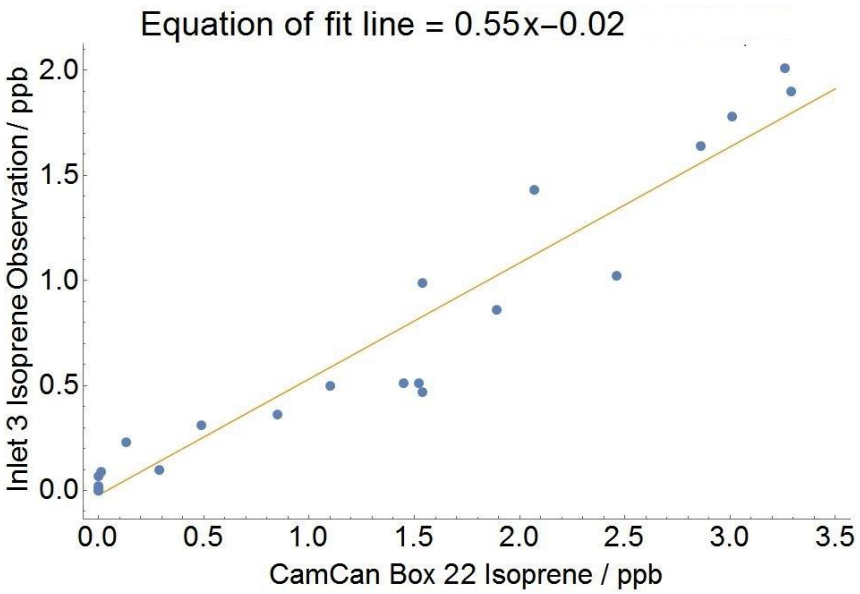

Figure 121 Example scatterplot on the 21st July of modelled output isoprene concentrations versus measured isoprene concentration showing line of best fit and equation with modelling efficiency factor of 0.55

When the model efficiency term for each day is plotted as a time series (Figure 122), it is observed that there is a seasonality to the profile for both CamCan and FORCAsT. The absence of a clear step change of this factor during the heatwave indicates that this factor is not a consequence of the temperature, but may be a result of the seasonality of the isoprene emission from the forest. It is also indicated that when the soil moisture increases due a rainfall event, there is a sharp decline in this efficiency factor and this is discussed further in Section 7.5.4. The emission factor taken from Lehning et al., (1999) was measured in the northern hemisphere in July and this result may indicate that a seasonality to the emission factor is required to capture the isoprene concentrations observed in the forest.

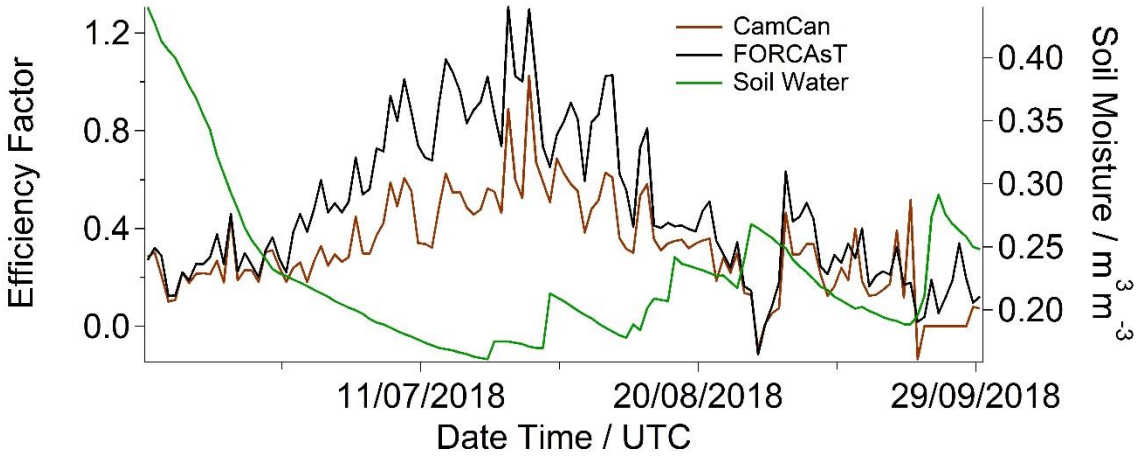

Figure 122 Model efficiency factor for CamCan and FORCAsT with the soil moisture also plotted

7.5.3 Effects of wind direction on model efficiency

Figure 120 shows the temperature profile alongside the measurements and model output and also shows the wind direction. It can be seen that there is an apparent correlation between the wind direction and times when the model discrepancy in Figure 120B was high, or relatively high.

It is hypothesised also that the wind direction may be key when thinking about this data. The forest in the model is assumed to be a continuous forest with an equally distributed source of isoprene that does not depend on wind direction. The tree cover is variable at Wytham and the distribution of *Q. robur* is not even, so different wind directions will effectively result in differing sources. In Figure 42 it can be seen that the distribution of *Q. robur* is random and a larger map of distribution would be required. In Section 6.4.1 there appears to be a link of isoprene concentration and wind direction and the potential sources do seem to be captured in the polar bivariate plots in Figure 82. This change in the source of isoprene may result in a discrepancy in the model. It is seen in Figure 120 that regions where the wind direction is from the north-east seems to coincide with times of elevated disagreement between the model and the measurements.

The mean daily wind direction is plotted against the daily efficiency factor between CamCan and FORCAsT outputs and the inlet 3 measurement in Figure 123. It is observed that there is no obvious relationship with the wind direction but that for the period from 0 – 50^{o} (northeast) the mean efficiency factor is 0.23 ± 0.07 and 0.37 ± 0.17 for CamCan and FORCAsT respectively and that for the period from 200-250^{o} (southwest) the mean

value is 0.34 ± 0.22 and 0.51 ± 0.34 for CamCan and FORCAsT respectively. This indicates that the model is better optimised when the wind is from 200-250^{o} (southwest) than from when the wind is from 0-50^{o} (north-northeast). It may be that the tree distribution from this direction is different to that of the southwest and that the training data (in which the wind is predominantly from the south west) does not represent every wind direction scenario in the forest. As the model is over estimating the isoprene it is hypothesised that the area has a depleted emission source, so may have a lower density of oak trees. This is an area for further discussion and study.

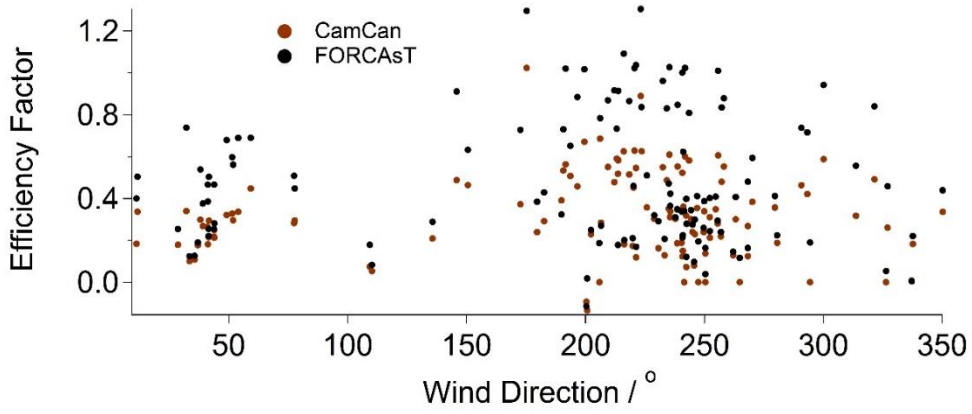

Figure 123 Relationship of mean wind direction for the period 1-5pm and the model daily efficiency factor for CamCan and FORCAsT model outputs

7.5.4 Effects of soil moisture on model efficiency

The soil moisture is currently not accounted for in either model. From Figure 122 it appears that the period where the efficiency factor is highest corresponds to the period when the soil moisture is the lowest. To investigate this the mean 1-5 pm soil moisture was plotted against the daily model efficiency factor for inlet 3. The plot is shown in Figure 124 and demonstrates that in general below a value of 0.22 m^3m^{-3} the frequency of high efficiency is increased. This may indicate that the model overestimation of isoprene is not factoring soil moisture and that the model output best represents the drought period.

It is also apparent from Figure 122 that where there is a large increase in soil moisture which is due to a rainfall event, there is a sharp fall in the efficiency factor. This effect is particularly evident on the 28th August. This behaviour highlight that the model does not represent the effect seen on isoprene after a rainfall event. This phenomenon requires further study to investigate further.

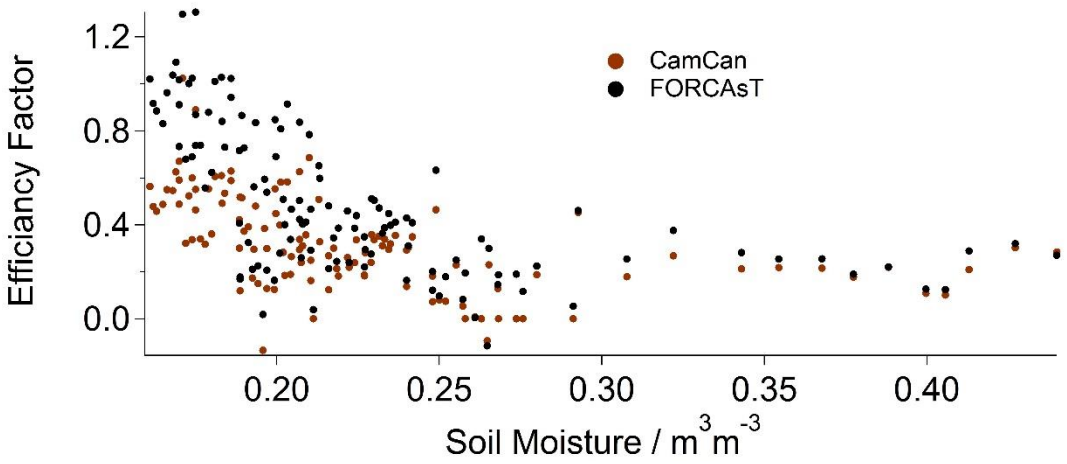

Figure 124 Mean soil moisture for the period 1-5pm plotted against the model daily efficiency factor

7.6 Fluxes calculated from CamCan

7.6.1 Calculating flux from CamCan

It is possible to calculate the flux from the top of the model in CamCan. The equation for flux is shown in *Equation 25*, where *l* is the height of the level. The level at the top of the model, level 50 has a transport term represented by the k_{diff} and the domain above the model is assumed to have an isoprene concentration of 0 ppb. Assuming a pressure of 100 kPa and a temperature of 298 K the concentration of isoprene can be calculated from the mixing ratio in the model level using the ideal gas law.

To constrain the model with the measurements, the model efficiency as described in Section 7.5.2 is multiplied by model output to increase confidence in the values of flux calculated.

$$Flux = \frac{\Delta[Isop] * k_{diff}}{l} \qquad \textit{Equation 25}$$

Hence using the k_{diff} for level 50 and the model calculated isoprene concentration corrected with the daily model efficiency factor, the flux is calculated and converted to $mgm^{-2}h^{-1}$. Figure 125 shows the values obtained across the season for the model output and the corrected model output. It is observed that the values are similar to those obtained in Alice Holt Forest, UK, a site 75 km southeast of Wytham that had isoprene fluxes measured in July and August 2005 and reached a maximum value of ~6 $mgm^{-2}h^{-1}$ (Langford et al., 2017). The flux values calculated are also comparable to values for other European oak forests. The flux here indicates that the values calculated for this time

period at Wytham occasionally exceed this maximum, which is likely due to the heatwave.

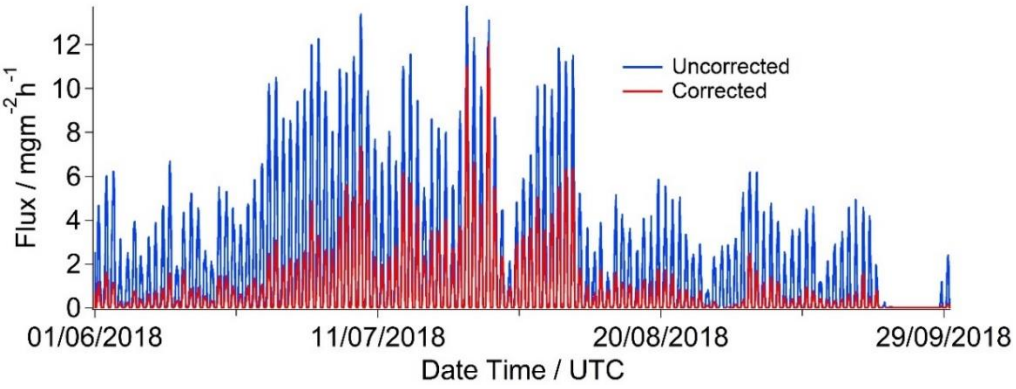

Figure 125 Flux calculated from 1st June to 30th September from isoprene concentrations and the diffusion coefficient from level 50 of the CamCan model into the region above the model domain showing both the original uncorrected model output (blue) and the corrected time series (red)

To examine what fraction of the isoprene is deposited to the ground, relative to this flux, the deposition flux is also calculated using *Equation 26*.

$$Flux_{dep} = \Delta[Isop] * K_{dep} \qquad \textit{Equation 26}$$

The value output is shown in Figure 126 and shows the diurnal profile and absolute values of the deposition flux. From this value, it is calculated that on average the flux of isoprene to the ground is 17.4 % of the flux to above the model domain. This has important implications for the fate of isoprene emitted from the trees. This is also a high value that drives the vertical canopy gradient during the day.

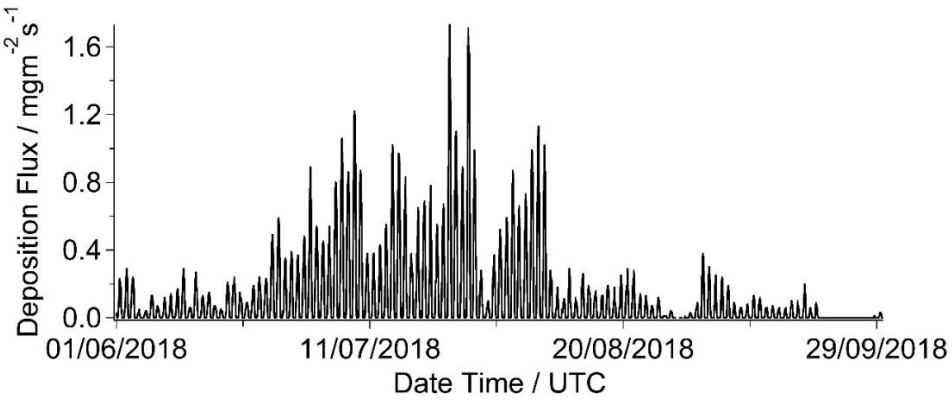

Figure 126 Deposition flux calculated from 1st June to 30th September from isoprene concentrations and the deposition velocity from level 1 of the CamCan model into the forest floor

7.6.2 Total flux from Wytham and estimates for UK isoprene emission

Using this profile of isoprene flux, it can be integrated over the entire period to obtain a value for total flux from the period 1st June to 30th September. Using some broad approximations, the isoprene emission rates for a number of different scales and locations are shown in Table 17.

Over the entire model period the flux is integrated to obtain a value of 4.8 gm^{-2}. It is assumed that that this value represents the growing season for the forest and that outside this time period the flux is zero, hence this value can be assumed to be a yearly flux value.

The percentage cover of *Q. robur* of a small transect of Wytham woods of (2000 m^2) was determined as 24% by Mihok et al., 2009. The total area of Wytham woods is 410 Ha and so the total flux for the oak coverage of the forest can be calculated. The value obtained is 2.0 Mg and as the other species at Wytham are assumed to be non-emitters the daily isoprene emission potential for the forest is 0.04 $kgha^{-1}d^{-1}$. The uncorrected value for isoprene emission potential is 0.10 $kgha^{-1}d^{-1}$ which highlights the over-prediction of the model and the necessity of constraining the results with the measurements. The heatwave period also showed double the rate of isoprene emission at 0.08 $kgha^{-1}d^{-1}$, indicating the importance of such climactic events.

In this calculation it is assumed that all the forest in the UK has the same composition and isoprene emission potential as Wytham and that none of the other land produces any isoprene. The total forest coverage of the UK is 13% and the total land area of the UK is 242,495 km^2 (Forestry Commission, 2018). Hence for the UK, with an emission potential of 0.01 $kgha^{-1}d^{-1}$ the estimation for total annual isoprene emission, assuming the measurement represents the growing period, is 15.1 Gg. The global yearly emission of isoprene is estimated at 600 Tg as calculated by MEGAN (Guenther et al., 2006) hence the value for the UK obtained using CamCan represents 0.004 % of the global emission of isoprene.

Table 17 Summary of isoprene emissions at different scales and locations with some values for tropical forests (David Fowler et al., 2011)

Factor calculated from CamCan	**Isoprene emission potential / kgha^{-1}d^{-1}**
Unconstrained mean emission potential for Wytham 1st June – 30th September	0.10
Constrained mean emission potential for Wytham 1st June – 30th September	0.04
Constrained mean emission potential for Wytham heatwave 23st June – 8th August	0.08
Constrained mean emission potential for UK 23st June – 8th August	0.01
Mean emission potential from OP3 for primary tropical forest (David Fowler et al., 2011)	0.60
Mean emission potential from OP3 for oil palm plantation (David Fowler et al., 2011)	3.00

To compare these value with global forest cover, which is estimated at 32,687,000 km^2 (Hansen, Stehman, & Potapov, 2010), this flux rate was calculate for the Earth. When the CamCan calculated flux is multiplied across the Earth's forest area the resulting isoprene emission potential is 0.3 kgha^{-1} which represents total annual emission of 15.6 Tg.

As shown in Table 17, emission potentials for primary forest and oil palm plantation measured during the OP3 campaign are order of magnitudes higher than that of Wytham. The emission potential for Wytham is 6.6 % that of the tropical primary forest, highlighting the importance of tropical forests on the global isoprene budget. The rate during the heatwave was also double that of the mean for the measurement period, indicating the importance of heatwaves on local atmospheric chemistry.

This result demonstrates that the forest at Wytham has lower, but comparable, magnitude for isoprene emission as other forests around the world. The value of 600 Tg globally calculated with MEGAN incorporates the emission from other land uses and plant species

and includes tropical areas of the Earth that have a higher emission potential.

These estimates use a vast array of broad assumptions and produces a feasible estimate for isoprene from the UK. However the uncertainty in this value is high and future refinement and research is required to increase confidence in these values.

7.6.3 Wytham flux at elevated temperature

To investigate the impact of a potentially warmer climate, a new run of CamCan was completed with temperatures elevated by 1^{o}C. In the model run, the only factor that is affected by temperature is the isoprene emission, hence the model output resulted in an increased isoprene concentration. The values obtained from the flux values are manipulated to calculate isoprene emission from Wytham and for the whole of the UK using the same set of assumptions as for Section 7.6.2. The results are shown in Table 18.

Table 18 Calculated values for isoprene emission for Wytham and the UK

CamCan Model Run	**Yearly isoprene emission / kgha^{-1}**	**Yearly Emission from Wytham / Mg**	**Yearly UK Isoprene Emission / Gg**
Standard Temperature	4.8	2.0	15.1
Temperature increase by 1^{o}C	5.39	2.2	17.0

The values indicate that an elevated temperature results in a higher emission of isoprene from Wytham and consequently for the UK. Just a 1^{o}C increase in average temperature results in a 12.3 % increase in isoprene emitted from Wytham Woods which represents 200 kg extra isoprene per year.

The implication of this on the future climate is significant. With the future climate predicted to be warmer than present temperature and global temperatures predicted to increase by 1.0 ^{o}C or greater by 2030 (IPCC, 2018). An increase in isoprene emission to the atmosphere of 12.3% is likely to strongly affect atmospheric chemistry and emissions of carbon from the biosphere. There will likely be changes in SOA and ozone concentrations in the atmosphere, with implications for radiation balance and human health. Future refinement of these calculations and investigation on the implications of these findings on atmospheric chemistry are required.

7.7 Simulating a tropical forest with CamCan

A further method to demonstrate the usefulness of CamCan is to ask what other scenarios can be simulated. As such, another forest type is examined that has repercussions for global isoprene emissions and is been investigated in this thesis; the tropical forest. This allows us to compare the model output with the measurements taken in these forests as described in Chapter 3.

In an attempt to model other types of forest, a different set of data is run to represent a tropical forest. CamCan was constructed for the forest system at Wytham, which is significantly different to the forests prevalent in Southeast Asia. A number of factors need to be changed before these models could be comparable.

Firstly the coordinates of a site in Malaysia are used. The location chosen was the Pekan oil palm site on Peninsular Malaysia with coordinates 3º26'28.9" N, 103º23'12.9" E. The latitude and longitude are important for determining the solar zenith angle which strongly influences the concentration of OH which is the primary oxidant for isoprene.

The structure of the forest is taken from various sources on tropical forests in Malaysian Borneo and it is assumed that these parameters also represented a tropical forest on the Malaysian Peninsula. The height of the canopy is assumed to be 60 m which is taken as an approximation from Riutta et al., 2018 representing the canopy height in a primary forest. The levels used in this simulation were 2.4 m high and extended to a height of 120 m. The leaf area index (LAI) is approximated for this test as 4 m^2m^{-2} and taken from Hardwick et al., 2015. It is understood that LAI changes significantly for the different conditions in the forest and factors such as season, aspect, climate and the influence of global shifts such as El Niño events (Hardwick et al., 2015), but for this model simulation it is assumed not to change for the period and location selected. An estimate of leaf area distribution which is scaled from the LAI is used and is shown in Figure 127.

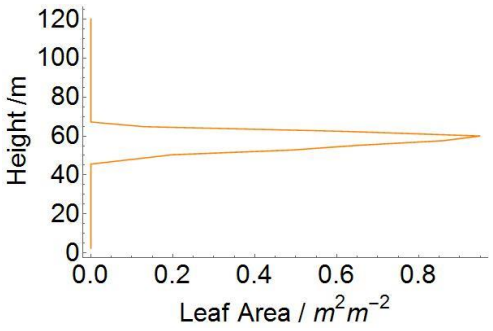

Figure 127 Tropical forest leaf area distribution showing the leaf area as a function of model height

The meteorological data used is taken from the Pekan oil palm plantation site. The site is the same one where isoprene was measured in Section 3.3.2. It is assumed that the meteorology of this site broadly represents the top of the canopy for a nearby mature forest. The wind speed was used to calculate the diffusion coefficient for the forest vertical transport and the temperature and solar radiation were used to calculate the emission rate from the leaves.

The species emission that is used was taken from values calculated in Section 3.4.1. The most abundant genera recorded in the tropical forests in 2018 are *Shorea, Parashorea, Dryobalanops, Diospyros* and *Syzygium* (Riutta et al., 2018). Trees from these genera were extracted from the list of recorded isoprene emission factors during the Plants Traits campaign in 2015 (Appendix 2) and contain trees that exhibit both emission and non-emission of isoprene. To increase confidence in these emission factors, they were filtered to exclude individual trees were the standard deviation is greater than 1000 $nmolm^{-2}s^{-1}$ and trees of the same species were averaged. The mean value used in these runs was 75.26 $nmolm^{-2}s^{-1}$.

Figure 128 shows the model output over 11 days in November 2015. This time period is chosen as it coincides with some time periods where measurements were taken. What is immediately striking about the model is the large difference in isoprene concentration between the upper canopy and the lower regions. This may reflect the longer distance the isoprene has to travel to get to the forest floor. Correspondingly, the ground level at 2.4 m has comparably low isoprene concentration. The values obtained for level 1 at 2.4m are similar to observations in the primary forest. In particular the sites at Belian and Seraya from Figure 32 and Figure 33 respectively have diurnal profiles that reach values of 2 ppb to 3 ppb. A direct comparison cannot be made as the meteorology was not the same for the measurement site and the model. These results are indicative however of the potential of CamCan to capture the tropical forest isoprene gradient.

The isoprene concetration at the top of the canopy reached maximum values of up to 50 ppb, which surpasses any observation made in any forest. Additionally, above canopy isoprene measurements were taken during aircraft flights in the OP3 campaign that was described in Section 1.7.1. These measurements were made at ~152m and report values of isoprene of 3.5 ppb (Jones et al., 2011) whereas in CamCan maximum concentrations predicted for 120 m are 2.2 ppb, which is comparable. This is further evidence that CamCan is predicting reasonable concentration values for the tropical forest. There is still some refinement of this model required and verification with a WISDOM type

experiment in the tropical forest would be able to verify and constrain the model results.

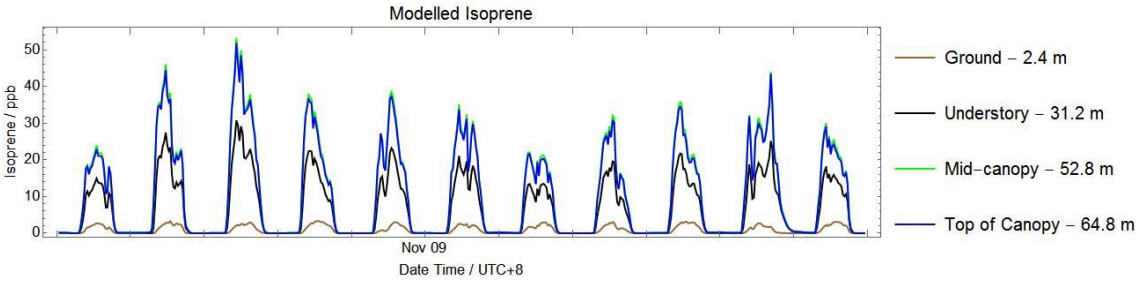

Figure 128 Modelled output of isoprene concentrations from CamCan at a tropical forest site over 11 days in November 2015

7.8 Simulating an oil palm plantation with CamCan

An adaption of the model is also run for an oil palm plantation. The meteorology and the coordinates were used as in Section 7.7. A number of factors were changed.

As the height of the oil palm plantation is ~20 m (Nadzir et al. in prep), the level distribution was changed so that the height of the canopy was 21.6 m and the level height was changed to 0.8 m, which puts the top of the model at 40 m. Based on this profile and an assumed constant LAI of 4.71 m^2m^{-2} (Corley, Hardon, & Tan, 1971) the estimated distribution of leaf area is shown in Figure 129 which shows a more symmetrical distribution than for the primary forest. The isoprene emission factor used is 31.9 $nmolm^{-2}s^{-1}$ (Misztal et al., 2011).

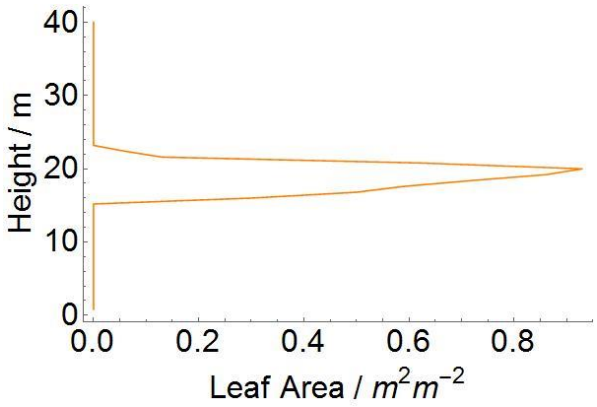

Figure 129 Leaf area distribution for the modelled hypothetical oil palm plantation as a function of model height showing a more symmetrical leaf profile than for the primary forest

Figure 130 shows the model output over 11 days in November 2015. The diurnal profile shape is the same as that for the primary forest (Figure 128) because the same meteorological data is used. The difference between the two outcomes is the magnitude

of the concentrations. The oil palm plantation concentration is much greater than that for the equivalent level in the primary forest. This can be due to two factors, one is the increased leaf area which provides a large emitting surface area which results in a larger emission, despite the lower emission factor. The other factor is that the canopy is smaller, so the isoprene emitted is being distributed into a smaller volume and hence this increases the observed concentrations.

The results shown in Section 3.5.4.3 show daily maxima of 20 – 30 ppb isoprene, which is the same order of magnitude as these modelled results. These results are similar in magnitude to those obtained by Misztal et al. (2011), indicating that this model produces reasonable output for the oil palm plantation.

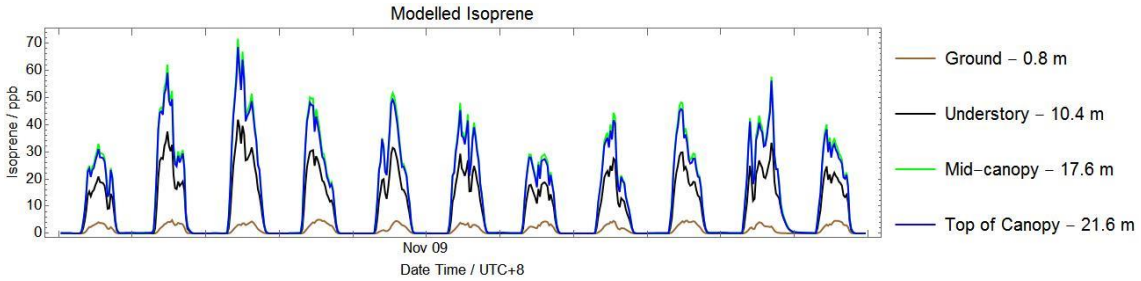

Figure 130 Model output for canopy vertical distribution of isoprene concentration in an oil palm plantation

The result of a higher concentration in the oil palm plantation is that more is transported to the free troposphere and less is lost to the forest canopy. This has repercussions for atmospheric chemistry of the troposphere, with a higher loading of isoprene the implication being that with increased NO_x from human activities, ozone concentrations may increase leading to a negative effect on human health.

7.9 Conclusions

This chapter concerned using the results from WISDOM to construct and constrain a new model called CamCan. In this section the key findings are summarised.

7.9.1 A new simple model, CamCan can describe isoprene in a canopy

The new CamCan model is described and characterised, with the chemical and physical processes involved described in detail. The model output is optimised for a select period and then run for the entire period where measurements were present. It is found that CamCan can simulate effectively the isoprene observed in a temperate forest canopy. CamCan is a simple model that can quickly and simply be adapted for new scenarios.

However, the model generally over-predicts isoprene and that this could be due to a number of processes that are not accounted for in the model. The processes that are concluded are the main causes of the over-estimation of isoprene in CamCan are:

- A lack of seasonal factor that reflects the changing emission factor of the leaves as a result of phenology and age
- Soil moisture and drought stress is not accounted for
- The wind direction and the horizontal fetch of the model is not represented as a variable source
- Over-simplified representation for diffusion and deposition

7.9.2 The FORCAsT model now represents isoprene in a canopy effectively

The FORCAsT model is run to compare with the observations and the output of CamCan. The benefit of FORCAsT is that it simulates a vast number of species so it is possible to gain an insight into the different interactions that occur besides isoprene, though this is not discussed here. FORCAsT now effectively simulates the absolute values of isoprene in a forest canopy and captures the vertical concentration gradient. Two factors that greatly improve the performance of FORCAsT were the inclusion of a new vertical transport scheme in the canopy and a better representation of deposition at the forest floor. FORCAsT overestimates isoprene to a lesser extent than CamCan. This is likely partially due to the expanded chemistry scheme, but as demonstrated in Section 7.3.5.3, the chemistry is in fact playing a minor role in determining the chemical distribution of isoprene. Another processes that may account for the improved simulation of isoprene is surface uptake of species.

7.9.3 Isoprene missions from Wytham Woods can be estimated using fluxes from CamCan

CamCan is used to calculate the flux of isoprene out of the forest. The values obtained from CamCan are comparable with those in the literature. Using this simulated flux, estimates for the annual emission of isoprene from Wytham Woods and the wider UK can be calculated. The total emission flux from Wytham Woods in 2018 was 2.0 Mg and from estimates of forest coverage and estimation, the emission of isoprene from the UK is calculated as 15.1 Gg. The emission from the UK represents 0.004 % of the 600 Tg global emission of isoprene.

In addition the model is run under a future climate scenario with a 1^{o}C increase in temperature to calculate fluxes under this scenario. The result shows an annual increase of 600 kg emitted from Wytham Woods, representing a 12.2% increase. This significant increase likely has implications for future climate and atmosphere.

CamCan is highly flexible and can be used to calculate fluxes for a number of scenarios which can be used to calculate emission potentials for forests.

7.9.4 Other types of forests can be investigated with CamCan

CamCan is run for a tropical forest and an oil palm plantation using representative meteorological data and forest parameters. It is concluded that this model can be used in a different forest setting and is easily customisable. The output from this model produces results that are comparable to the measurements that were made previously in primary tropical forests in 2015. A large factor for uncertainty is the calculation of an average emission factor for the trees and further research in this area should focus on improving this estimation.

8 Conclusions and Future Work

8.1 Introduction

Research into isoprene emission from plants and how it interacts in forests was limited by the availability of suitable instrumentation. Here a summary of the iDirac is presented, and how it is used to take measurements in tropical and temperate forests and to inform a modelling study.

This chapter provides a summary of the research conducted in this thesis. Forest isoprene emissions are described and how the iDirac is used to analyse isoprene distribution in a forest. This study provided an opportunity to evaluate the iDirac, a portable instrument developed in-house for the measurement of isoprene in challenging field conditions as described in Chapter 2. It provides some insight into under-sampled tropical forests in Southeast Asia as described in Chapter 3. The WISDOM campaign is described in Chapters 4–6 to gain insight into the vertical distribution of isoprene in the canopy as highlighted as a poorly understood aspect of isoprene research in Chapter 1. Finally, the model CamCan, described in Chapter 7, improves vertical modelling of isoprene in a canopy and provides a link between the WISDOM campaign and those measurements in the tropical areas. Here the model findings are summarised and the model performance is evaluated.

In brief, the aims of first part of this final chapter are to summarise:

1. the performance, strengths and weaknesses of the new iDirac instrument;
2. results from (i) tree emissions; (ii) primary and secondary forests and (iii) a palm oil plantation from preliminary measurements in Borneo;
3. the design and results from WISDOM, a five month field study in Wytham Woods;
4. the development of the new CamCan model to address specific questions related to isoprene measurements in a forest canopy; and
5. the performance of CamCan and the improvement of the established FORCAsT model in reproducing the WISDOM results, and the use of CamCan to simulate

isoprene in tropical forests.

In the second part, suggestions are presented for further work which are related to possible modifications to the iDirac, opportunities for new field measurements where the iDirac would enhance current instrumental capability; and potential modelling studies.

8.2 Summary of research findings

8.2.1 The iDirac as a new field instrument

This PhD thesis focussed on the development and deployment of the iDirac portable gas chromatograph. The need for such an instrument was evaluated and the construction of the iDirac is described in detail. Early deployments were also described using this instrument to measure isoprene.

The iDirac software and design is proven in field deployments. The iDirac is found to be suitable for use in field campaigns. The modular design of the instrument means that maintenance is straightforward and parts are accessible. Various features mean that adaptions and field repairs are straightforward, these include use of the open source Arduino language, the solderless connections and the intuitive design. Several design issues and potential developments are highlighted including the high number of electrical connections, the fragility of several transfer tubes and the sensitivity of the Raspberry Pi to unstable power supplies.

The iDirac is robust. The Pelicase exterior allows the instrument to be transported with ease and not suffer damage. The foam packing inside the instrument absorbs shock and prevents damage to the fragile components. Particularly in the tropical forest the instrument was transported very roughly to remote places and never suffered any damage. The protection afforded by the casing also prevents ingress of water, dust or wildlife. The Pelicase does however add most of the weight to the instrument.

The instrument has good sensitivity and low detection limit for isoprene. The typical limit of detection in the field for isoprene is 35-40 ppt. The iDirac is suited to deployment in forests where the night-time concentration drops to below detection limit or even zero and the iDirac is hence able to track the evening decay or early morning levels of isoprene which are key for understanding mixing and chemistry in the forest environment. In addition the instrument is capable of measuring isoprene in areas where it is important but is in very low concentration such as over remote oceans.

The instrument can run stably over long periods. The WISDOM campaign showed continuous operation for five months running autonomously using a solar power supply. Issues arose from the gradually decreasing sensitivity of the absorbent trap and the performance of the internal pump. These result in a small reduction in the measurement quality.

8.2.2 Isoprene in a tropical forest

The deployment of the iDirac in a tropical forest led to several conclusions regarding the emission of isoprene in this environment which are presented and discussed in this research. The experimental technique utilised in this environment has the potential for greater improvement and refinement.

Land use change in Borneo has a large effect on the atmospheric abundance of isoprene. The day-time concentration of isoprene is generally highest above the canopy in the oil palm plantations, with peak isoprene concentration measured of 35 ppb and lowest at the forest floor in the primary forest with daily maximum of 3.5 ppb. The implication for such observation is that the atmospheric chemistry will change as the land is converted to oil palm and have repercussions on human health as ozone is produced, particularly when in proximity to large urban centres.

Land-use change in Borneo influences the variation of isoprene at the forest floor. The variation of the isoprene concentrations are highest in disturbed forest such as the secondary forest on the periphery of the oil palm plantation. The least variation is observed in the primary forest due to the dense tree canopy which likely slows the transport of isoprene to the forest floor.

A single inlet limits understanding of the entire forest. The research from the primary forest highlights questions about the distribution of isoprene through a canopy and how a forest can be sampled with one inlet. One inlet is not enough and measurements made at the forest floor are not representative of that forest.

There is large variation between individual branches isoprene emission factors. In total the isoprene emission factor of 173 branches, 162 individual trees and 80 species are recorded. There is large variation in the isoprene emission factors measured from different branches. Several measured species are very strong emitters and some did not emit any isoprene. Many of these tree species had not been previously measured. The tree species at the secondary forest have a higher emission factor than at the primary forest sites. The

experimental technique and the many assumptions used to calculate these emission factors incurs a large uncertainty on the values.

8.2.3 Conclusions on canopy isoprene from WISDOM

The WISDOM campaign in 2018 was successful in collected data on isoprene concentration across the summer and a range of other parameters. This has allowed detailed analysis of the vertical forest isoprene in a temperate forest. The data revealed some key relationships of isoprene with the forest and the meteorology.

Isoprene strongly correlates with temperature but weakly with light. Isoprene concentration visually showed a strong correlation with temperature and is depended on light, but shows a weak correlation. The implication of this is that as the climate warms and temperature extremes are more frequent the isoprene emission will increase.

The vertical gradient of isoprene strongly correlates with the top-of-canopy PAR. The light intensity at the top of the canopy, through localised heating and the creation of a temperature difference between the top of the canopy and the ground is the main determining factor of the mixing. There is a strong observed correlation of the top of the canopy PAR and the difference in temperature between the top and bottom of the forest.

The Wytham trees were under heat and drought stress during the 2018 heatwave. The forest experienced conditions that induced a heightened isoprene response both as a response to temperature and as a response to low soil water. This heatwave response is not well represented by the Guenther equations for isoprene emission which only represents isoprene under ‘normal’ conditions. The implication of these findings have repercussions for future climate, where heightened extreme weather events such as heatwaves are more likely to occur.

The Wytham trees did not get damaged during the 2018 heatwave. Though an extreme and exceptional weather event, the 2018 heatwave did not cause the *Q. robur* individuals to experience visible damage or wilting. This is likely due to the deep and broad rooting system of the trees. The minimum soil moisture recorded in the summer was 0.161 m^3m^{-3} on the 20th July and the wilting point used in MEGAN is 0.171 m^3m^{-3}. This indicates that that threshold was crossed but that there was no visible wilting which is likely dependant on the soil type and specific conditions at Wytham. The tree was highly stressed but a ‘drop’ of isoprene was not observed. The reason for this is not known and is worthy of future study.

The experimental design is suitable for investigating the canopy isoprene gradient. In general the design of the WISDOM experiment is appropriate for investigating the isoprene from the forest in full. The experiment allows an analysis of the isoprene both as a function of time and as a function of height, allowing a full analysis of the factors affecting the vertical gradient of the forest.

8.2.4 Conclusions from modelling WISDOM

The WISDOM experiment served as an ideal dataset for developing a 1D canopy model of the forest called CamCan, which improves on existing models to simulate isoprene in a canopy. The presence of the vertically distributed inlets allowed verification of CamCan and the FORCAsT model, and allowed the model results to be constrained to calculate isoprene emission into the atmosphere.

CamCan can calculate the vertical distribution of isoprene in a temperate forest canopy. The processes described in CamCan adequately describe the system measured and closely recreate the observations. The approximations and assumptions put forward in CamCan are appropriate for this system and isoprene can be adequately predicted for the region sampled and for other time periods. This is an improvement on existing models, which had failed to capture the vertical profile. CamCan has also suggested that horizontal advection has a strong effect on isoprene concentration and that vertical transport of isoprene may not be as relevant higher in the PBL.

FORCAsT has been improved to provide a better simulation of forest isoprene. Using CamCan, the FORCAsT model has been improved to reconstruct the forest isoprene gradient and concentrations effectively, showing great improvement on past performance. A number of processes in FORCAsT are better represented than in CamCan such as deposition and chemistry that allow a better calculation of isoprene concentrations.

Some factors are not well represented in either CamCan or FORCAsT. Differences for both models to the measurements are due to various factors that are absent from the model. Varying sources from different wind directions likely change the source term. The absence of any term that accounts for soil moisture means tree stress is not factored into the model. The lack of a factor for leaf maturity or aging, reflecting a changing emission factor fails to capture the seasonality of the measurements. These highlight a clear route for further developments for either model.

CamCan predicts a flux of isoprene from Wytham of 0.04 kgha^{-1}d^{-1}. The flux from the forest can be calculated with CamCan. Values obtained from Wytham are comparable to other similar forests. With some assumptions, the annual isoprene emission from the UK is estimated at 22.3 Gg which represents 0.004% of global isoprene emission estimates. 17.4% of the flux to the troposphere is deposited to the forest floor, representing a large loss of isoprene that drives a strong vertical gradient.

CamCan can predict isoprene in a tropical forests. It is demonstrated that with simple alterations, CamCan produces feasible results for tropical forests. A simulation for the primary forest produces comparable concentrations to measurements taken at the forest floor and concentrations above the canopy in the literature. A CamCan simulation for the oil palm plantation produces concentrations that are similar to measurements of isoprene concentration at the equivalent site and are generally higher than those is the primary forest.

8.3 Future recommendations

With the development of the iDirac and the measurements that have been made in the course of this thesis, it is apparent that there is still failure to understand many of the processes that occur in the natural environment. The fieldwork and an analysis of the measurements have raised new questions about isoprene in a forest and with the iDirac and the CamCan model, there are now these new tools to address them. These potential future research areas are discussed here.

8.3.1 Further instrument development

The iDirac has proven itself to be a valuable tool for understanding isoprene patterns in forest environments. The instrument was conceived in 2014 and has since been developed to become fully functioning and has already been used in several large field campaigns. However, the iDirac is still a new instrument and summarised here are five instrumental upgrades and developments that could potentially further the usefulness of the iDirac.

Reduce dependence on carrier gas. The instrument timeframe is limited by nitrogen which can be both impractical and is limited by volume. The use of air would allow the deployment of the instrument indefinitely, save space and reduce the safety risk of using a pressurised container. The absorbent in the columns is sensitive to oxygen, hence may need changed. It would be possible to run the instrument oven at a lower temperature to reduce damage and save power.

Wireless data uploading. Manually downloading the data can be time consuming or difficult, if the iDirac is located in an inaccessible or remote location. The Raspberry Pi can connect to a Wi-Fi network and with 4G coverage, the apparatus could access the internet and automatically upload files to a server which can be remotely accessed.

Dynamic volume sampling. The large changes in isoprene concentration through the day leads to inefficient sampling of either too large or too small a sample volume. Currently a single volume is used such that the appropriate sensitivity is achieved for a given environment. A proposed dynamic volume system would increase the frequency of measurement and capture lower concentrations. If a smaller volume was used for the higher concentrations, the pump would sample for a shorter time to reach the desired volume and save time and power. In the inverse situation a low concentration requires a large sampling volume for increased sensitivity. This would be possible with a peak finding function in the in-built Python script run from the Raspberry Pi and resetting the volume for the next run based on peak height.

Improve absorbent trap lifetime. The gradual desensitising of the absorbent trap in a problem in a long deployment. A solution is to use a multi-absorbent trap to sacrificially absorb different VOCs and prevent the poisoning of the absorbent for isoprene.

Adapt the iDirac to measure other species. For forest studies monoterpenes would be a valuable addition, but any particular species could be measured. To achieve such an enhancement, different absorbents and different column packing materials would need to be investigated.

8.3.2 Further measurement

This thesis has brought about many new questions about the forest canopy, how the isoprene is distributed and how the forest responds to a heatwave. In general, how specific factors affect isoprene emission could be investigated further and there is the potential for controlled chamber studies on this.

8.3.2.1 WISDOM2

The WISDOM campaign was the first such experiment of its type. Carried out in 2018, it used the new iDirac instrument to ask simple questions of the forest canopy. Having been the first experiment of its kind it raised many questions of the forest canopy.

Capture the bud-burst. Measurements should begin earlier in the season to capture the periods before and during the bud burst period. Literature suggests that isoprene does not

come immediately with bud burst and there is a lag. It would be interesting to demonstrate this at Wytham and attempt to quantify this time-lag and also analyse how rapidly the concentration increases at the start of the season.

Horizontal wind across the forest. Another question that has arisen from the WISDOM campaign and the CamCan model is that of horizontal isoprene transport. CamCan2D has offered the possibility that the isoprene measured is a cumulative concentration from advection across a forest. With a set-up similar to WISDOM, but with the inlets orientated horizontally and comprehensive wind data, an understanding could be sought of how the isoprene is transported across the canopy. The inlets could also be strategically placed to investigate if the location in the forest determines the concentration, for example on the edge of the forest versus in the centre of the forest. The effect of topography and aspect of the forest has also not been investigated and may lead to differing forest emission profiles.

8.3.2.2 Plant response to stress

It is inherently difficult to study such conditions as high temperatures or low soil moisture in a natural field site because it relies on the chance occurrence of an extreme event of sufficient scale to test certain hypotheses. Here an investigation is proposed of isoprene emission from plant individuals in a chamber study. Under controlled conditions, the soil moisture could be lowered systematically and the isoprene monitored. In this study it would be possible to test the soil moisture against the isoprene without the influence of temperature or light intensity. In a similar experiment, testing different temperatures at each level of soil moisture might also allow the quantification of the response to stress which could be factored into CamCan.

8.3.2.3 Forest chemistry

An increased suite of measurements could also lend new insights into the forest dynamics, measurements of ozone and NO_x would expand understanding of the forest chemistry and the effect that anthropogenic pollution is having on the forest. In particular the ozone concentration measurements would allow the calculation of a more accurate concentration of OH in the air, key for the reactions with isoprene.

An investigation of the oxidised species of isoprene may also lend insight into the forest canopy and the oxidising capacity for the canopy air mass. With NO_x, the chemistry of the formation of other important species such as peroxyacetyl nitrate could be investigated. The implication of this on the health of the trees, or the isoprene emission

rate could be assessed.

8.3.2.4 Tropical forests and other types of forest

With the framework for an experiment such as WISDOM, there are many possibilities for new experiments using the iDirac, or multiple iDiracs, in such a way. Across different biomes there are many different types of forests and each has a unique VOC emission 'footprint'. WISDOM-type experiments are able to lend insight to the dynamics of isoprene, or even other VOCs, emission into the atmosphere.

WISDOM in tropical forests. The measurements described in this thesis from the tropical forests give a clue about the vertical isoprene gradient, and suggest that the measurements are not representative of the whole forest. A proposed experiment is to set up a WISDOM-type installation in a primary tropical forest. Using this set-up it would be possible to verify the model results discussed in Chapter 7 and constrain the model further. It would then be possible then to predict the flux of isoprene from the top of the forests into the free boundary layer and be able to constrain the global emission models that highlight the tropics as an important isoprene emission area. The isoprene profile from oil palm plantations could also be investigated with a WISDOM-type experiment. This experiment would be able to constrain those model runs performed in Section 7.8 and also calculate flux from the forest canopy.

How is the vertical gradient affected by land-use change? The forests of Borneo are changing and it is expected that the isoprene profile will also change. Using the framework of WISDOM it may be possible to examine how the isoprene is distributed in disturbed forests and verify the conclusions from the isoprene measurements in the secondary forest.

Set-up in a coniferous forest. A similar set-up could study the emission of monoterpenes from a coniferous forest. A different emission mechanism for these species would likely lead to a differing tree response and daily profile and likely lead to a different vertical concentration gradient. The leaf distribution of a coniferous forest is also markedly different from a broadleaved forest. An experiment such as WISDOM, with an iDirac modified to measure monoterpenes, would lead to a greater understanding of this important type of forest.

8.3.3 Modelling future work

There are some clear areas of improvement for CamCan that are focussed on developing some of the assumptions used in constructing the model.

More developed chemistry scheme. The current assumption for OH concentration and reaction with isoprene is vastly over simplified, and even the addition of a couple of other reactions such as oxidation by O_3 or NO_3 could improve simulations, particularly of the night-time values.

Improve treatment of heatwaves. For both CamCan and FORCAsT, it is clear that the heatwave period of stress is not represented and that this is primarily due to the Guenther emission rate equation not well representing exceptional stress. Three developments have been proposed that aim to improve this performance:

- A seasonal factor would account for the changes in emission factor based on the age of the leaves and decline later in the season, such a term could be a scaling factor for the emission factor.
- A term for the soil moisture could take a form similar to those in MEGAN, with a 'stress threshold' and a shut-off point. From the measurements, this stress value has been highlighted at ~0.2 m^3m^{-3}.
- It is proposed that a wind direction-dependant source term would improve results. This would require further knowledge of the *Q. robur* distribution at Wytham and the fetch of the air masses that reach the measurement site.

Model of horizontal air movement. From preliminary calculations, there is evidence that the isoprene observed is likely due to horizontal advection and that the drop-off of isoprene in the evening may be a result of advection from beyond the boundary of the forest. Hence it would be possible to refine this model with this in mind and simulate different sizes of forests or different distributions of emitting trees. There is also the possibility of constraining such a 2D model with a series of experiments located in different portions of Wytham Woods. Observations could be made of the evening drop off of isoprene and whether this was different as a result of low-isoprene air arriving from the edge of the forest. A very large forest, which could represent an infinite forest, would provide an interesting comparison with Wytham and the evening decline of isoprene concentration could reveal if the horizontal transport is important.

8.4 Closing remarks

The natural environment is a complex place and this study has investigated only a small part of the complete picture. We are only starting to understand the role of VOCs in the environment and how they are used in defence of stress, as signalling factors and a multitude of other functionalities. How isoprene distributes in a forest canopy is key both to its ecosystem function and also to its effect on the atmosphere. By beginning to understand the emission of isoprene and how the trees react to environmental stimuli a small piece of this puzzle can be put in place.

The work in this thesis has demonstrated the usefulness of small portable gas chromatographs for measurement of isoprene. Much of the environmental interactions of isoprene are poorly understood and are limited by available instrumentation. Several decades of measurement data using conventional bench-top instruments have limited understanding to accessible and convenient locations. With a new instrument such as the iDirac the door is opened to new possibilities. It is now possible to take measurements in challenging and inaccessible places where key processes affecting the emission of isoprene are taking place. These new opportunities will allow us to ask new questions, gain a new understanding and progress our appreciation of this important atmospheric constituent.

9 REFERENCES

Achakulwisut, P., Mickley, L. J., Murray, L. T., Tai, A. P. K., Kaplan, J. O., & Alexander, B. (2015). Uncertainties in isoprene photochemistry and emissions : implications for the oxidative capacity of past and present, 7977–7998. http://doi.org/10.5194/acp-15-7977-2015

Allen, N. D. C., Worton, D. R., Brewer, P. J., Pascale, C., & Niederhauser, B. (2018). The importance of cylinder passivation for preparation and long-term stability of multicomponent monoterpene primary reference materials, 6429–6438.

Andreae, M. O. (1997). Atmospheric Aerosols: Biogeochemical Sources and Role in Atmospheric Chemistry. *Science*, *276*(5315), 1052–1058. http://doi.org/10.1126/science.276.5315.1052

Andreae, M. O., Artaxo, P., Brandao, C., Carswell, F. E., Ciccioli, P., Da Costa, A. L., … Waterloo, M. J. (2002). Biogeochemical cycling of carbon, water, energy, trace gases, and aerosols in Amazonia: The LBA-EUSTACH experiments. *Journal of Geophysical Research D: Atmospheres*, *107*(20). http://doi.org/10.1029/2001JD000524

Aneja, V., Blunden, J., Claiborn, C., Rogers, H., Barnes, I., & Rudzinski, K. (2006). Dynamic Chamber System to Measure Gaseous Compounds Emissions and Atmospheric-Biospheric Interactions. *Environmental Simulation Chambers: Application to Atmospheric Chemical Processes*, *62*, 97–109. Retrieved from http://dx.doi.org/10.1007/1-4020-4232-9_7

Archibald, A. T., Cooke, M. C., Utembe, S. R., Shallcross, D. E., Derwent, R. G., & Jenkin, M. E. (2010). Impacts of mechanistic changes on HOx formation and recycling in the oxidation of isoprene. *Atmospheric Chemistry and Physics*, *10*(17), 8097–8118. http://doi.org/10.5194/acp-10-8097-2010

Ashworth, K., Chung, S. H., Griffin, R. J., Chen, J., Forkel, R., Bryan, A. M., & Steiner, A. L. (2015). FORest Canopy Atmosphere Transfer (FORCAsT) 1.0: A 1-D model of biosphere-atmosphere chemical exchange. *Geoscientific Model Development*, *8*(11), 3765–3784. http://doi.org/10.5194/gmd-8-3765-2015

Bäck, J., Aaltonen, H., Hellén, H., Kajos, M. K., Patokoski, J., Taipale, R., … Heinonsalo,

J. (2010). Variable emissions of microbial volatile organic compounds (MVOCs) from root-associated fungi isolated from Scots pine. *Atmospheric Environment*, *44*(30), 3651–3659. http://doi.org/10.1016/j.atmosenv.2010.06.042

Baldocchi, D. (1988). A multi-layer model for estimating sulfur dioxide deposition to a deciduous oak forest canopy. *Atmospheric Environment*, *22*(5), 869–884.

Baldocchi, D. (1995). The fluxes and air chemistry of isoprene above a deciduous hardwood forest. *Philosophical Transactions - Royal Society of London, A*, *351*(1696), 279–296. http://doi.org/10.1098/rsta.1995.0034

Bamberger, I., Ruehr, N. K., Schmitt, M., Gast, A., Wohlfahrt, G., & Arneth, A. (2017). Isoprene emission and photosynthesis during heatwaves and drought in black locust. *Biogeosciences*, *14*, 3649–3667. http://doi.org/10.5194/bg-14-3649-2017

Batterman, S., Metts, T., Kalliokoski, P., & Barnett, E. (2002). Low-flow active and passive sampling of VOCs using thermal desorption tubes: theory and application at an offset printing facility. *Journal of Environmental Monitoring*, *4*(3), 361–370. http://doi.org/10.1039/b203289a

Beer, C., Reichstein, M., Tomelleri, E., Ciais, P., Jung, M., Carvalhais, N., … Papale, D. (2010). Terrestrial Gross Carbon Dioxide Uptake: Global Distribution and Covariation with Climate. *Science*, *329*(August), 834–839.

Bieri, G., Burger, F., Heilbronner, E., & Maier, J. P. (1977). Valence Ionization Energies of Hydrocarbons. *Helvetica Chimica Acta*, *60*(7), 2213–2233. http://doi.org/10.1002/hlca.19770600714

Blackadar, A. (1962). The Vertical Distribution of Wind and Turbulent Exchange in a Neutral Atmosphere. *Journal of Geophysical Research*, *67*(8), 3095–3102.

Both, S., Riutta, T., Paine, C. E. T., Elias, D. M. O., Cruz, R. S., Jain, A., … Burslem, D. F. R. P. (2019). Logging and soil nutrients independently explain plant trait expression in tropical forests. *New Phytologist*, *221*, 1853–1865. http://doi.org/10.1111/nph.15444

Breitmaier, E. (2006). Terpenes: flavours, fragrances, pharmaca, pheromons, 711–713. http://doi.org/10.1021/np078143n

Brilli, F., Barta, C., Fortunati, A., Lerdau, M., Loreto, F., & Centritto, M. (2007). Response of isoprene emission and carbon metabolism to drought in white poplar (Populus alba) saplings. *New Phytologist*, *175*(2), 244–254. http://doi.org/10.1111/j.1469-8137.2007.02094.x

Butt, N., Campbell, G., Malhi, Y., Morecroft, M., Fenn, K., Thomas, M., … Hill, R. (2009). Initial Results from Establishment of a Long-term Broadleaf Monitoring Plot at Wytham Woods , Oxford , UK. *University of Oxford*.

Carlton, A. G., Wiedinmyer, C., & Kroll, J. H. (2009). A review of Secondary Organic Aerosol (SOA) formation from isoprene. *Atmospheric Chemistry and Physics*, *9*(14), 4987–5005. http://doi.org/10.5194/acp-9-4987-2009

Chaves, J. E., Rueda-romero, P., Kirst, H., & Melis, A. (2017). Engineering Isoprene Synthase Expression and Activity in Cyanobacteria. *ACS Synthetic Biology*, *6*, 2281−2292. http://doi.org/10.1021/acssynbio.7b00214

Chen, J., & Ã, R. J. G. (2005). Modeling secondary organic aerosol formation from oxidation of a -pinene , b -pinene , and d -limonene. *Atmospheric Environment*, *39*, 7731–7744. http://doi.org/10.1016/j.atmosenv.2005.05.049

Christensen, L. E., Okumura, M., Sander, S. P., Salawitch, R. J., Toon, G. C., Sen, B., … Jucks, K. W. (2002). Kinetics of HO2 + HO2 - H2O2 + O2 : Implications for Stratospheric H2O2. *Geophysical Research Letters*, *29*(9), 2–5.

Claeys, M. (2004). Formation of Secondary Organic Aerosols Through Photooxidation of Isoprene. *Science*, *303*(5661), 1173–1176. http://doi.org/10.1126/science.1092805

Cleveland, C. C., & Yavitt, B. (1997). Consumption of atmospheric isoprene in soil. *Geophysical Research Letters*, *24*(19), 2379–2382. http://doi.org/10.1029/97GL02451

Corley, R. H. V., Hardon, J. J., & Tan, G. Y. (1971). Analysis of growth of the oil palm (Elaeis guineensisJacq.) I. Estimation of growth parameters and application in breeding. *Euphytica*, *20*(2), 307–315. http://doi.org/10.1007/BF00056093

Darer, A. I., Cole-Filipiak, N. C., O'Connor, A. E., & Elrod, M. J. (2011). Formation and stability of atmospherically relevant isoprene-derived organosulfates and organonitrates. *Environmental Science and Technology*, *45*(5), 1895–1902. http://doi.org/10.1021/es103797z

Deardorff, J. W. (1972). Parameterization of the Planetary Boundary layer for Use in General Circulation Models 1. *Monthly Weather Review*, *100*(2), 93–106. http://doi.org/10.1175/1520-0493(1972)100<0093:potpbl>2.3.co;2

Edney, E. O., Jaoui, M., Offenberg, J. H., Kleindienst, T. E., Lewandowski, M., Wang, W., & Claeys, M. (2005). Formation of 2-methyl tetrols and 2-methylglyceric acid in secondary organic aerosol from laboratory irradiated isoprene/NOX/SO2/air mixtures

and their detection in ambient PM2.5 samples collected in the eastern United States. *Atmospheric Environment*, *39*(29), 5281–5289. http://doi.org/10.1016/j.atmosenv.2005.05.031

Edwards, P. M., Evans, M. J., Furneaux, K. L., Hopkins, J., Ingham, T., Jones, C., … Heard, D. E. (2013). OH reactivity in a South East Asian tropical rainforest during the oxidant and particle photochemical processes (OP3) project. *Atmos. Chem. Phys*, *13*(18), 9497–9514. http://doi.org/10.5194/acp-13-9497-2013

Ehn, M., Thornton, J. A., Kleist, E., Sipilä, M., Junninen, H., Pullinen, I., … Mentel, T. F. (2014). A large source of low-volatility secondary organic aerosol. *Nature*, *506*(7489), 476–479. http://doi.org/10.1038/nature13032

Ewers, R. M., Didham, R. K., Fahrig, L., Ferraz, G., Hector, a., Holt, R. D., … Turner, E. C. (2011). A large-scale forest fragmentation experiment: the Stability of Altered Forest Ecosystems Project. *Philosophical Transactions of the Royal Society B: Biological Sciences*, *366*(1582), 3292–3302. http://doi.org/10.1098/rstb.2011.0049

Fall, R., & Monson, R. K. (1992). Isoprene Emission Rate and Intercellular Isoprene Concentration as Influenced by Stomatal Distribution and Conductance. *Plant Physiology*, *100*(2), 987–992. http://doi.org/10.1104/pp.100.2.987

Fares, S., Barta, C., Brilli, F., Centritto, M., Ederli, L., Ferranti, F., … Loreto, F. (2006). Impact of high ozone on isoprene emission, photosynthesis and histology of developing Populus alba leaves directly or indirectly exposed to the pollutant. *Physiologia Plantarum*, *128*(3), 456–465. http://doi.org/10.1111/j.1399-3054.2006.00750.x

Ferreira, J., Reeves, C. E., Murphy, J. G., Parker, D. J., & Oram, D. E. (2010). Isoprene emissions modelling for West Africa : MEGAN model evaluation and sensitivity analysis. *Atmos. Chem. Phys*, *10*, 8453–8467. http://doi.org/10.5194/acp-10-8453-2010

Fiala, B., Grunsky, H., Maschwitz, U., & Linsenmair, K. E. (1994). Diversity of ant-plant interactions : protective efficacy in Macaranga species with different degrees of ant association. *Oecologia*, *97*, 186–192.

Forestry Commission. (2018). Forestry Statistics 2018 - Forest Research, (September). Retrieved from https://www.forestresearch.gov.uk/tools-and-resources/statistics/forestry-statistics/forestry-statistics-2018/

Forkel, R., Klemm, O., Graus, M., Rappenglu, B., Stockwell, W. R., Grabmer, W., … Steinbrecher, R. (2006). Trace gas exchange and gas phase chemistry in a Norway spruce

forest : A study with a coupled 1-dimensional canopy atmospheric chemistry emission model. *Atmospheric Environment*, *40*, 28–42. http://doi.org/10.1016/j.atmosenv.2005.11.070

Fowler, D., Nemitz, E., Misztal, P., Di Marco, C., Skiba, U., Ryder, J., … Hewitt, C. N. (2011). Effects of land use on surface–atmosphere exchanges of trace gases and energy in Borneo: comparing fluxes over oil palm plantations and a rainforest. *Philosophical Transactions of the Royal Society of London. Series B, Biological Sciences*, *366*, 3196–3209. http://doi.org/10.1098/rstb.2011.0055

Fowler, D., Pilegaard, K., Sutton, M. A., Ambus, P., Raivonen, M., Duyzer, J., … Erisman, J. W. (2009). Atmospheric composition change: Ecosystems-Atmosphere interactions. *Atmospheric Environment*. http://doi.org/10.1016/j.atmosenv.2009.07.068

Funk, J. L., Mak, J. E., & Lerdau, M. T. (2004). Stress-induced changes in carbon sources for isoprene production in Populus deltoides. *Plant, Cell and Environment*, *27*(6), 747–755. http://doi.org/10.1111/j.1365-3040.2004.01177.x

Gabey, A. M., Gallagher, M. W., Whitehead, J., Dorsey, J. R., Kaye, P. H., & Stanley, W. R. (2010). Measurements and comparison of primary biological aerosol above and below a tropical forest canopy using a dual channel fluorescence spectrometer. *Atmospheric Chemistry and Physics*, *10*(10), 4453–4466. http://doi.org/10.5194/acp-10-4453-2010

Gao, W., Wesely, M. L., & Doskey, P. V. (1993). Numerical Modeling of the Turbulent Diffusion and Chemistry of NOx , 03 , Isoprene , and Other Reactive Trace Gases in and Above a Forest Canopy. *Journal of Geophysical Research*, *98*(10), 18339–18353.

Gebhardt, S., Colomb, A., Hofmann, R., Williams, J., & Lelieveld, J. (2008). Halogenated organic species over the tropical South American rainforest. *Atmos. Chem. Phys*, *8*, 3185–3197. http://doi.org/10.5194/acp-8-3185-2008

Geiger, H., Barnes, I., Bejan, I., Benter, T., & Spittler, M. (2003). The troposhperic degredation of isoprene: an updated module for the regional atmospheric chemistry mechanism. *Atmos. Environ.*, *37*, 1503–1519.

Gelmont, D., Mead, J. F., & Stein, R. A. (1981). Isoprene - The Main Hydrocarbon in Human Breath. *Biochemical and Biophysical Research Communications*, *99*(4), 1456–1460.

Geron, C., Guenther, a, Greenberg, J., Loescher, H. W., Clark, D., & Baker, B. (2002).

Biogenic volatile organic compound emissions from a lowland tropical wet forest in Costa Rica. *Atmospheric Environment*, *36*(23), 3793–3802. http://doi.org/Pii S1352-2310(02)00301-1\rDoi 10.1016/S1352-2310(02)00301-1

Givnish, T. J. (1988). Adaption to Sun and Shade: A Whole-plant Perspective. *Journal of Plant Physiology*, *15*, 63–92.

Gostlow, B., Robinson, A. D., Harris, N. R. P., O'Brien, L. M., Oram, D. E., Mills, G. P., … Pyle, J. A. (2010). μdirac: An autonomous instrument for halocarbon measurements. *Atmospheric Measurement Techniques*, *3*(2), 507–521. http://doi.org/10.5194/amt-3-507-2010

Griffin, R. J., Dabdub, D., & Seinfeld, J. H. (2002). Secondary organic aerosol 1 . Atmospheric chemical mechanism for production of molecular constituents. *Journal of Geophysical Research*, *107*(17), 4332. http://doi.org/10.1029/2001JD000541

Griffin, R. J., Dabdub, D., & Seinfeld, J. H. (2005). Development and initial evaluation of a dynamic species-resolved model for gas phase chemistry and size-resolved gas/particle partitioning associated with secondary organic aerosol formation. *Journal of Geophysical Research*, *110*, 1–16. http://doi.org/10.1029/2004JD005219

Guenther, a., Karl, T., Harley, P., Wiedinmyer, C., Palmer, P. I., & Geron, C. (2006). Estimates of global terrestrial isoprene emissions using MEGAN (Model of Emissions of Gases and Aerosols from Nature). *Atmospheric Chemistry and Physics*, *6*(11), 3181–3210. http://doi.org/10.5194/acpd-6-107-2006

Guenther, A. B., Jiang, X., Heald, C. L., Sakulyanontvittaya, T., Duhl, T., Emmons, L. K., & Wang, X. (2012). The model of emissions of gases and aerosols from nature version 2.1 (MEGAN2.1): An extended and updated framework for modeling biogenic emissions. *Geoscientific Model Development*, *5*(6), 1471–1492. http://doi.org/10.5194/gmd-5-1471-2012

Guenther, A., Nicholas, C., Fall, R., Klinger, L., Mckay, W. a, Scholes, B., … Zimmerman, P. (1995). A global model of natural volatile organic compound emissions. *Journal of Geophysical Research*, *100*(D5), 8873–8892. http://doi.org/10.1029/94JD02950

Guenther, A., Zimmerman, P. R., Harley, P. C., & Monson, R. K. (1993). Isoprene and Monoterpene Emission Rate Variability' Model Evaluations and Sensitivity Analyses. *Journal of Geophysical Research*, *98*(7), 12609–12617.

http://doi.org/10.1029/93JD00527

Hall, S. J., Matson, P. A., & Roth, P. M. (1996). NOx Emissions from Soil: Implications for Air Quality Modeling in Agricultural Regions. *Annual Review of Energy & the Environment*, *21*(1), 311. http://doi.org/10.1146/annurev.energy.21.1.311

Hansen, M. C., Stehman, S. V., & Potapov, P. V. (2010). Quantification of global gross forest cover loss. *Proceedings of the National Academy of Sciences*, *107*(19), 8650–8655. http://doi.org/10.1073/pnas.0912668107

Hardwick, S. R., Toumi, R., Pfeifer, M., Turner, E. C., Nilus, R., & Ewers, R. M. (2015). Agricultural and Forest Meteorology The relationship between leaf area index and microclimate in tropical forest and oil palm plantation : Forest disturbance drives changes in microclimate. *Agricultural and Forest Meteorology*, *201*, 187–195. http://doi.org/10.1016/j.agrformet.2014.11.010

Harley, P., Guenther, A., Li, G., Geng, F., Tie, X., & Cao, J. (2011). Effect of isoprene emissions from major forests on ozone formation in the city of Shanghai, China. *Atmospheric Chemistry and Physics*, *11*(20), 10449–10459. http://doi.org/10.5194/acp-11-10449-2011

Heard, D. E. (2006). Analytical Techniques for Atmospheric Measurement.

Helmig, D., Greenberg, J., Guenther, A., Zimmerman, P., & Geron, C. (2002). Volatile organic compounds and isoprene oxidation products at a temperate deciduous forest site. *Journal of Geophysical Research: Atmospheres*, *103*(D17), 22397–22414. http://doi.org/10.1029/98jd00969

Herbst, M., Rosier, P. T. W., Morecroft, M. D., & Gowing, D. J. (2008). Comparative measurements of transpiration and canopy conductance in two mixed deciduous woodlands differing in structure and species composition. *Tree Physiology*, *28*, 959–970.

Hewitt, C. N., Lee, J. D., MacKenzie, A. R., Barkley, M. P., Carslaw, N., Carver, G. D., … Yin, X. (2010). Overview: oxidant and particle photochemical processes above a south-east Asian tropical rainforest (the OP3 project): introduction, rationale, location characteristics and tools. *Atmospheric Chemistry and Physics*, *10*(1), 169–199. http://doi.org/10.5194/acp-10-169-2010

Hewitt, C. N., Mackenzie, A. R., Carlo, P. Di, Marco, C. F. Di, Dorsey, J. R., Evans, M., … Moller, S. J. (2009). Nitrogen management is essential to prevent tropical oil palm plantations from causing ground-level ozone pollution. *PNAS*, *106*(44), 18447–18451.

Hough, A. M. (1988). The calculation of photolysis rates for use in global modelling studies. Tech. rep. *UK Atomic Energy Authority, Harwell, Oxon., UK, 1988*.

IPCC. (2018). Global warming of 1.5oC: Summary for policymakers.

Ishii, H. T., Tanabe, S., Hiura, T., Hiroaki T. Ishii, Shin-ichi Tanabe, Tsutom Hiura, … Hiura, T. (2004). Canopy Structure , Stand Productivity , and Biodiversity of Temperate Forest Ecosystems. *Forest Science*, *50*(3), 342–355.

Jacob, D. J., & Wofsy, S. C. (1988). Photochemistry of biogenic emissions over the Amazon Forest. *Journal of Geophysical Research*, *93*(D2), 1477–1486. http://doi.org/10.1029/JD093iD02p01477

Jardine, K. J., Meyers, K., Abrell, L., Alves, E. G., Yanez Serrano, A. M., Kesselmeier, J., … Chambers, J. Q. (2013). Emissions of putative isoprene oxidation products from mango branches under abiotic stress. *Journal of Experimental Botany*, *64*(12), 3697–3709. http://doi.org/10.1093/jxb/ert202

Jiang, X., Guenther, A., Potosnak, M., Geron, C., Seco, R., Karl, T., … Pallardy, S. (2018). Isoprene emission response to drought and the impact on global atmospheric chemistry. *Atmospheric Environment*, *183*, 69–83. http://doi.org/10.1016/j.atmosenv.2018.01.026

Johan, E. T., Vlieg, H., Leemhuis, H., Spelberg, J. H. L., & Janssen, D. B. (2000). Characterization of the Gene Cluster Involved in Isoprene Metabolism in Rhodococcus sp. Strain AD45. *Journal of Bacteriology*, *182*(7), 1956–1963.

Jones, C. E., Hopkins, J. R., & Lewis, A. C. (2011). In situ measurements of isoprene and monoterpenes within a south-east Asian tropical rainforest. *Atmospheric Chemistry and Physics*, *11*(14), 6971–6984. http://doi.org/10.5194/acp-11-6971-2011

Josef, R., Staudt, M., Zimmer, I., Rambal, S., & Schnitzler, J. (2002). Seasonal pattern of monoterpene synthase activities in leaves of the evergreen tree Quercus ilex. *Physiologia Plantarum*, *114*, 354–360.

Karl, M., Brauers, T., Dorn, H., Holland, F., Komenda, M., Poppe, D., … Wahner, A. (2004). Kinetic Study of the OH-isoprene and O3-isoprene reaction in the atmosphere simulation chamber, SAPHIR. *Geophysical Research Letters*, *31*, 4–7. http://doi.org/10.1029/2003GL019189

Karl, T., Guenther, A., Yokelson, R. J., Greenberg, J., Potosnak, M., Blake, D. R., & Artaxo, P. (2007). The tropical forest and fire emissions experiment: Emission, chemistry,

and transport of biogenic volatile organic compounds in the lower atmosphere over Amazonia. *Journal of Geophysical Research*, *112*, 1–17. http://doi.org/10.1029/2007JD008539

Keenan, T., Niinemets, Ü., Sabate, S., Gracia, C., & Peñuelas, J. (2009). Process based inventory of isoprenoid emissions from European forests: Model comparisons, current knowledge and uncertainties. *Atmospheric Chemistry and Physics*, *9*(12), 4053–4076. http://doi.org/10.5194/acp-9-4053-2009

Keller, M., Goreau, T. ., Wofsy, S. ., Kaplan, W. ., & McElroy, M. . (1983). Production of Nitrous Oxide and Consumption of Methane by Forest Soils. *Geophysical Research Letters*, *10*(12), 1156–1159.

Keller, M., & Lerdau, M. (1999). Isoprene emission from tropical forest canopy leaves. *Global Biogeochemical Cycles*, *13*(1), 19–29.

Kleinman, L. I., Springston, S. R., Nunnermacker, L. J., Rudolph, J., Lee, Y.-N., Weinstein-Lloyd, J., … Daum, P. H. (2003). Correction to "Ozone production rate and hydrocarbon reactivity in 5 urban areas: A cause of high ozone concentration in Houston." *Geophysical Research Letters*, *30*(12), 1–4. http://doi.org/10.1029/2003gl017485

Knowlton, K., Rosenthal, J. E., Hogrefe, C., Lynn, B., Gaffin, S., Goldberg, R., … Rosenthal, E. (2004). Assessing Ozone-Related Health Impacts Under a Chaning Climate. *Environmental Health Perspectives*, *112*(15), 1557–1563. http://doi.org/10.1289/ehp.7l63

Koken, P. J. M., Piver, W. T., Ye, F., Elixhauser, A., Olsen, L. M., & Portier, C. J. (2003). Temperature, air pollution, and hospitalization for cardiovascular diseases among elderly people in Denver. *Environmental Health Perspectives*, *111*(10), 1312–1317. http://doi.org/10.1289/ehp.5957

Kuhn, U., Andreae, M. O., Ammann, C., Araújo, a. C., Brancaleoni, E., Ciccioli, P., … Kesselmeier, J. (2007). Isoprene and monoterpene fluxes from Central Amazonian rainforest inferred from tower-based and airborne measurements, and implications on the atmospheric chemistry and the local carbon budget. *Atmospheric Chemistry and Physics Discussions*, *7*(1), 641–708. http://doi.org/10.5194/acpd-7-641-2007

Kuzma, J., Nemecek-marshall, M., Pollock, W. H., & Fall, R. (1995). Microbiology Bacteria Produce the Volatile Hydrocarbon Isoprene. *Current Microbiology*, *30*, 97–103.

Lamb, B., Gay, D., Westberg, H., & Pierce, T. (1993). A biogenic hydrocarbon emission

inventory for the U.S.A using a simple forest canopy model. *Atmospheric Environment*, *27*(11), 1673–1690.

Lamb, B., Pierce, T., Baldocchi, D., Allwine, E., Dilts, S., Westberg, H., … Zimmerman, P. (1996). Evaluation of forest canopy models for estimating isoprene emissions. *Journal of Geophysical Research: Atmospheres*, *101*(D17), 22787–22797. http://doi.org/10.1029/96jd00056

Lamb, B., Westberg, H. A. L., & Quarles, T. I. M. (1985). Biogenic Hydrocarbon Emissions From Deciduous and Coniferous Trees in the United States. *Journal of Geophysical Research*, *90*, 2380–2390.

Langford, B., Cash, J., Acton, W. J. F., Valach, A. C., Hewitt, C. N., Fares, S., … Nemitz, E. (2017). Isoprene emission potentials from European oak forests derived from canopy flux measurements: An assessment of uncertainties and inter-algorithm variability. *Biogeosciences*, *14*, 5571–5594. http://doi.org/10.5194/bg-14-5571-2017

Langford, B., Misztal, P. K., Nemitz, E., Davison, B., Helfter, C., Pugh, T. A. M., … Hewitt, C. N. (2010). Fluxes and concentrations of volatile organic compounds from a South-East Asian tropical rainforest. *Atmospheric Chemistry and Physics*, *10*(17), 8391–8412. http://doi.org/10.5194/acp-10-8391-2010

Laothawornkitkul, J., Paul, N. D., Vickers, C. E., Possell, M., Mullineaux, P. M., Hewitt, C. N., & Taylor, J. E. (2008). The role of isoprene in insect herbivory. *Plant Signaling and Behavior*, *3*(12), 1141–1142. http://doi.org/10.4161/psb.3.12.7171

Laothawornkitkul, J., Paul, N. D., Vickers, C. E., Possell, M., Taylor, J. E., Mullineaux, P. M., & Hewitt, C. N. (2008). Isoprene emissions influence herbivore feeding decisions. *Plant, Cell and Environment*, *31*(10), 1410–1415. http://doi.org/10.1111/j.1365-3040.2008.01849.x

Latif, M. T., Dominick, D., Ahamad, F., Ahamad, N. S., Khan, M. F., Juneng, L., … Harris, N. R. P. (2016). Seasonal and long term variations of surface ozone concentrations in Malaysian Borneo. *Science of the Total Environment*, *573*, 494–504. http://doi.org/10.1016/j.scitotenv.2016.08.121

Lee, A., Goldstein, A. H., Kroll, J. H., Ng, N. L., Varutbangkul, V., Flagan, R. C., & Seinfeld, J. H. (2006). Gas-phase products and secondary aerosol yields from the photooxidation of 16 different terpenes. *Journal of Geophysical Research*, *111*, 1–25. http://doi.org/10.1029/2006JD007050

Lee, J., Cai, X., Lellmann, J., Dalponte, M., Malhi, Y., Butt, N., … Coomes, D. A. (2016). Individual Tree Species Classification from Airborne Multisensor Imagery Using Robust PCA. *IEEE Journal of Selected Topics in Applied Earth Observations and Remote Sensing*, *9*(6), 2554–2567. http://doi.org/10.1109/JSTARS.2016.2569408

Lee, J. D., Lewis, A. C., Monks, P. S., Jacob, M., Hamilton, J. F., Hopkins, J. R., … Jenkin, M. E. (2006). Ozone photochemistry and elevated isoprene during the UK heatwave of august 2003. *Atmospheric Environment*, *40*, 7598–7613. http://doi.org/10.1016/j.atmosenv.2006.06.057

Lehning, a, Zimmer, I., Steinbrecher, R., Bruggemann, N., & Schnitzler, J. P. (1999). Isoprene synthase activity and its relation to isoprene emission in Quercus robur L. leaves. *Plant Cell and Environment*, *22*(5), 495–504. http://doi.org/10.1046/j.1365-3040.1999.00425.x

Lehning, A., Zimmer, I., Steinbrecher, R., Brüggemann, N., & Schnitzler, J. P. (1999). Isoprene synthase activity and its relation to isoprene emission in Quercus robur L. leaves. *Plant, Cell and Environment*, *22*, 495–504. http://doi.org/10.1046/j.1365-3040.1999.00425.x

Lerdau, M., & Keller, M. (1997). Controls on isoprene emission from trees in a subtropical dry forest. *Plant, Cell and Environment*, *20*, 569–578.

Li, G., Guenther, A., Tie, X., Madronich, S., & Ying, Z. (2006). Biogenic emissions of isoprenoids and NO in China and comparison to anthropogenic emissions. *Science of The Total Environment*, *371*(1–3), 238–251. http://doi.org/10.1016/j.scitotenv.2006.06.025

Li, Z., Ratliff, E. A., & Sharkey, T. D. (2011). Effect of Temperature on Postillumination Isoprene Emission in Oak and Poplar. *Plant Physiology*, *155*, 1037–1046. http://doi.org/10.1104/pp.110.167551

Lieberman, D., Lieberman, M., Peralta, R., & Hartshorn, G. S. (2006). Tropical Forest Structure and Composition on a Large-Scale Altitudinal Gradient in Costa Rica. *The Journal of Ecology*, *84*(2), 137–152. http://doi.org/10.2307/2261350

Liu, Y., & Sander, S. P. (2015). Rate Constant for the OH + CO Reaction at Low Temperatures. *Journal of Physical Chemistry A*, *119*, 10060–10066. http://doi.org/10.1021/acs.jpca.5b07220

Llusia, J., Sardans, J., Niinemets, Ü., Owen, S. M., & Peñuelas, J. (2014). A screening study of leaf terpene emissions of 43 rainforest species in Danum Valley Conservation

Area (Borneo) and their relationships with chemical and morphological leaf traits. *Plant Biosystems*, *148*(2), 307–317. http://doi.org/10.1080/11263504.2013.770803

Loivamaki, M., Mumm, R., Dicke, M., & Schnitzler, J. (2008). Isoprene interferes with the attraction of bodyguards by herbaceous plants. *PNAS*, *105*(45), 17430–17435. http://doi.org/10.1073/pnas.0804488105

Loreto, F., & Velikova, V. (2001). Isoprene Produced by Leaves Protects the Photosynthetic Apparatus against Ozone Damage, Quenches Ozone Products, and Reduces Lipid Peroxidation of Cellular Membranes. *Plant Physiology*, *127*, 1781–1787. http://doi.org/10.1104/pp.010497.Sharkey

Lowman, M. D., & Schowalter, T. D. (2012). Plant science in forest canopies - the first 30 years of advances and challenges (1980-2010). *New Phytologist*, *194*(1), 12–27. http://doi.org/10.1111/j.1469-8137.2012.04076.x

Marais, E. A., Jacob, D. J., Guenther, A., Chance, K., Kurosu, T. P., Murphy, J. G., & Reeves, C. E. (2014). Improved model of isoprene emissions in Africa using Ozone Monitoring Instrument (OMI) satellite observations of formaldehyde : implications for oxidants and particulate matter. *Atmos. Chem. Phys*, *14*(2), 7693–7703. http://doi.org/10.5194/acp-14-7693-2014

Mauzerall, D. L., & Wang, X. (2001). Protecting Agricultural Crops from the Effects of Tropospheric Ozone Exposure: Reconciling Science and Standard Setting in the United States, Europe and Asia. *Annu. Rev. Energy Environ.*, (26), 237–268.

Mcfiggans, G., Mentel, T. F., Wildt, J., Pullinen, I., Kang, S., Kleist, E., … Kiendler-scharr, A. (2019). Secondary organic aerosol reduced by mixture of atmospheric vapours. *Nature*, 0–6. http://doi.org/10.1038/s41586-018-0871-y

Mcgenity, T. J., Crombie, A. T., & Murrell, J. C. (2018). Microbial cycling of isoprene , the most abundantly produced biological volatile organic compound on Earth. *The ISME Journal*, *12*, 931–941. http://doi.org/10.1038/s41396-018-0072-6

Met Office. (2018). Summer 2018. Retrieved from https://www.metoffice.gov.uk/climate/uk/interesting/summer_2018

Mihok, B., Paviour-Smith, K., Kirby, K. J., Elbourn, C. A., & Kenderes, K. (2009). Forty-year changes in the canopy and the understorey in Wytham Woods. *Forestry*, *82*(5), 515–527. http://doi.org/10.1093/forestry/cpp021

Miller, B., Oschinski, C., & Zimmer, W. (2001). First isolation of an isoprene synthase

gene from poplar and successful expression of the gene in Escherichia coli. *Planta*, *213*, 483–487. http://doi.org/10.1007/s004250100557

Misztal, P. K., Nemitz, E., Langford, B., Marco, C. F. Di, Phillips, G. J., Hewitt, C. N., & Mackenzie, A. R. (2011). Direct ecosystem fluxes of volatile organic compounds from oil palms in South-East Asia. *Atmospheric Chemistry and Physics*, *11*, 8995–9017. http://doi.org/10.5194/acp-11-8995-2011

Monson, R. K., Harley, P. C., Litvak, M. E., Wildermuth, M., Guenther, A. B., Zimmerman, P. R., & Fall, R. (1994). Environmental and developmental controls over the seasonal pattern of isoprene emission from aspen leaves. *Oecologia*, *99*(3–4), 260–270. http://doi.org/10.1007/BF00627738

Moore, R. M., Oram, D. E., & Penkett, S. A. (1994). Production of isoprene by marine phytoplankton cultures. *Geophysical Research Letters*, *21*(23), 2507–2510.

Moukhtar, S., Bessagnet, B., Rouil, L., & Simon, V. (2005). Monoterpene emissions from Beech (Fagus sylvatica) in a French forest and impact on secondary pollutants formation at regional scale. *Atmospheric Environment*, *39*, 3535–3547. http://doi.org/10.1016/j.atmosenv.2005.02.031

Muller, J. F. (1992). Geographical distribution and seasonal variation of surface emissions and deposition velocities of atmospheric trace gases. *Journal of Geophysical Research*, *97*(D4), 3787–3804. http://doi.org/10.1029/91JD02757

Murphy, J. G., Oram, D. E., & Reeves, C. E. (2010). Measurements of volatile organic compounds over West Africa. *Atmos*, *10*, 5281–5294. http://doi.org/10.5194/acp-10-5281-2010

Nadzir, M. S. M., Cain, M., Robinson, A. D., Bolas, C., Harris, N. R. P., Parnikoza, I., … Noor, A. Y. M. (2019). Isoprene hotspots at the Western Coast of Antarctic Peninsula during MASEC′16. *Polar Science*. http://doi.org/10.1016/j.polar.2018.12.006

Nadzir, M. S. M., Harris, N. R., Bolas, C., Bran, S. H., Macatangay, R., Ooi, C. G., … Bakar, M. A. A. (n.d.). Driving factors for isoprene chemistry over an oil palm plantation in Malaysia. *In Preparation*.

Ng, N. L., Chhabra, P. S., Chan, A. W. H., Surratt, J. D., Kroll, J. H., Kwan, A. J., … Wennberg, P. O. (2007). Effect of NO x level on secondary organic aerosol (SOA) formation from the photooxidation of terpenes. *Atmospheric Chemistry and Physics*, *7*, 5159–5174.

Noe, S. M., Peñuelas, J., & Niinemets, Ü. (2008). Monoterpene emissions from ornamental trees in urban areas: A case study of Barcelona, Spain. *Plant Biology*, *10*, 163–169. http://doi.org/10.1111/j.1438-8677.2007.00014.x

Noelscher, A. C., Yan˜ez-Serrano, A. M., Wolff, S., Carioca de Araujo, A., Lavric, J. V., Kesselmeier, J., Williams, J. (2016). Unexpected seasonality in quantity and composition of Amazon rainforest air reactivity. *Nature Communications*, *7*. http://doi.org/10.1038/ncomms10383

Norman, J. M. (1979). Modelling the complete crop canopy. *Am. Soc. Agr. Eng. Monograph*, *2*, 249–277.

Norman, J. M., & Campbell, G. S. (1983). Application of a plant environment model to problems in irrigation. *Advances in Irrigation*, *II*, 155–188.

Oa, B. T. W., Sharkey, T. D., Loreto, F., Peeva, V., & Busheva, M. (2011). Increased Thermostability of Thylakoid Membranes in Isoprene-Emitting Leaves Probed with Three Biophysical Techniques. *Plant Physiology*, *157*, 905–916. http://doi.org/10.1104/pp.111.182519

Oke, T. R. (1995). The Heat Island of the Urban Boundary Layer : Characteristics , Causes and Effects. *Wind Climate in Cities*, 81–107. http://doi.org/10.1007/978-94-017-3686-2

Pacifico, F., Harrison, S. P., Jones, C. D., & Sitch, S. (2009). Isoprene emissions and climate. *Atmospheric Environment*, *43*(39), 6121–6135. http://doi.org/10.1016/j.atmosenv.2009.09.002

Padhy, P. K., & Varshney, C. K. (2005). Emission of volatile organic compounds (VOC) from tropical plant species in India. *Chemosphere*, *59*(11), 1643–1653. http://doi.org/10.1016/j.chemosphere.2005.01.046

Paulot, F., Henze, D. K., & Wennberg, P. O. (2012). Impact of the isoprene photochemical cascade on tropical ozone. *Atmospheric Chemistry and Physics*, *12*, 1307–1325. http://doi.org/10.5194/acp-12-1307-2012

Pegoraro, E., Rey, A., Greenberg, J., Harley, P., Grace, J., Malhi, Y., & Guenther, A. (2004). Effect of drought on isoprene emission rates from leaves of Quercus virginiana Mill. *Atmospheric Environment*, *38*(36), 6149–6156. http://doi.org/10.1016/j.atmosenv.2004.07.028

Peñuelas, J., Llusià, J., Asensio, D., & Munné-Bosch, S. (2005). Linking isoprene with

plant thermotolerance, antioxidants and monoterpene emissions. *Plant, Cell and Environment*, *28*(3), 278–286. http://doi.org/10.1111/j.1365-3040.2004.01250.x

Pérez-Harguindeguy, N., Díaz, S., Garnier, E., Lavorel, S., Poorter, H., Jaureguiberry, P., … Cornelissen, J. H. C. (2016). New handbook for standardised measurement of plant functional traits worldwide. *Australian Journal of Botany*, *61*(3), 167–234.

Pierce, T., Dennis, R., Tonnesen, G., Geron, C., Bender, L., & Guenther, A. (1998). Influence of increased isoprene emissions on regional ozone modeling. *Journal of Geophysical Research: Atmospheres*, *103*(D19), 25611–25629. http://doi.org/10.1029/98jd01804

Pöschl, U., Kuhlmann, R. V. O. N., Poisson, N., & Crutzen, P. J. (2000). Development and Intercomparison of Condensed Isoprene Oxidation Mechanisms for Global Atmospheric Modeling. *Journal of Atmospheric Chemistry*, *37*, 29–52.

Pyle, J. A., Ashfold, M. J., Harris, N. R. P., Robinson, A. D., Warwick, N. J., Carver, G. D., … Ong, S. (2011). Bromoform in the tropical boundary layer of the Maritime Continent during OP3. *Atmospheric Chemistry and Physics*, *11*(2), 529–542. http://doi.org/10.5194/acp-11-529-2011

RCSB. (2015). Isoprene Synthase. *Protein Data Bank, RCSB*. Retrieved from https://pdb101.rcsb.org/motm/201

Riutta, T., Malhi, Y., Khoon, L., Marthews, T. R., Huaraca, W., Minsheng, H., … Ewers, R. M. (2018). Logging disturbance shifts net primary productivity and its allocation in Bornean tropical forests. *Global Change Biology*, *24*, 2913–2928. http://doi.org/10.1111/gcb.14068

Rosenstiel, T. N., Ebbets, A. L., Khatri, W. C., Fall, R., & Monson, R. K. (2004). Induction of Poplar Leaf Nitrate Reductase: A Test of Extrachloroplastic Control of Isoprene Emission Rate. *Plant Biology*, *6*(1), 12–21. http://doi.org/10.1055/s-2003-44722

Sanadze, G. A. (1990). The principal scheme of photosynthetic carbon conversion in cells of isoprene releasing plants. *Current Research in Photosynthesis*, *IV*, 231–232.

Sanderson, M. G., Jones, C. D., Collins, W. J., Johnson, C. E., & Derwent, R. G. (2003). Effect of climate change on isoprene emissions and surface ozone levels. *Geophysical Research Letters*, *30*(18), 10–13. http://doi.org/10.1029/2003GL017642

Seco, R., Karl, T., Guenther, A., Hosman, K. P., Pallardy, S. G., Gu, L., … Kim, S. (2015). Ecosystem-scale volatile organic compound fluxes during an extreme drought in

a broadleaf temperate forest of the Missouri Ozarks (central USA). *Global Change Biology*, *21*(10), 3657–3674. http://doi.org/10.1111/gcb.12980

Seinfeld, J. H., & Pandis, S. N. (2006). Atmospheric Chemistry and Physics: From Air Pollution to Climate Change, *Second Edi*.

Sharkey, T. D. (2001). Isoprene Increases Thermotolerance of Fosmidomycin-Fed Leaves. *Plant Physiology*, *125*(4), 2001–2006. http://doi.org/10.1104/pp.125.4.2001

Sharkey, T. D. (2013). Is it useful to ask why plants emit isoprene? *Plant, Cell and Environment*, *36*(3), 517–520. http://doi.org/10.1111/pce.12038

Sharkey, T. D., & Loreto, F. (1993). Water stress, temperature, and light effects on the capacity for isoprene emission and photosynthesis of kudzu leaves. *Oecologia*, *95*, 328–333.

Sharkey, T. D., & Monson, R. K. (2014). The future of isoprene emission from leaves, canopies and landscapes. *Plant, Cell and Environment*, *37*(8), 1727–1740. http://doi.org/10.1111/pce.12289

Sharkey, T. D., & Singsaas, E. L. (1995). Why plants emit isoprene. *Nature*. http://doi.org/10.1038/374769a0

Sharkey, T. D., Wiberley, A. E., & Donohue, A. R. (2008). Isoprene emission from plants: Why and how. *Annals of Botany*, *101*(1), 5–18. http://doi.org/10.1093/aob/mcm240

Sharkey, T. D., & Yeh, S. (2001). Isoprene Emission from Plants. *Annu. Rev. Plant Physiol. Plant Mol. Biol.*, *52*, 407–436.

Silver, G. M., & Fall, R. (1991). Enzymatic Synthesis of Isoprene from Dimethylallyl Diphosphate in Aspen Leaf Extracts. *Plant Physiology*, *97*(4), 1588–1591. http://doi.org/10.1104/pp.97.4.1588

Singsaas, E. L., & Sharkey, T. D. (2000). The effects of high temperature on isoprene synthesis in oak leaves. *Plant, Cell and Environment*, *23*(7), 751–757. http://doi.org/10.1046/j.1365-3040.2000.00582.x

Sinha, A., Lovejoy, E. R., & Howard, C. J. (1987). Kinetic study of the reaction of HO2 with ozone. *The Journal of Chemical Physics*, *87*(4), 2122–2128. http://doi.org/10.1063/1.453136

Siwko, M. E., Marrink, S. J., de Vries, A. H., Kozubek, A., Schoot Uiterkamp, A. J. M., & Mark, A. E. (2007). Does isoprene protect plant membranes from thermal shock? A

molecular dynamics study. *Biochimica et Biophysica Acta - Biomembranes*, *1768*(2), 198–206. http://doi.org/10.1016/j.bbamem.2006.09.023

Smith, I. M. (2010). Software for Determining Polynomial Calibration Functions by Generalised Least Squares: User Manual. *NPL Report MS11, Teddington*.

Smith, P. A., Koch, D., Hook, G. L., Erickson, R. P., Jackson Lepage, C. R., Wyatt, H. D. M., … Eckenrode, B. A. (2004). Detection of gas-phase chemical warfare agents using field-portable gas chromatography-mass spectrometry systems: Instrument and sampling strategy considerations. *TrAC - Trends in Analytical Chemistry*, *23*(4), 296–306. http://doi.org/10.1016/S0165-9936(04)00405-4

Song, M., Liu, P. F., Hanna, S. J., Li, Y. J., Martin, S. T., & Bertram, A. K. (2015). Relative humidity-dependent viscosities of isoprene-derived secondary organic material and atmospheric implications for isoprene-dominant forests. *Atmospheric Chemistry and Physics*, *15*, 5145–5159. http://doi.org/10.5194/acp-15-5145-2015

Staudt, M., Bertin, N., Frenzel, B., & Seufert, G. (2000). Seasonal Variation in Amount and Composition of Monoterpenes Emitted by Young Pinus pinea Trees – Implications for Emission Modeling. *Journal of Atmospheric Chemistry*, *35*, 77–99.

Stavrakou, T., Müller, J. F., Bauwens, M., De Smedt, I., Van Roozendael, M., Guenther, A., … Xia, X. (2014). Isoprene emissions over Asia 1979-2012: Impact of climate and land-use changes. *Atmospheric Chemistry and Physics*, *14*(9), 4587–4605. http://doi.org/10.5194/acp-14-4587-2014

Steinbrecher, R., Hauff, K., Hakola, H., & Rössler, J. (1999). A revised parameterisation for emission modelling of isoprenoids for boreal plants. *Air Pollution Research Report*, *70*, 29–44.

Stockwell, W. R., Kirchner, F., Kuhn, M., & Seefeld, S. (1997). A new mechanism for regional atmospheric chemistry modeling. *Journal of Geophysical Research*, *102*(97), 25847–25879.

Stone, D., Evans, M. J., Edwards, P. M., Commane, R., Ingham, T., Rickard, A. R., … Heard, D. E. (2011). Isoprene oxidation mechanisms: Measurements and modelling of OH and HO2 over a South-East Asian tropical rainforest during the OP3 field campaign. *Atmospheric Chemistry and Physics*, *11*, 6749–6771. http://doi.org/10.5194/acp-11-6749-2011

Taraborrelli, D., Lawrence, M. G., Crowley, J. N., Dillon, T. J., Gromov, S., Groß, C. B.

M., … Lelieveld, J. (2012). Hydroxyl radical buffered by isoprene oxidation over tropical forests. *Nature Geoscience*, *5*(4), 300–300. http://doi.org/10.1038/ngeo1433

Thomas, M. V., Malhi, Y., Fenn, K. M., Fisher, J. B., Morecroft, M. D., Lloyd, C. R., … McNeil, D. D. (2011). Carbon dioxide fluxes over an ancient broadleaved deciduous woodland in southern England. *Biogeosciences*, *8*(6), 1595–1613. http://doi.org/10.5194/bg-8-1595-2011

University of Oxford. (2013). Tree-related research at Wytham Woods.

Velikova, V., & Loreto, F. (2005). On the relationship between isoprene emission and thermotolerance in Phragmites australis leaves exposed to high temperatures and during the recovery from a heat stress. *Plant, Cell and Environment*, *28*(3), 318–327. http://doi.org/10.1111/j.1365-3040.2004.01314.x

Visakorpi, K., Gripenberg, S., Malhi, Y., Bolas, C., Oliveras, I., Harris, N., … Riutta, T. (2018). Small-scale indirect plant responses to insect herbivory could have major impacts on canopy photosynthesis and isoprene emission. *New Phytologist*, *220*, 799–810. http://doi.org/10.1111/nph.15338

Wennberg, P. O., Bates, K. H., Crounse, J. D., Dodson, L. G., Mcvay, R. C., Mertens, L. A., … Seinfeld, J. H. (2018). Gas-Phase Reactions of Isoprene and Its Major Oxidation Products. *Chem. Rev.*, *118*, 3337–3390. http://doi.org/10.1021/acs.chemrev.7b00439

Wiedinmyer, C., Greenberg, J., Guenther, A., Hopkins, B., Baker, K., Geron, C., … Janssen, M. (2005). Ozarks Isoprene Experiment (OZIE): Measurements and modeling of the "isoprene volcano." *Journal of Geophysical Research D: Atmospheres*, *110*(18), 1–17. http://doi.org/10.1029/2005JD005800

Wolfe, G. M., & Thornton, J. A. (2011). The Chemistry of Atmosphere-Forest Exchange (CAFE) Model – Part 1 : Model description and characterization. *Atmospheric Chemistry and Physics*, *11*, 77–101. http://doi.org/10.5194/acp-11-77-2011

Wolfe, G. M., Thornton, J. a., Bouvier-Brown, N. C., Goldstein, A. H., Park, J.-H., McKay, M., … Keutsch, F. N. (2011). The Chemistry of Atmosphere-Forest Exchange (CAFE) Model – Part 2: Application to BEARPEX-2007 observations. *Atmospheric Chemistry and Physics*, *11*(3), 1269–1294. http://doi.org/10.5194/acp-11-1269-2011

World Health Organisation, T. (2005). WHO Air quality guidelines for particulate matter, ozone, nitrogen dioxide and sulfur dioxide.

Yáñez-Serrano, A. M., Nölscher, A. C., Williams, J., Wolff, S., Alves, E., Martins, G. A.,

… Kesselmeier, J. (2015). Diel and seasonal changes of biogenic volatile organic compounds within and above an Amazonian rainforest. *Atmospheric Chemistry and Physics*, *15*(6), 3359–3378. http://doi.org/10.5194/acp-15-3359-2015

Yi, C. (2007). Momentum Transfer within Canopies, (2005), 262–275. http://doi.org/10.1175/2007JAMC1667.1

Yu, H., Guenther, A., Gu, D., Warneke, C., Geron, C., Goldstein, A., … Yuan, B. (2017). Airborne measurements of isoprene and monoterpene emissions from southeastern U.S. forests. *Science of the Total Environment*, *595*, 149–158. http://doi.org/10.1016/j.scitotenv.2017.03.262

Zheng, Y., Unger, N., Tadić, J. M., Seco, R., Guenther, A. B., Barkley, M. P., … Pallardy, S. G. (2017). Drought impacts on photosynthesis, isoprene emission and atmospheric formaldehyde in a mid-latitude forest. *Atmospheric Environment*, *167*, 190–201. http://doi.org/10.1016/j.atmosenv.2017.08.017

10 APPENDICES

APPENDIX 1: CODES FOR IDIRAC CONTROL, DATA ANALYSIS AND CAMCAN

Each of the scripts described in this thesis can be found on the public GitHub repository, iDirac-scripts.

The repository can be accessed here:

https://github.com/cgb36/iDirac-scripts

This repository contains the following scripts.

Arduino

adr_isoprene_gc.ino iDirac V1 script for the Arduino Mega inside the instrument. Controls the internal components of the iDirac and the various sensors that compose the instrument. This is the Version 1 script, used only on the Yellow iDirac. Described in Chapter 2.

adr_isoprene_gc_v2.ino iDirac V2 script for the Arduino Mega inside the instrument. Controls the internal components of the iDirac and the various sensors that compose the instrument. This is the Version 1 script, used on the orange and grey iDiracs. Described in Chapter 2.

adr_flowmeter_altimeter.ino iDirac script for the Arduino Micro that controls the integration of the flow through the instrument. Used on all iDiracs. Described in Chapter 2.

Python 2.7

ard_listen.py Script that communicates with the Arduino from the on-board Raspberry Pi. Uses Python 2.7 commands to manipulate a command line terminal that different parameters for the iDirac can be configured from. Described in Chapter 2.

Mathematica

Chromatogram Analysis.nb Mathematica (v11.1.1) script that processes raw chromatograms from the iDirac. Described in Chapter 2.

CamCan.nb Mathematica (v11.1.1) model that takes meteorological data and simulates isoprene at different levels in a forest canopy. Described in Chapter 7.

APPENDIX 2: TROPICAL FOREST TREE ISOPRENE EMISSION FACTORS

Species	**Tree No.**	**Site**	**Sun or Shade**	**Measured emission rate / nmolm^{-2}s^{-1}**	**Measured emission rate standard deviation / nmolm^{-2}s^{-1}**	**Emission factor / nmolm^{-2}s^{-1}**	**Emission factor standard deviation / nmolm^{-2}s^{-1}**
Litsea graciae	3577	Plot E, SAFE	Sun	71704.21	36643.24	3014096.99	1540304.03
Artocarpus anisophyllus	15	Plot E, SAFE	Sun	2354.06	2156.25	620619.19	568467.83
Macaranga pearsonii	379	Plot E, SAFE	Sun	1298.46	1306.00	171901.32	172899.94
Cleistanthus paxii	152	Plot E, SAFE	Sun	3090.00	4208.08	93980.99	127986.84
To be identified	377	Plot E, SAFE	Sun	739.51	1013.84	73670.92	101000.97
Macaranga gigantea	42	Plot E, SAFE	Sun	91.19	87.03	72936.63	69609.44
Macaranga pearsonii	378	Plot E, SAFE	Sun	963.40	1253.93	40796.27	53099.14
Macaranga pearsonii	383	Plot E, SAFE	Sun	56.14	41.75	35422.45	26341.56
Dryobalanops lanceolata	297	Belian, Maliau	Sun	2.05	1.68	26706.74	21853.35
Glochidion lutescens	176	Plot E, SAFE	Sun	498.42	571.05	20375.78	23344.66
Horsfielda	358	Belian,	Sun	6.17	2.87	19608.45	9104.51

walichii		Maliau					
Lithorcarpus gracilis	101	Belian, Maliau	Sun	2.21	5.49	14236.44	35335.13
Sindora irpicina	97	Seraya, Maliau	Sun	12.63	5.48	12112.54	5255.51
Lithocarpus orocola	241	Plot E, SAFE	Sun	19.56	29.46	11162.47	16814.12
Reinwardtiodend-ron humile	285	Belian, Maliau	Sun	3.15	2.86	9776.37	8864.58
Macaranga pearsonii	391	Plot E, SAFE	Sun	21.49	12.58	9622.21	5632.91
Ochanostachys amentacea	217	Seraya, Maliau	Sun	2.87	5.15	9134.33	16374.54
Antidesma stipulane	211	Plot E, SAFE	Sun	53.28	72.32	8420.07	11429.60
Crotoxylum cochinchinense	50	Plot E, SAFE	Sun	50.82	25.29	7946.09	3954.72
Macaranga pearsonii	376	Plot E, SAFE	Sun	149.30	104.87	7717.84	5421.00
Myristica smythiesii	365	Plot E, SAFE	Sun	153.23	291.82	7348.89	13995.75
Macaranga pearsonii	402	Plot E, SAFE	Sun	60.39	11.08	6425.71	1179.33
Parartocarpus bracteatus	471	Seraya, Maliau	Sun	8.27	3.22	6234.68	2423.22

Glochidion borneensis	509	Plot E, SAFE	Sun	47.71	57.30	5657.37	6794.43
Canarium decumanum	309	Seraya, Maliau	Sun	7.36	6.63	5507.77	4963.79
Syzygium racemosum	273	Plot E, SAFE	Sun	61.33	65.53	5239.09	5597.94
Hydnocarpus woodii	337	Belian, Maliau	Sun	9.25	12.41	5110.01	6858.60
Macaranga pearsonii	380	Plot E, SAFE	Sun	42.09	13.54	5044.02	1622.25
Reinwardtiodend-ron humile	214	Plot E, SAFE	Sun	4.64	10.93	4997.11	11766.81
Litsea angulata	160	Plot E, SAFE	Sun	119.52	185.10	4721.19	7312.15
Litsea angulata	160	Plot E, SAFE	Sun	47.15	8.24	3896.14	681.23
Dryobalanops lanceolata	308	Seraya, Maliau	Sun	0.72	7.48	3574.10	37336.68
Neonauclea gigantea	189	Seraya, Maliau	Sun	0.95	0.49	3014.32	1539.30
Pometia pinnata	11	Seraya, Maliau	Sun	1.62	1.65	2833.17	2888.24
Shorea parvifolia	195	Belian, Maliau	Sun	0.88	0.84	2780.58	2678.61
Eusideroxylo	275	Belian,	Sun	1.13	0.65	2757.30	1573.58

n zwageri		Maliau					
Payena acuminata	84	Plot E, SAFE	Sun	67.12	29.58	2546.94	1122.39
Glochidion lutescens	176	Plot E, SAFE	Sun	38.51	53.96	2523.53	3535.70
Duabanga moluccana	35	Seraya, Maliau	Sun	5.91	14.58	2318.88	5718.59
Knema oblongata	32	Plot E, SAFE	Sun	17.20	26.07	1780.52	2698.72
Dryobalanops lanceolata	352	Belian, Maliau	Sun	0.67	0.23	1754.52	598.34
Shorea laevis	79	Plot E, SAFE	Sun	26.71	49.93	1744.33	3261.03
Myristica smythiesii	365	Plot E, SAFE	Sun	2.76	14.20	1652.49	8514.29
Dacryodes rugosa	294	Belian, Maliau	Sun	3.50	2.87	1587.85	1301.09
Dialium kunstleri	1056	Plot E, SAFE	Sun	12.42	25.09	1447.51	2923.27
Eusideroxylon zwageri	343	Belian, Maliau	Sun	0.58	0.61	1433.59	1510.63
Bauccaurea latifolia	230	Plot E, SAFE	Sun	14.43	15.41	1358.46	1450.96
Litsea caulocarpa	136	Plot E, SAFE	Sun	22.70	26.59	1162.84	1362.02
Hopea plagata	287	Seraya, Maliau	Sun	2.67	2.06	1045.74	805.00
Neoscortechi	163	Plot E,	Sun	43.52	76.91	1001.85	1770.66

nia philippinensis		SAFE					
Blumeodendron tokbrai	59	Belian, Maliau	Shade	1.19	1.19	867.94	869.52
Quercus argentata	569	Plot E, SAFE	Sun	12.50	20.07	853.10	1369.68
Shorea ovata	253	Plot E, SAFE	Sun	6.69	11.86	788.34	1396.98
Santiria laevigata	3516	Plot E, SAFE	Sun	12.27	9.04	786.48	579.61
Dimocarpus longan	219	Plot E, SAFE	Sun	3.29	3.02	662.93	607.19
Shorea johorensis	80	Belian, Maliau	Sun	0.46	0.75	655.37	1081.38
Sageraea elliptica	5	Plot E, SAFE	Sun	2.47	2.22	597.29	535.72
Shorea pauciflora	97	Belian, Maliau	Sun	1.29	0.40	595.35	187.16
Shorea macroptera	342	Seraya, Maliau	Sun	1.01	1.39	556.30	761.61
Gluta aptera	149	Plot E, SAFE	Sun	2.96	3.20	543.97	588.01
Madhuca korthalsii	577	Plot E, SAFE	Sun	1.17	1.83	533.35	832.79
Shorea parvifolia	455	Seraya, Maliau	Sun	0.66	0.34	465.91	239.40
Cyathocalyx	105	Belian,	Sun	0.43	0.88	427.97	871.93

deltoideus		Maliau					
Blumeodendron tokbrai	3519	Plot E, SAFE	Shade	2.88	1.29	423.43	189.39
Elaeocarpus stipularis	343	Seraya, Maliau	Sun	0.30	0.35	419.55	497.95
Eusideroxylon zwageri	336	Belian, Maliau	Sun	0.22	0.18	331.41	269.99
Dysoxylum cyrtobotryum	276	Belian, Maliau	Sun	1.92	0.83	316.68	137.27
Eusideroxylon zwageri	290	Belian, Maliau	Sun	0.47	0.70	287.61	427.47
Dysoxylum cauliflora	345	Belian, Maliau	Sun	0.95	0.22	283.07	64.56
Alangium javanicum	347	Belian, Maliau	Sun	0.33	0.39	281.30	329.62
Dipterocarpus caudiferus	109	Seraya, Maliau	Sun	0.29	0.67	252.37	586.62
Parashorea smythiesii	305	Seraya, Maliau	Sun	0.66	0.34	177.24	91.94
Shorea beccariana	3520	Plot E, SAFE	Sun	6.37	8.82	166.39	230.26
Eusideroxylon zwageri	138	Belian, Maliau	Sun	0.32	0.44	153.45	209.28
Syzygium havilandii	280	Belian, Maliau	Sun	0.60	3.95	146.08	968.69
Dimocarpus longan	219	Plot E, SAFE	Sun	1.47	0.91	133.44	82.32

Eusideroxylon zwageri	338	Belian, Maliau	Sun	0.38	0.66	113.30	197.08
Eusideroxylon zwageri	278	Belian, Maliau	Sun	1.09	1.05	111.76	107.20
Dryobalanops lanceolata	95	Belian, Maliau	Sun	2.28	4.54	100.58	199.86
Castanopsis hypophoenicea	480	Seraya, Maliau	Sun	0.16	4.30	92.43	2555.33
Eusideroxylon zwageri	138	Belian, Maliau	Sun	2.17	1.57	92.30	66.95
Dryobalanops lanceolata	137	Belian, Maliau	Sun	3.50	3.11	83.55	74.27
Scaphium macropodum	30	Plot E, SAFE	Shade	0.60	4.90	76.78	629.15
Reinwardtiodendron humile	214	Plot E, SAFE	Sun	0.29	2.36	71.58	582.15
Eusideroxylon zwageri	58	Belian, Maliau	Shade	0.05	0.09	57.42	96.03
Shorea almon	300	Plot E, SAFE	Sun	0.39	2.13	53.05	288.73
Eusideroxylon zwageri	62	Seraya, Maliau	Shade	0.24	0.43	48.14	86.34
Ryparosa acuminata	56	Belian, Maliau	Shade	2.16	1.55	45.61	32.72
Baccaurea latifolia	392	Plot E, SAFE	Sun	0.45	2.39	43.42	230.89
Vatica	474	Seraya	Sun	0.05	2.07	16.30	639.97

dulitensis		, Maliau					
Ochanostachys amentacea	339	Belian, Maliau	Sun	0.02	1.51	15.32	1242.88
Shorea beccariana	125	Plot E, SAFE	Sun	0.14	0.58	8.72	35.50
Shorea leprosula	128	Belian, Maliau	Sun	0.29	4.81	7.00	117.53
Shorea fallax	47	Plot E, SAFE	Sun	0.01	6.10	2.08	879.47
Knema laurina	31	Plot E, SAFE	Sun	0.00	10.38	0.00	299.12
Eusideroxylon zwageri	109	Belian, Maliau	Sun	0.00	0.07	0.00	49.35
Lophopethalum beccariana	424	Plot E, SAFE	Sun	0.00	3.11	0.00	71.95
Parashorea tomentella	46	Seraya , Maliau	Sun	0.00	1.39	0.00	257.25
Eusideroxylon zwageri	281	Plot E, SAFE	Sun	0.00	2.23	0.00	328.66
Ochanostachys amentacea	151	Plot E, SAFE	Sun	0.00	2.42	0.00	1166.04
Chisocheton pentandrus	243	Plot E, SAFE	Sun	0.00	0.34	0.00	30.36
Shorea leprosula	341	Belian, Maliau	Sun	0.00	0.13	0.00	5.54
Naotaphoebe umbelliflora	567	Plot E, SAFE	Sun	0.00	2.76	0.00	92.53
Dialium	239	Seraya	Sun	0.00	0.04	0.00	58.82

indum		, Maliau					
Parashorea malaanonan	104	Belian, Maliau	Sun	0.00	0.25	0.00	629.14
Shorea guiso	337	Seraya , Maliau	Sun	0.00	0.74	0.00	5264.86
Diospyros curranii	299	Plot E, SAFE	Sun	0.00	1.80	0.00	164.46
Dryobalanops lanceolata	351	Belian, Maliau	Sun	0.00	0.24	0.00	356.54
Eusideroxylon zwageri	281	Plot E, SAFE	Sun	0.00	0.56	0.00	226.14
Shorea faguetiana	60	Belian, Maliau	Sun	0.00	7.25	0.00	134.36
Dialium indum	49	Plot E, SAFE	Shade	0.00	5.38	0.00	354.63
Aglaia angustifolia	25	Seraya , Maliau	Sun	0.00	0.71	0.00	358.39
Melanochyla tomentosa	340	Belian, Maliau	Sun	0.00	0.48	0.00	330.61
Paranephelium xestophyllum	13	Seraya , Maliau	Shade	0.00	1.21	0.00	548.00
Parashorea tomentella	49	Seraya , Maliau	Sun	0.00	0.86	0.00	806.87
Lophopetalum glabrum	92	Seraya , Maliau	Sun	0.00	4.61	0.00	2305.20

Chisocheton sarawakensis	257	Plot E, SAFE	Sun	0.00	0.85	0.00	181.11
Shorea ovalis	275	Plot E, SAFE	Sun	0.00	6.10	0.00	224.38
Payena acuminata	84	Plot E, SAFE	Shade	0.00	34.82	0.00	1989.59
Macaranga winkleri	1172	Plot E, SAFE	Sun	0.00	15.80	0.00	1343.03
Dysoxylum densiflorum	559	Plot E, SAFE	Sun	0.00	9.29	0.00	439.50
Pentace laxiflora	41	Plot E, SAFE	Sun	0.00	3.24	0.00	552.77
Vatica rasak	309	Plot E, SAFE	Sun	0.00	18.00	0.00	1196.37
Ficus sp	289	Plot E, SAFE	Sun	0.00	1.75	0.00	613.67
Pterygota alata	326	Seraya, Maliau	Sun	0.00	2.30	0.00	1067.85
Pyrenaria tawauensis	365	Seraya, Maliau	Sun	0.00	0.44	0.00	1514.12
Eusideroxylon zwageri	282	Belian, Maliau	Sun	0.00	1.64	0.00	761.29
Eusideroxylon zwageri	62	Seraya, Maliau	Sun	0.00	0.33	0.00	256.33
Syzygium grande	171	Plot E, SAFE	Sun	0.00	1.12	0.00	240.10
Shorea ovalis	54	Seraya	Sun	0.00	1.06	0.00	1240.45

		, Maliau					
Syzygium tawahense	349	Belian, Maliau	Sun	0.00	3.50	0.00	2042.68
Parashorea malaanonan	267	Belian, Maliau	Sun	0.00	0.57	0.00	577.25
Syzygium grande	171	Plot E, SAFE	Sun	0.00	1.08	0.00	150.73
Parashorea tomentella	37	Seraya , Maliau	Sun	0.00	0.51	0.00	355.43
Litsea accedens	494	Plot E, SAFE	Sun	0.00	10.49	0.00	1573.60
Cleistanthus pubens	57	Seraya , Maliau	Shade	0.00	0.36	0.00	5487.39
Shorea leprosula	390	Seraya , Maliau	Sun	0.00	3.07	0.00	3161.09
Shorea johorensis	46	Plot E, SAFE	Sun	0.00	5.92	0.00	1074.87
Lithocarpus blumeanus	96	Plot E, SAFE	Sun	0.00	8.19	0.00	535.56
Vatica albiramis	164	Plot E, SAFE	Sun	0.00	3.86	0.00	1808.90
Vatica dulitensis	469	Seraya , Maliau	Sun	0.00	1.17	0.00	1368.82
Blumeodendron kurzii	232	Plot E, SAFE	Sun	0.00	23.11	0.00	2035.63

Pentace laxiflora	166	Plot E, SAFE	Sun	0.00	22.41	0.00	1769.59
Hopea sangal	30	Belian, Maliau	Sun	0.00	3.21	0.00	820.68
Santiria laevigata	236	Plot E, SAFE	Sun	0.00	6.06	0.00	1987.04
Shorea parvistipulata	526	Plot E, SAFE	Sun	0.00	8.35	0.00	721.82
Shorea faguetiana	102	Belian, Maliau	Sun	0.00	3.09	0.00	2963.38
Dipterocarpus caudiferus	589	Plot E, SAFE	Sun	0.00	17.27	0.00	1291.89
Shorea macroptera	81	Plot E, SAFE	Sun	0.00	7.65	0.00	675.79
Adinandra dumosa	364	Seraya, Maliau	Sun	0.00	0.79	0.00	1227.91
Shorea macroptera	81	Plot E, SAFE	Shade	0.00	18.60	0.00	1373.98
Maasua sumatrana	3578	Plot E, SAFE	Shade	0.00	5.49	0.00	471.59
To be identified	395	Plot E, SAFE	Sun	0.00	1.79	0.00	642.39
Parashorea tomentella	222	Seraya, Maliau	Sun	0.00	1.40	0.00	4038.77
Naotaphoebe umbelliflora	567	Plot E, SAFE	Sun	0.00	6.17	0.00	6336.33
Knema pulcha	233	Seraya,	Sun	0.00	0.36	0.00	404.51

		Maliau					
Durio graveolens	289	Belian, Maliau	Sun	0.00	0.55	0.00	6786.95
Shorea beccariana	2832	Seraya, Maliau	Sun	0.00	1.16	0.00	2103.89
Parashorea tomentella	348	Belian, Maliau	Sun	0.00	0.51	0.00	1728.17
Vatica dulitensis	477	Seraya, Maliau	Sun	0.00	3.89	0.00	2864.31
Shorea leprosula	59	Plot E, SAFE	Sun	0.00	45.03	0.00	3824.43
Spathiostemon javanensis	231	Seraya, Maliau	Sun	0.00	6.04	0.00	4252.46
Vatica dulitensis	479	Seraya, Maliau	Sun	0.00	2.81	0.00	8606.97
Vatica odorata	386	Plot E, SAFE	Sun	0.00	3.48	0.00	3308.13
Syzygium murtifolium	481	Plot E, SAFE	Sun	0.00	29.84	0.00	1713.49
Scorodocarpus borneensis	112	Seraya, Maliau	Sun	0.00	0.48	0.00	7117.00
Quercus argentata	278	Seraya, Maliau	Sun	0.00	0.37	0.00	5237.78
To be identified	48	Plot E, SAFE	Shade	0.00	6.23	0.00	1232.98

Pseuduvaria borneensis	114	Plot E, SAFE	Sun	0.00	20.83	0.00	9713.33
Vatica dulitensis	473	Seraya, Maliau	Sun	0.00	1.33	0.00	5446.38
Pterygota alata	227	Seraya, Maliau	Sun	0.00	2.26	0.00	27386.54
Vatica dulitensis	476	Seraya, Maliau	Sun	0.00	2.21	0.00	25480.90
Pterygota alata	326	Seraya, Maliau	Sun	0.00	3.12	0.00	39683.73